ANALYSIS OF BIOLOGICAL PATTERN FORMATION MODELS

by

David Michael Crawford

Thesis submitted in partial fulfillment of

the requirements for the degree of

Doctor of Philosophy

at the University of Oxford

Jesus College, Oxford

Michaelmas Term 1989

ANALYSIS OF BIOLOGICAL PATTERN FORMATION MODELS

by
David Michael Crawford,
Jesus College, Oxford.

Thesis submitted for the degree of D. Phil.
Michaelmas term 1989.

In this thesis we examine mathematical models which have been suggested as possibile mechanisms for forming certain biological patterns. We analyse them in detail attempting to produce the requisite patterns both analytically and numerically. A reaction diffusion system in two spatial dimensions with anisotropic diffusion is examined in detail and the results compared with certain snakeskin patterns. We examine two other variants to the standard reaction diffusion system: a system where the reaction kinetics and the diffusion coefficients depend upon the cell density suggested as a possible model for the segmentation sequence in *Drosophila* and a system where the model parameters have one dimensional spatial gradients.

We also analyse a model derived from known cellular processes used to model the branching behaviour in bryozoans and show that, in one dimension, such a model can, in theory, give all the required solution behaviour. A genetic switch model for pattern elements on butterfly wings is also briefly examined to obtain expressions for the solution behaviour under coldshock.

Contents.

Acknowledgements.

I would like to thank my supervisor Professor J.D. Murray for all his help and encouragement throughout my studies. I would also like to thank Dr. Philip Maini and Dr. Peter Grindrod for all their suggestions and assistance.

I acknowledge the assistance, especialy in matters computational, of my fellow students in Mathematical Biology; Louisa Shaw, Mick Jenkins, Meghan Burke and Mark Lewis who created a very relaxed work atmosphere. I would also like to thank the faculty, students and staff of the Dept. of Applied Math. at the University of Washington in Seattle where I spent an enjoyable nine months in 1988/89. Special thanks are also due to Jesus College, Oxford and the Mathematical Institute, Oxford for generous travel grants which made this trip possible.

I gratefully acknowledge the Science and Engineering Research Council of Great Britain for the grant under which this work was carried out.

Introduction.

The development of pattern and form in biology, known as morphogenesis, is one of the great unsolved mysteries in science. When cell division first begins in an embryo, the original mass of cells is homogeneous so a mechanism is required to account for the organisation of the cells into the different organs. The concept of positional information, suggested by Wolpert (1969), says that the cells are pre-programmed to differentiate into different types of cells depending upon the concentration of a chemical they experience. This idea divides development into several separate stages; the first being the establishment of the chemical or morphogen pre-pattern.

The two most widely studied mechanisms for producing morphological patterns are reaction diffusion mechanisms based on the pioneering work of Turing (1952) and the more recent mechanochemical models as discussed by Murray and Oster (1984a,b). This latter type of system considers pattern formation and morphogenesis to go on simultaneously - the chemical patterning and the form shaping movements of the cells and the embryological tissue are thought to be continuously interacting to produce the observed spatial pattern. These models use the fact that the individual cells move by exerting traction forces upon their surroundings, which consist of the fibrous extracellular matrix and the surfaces of other cells. These traction forces deform the matrix which in turn affects the cell movements. A detailed bi-

ological description of how each term in the equations is derived is given in Oster, Murray and Harris (1983).

Reaction diffusion mechanisms, on the other hand, have pattern formation and morphogenesis occuring sequentially. Chemicals, called morphogens, form a concentration pattern which then assigns positional values to the cells. Models of this type use the morphogen concentrations as variables and are capable of forming heterogeneous steady state patterns from small disturbances about a uniform steady state. This is the property that has most attracted the attention of theoretical biologists. Contrary to its normal behaviour, in these models, diffusion is acting as a destabilizing factor.

There are two major drawbacks to the chemical theory of morphogenesis. The first is that the morphogens themselves are purely hypothetical. Recently retinoic acid (Tickle (1983)) and calcium (Goodwin (1984)) have been put forward as morphogen candidates but the role they play in positional signalling and experimental evidence for their existence is, at present, inconclusive. The second problem concerns the solution's sensitivity to alterations in the domain size and shape or in the initial conditions. The need for the accurate pattern reproduction found in most areas of morphogenesis has given rise to suggestions that more stable patterns, such as simple gradients, when coupled with threshold mechanisms of the type discussed by Lewis *et al.* (1977) could prove to be the basis for producing the positional information necessary for Wolpert's theory. These simple gradients however are not capable of producing the more elaborate patterns observed.

In this thesis we discuss, in the main, models of the reaction diffusion type with slight modifications to the norm to see what patterns we can produce. In Chapter One we review reaction diffusion theory, apply it to a simple example of a reaction kinetics set and illustrate the effects changing certain parameters can have upon the model solutions by means of numerical simulations. In Chapter Two we discuss the possibility of using anisotropy in the diffusion coefficients and analyse in depth the effect this has on the solution patterns. In Chapter Three we consider the reaction diffusion model of Nagorcka (1988) as applied to the problem of segmentation in the embryo of the fruit fly *Drosophila Melanogaster*. The point of interest of this chapter is the incorporation of the cell density into the reaction kinetics and the diffusion coefficients to try to obtain the effect of period doubling. In Chapter Four we briefly examine the effects of one dimensional gradients in the reaction parameters upon the patterns formed on a two dimensional domain.

In Chapter Five we examine a slightly different model suggested by Goldwasser, Maini and Murray (1989) with a more mechanochemical basis to attempt to explain the phenomena of branching in bryozoans. In Chapter Six we briefly consider a genetic switch model first proposed by Murray (1981a) to model pattern formation on butterfly wings and use it to examine the behaviour of eyespot patterns under coldshock.

Chapter 1

A Brief Review of the Reaction Diffusion Theory of Pattern Formation.

1.1 Background.

In his seminal paper Turing (1952) suggested that, under certain conditions, chemicals could react together and diffuse through the surrounding medium in such a way as to produce spatially heterogeneous steady state patterns of chemical or morphogen concentration. The process could be triggered by a random disturbance about a uniform steady state and the resulting morphogen landscape used to provide a blueprint for cell differentiation in morphogenesis. This is the basis for Wolpert's (1969,1981) theory of positional information. In particular Turing considered systems of two or three morphogens interacting on a ring of cells or tissue. He suggested that this could be used to model, among other things, tentacle development in *Hydra*, an idea subsequently developed by Gierer and Meinhardt (1972). The equations for the reaction diffusion mechanisms we consider in this thesis are of

the general form

$$\frac{\partial \underline{c}}{\partial t} = \underline{f}(\underline{c}) + D\nabla^2 \underline{c} \tag{1.1}$$

where

$\underline{c}$ is the vector of morphogen concentrations.

$\underline{f}$ represents the reaction-kinetics interactions between the chemicals.

D is the (generally) diagonal matrix of positive diffusion coefficients.

Since Turing's classic paper, a number of specific, two reactant, model mechanisms have been proposed, studied extensively and applied, with varying degrees of plausibility, to a large number of problems in developmental biology. These mechanisms can exhibit an amazing richness of spatial and temporal patterns that are diffusion driven in the Turing sense. Two particularly widely studied systems are the autocatalytic activator-inhibitor model of Gierer and Meinhardt (1972), used in several varying forms to model the morphogenesis of *Hydra* and in the formation of slime mould *Dictyostelium discoideum* slugs (*cf.* Lacalli and Harrison (1979)) and the experimental substrate inhibition model of Thomas (1976), used as the model mechanism for generating mammalian coat patterns (Murray 1981a,b) and by Bunow *et al.* (1980) to model compartment formation on the wings of the fruit fly *Drosophila.* Another class of mechanisms, of a more hypothetical nature but algebraically simpler to deal with, are the trimolecular autocatalytic reactions involving two chemicals as categorised by Schnackenberg (1979). Murray (1982) shows that all the particular reaction diffusion mechanisms are qualitatively the same, as regards pattern formation potential in a Turing sense, and we make use of this by employing the simplest of the Schnacken-

berg (1979) mechanisms, described in Section 1.3 below, to illustrate many of the analytical results in later chapters of this thesis.

Reaction diffusion systems can have solutions falling into two qualitative groups: the type we are concerned with which are asymptotically stationary and spatially heterogeneous and solutions which vary periodically in time. For completeness we mention here the classic real example of the time varying solution type, namely the Belousov-Zhabotinski reaction which has generated so much mathematical interest. This chemical oscillator can exhibit both periodic travelling waves and spiral waves. A review of the models suggested to explain this phenomena is given by Tyson (1976). A real biological example which exhibits rotating spiral waves, and for which a realistic reaction diffusion model exists, has recently been described by Tyson, Alexander, Manoranjan and Murray (1989). In this example experimental parameter values are available. The analytical results from this model are in good agreement with the experimental data.

With our current state of knowledge, or rather lack of it, concerning the identity of morphogens taking part in almost all morphogenetic pattern formation, we cannot really say that any particular model is the 'best' biologically. We can, however, compare the models' sensitivity to initial or boundary conditions, the time scale of pattern formation and the stability of the final pattern. Under zero flux boundary conditions both the solution patterns obtained and the pattern's polarity are sensitive to changes in the initial conditions and in the domain's size and shape. This sensitivity

has prompted some workers to question the biological applicability of reaction diffusion systems (for example Bunow *et al.* (1980), Bard and Lauder (1974)). In some situations however, this sensitivity is a positive attribute of the model. This is the case in Murray's (1981a) reaction diffusion model for animal coat markings. For given initial conditions the heterogeneous steady state was found to be unique: small variations in the initial conditions resulting in quite different spatial patterns although the general qualitative character was similar. This is obviously an advantage when attempting to model animal markings which exhibit, within the same species, randomness but only within certain limits. For example all leopards are spotted but the distribution of the spots is unique to each animal.

The question of the time scale of the pattern formation is closely related to the magnitude of the diffusion coefficients for morphogen candidates. In order for the morphogen to be able to diffuse across cells it would be expected to have a diffusion coefficient of $O(10^{-7}\text{cm}^2\text{sec}^{-1})$, probably much smaller in fact. This would suggest that to establish, for example, a gradient in a domain of size O(1cm) using a simple diffusion process would need about one day. This is longer than would be reasonable in many biological situations. This does not imply that reaction diffusion systems cannot successfully model many biological patterning phenomena as the time required to generate a reaction diffusion pattern can be much shorter than by pure diffusion. Some of the varied practical applications of reaction diffusion theory are given in the books by Murray (1977,1989). The lecture notes by Fife (1979) and the

book by Britton (1986) survey the more mathematical results.

In one space dimension, Mimura and Murray (1978) considered a model predator-prey system which could be driven unstable by diffusion in the Turing sense. They thought that this could be a possible contributing factor to the observed planktonic patchiness in the sea. They found that numerical simulation of the finite amplitude solution from the full nonlinear equations showed that the linear theory, which predicted a fastest growing linearly unstable mode, gave an accurate prediction of the ultimate heterogeneous structure. Murray (1979) showed that in two (or higher) spatial dimensions the finite amplitude structure bears no obvious relation to the fastest growing linearly unstable mode. Except for the simplest patterns we should only use two (and higher) dimensional linear theory as a guide to the range of patterns the model can generate and as a method for determining the parameter ranges necessary for pattern generation. The finite amplitude structure depends upon the initial and boundary conditions. Arcuri and Murray (1986) showed in the case of the Thomas (1976) mechanism that, in one dimension, nonhomogeneous boundary conditions give rise to patterns which are much more robust than those with zero-flux boundary conditions. This is intuitively as we would expect. This would correspond to a biological system exchanging material with its immediate surroundings which is not an unreasonable assumption in many biological situations.

Many workers have suggested slightly altered reaction diffusion systems to produce some differing patterns not obtained from normal reaction diffusion

systems. Meinhardt and Klinger (1987), for example, discuss the possibilities of the patterns found on the shells of certain molluscs being formed by such a mechanism. A more realistic model for shell patterns however has been proposed by Ermentrout, Campbell and Oster (1986). The former solve the system on a two dimensional (one space-one time) domain as the pattern is only laid down at the growing edge and so is one dimensional while the second dimension comes from shell growth. In later chapters of this thesis we discuss other such variations: anisotropic diffusion in Chapter Two, cell density dependent diffusion coefficients and reaction strengths in Chapter Three and space varying parameters in Chapter Four.

In the rest of this chapter we give a review of the basic theory which we need for the analysis to follow. In Section 1.2 we establish the conditions necessary for diffusion driven instability for general reaction kinetics. In Section 1.3 we carry out a more specific analysis for the simple trimolecular system of Schnackenberg (1979) and establish what is generally known as the Turing space (region in the parameter space where diffusion driven instability can occur) *cf.* Murray (1982). In Section 1.4 we illustrate, with numerical simulations, the effects that changing certain model parameters can have on the patterns formed.

1.2 Reaction Diffusion Theory.

A reaction diffusion system is said to exhibit diffusion driven or Turing instability if the uniform steady state is stable to small spatially homogeneous

perturbations but becomes unstable when spatially heterogeneous perturbations are introduced. In this section we derive the conditions necessary for this behaviour for a general dimensionless reaction diffusion system, namely

$$\begin{aligned} u_t &= \gamma f(u,v) + \nabla^2 u \\ v_t &= \gamma g(u,v) + d\nabla^2 v \end{aligned} \tag{1.2}$$

where u and v are the morphogen concentrations and d is the ratio of the diffusion coeffients D_v/D_u of the two morphogens. The parameter γ can be interpreted in at least three ways (Arcuri and Murray (1986)).

1. γ is directly proportional to the area of the domain.
2. γ is inversely proportional to the absolute size of the diffusivities in such a way that if d is kept constant then an increase in γ is equivalent to a proportional decrease in both D_u and D_v.
3. γ represents the strength of the overall reaction terms.

We assume the system has a unique positive homogeneous steady state (u_0, v_0) given by the solution of

$$f(u,v) = g(u,v) = 0 \quad \Rightarrow u = u_0, v = v_0. \tag{1.3}$$

The first stage of the analysis is to obtain conditions for the linear stability of this steady state in the absence of diffusion. To do this we consider

$$\begin{aligned} u_t &= \gamma f(u,v) \\ v_t &= \gamma g(u,v). \end{aligned} \tag{1.4}$$

Linearising about the steady state (u_0, v_0), we set

$$\underline{w} = \begin{pmatrix} u - u_0 \\ v - v_0 \end{pmatrix} \tag{1.5}$$

to obtain

$$\underline{w}_t = \gamma M \underline{w} + h(\underline{w}, \gamma) \tag{1.6}$$

where the stability matrix M is given by

$$M = \left(\begin{array}{cc} f_u & f_v \\ g_u & g_v \end{array} \right)_{u_0, v_0}$$

and $h(\underline{w}, \gamma)$ contains the nonlinear terms. For $|u - u_0|$, $|v - v_0| \ll 1$ the nonlinear terms are negligable so we look for solutions of the form

$$\underline{w} \propto e^{\lambda t} \tag{1.7}$$

which gives λ as the solutions of

$$\lambda^2 - \gamma\lambda(f_u + g_v) + \gamma^2(f_u g_v - f_v g_u) = 0 \tag{1.8}$$

namely

$$2\lambda = \gamma(f_u + g_v) \pm \gamma\sqrt{(f_u + g_v)^2 - 4(f_u g_v - f_v g_u)}. \tag{1.9}$$

The steady state $\underline{w}$=0 is linearly stable if and only if $\underline{w} \to 0$ as $t \to \infty$ which will only occur if both roots of (1.9) have $\Re(\lambda) < 0$. This gives the conditions for the steady state to be stable in the absence of diffusion as

$$i) \quad f_u + g_v < 0 \qquad ii) \quad \det M = f_u g_v - f_v g_u > 0. \tag{1.10}$$

Now consider the full system (1.2), substitute for $\underline{w}$ and linearise about $\underline{w}$=0 to obtain

$$\underline{w}_t = \gamma M \underline{w} + D\nabla^2 \underline{w} \tag{1.11}$$

where

$$D = \left(\begin{array}{cc} 1 & 0 \\ 0 & d \end{array} \right).$$

To solve (1.11) we define $\underline{X}$ to be the time independent solution of the eigenvalue problem

$$\nabla^2 \underline{X} + k^2 \underline{X} = 0 \tag{1.12}$$

where k is the eigenvalue and $\underline{X}$ satisfies the relevant boundary conditions of the problem. We let $\underline{X}_k$ be the eigenfunction satisfying the eigenvalue problem (1.12) for each specific k. Each eigenfunction satisfies the boundary conditions so we look for solutions of the form

$$\underline{w} = \sum_k p_k \underline{X}_k e^{\lambda t} \tag{1.13}$$

where the p_k are determined from a Fourier expansion of the initial conditions. Substituting this expression in (1.11) gives

$$\lambda \underline{X}_k = \gamma M \underline{X}_k - D k^2 \underline{X}_k \quad \text{for each } k. \tag{1.14}$$

This gives the dispersion relation $\lambda(k^2)$ as the solution of the following equation

$$\lambda^2 + \lambda[-\gamma(f_u + g_v) + k^2(1+d)] + H(k^2) = 0 \tag{1.15}$$

where

$$H(k^2) = dk^4 - \gamma(df_u + g_v)k^2 + \gamma^2 \det M. \tag{1.16}$$

The dispersion relation is thus

$$2\lambda(k^2) = \gamma(f_u + g_v) - k^2(1+d) \pm \sqrt{(-\gamma(f_u + g_v) + k^2(1+d))^2 - 4H(k^2)}. \tag{1.17}$$

For diffusion driven instability we require $\Re(\lambda(k^2)) > 0$ for some values of $k^2 \neq 0$ so that the contribution of at least one eigenfunction grows with

time. Relations (1.10) tell us that $f_u + g_v < 0$ so for instability we require $H(k^2) < 0$ for some k^2. As $\det M > 0$ from (1.10) a necessary condition for this to occur is therefore

$$iii) \quad df_u + g_v > 0, \quad d \neq 1. \tag{1.18}$$

Figure 1.1 shows the effect of increasing d on the values of $H(k^2)$ and $\lambda(k^2)$. As we can see $H(k^2)$ becomes negative for a range of values $k^2 > 0$ when the diffusion ratio d exceeds the critical value. For this range of k^2 the larger eigenvalue $\lambda(k^2)$ becomes positive and so these wavenumbers are unstable and hence pattern will form (*i.e.* $H(k^2)$ decreases as d increases and $\lambda(k^2)$ increases). We also need the condition that the minimum of $H(k^2) < 0$. From (1.16) we obtain

$$\frac{\partial H}{\partial k^2} = 2dk^2 - \gamma(df_u + g_v) \tag{1.19}$$

so the minimum value occurs at

$$k^2 = \frac{\gamma(df_u + g_v)}{2d} \tag{1.20}$$

giving

$$H_{min} = \gamma^2 \left[\det M - \frac{(df_u + g_v)^2}{4d} \right]. \tag{1.21}$$

This leads to a fourth condition for Turing instability, namely

$$iv) \quad (df_u + g_v)^2 - 4d \det M > 0. \tag{1.22}$$

We now have four inequalities which define a region in the $(a_1, a_2, ...a_n, d)$ parameter space where diffusion driven instability is possible where $a_1, a_2, ...a_n$

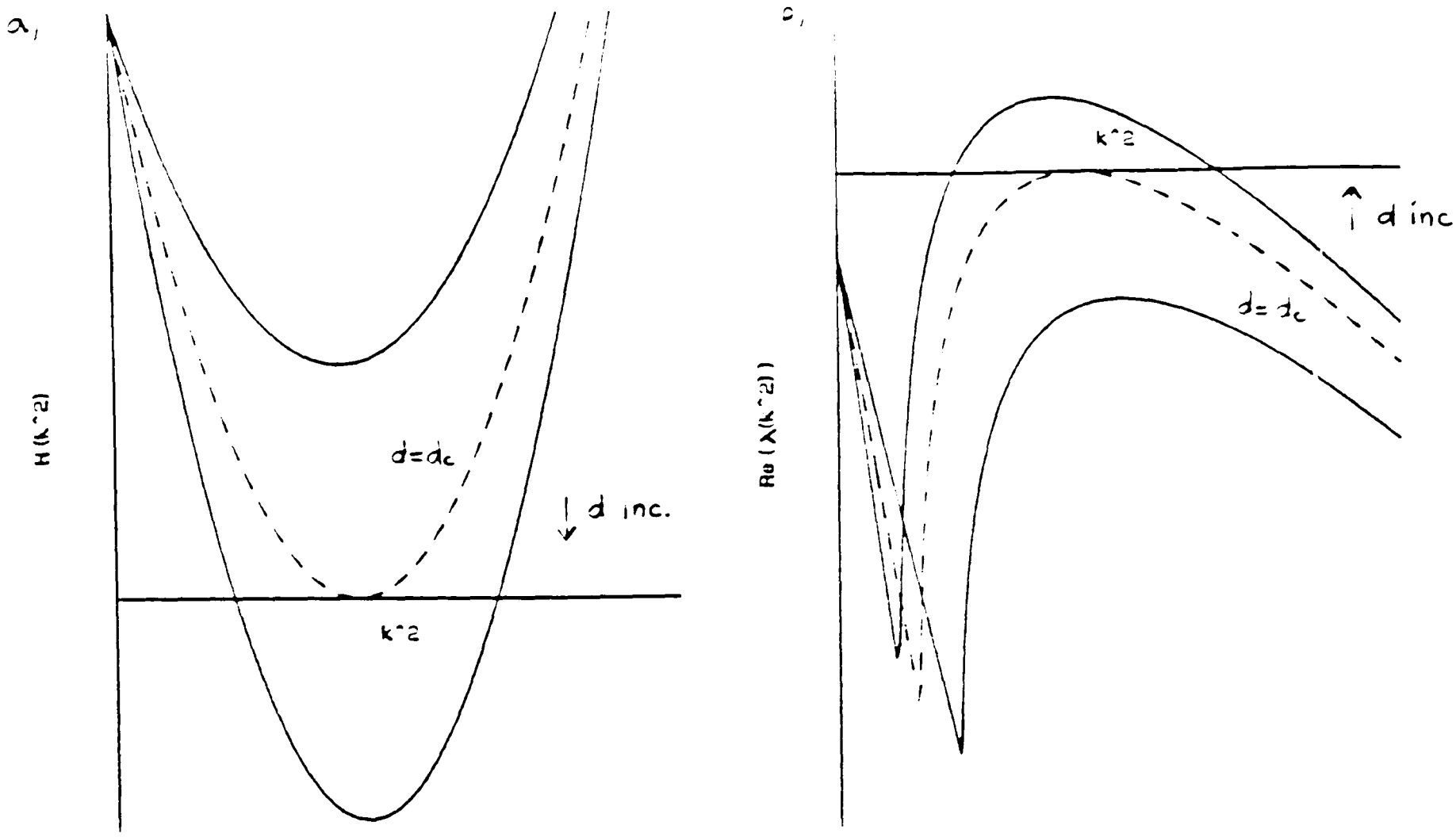

Figure 1.1: a) Plot of $H(k^2)$ defined in (1.16) drawn for the Schnackenberg kinetics. b) Plot of the real part of the larger eigenvalue $\lambda(k^2)$ defined in (1.17) also drawn for the same kinetics. In both cases the dotted curve has $d = d_c$.

are the parameters in the reaction terms f, g. We call this region the Turing space (Murray (1982)). Note that (1.10) and (1.18) imply that f_u and g_v must have different signs. If $f_u > 0$ then we require $d > 1$ while if $f_u < 0$ we require $d < 1$. At the bifurcation point we have $H_{min} = 0$ and so

$$(d_c f_u + g_v)^2 = 4 d_c \det M. \tag{1.23}$$

Taking the case where $f_u > 0$ this determines the critical diffusion coefficient $d_c > 1$, the minimum value of d necessary for pattern formation, to be the larger of the two roots of

$$d_c^2 f_u^2 + 2(2 f_v g_u - f_u g_v) d_c + g_v^2 = 0 \tag{1.24}$$

which gives

$$d_c = \frac{-(2f_v g_u - f_u g_v) \pm \sqrt{(2f_v g_u - f_u g_v)^2 - f_u^2 g_v^2}}{f_u^2} \tag{1.25}$$

and thus the critical wavenumber at bifurcation, k_c, is given by

$$k_c^2 = \frac{\gamma(d_c f_u + g_v)}{2d_c} = \gamma \left[\frac{f_u g_v - f_v g_u}{d_c} \right]^{\frac{1}{2}}. \tag{1.26}$$

The range of unstable wavenumbers $k_1^2 < k^2 < k_2^2$ is given by the zeros of $H(k^2)$, namely

$$\begin{aligned} k_1^2 = \; & \frac{\gamma}{2d} \left[(df_u + g_v) - \sqrt{(df_u + g_v)^2 - 4d\det M} \right] \quad < k^2 \\ < \; & \frac{\gamma}{2d} \left[(df_u + g_v) + \sqrt{(df_u + g_v)^2 - 4d\det M} \right] = k_2^2. \end{aligned} \tag{1.27}$$

In (1.13) the dominant contributions come from the values of k^2 which have $\Re(\lambda(k^2)) > 0$ as all the other modes tend to zero exponentially. Thus the solution $\underline{w}$ is of the form

$$\underline{w} \sim \sum_{k_1}^{k_2} p_k \underline{X}_k e^{\lambda(k^2)t}. \tag{1.28}$$

This exponentially growing solution would become unbounded for large t and only describes $\underline{w}$ near 0. As $\underline{w}$ grows the neglected nonlinear terms $h(\underline{w}, \gamma)$ become large and eventually bound the linearly unstable modes. It can be proved (Smoller (1983)) that if there exists a confined set for the reaction kinetics then, if this set is of a certain shape (rectangular in the case of models of the form we are considering), it will also act as a confining set for the full nonlinear partial differential equations (*cf.* Section 3.7). Lara-Ochoa and Murray (1983), for example, carried out a nonlinear bifurcation analysis for d in the vicinity of d_c to show that spatially heterogeneous steady state

solutions do indeed occur. In the next section we consider a specific set of reaction kinetics and carry out the linear analysis and obtain the results for the parameter regions in graphical form.

1.3 Analysis of a Specific Mechanism.

In this section we carry out the analysis for the simple tri-molecular model of Schnackenberg (1979) which is given by the chemical reaction sequence

$$X \underset{k_1}{\overset{k_2}{\rightleftharpoons}} A \qquad B \xrightarrow{k_4} Y \qquad 2X + Y \xrightarrow{k_3} 3X. \tag{1.29}$$

Using the law of mass action we obtain

$$\begin{aligned} \frac{\partial [X]}{\partial t} &= k_1 - k_2[X] + k_3[X]^2[Y] + D_X \nabla^2 [X] \\ \frac{\partial [Y]}{\partial t} &= k_4 - k_3[X]^2[Y] + D_Y \nabla^2 [Y] \end{aligned} \tag{1.30}$$

where $[X]$,$[Y]$ represent the concentrations of chemicals X and Y respectively.

We nondimensionalise the equations by setting

$$\begin{aligned} u &= [X]\sqrt{\frac{k_3}{k_2}} \quad a = \frac{k_1}{k_2}\sqrt{\frac{k_3}{k_2}} \quad t^* = \frac{D_X t}{L} \quad \underline{x}^* = \frac{\underline{x}}{L} \\ v &= [Y]\sqrt{\frac{k_3}{k_2}} \quad b = \frac{k_4}{k_2}\sqrt{\frac{k_3}{k_2}} \quad d = \frac{D_Y}{D_X} \quad \gamma = \frac{L^2 k_2}{D_X} \end{aligned} \tag{1.31}$$

where L is a typical length, to obtain the nondimensionalised system (dropping the asterisks for notational convenience),

$$\begin{aligned} u_t = \quad & \gamma(a - u + u^2 v) + \nabla^2 u \quad = \gamma f(u,v) + \nabla^2 u \\ v_t = \quad & \gamma(b - u^2 v) + d\nabla^2 v \qquad = \gamma g(u,v) + d\nabla^2 v. \end{aligned} \tag{1.32}$$

Figure 1.2 shows a typical nullcline diagram for this system.

From the analysis carried out for a general reaction diffusion system in Section 1.2 we see that the conditions for diffusion driven instability are

$$\begin{aligned} & f_u + g_v < 0 \quad f_u g_v - f_v g_u > 0 \\ & df_u + g_v > 0 \quad (df_u + g_v)^2 - 4d\det M > 0. \end{aligned} \tag{1.33}$$

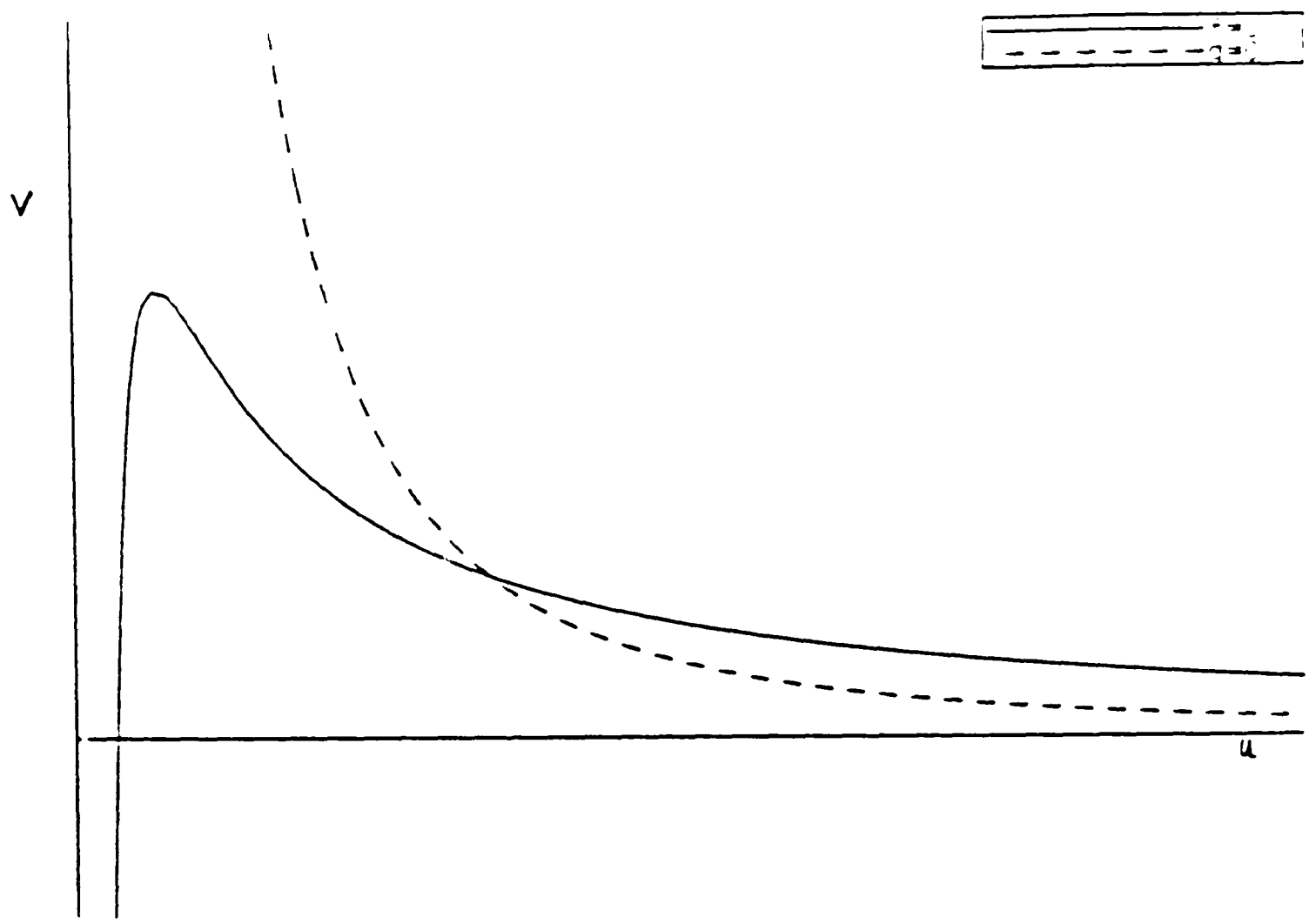

Figure 1.2: Nullcline diagram for (1.32) drawn here for $a = 0.1$ and $b = 0.9$.

For the Schnackenberg kinetics we have

$$\begin{aligned} f_u &= -1 + 2u_0v_0 \quad f_v = u_0^2 \qquad u_0 = a + b \\ g_u &= -2u_0v_0 \qquad\quad g_v = -u_0^2 \quad v_0 = \frac{b}{(a+b)^2}. \end{aligned} \tag{1.34}$$

Substituting these into (1.33) we obtain the following inequalities:

$$\begin{aligned} f_u + g_v < 0 \qquad &\Rightarrow \quad 0 < (b-a) < (b+a)^3 \\ f_u g_v - f_v g_u > 0 \qquad &\Rightarrow \quad (b+a)^2 > 0 \\ df_u + g_v > 0 \qquad &\Rightarrow \quad d(b-a) > (b+a)^3 \\ (df_u + g_v)^2 > 4d\det M \quad &\Rightarrow \quad [d(b-a) + (b+a)^3]^2 > 8db(b+a)^3. \end{aligned} \tag{1.35}$$

These define a domain in the (a, b, d) parameter space called the Turing space (see Murray (1982)). To plot the Turing space it is easier to consider a parametric representation of (1.35) in terms of the non-negative u_0. Here

$$v_0 = \frac{(u_0 - a)}{u_0^2} \qquad b = u_0 - a, \tag{1.36}$$

and the first condition now reads

$$\begin{aligned} f_u + g_v < 0 \qquad & \Rightarrow 1 - \frac{2a}{u_0} - u_0^2 < 0 \\ a > \tfrac{u_0}{2}(1 - u_0^2) \quad & b = \tfrac{u_0}{2}(1 + u_0^2). \end{aligned} \tag{1.37}$$

When these inequalities are replaced by equalities they define a boundary curve in the $a - b$ parameter space if we let u_0 take on all positive values. The other conditions in (1.35) give

$$f_u g_v - f_v g_u > 0 \quad \Rightarrow \quad u_0^2 > 0 \tag{1.38}$$

which is satisfied automatically and

$$df_u + g_v > 0 \quad \Rightarrow a < \frac{u_0}{2d}(d - u_0^2) \quad b = \frac{u_0}{2d}(d + u_0^2) \tag{1.39}$$

$$(df_u + g_v)^2 > 4d \det M \quad \Rightarrow [u_0(d - u_0^2) - 2ad]^2 > 4du_0^4. \tag{1.40}$$

The inequality (1.40) results in two curves as it is quadratic in a, namely

$$\begin{aligned} a < \tfrac{u_0}{2}\left[1 - \frac{2u_0}{\sqrt{d}} - \frac{u_0^2}{d}\right] \qquad & b = u_0 - a = \tfrac{u_0}{2}\left[1 + \frac{2u_0}{\sqrt{d}} + \frac{u_0^2}{d}\right] \\ a > \tfrac{u_0}{2}\left[1 + \frac{2u_0}{\sqrt{d}} - \frac{u_0^2}{d}\right] \qquad & b = u_0 - a = \tfrac{u_0}{2}\left[1 - \frac{2u_0}{\sqrt{d}} + \frac{u_0^2}{d}\right]. \end{aligned} \tag{1.41}$$

We now let u_0 take on a range of positive values and calculate the values of a and b for a given value of d to give the boundary curves. However, in this case, some of the curves are redundant as they are enclosed within one of the others. For the Schnackenberg kinetics $d > 1$ and hence

$$\frac{u_0}{2}\left[1 - \frac{u_0^2}{d}\right] < \frac{u_0}{2}(1 - u_0^2) < a \tag{1.42}$$

which shows that the curve defined in (1.39) lies below the curve defined in (1.37). Also as

$$\frac{u_0}{2}\left[1 - \frac{u_0^2}{d}\right] < \frac{u_0}{2}\left[1 - \frac{u_0^2}{d} + \frac{2u_0}{\sqrt{d}}\right] \tag{1.43}$$

we cannot have a domain satisfying the second of (1.41) and (1.39). This leads to two parametric curves for the Turing space, namely

$$\begin{aligned} a &> \tfrac{u_0}{2}(1-u_0^2) & b &= \tfrac{u_0}{2}(1+u_0^2) \\ a &< \tfrac{u_0}{2}\left[1-\tfrac{2u_0}{\sqrt{d}}-\tfrac{u_0^2}{d}\right] & b &= \tfrac{u_0}{2}\left[1+\tfrac{2u_0}{\sqrt{d}}+\tfrac{u_0^2}{d}\right]. \end{aligned} \tag{1.44}$$

Figure 1.3 shows the Turing space for the Schnackenberg system for several given values of d. For parameter values lying within the two appropriate boundary curves diffusion driven instability can occur. In the next section we give a few examples of numerical solutions of the Schnackenberg kinetics on a two dimensional domain and illustrate the effect that changes in the diffusion ratio d and the space parameter γ can have upon the pattern formed.

1.4 Numerical Simulations on a Rectangular Domain.

Here we solve (1.32) on a two dimensional rectangular domain A defined by $0 \leq x \leq r$, $0 \leq y \leq q$. The related eigenvalue problem (*cf.* (1.12)) is

$$\nabla^2 \underline{W} + k^2 \underline{W} = 0. \tag{1.45}$$

We take zero flux boundary conditions

$$(\underline{n}.\underline{\nabla})\underline{W} = 0 \quad \text{on} \quad \partial A \tag{1.46}$$

to demonstrate our results. The eigenfunctions are thus of the form

$$\underline{W}(x,y) = \underline{P}_k \cos\frac{n\pi x}{r}\cos\frac{m\pi y}{q} \quad \text{with} \quad k^2 = \pi^2\left(\frac{n^2}{r^2}+\frac{m^2}{q^2}\right) \tag{1.47}$$

for integers n and m. From (1.27) the linearly unstable modes are the ones satisfying

$$k_1^2 = \frac{\gamma}{2d}[L-J] < k^2 < \frac{\gamma}{2d}[L+J] = k_2^2 \tag{1.48}$$

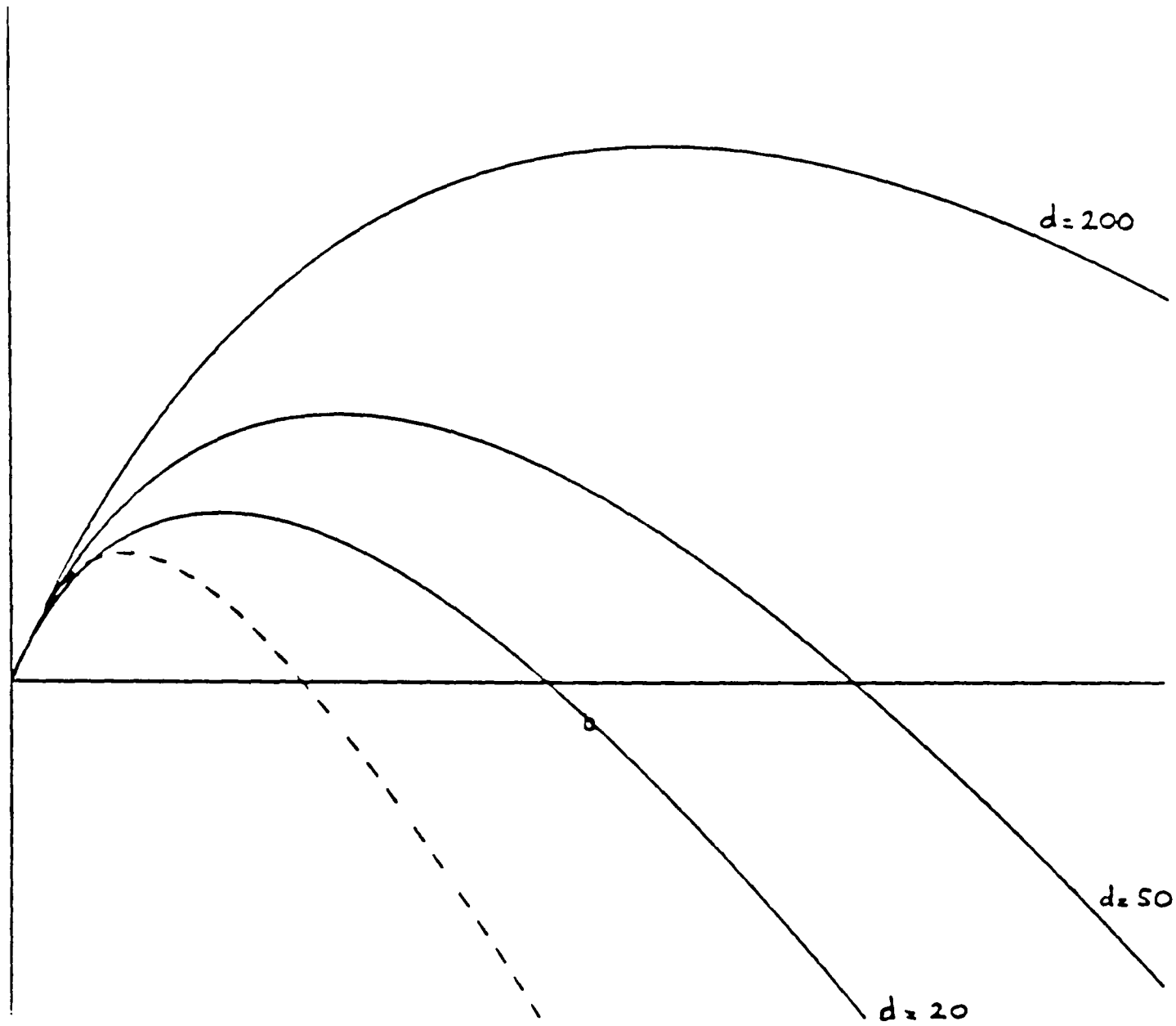

Figure 1.3: Turing space for the Schnackenberg system: $d = 20$, $d = 50$, $d = 200$. The dotted curve shows the first curve from (1.44) while the other curves show the second curve from (1.44) for the different values of d.

where

$$L = [d(b-a) - (a+b)^3] \quad J = [L^2 - 4d(a+b)]^{\frac{1}{2}}. \tag{1.49}$$

This gives the linear approximation $\underline{w}$ to the solution as

$$\underline{w}(x,y,t) = \sum_{k_1}^{k_2} \underline{P}_k e^{\lambda(k^2)t} \cos\frac{n\pi x}{r} \cos\frac{m\pi y}{q} \tag{1.50}$$

where the sum is over all the pairs n, m satisfying (1.47). If, for example, we examine the effect of varying γ upon the possible unstable modes using parameter values $a = 0.1$, $b = 0.9$ and $d = 8.8$ (just greater than d_c=8.65 for

these values) (1.47) gives

$$\frac{\gamma}{2}[0.0565] < \frac{n^2}{r^2} + \frac{m^2}{q^2} < \frac{\gamma}{2}[0.0826]. \tag{1.51}$$

Taking a domain of size 6×12 we have only one possible unstable mode for γ=2, namely n=0, m=3 whereas for γ=4 we have the modes n=1, m=4 and n=2, m=1-2 unstable. The effect of increasing γ is to increase the activity or heterogeneity of the pattern formed (see Berding (1987) for a discussion of this concept). This occurs because the curve $\Re(\lambda(k^2))$ has moved its intersections with the k^2 axis to the right as is shown in Figure 1.4a) and so higher values of n and m are possible. Increasing γ changes the fastest growing linearly unstable mode and so the resulting pattern from the nonlinear system will be quite different. Figure 1.4b) schematically shows the different patterns that can result: here the shaded regions represent concentrations of u that are greater than the steady state. The numerical simulations were carried out using a modified version of MORPHO4 developed by Dr. Leah Edelstein-Keshet.

If we vary d with γ fixed we do not find such a marked change in pattern. Taking γ=2 and d = 17.6 we find that the modes n=0, m=2-4; n=1, m=0-3 and n=2, m=0-1 to be unstable. The increased number of unstable modes occurs because the curve $\Re(\lambda(k^2))$ has been raised. Figure 1.5a) shows this effect. Here however the maximum value of the curve still occurs at approximately the same value of k^2 so the fastest growing linearly unstable mode does not alter markedly. The resulting steady state patterns are shown in Figure 1.5b).

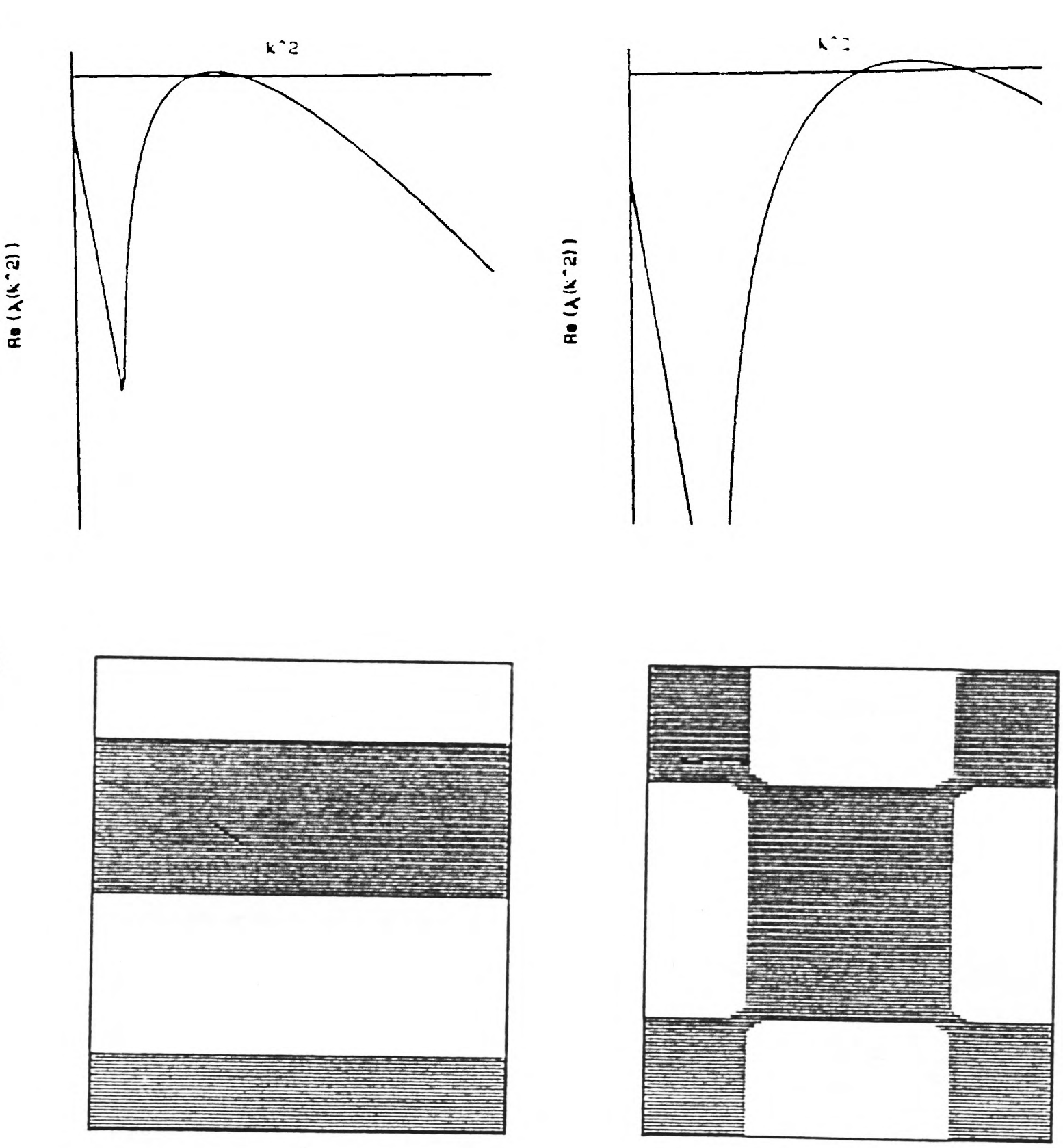

Figure 1.4: a) $\Re(\lambda(k^2))$ as defined in (1.17) for increasing values of γ. Drawn for the Schnackenberg system with parameters $a = 0.1$, $b = 0.9$, $d = 8.8$ and $\gamma = 2, 4$. b) Effect of increasing γ on the heterogeneous steady state patterns with parameters as in a).

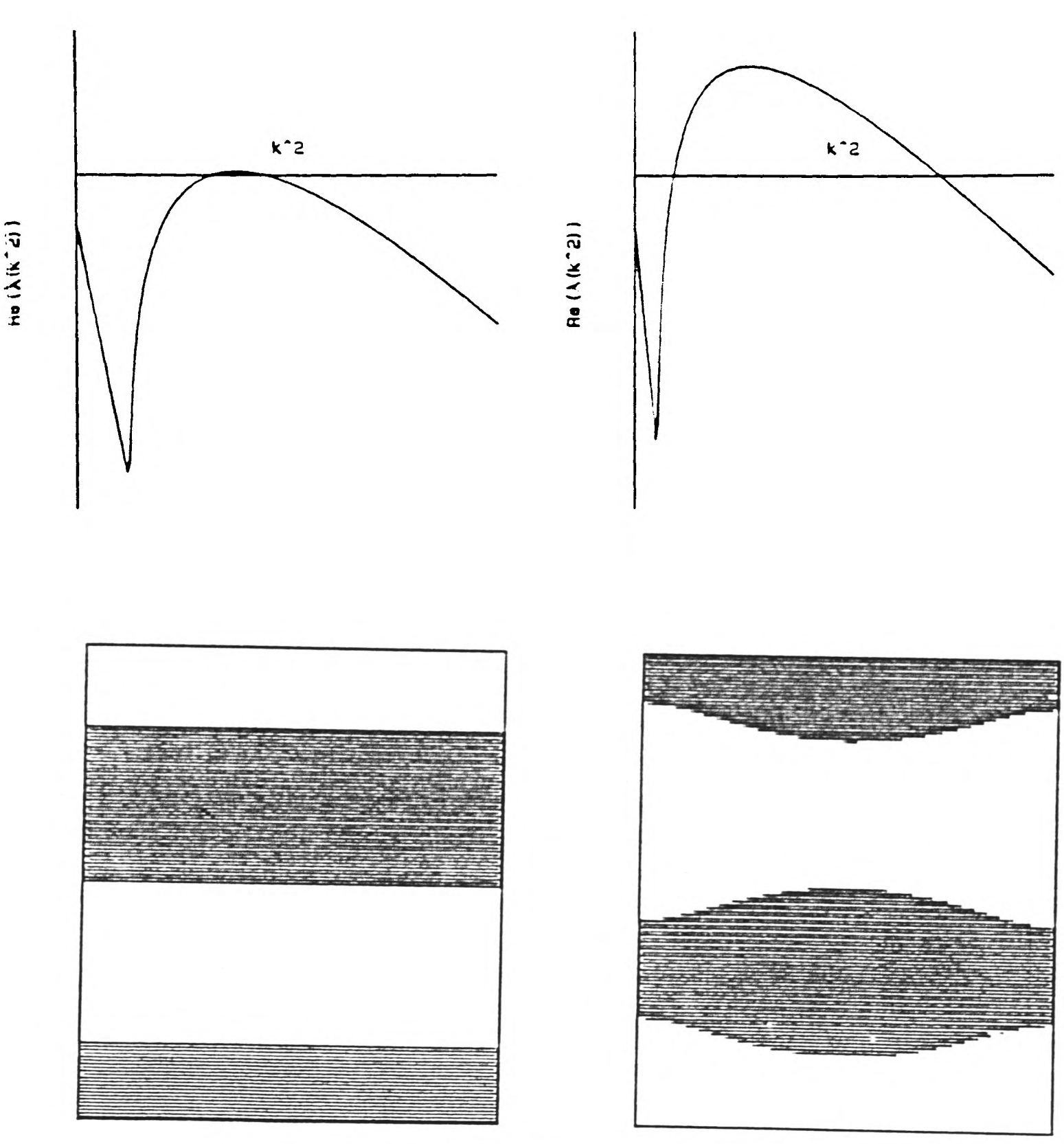

Figure 1.5: a)$\Re(\lambda(k^2))$ as defined in (1.17) for increasing values of d. Drawn for the Schnackenberg system with parameters $a = 0.1$, $b = 0.9$, $\gamma = 2$ and $d = 8.8, 17.6$. b) Effect of increasing d on heterogeneous steady state patterns with parameters as in a).

As was mentioned in Section 1.1, in two space dimensions, a linear analysis cannot fully predict the pattern that is formed. The first patterns in both Figures 1.4b) and 1.5b) can be predicted from the linear analysis as only one mode n=0, m=3 is unstable. For the second pattern in Figure 1.4b) the dominant linearly unstable mode is n=2, m=2 which is clearly the form of the final pattern formed from the nonlinear equations. However this is not the case for the second pattern in Figure 1.5b) where the dominant mode is n=1, m=2 which would imply that, on the basis of a linear analysis, the final nonlinear pattern would be similar to the one shown in Figure 1.6. The difference between the expected and the actual pattern has occured because the unstable modes interact together in a nonlinear manner which is impossible to predict by means of a linear analysis. This agrees with the findings of Arcuri and Murray (1986).

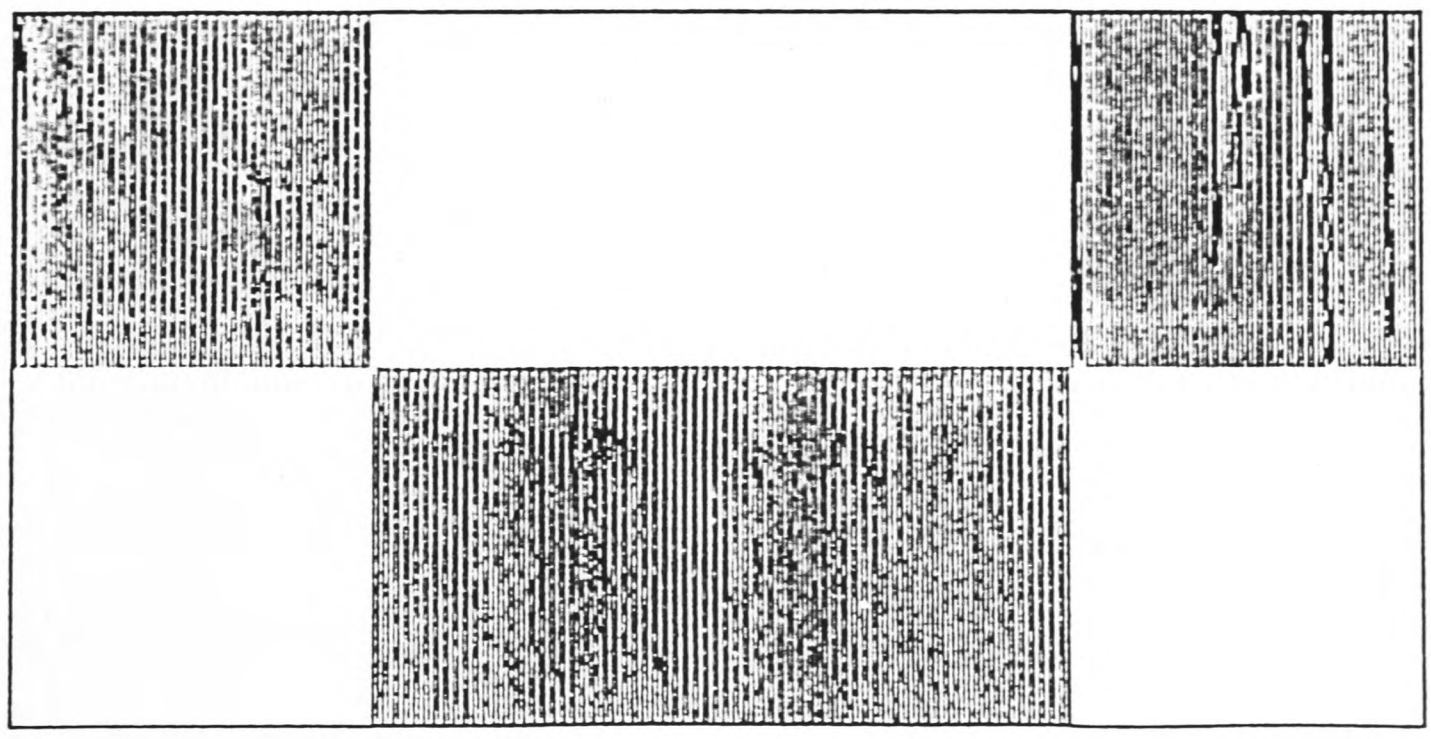

Figure 1.6: Sketch of the predicted pattern based on the fastest growing linearly unstable mode for the parameter values used in the second picture of Figure 1.5b).

In the next chapter we examine the effects of anisotropy upon the steady state patterns of reaction diffusion systems.

Chapter 2

Anisotropy in Reaction Diffusion Models.

2.1 Introduction.

In this chapter we consider reaction diffusion systems with anisotropic diffusion. This means that the diffusion coefficients in the different spatial directions are not the same and so the model potentially has a richer spectrum of patterns.

Little work has been carried out on models involving anisotropic diffusion. Anisotropy has been suggested recently (Nijhout pers. comm. to Murray) as a possible method for obtaining some of the particular patterns found on butterfly wing cells. Models with isotropic diffusion do not seem to be sufficiently flexible to explain many of these patterns.

In Section 2.2 we carry out a linear analysis of a general two dimensional reaction diffusion model with anisotropic diffusion. This gives rise to the parameter conditions necessary for diffusion driven instability and hence a non-uniform steady state pattern to occur. In Section 2.3, for parameter values satisfying these conditions, we carry out a nonlinear bifurcation analysis,

using the Schnackenberg kinetics analysed in Chapter One, for the simplest example of anisotropic diffusion. A more complex example of anisotropic diffusion giving rise to a specific type of pattern is then analysed in full in Section 2.4. Throughout the chapter we present numerical simulations of the model for the various cases analysed to support the claims made by the bifurcation analyses and to illustrate the possible finite amplitude patterns this type of model can generate.

2.2 Linear Analysis.

Consider the reaction diffusion system discussed in Section 1.2 but now with anisotropic diffusion, namely

$$\begin{aligned} u_t &= \gamma f(u,v) + d_1 u_{xx} + d_2 u_{yy} \\ v_t &= \gamma g(u,v) + d_3 v_{xx} + d_4 v_{yy}. \end{aligned} \tag{2.1}$$

We proceed as in Section 1.2. Linearising about the steady state with

$$\underline{w} = \begin{pmatrix} u-u_0 \\ v-v_0 \end{pmatrix} \qquad D_x = \begin{pmatrix} d_1 & 0 \\ 0 & d_3 \end{pmatrix} \qquad D_y = \begin{pmatrix} d_2 & 0 \\ 0 & d_4 \end{pmatrix} \tag{2.2}$$

we obtain

$$\underline{w}_t = \gamma M \underline{w} + D_x \underline{w}_{xx} + D_y \underline{w}_{yy} \tag{2.3}$$

where $M = \begin{pmatrix} f_u & f_v \\ g_u & g_v \end{pmatrix}$ is evaluated at the steady state.

We look for solutions of the form

$$\underline{w} = \exp(\lambda t + i(k_x x + k_y y)) = \exp(\lambda t + i\underline{k}.(x,y)) \tag{2.4}$$

where $\underline{k}$ is the wavenumber vector. Solutions are only possible if

$$\begin{vmatrix} \lambda - \gamma f_u + d_1 k_x^2 + d_2 k_y^2 & -\gamma f_v \\ -\gamma g_u & \lambda - \gamma g_v + d_3 k_x^2 + d_4 k_y^2 \end{vmatrix} = 0 \qquad (2.5)$$

which gives the dispersion relation $\lambda = \lambda(k_x^2, k_y^2)$ as the appropriate solution of

$$\lambda^2 + \lambda(-\gamma(f_u + g_v) + k_x^2(d_1 + d_3) + k_y^2(d_2 + d_4)) + H(k_x^2, k_y^2) = 0 \qquad (2.6)$$

where

$$\begin{aligned} H(k_x^2, k_y^2) = d_1 d_3 k_x^4 \; &+ \; (d_1 d_4 + d_2 d_3) k_x^2 k_y^2 + d_2 d_4 k_y^4 - \gamma k_x^2 (d_3 f_u + d_1 g_v) \\ &- \; \gamma k_y^2 (d_4 f_u + d_2 g_v) + \gamma^2 \det M. \end{aligned} \qquad (2.7)$$

A preliminary requirement for diffusion driven instability is that the steady state is stable in the absence of diffusion, that is, we require $\Re(\lambda) < 0$ for $k_x = k_y = 0$. In this case

$$2\lambda = \gamma(f_u + g_v) \pm \gamma\sqrt{(f_u + g_v)^2 - 4\det M}. \qquad (2.8)$$

So, as in (1.10), we obtain the conditions

$$f_u + g_v < 0 \qquad\qquad f_u g_v - f_v g_u > 0. \qquad (2.9)$$

When diffusion is included, we wish the steady state to be unstable to small perturbations, that is $\Re(\lambda) > 0$ for some non-zero $\underline{k}$. Again using the same arguments as in Chapter One we find that the necessary condition is

$$H(k_x^2, k_y^2) < 0 \qquad \text{for some} \quad k_x^2, k_y^2 \neq 0. \qquad (2.10)$$

Since H is a quadratic in k_x^2, k_y^2, consider the conic section

$$ax^2 + 2cxy + by^2 + dx + ey + f = 0. \tag{2.11}$$

This is a hyperbola if $c^2 > ab$, a parabola if $c^2 = ab$ and $\Delta \neq 0$, a degenerate line pair if $c^2 = ab$ and $\Delta = 0$ or an ellipse if $c^2 < ab$ where

$$\Delta = \begin{vmatrix} a & c & d \\ c & b & e \\ d & e & f \end{vmatrix}.$$

Considering H = constant as a conic in k_x^2, k_y^2 we have

$$c^2 - ab = \frac{(d_1 d_4 - d_2 d_3)^2}{4} \geq 0. \tag{2.12}$$

In the case of equal diffusion coefficients in different spatial directions or a constant ratio of diffusion coefficients in the different directions for the reacting substances we have $c^2 = ab$ and $\Delta = 0$ so we have a degenerate straight line pair. In all other cases we have a hyperbola. In Figure 2.1 we show the shape of the curve $H(k_x^2, k_y^2) = 0$ for the Schnackenberg system with reaction parameters $a = 0.1$ and $b = 0.9$ in the isotropic case with $d_1 = d_2 = 1$, $d_3 = d_4 = 12$ and $\gamma = 15$ and in the anisotropic case with the same parameter values except for $d_3 = 15$, $d_4 = 7$ and $\gamma = 3$.

To find the minimum point of $H(k_x^2, k_y^2)$ we consider

$$\frac{\partial H}{\partial k_x^2} = 2d_1 d_3 k_x^2 + (d_1 d_4 + d_2 d_3) k_y^2 - \gamma(d_3 f_u + d_1 g_v) = 0 \tag{2.13}$$

$$\frac{\partial H}{\partial k_y^2} = 2d_2 d_4 k_y^2 + (d_1 d_4 + d_2 d_3) k_x^2 - \gamma(d_4 f_u + d_2 g_v) = 0 \tag{2.14}$$

which gives

$$\begin{pmatrix} k_x^2 \\ k_y^2 \end{pmatrix} = \frac{-\gamma}{(d_1 d_4 + d_2 d_3)^2} \begin{pmatrix} 2d_2 d_4 & -(d_1 d_4 + d_2 d_3) \\ -(d_1 d_4 + d_2 d_3) & 2d_1 d_3 \end{pmatrix} \begin{pmatrix} d_3 f_u + d_1 g_v \\ d_4 f_u + d_2 g_v \end{pmatrix} \tag{2.15}$$

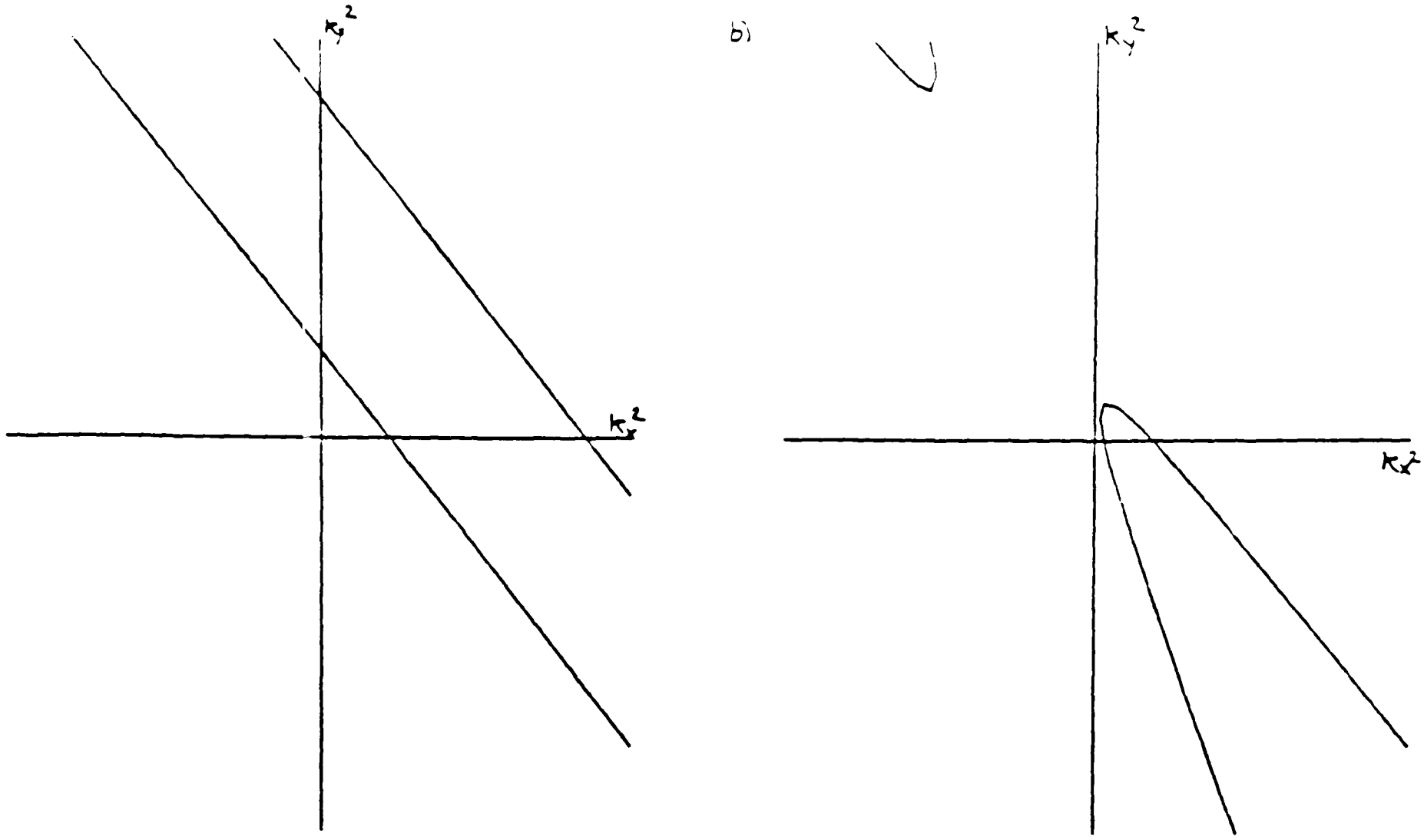

Figure 2.1: Contour diagrams showing $H(k_x^2, k_y^2) = 0$ from (2.7) for a) the isotropic case, b) the anisotropic case.

and so

$$\begin{pmatrix} k_x^2 \\ k_y^2 \end{pmatrix} = \frac{\gamma(d_1 d_4 - d_3 d_2)}{-(d_1 d_4 + d_2 d_3)^2} \begin{pmatrix} -d_4 f_u + d_2 g_v \\ d_3 f_u - d_1 g_v \end{pmatrix}. \tag{2.16}$$

Now for k_x, k_y to be real and non-zero we require

$$(d_1 d_4 - d_2 d_3) \begin{pmatrix} -d_4 f_u + d_2 g_v \\ d_3 f_u - d_1 g_v \end{pmatrix} < \begin{pmatrix} 0 \\ 0 \end{pmatrix}. \tag{2.17}$$

There are 2 cases to consider:
1) $(d_1 d_4 - d_3 d_2) > 0.$
2) $(d_1 d_4 - d_3 d_2) < 0.$

Case 1) implies

$$d_4 f_u - d_2 g_v > 0$$

$$-d_3 f_u + d_1 g_v > 0$$

$$\Rightarrow \quad (d_1 d_4 - d_2 d_3) f_u > 0 \qquad \text{and} \quad (d_1 d_4 - d_3 d_2) g_v > 0$$

$$\Rightarrow \qquad f_u > 0 \quad g_v > 0 \tag{2.18}$$

which contradicts the assumption of (2.9) that $f_u + g_v < 0$.

Case 2) implies

$$d_4 f_u - d_2 g_v < 0$$

$$-d_3 f_u + d_1 g_v < 0$$

$$\Rightarrow \quad (d_1 d_4 - d_2 d_3) f_u < 0 \qquad \text{and} \quad (d_1 d_4 - d_2 d_3) g_v < 0$$

$$\Rightarrow \qquad f_u > 0 \quad g_v > 0 \tag{2.19}$$

which also contradicts (2.9).

Thus the minimum of H does not lie in the first quadrant of the $k_x^2 - k_y^2$ plane. This implies that diffusion driven instability for models with anisotropic diffusion *must first occur on a boundary of the positive quadrant in* $k_x^2 - k_y^2$ space when the region bounded by the curve H = 0 first intersects the positive quadrant. Consider the intersection of H = 0 with $k_x^2 = 0$.

$$d_2 d_4 k_y^4 - \gamma(d_4 f_u + d_2 g_v) k_y^2 + \gamma^2 \det M = 0 \tag{2.20}$$

that is

$$k_y^2 = \frac{\gamma(d_4 f_u + d_2 g_v) \pm \gamma\sqrt{(d_4 f_u + d_2 g_v)^2 - 4 d_2 d_4 \det M}}{2 d_2 d_4}. \tag{2.21}$$

For k_y^2 to be real we require

$$(d_4 f_u + d_2 g_v)^2 > 4 d_2 d_4 \det M. \tag{2.22}$$

For k_y^2 to be positive we require

$$(d_4 f_u + d_2 g_v) > 0. \tag{2.23}$$

Similarly, considering the intersection of H = 0 with $k_y^2 = 0$ we obtain the conditions

$$(d_3 f_u + d_1 g_v)^2 > 4 d_1 d_3 \det M, \qquad (d_3 f_u + d_1 g_v) > 0. \tag{2.24}$$

However these are precisely the conditions one would obtain by considering the one dimensional problem (*cf.* (1.18))

$$\underline{w}_t = \gamma \begin{pmatrix} f(u,v) \\ g(u,v) \end{pmatrix} + D\underline{w}_{zz} \tag{2.25}$$

with

$$\text{a)} \quad D = \begin{pmatrix} d_2 & 0 \\ 0 & d_4 \end{pmatrix} \qquad \text{b)} \quad D = \begin{pmatrix} d_1 & 0 \\ 0 & d_3 \end{pmatrix}. \tag{2.26}$$

So a necessary condition for diffusion driven instability is

$$\frac{d_3}{d_1} > d_c \quad \text{and/or} \quad \frac{d_4}{d_2} > d_c \tag{2.27}$$

where d_c is the critical value of d given by

$$d_c = \frac{-(2 f_v g_u - f_u g_v) + \sqrt{(2 f_v g_u - f_u g_v)^2 - f_u^2 g_v^2}}{f_u^2} \tag{2.28}$$

as found in Section 1.3.

When these conditions are satisfied there exists a region in the positive quadrant of $k_x^2 - k_y^2$ space where H < 0. This region always has an axis as part of its boundary. Increasing the ratio of either $\frac{d_3}{d_1}$ or $\frac{d_4}{d_2}$, holding the other fixed, leads to an increase in the area of the region enclosed and so to the possibility of more modes being unstable when the system is solved on a finite domain. Figure 2.2 shows the contour values (measured in 100's) of H. The parameter values used for the Schnackenberg system are $a = 0.1$,

$b = 0.9$, $d_1 = d_2 = 1$, $\gamma = 10$ and a) $d_3 = 6$, $d_4 = 4$; b) $d_3 = 10$, $d_4 = 4$; c) $d_3 = 20$, $d_4 = 4$; d) $d_3 = 4$, $d_4 = 6$; e) $d_3 = 4$, $d_4 = 10$; f) $d_3 = 4$, $d_4 = 20$.

Note 1: Intersection of $H(k_x^2, k_y^2)$ with $k_x = 0$ only, does not necessarily imply that the pattern formed by such a mechanism when solved on a two dimensional rectangular domain would be one dimensional as two dimensional modes can also be unstable. Figure 2.3 illustrates this for the Schnackenberg system using the same parameters as in Figure 2.2 b) except for $d_4 = 8.5$. The horizontal lines represent $k_y^2 = \frac{m^2\pi^2}{s^2}$ for integer values of m where s is the y length of the domain upon which the system is being considered. The vertical lines represent $k_x^2 = \frac{n^2\pi^2}{r^2}$ for integer values of n where r is the x length of the domain. For this figure we have taken $r = 6$ and $s = 12$. The intersections of the lines enclosed by the curve $H = 0$ give values of n and m which correspond to the possible unstable modes.

2.3 Nonlinear Analysis (i).

In this and the following section we consider nonlinear bifurcation analyses of the model first considered in Section 2.2 for various different cases. In this section we examine the case when only one of the ratios $\frac{d_3}{d_1}$, $\frac{d_4}{d_2}$ exceeds the critical value. In the next section we consider what types of pattern are possible when both exceed the critical value. For ease in the analysis to follow we take $\gamma = 1$, $d_1 = 1$ and use the Schnackenberg reaction kinetics.

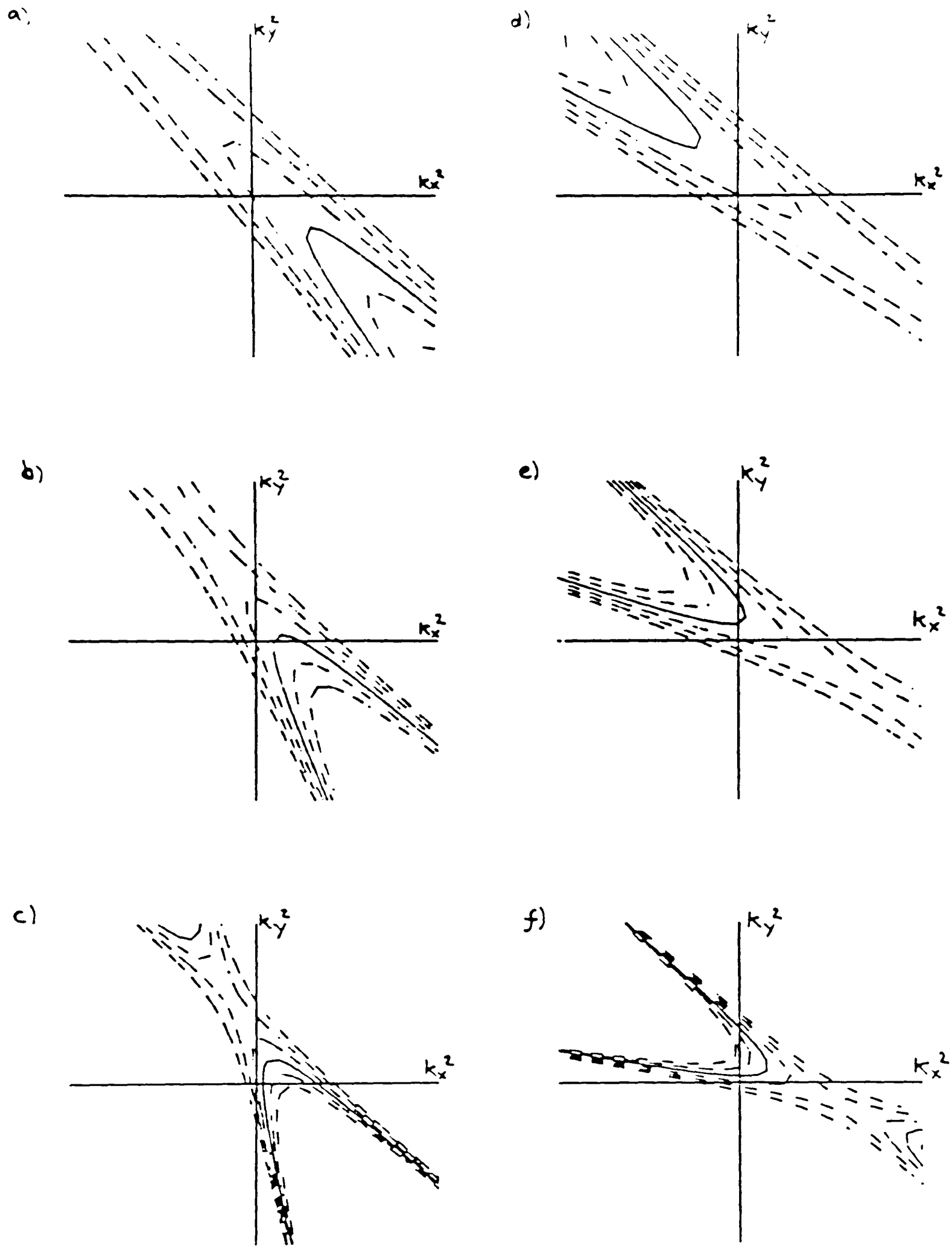

Figure 2.2: Contour diagrams showing the effect of increasing the ratios $\frac{d_3}{d_1}$ and $\frac{d_4}{d_2}$ on the areas enclosed by the curve H = 0 and the positive quadrant. The solid line shows H=0.

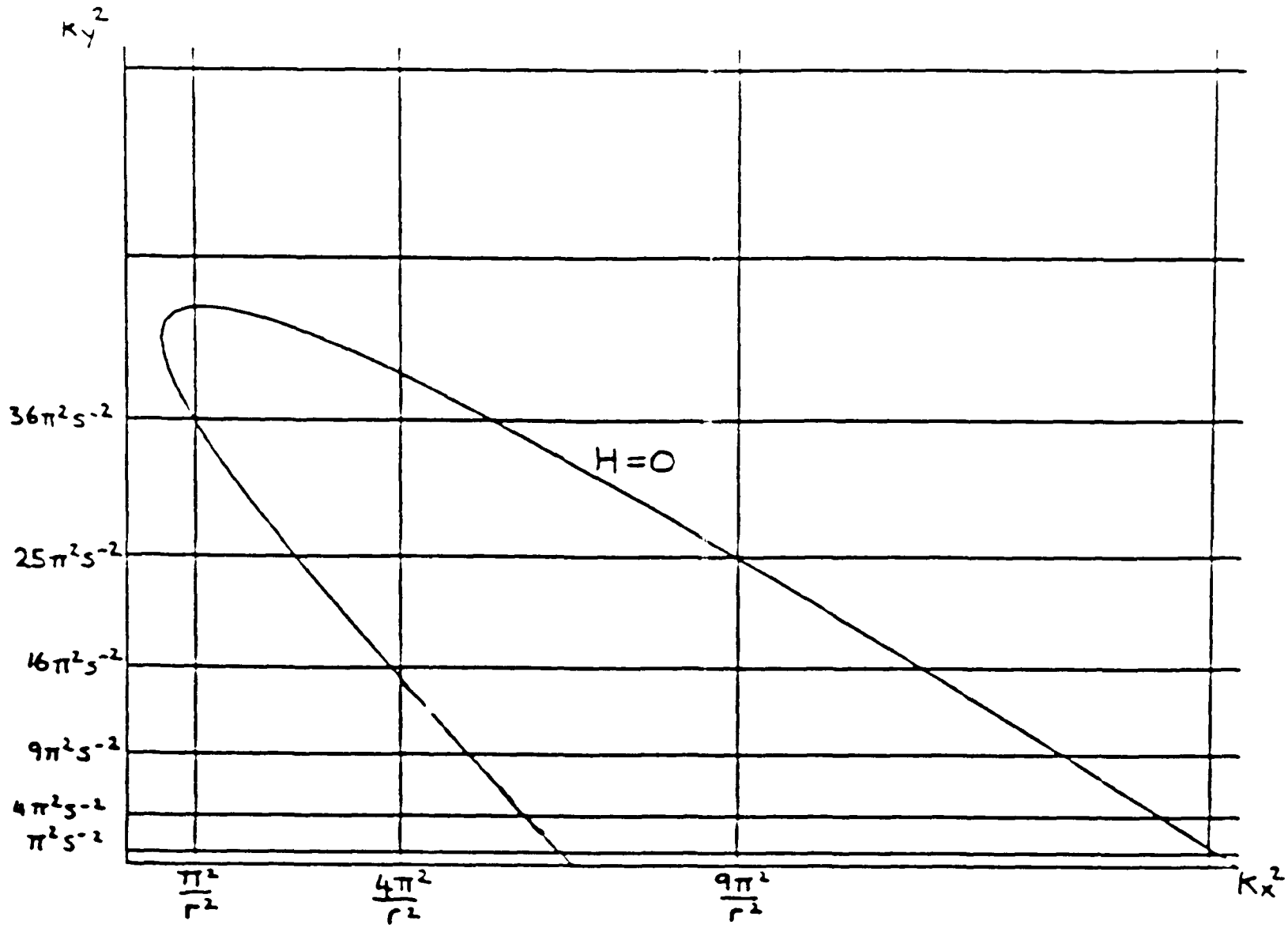

Figure 2.3: Diagram to show that 2 dimensional modes can be unstable when only one of the ratios $\frac{d_3}{d_1}, \frac{d_4}{d_2} > d_c$. The intersections of the lines in the region enclosed by the curve correspond to the unstable modes.

The specific system we consider is of the form

$$\begin{pmatrix} u \\ v \end{pmatrix}_t = \begin{pmatrix} a - u + u^2 v \\ b - u^2 v \end{pmatrix} + \begin{pmatrix} 1 & 0 \\ 0 & D \end{pmatrix} \begin{pmatrix} u \\ v \end{pmatrix}_{xx} + \begin{pmatrix} d_2 & 0 \\ 0 & d_4 \end{pmatrix} \begin{pmatrix} u \\ v \end{pmatrix}_{yy} \tag{2.29}$$

where

$$\frac{d_4}{d_2} < d_c \qquad d_c - \frac{d_4}{d_2} = O(1). \tag{2.30}$$

The problem is to calculate the bifurcation behaviour for D in the vicinity of d_c. We use a multi-scale perturbation procedure. Let D be close to d_c and define a small parameter ϵ $(0 < \epsilon \ll 1)$ by

$$D = d_c + \epsilon^2 \tag{2.31}$$

where we have chosen ϵ^2 rather than ϵ for algebraic simplicity in what follows. Define a slow time variable τ and a fast time t^* by

$$\tau = \epsilon^2 t \qquad\qquad t^* = t. \tag{2.32}$$

For $0 < (D - d_c) \ll 1$ the surface $H(k_x^2, k_y^2)$ only just crosses the plane H = 0 at $k_x^2 = p^2$ and $k_y^2 = O(\epsilon)$.

We look for solutions of the form

$$\underline{u} = \underline{u}_0 + \sum_j \epsilon^j \underline{u}_j(x, \epsilon y, \tau, t^*) \tag{2.33}$$

where we have chosen x and ϵy rather than ϵx and y because only the diffusion ratio in the x direction is greater than the critical value so it seems likely that patterns in the x direction will be dominant with respect to patterns in the y direction. In the nonlinear analysis there are essentially three time regions:

$0 \leq t^*$	:	evolution from initial conditions.
$\tau = O(1)$	:	nonlinear effects.
$\tau \to \infty$	:	steady state.

Expanding $\underline{F}(\underline{a}, \underline{u}) = \begin{pmatrix} a - u + u^2 v \\ b - u^2 v \end{pmatrix}$ in a Taylor series to $O(\epsilon^3)$ on using (2.33) we obtain

$$\begin{aligned} \underline{F}(\underline{a}, \underline{u}) &= \underline{F}(\underline{a}, \underline{u}_0) + \epsilon M \underline{u}_1 + \epsilon^2 (M \underline{u}_2 + \frac{1}{2} u_1^2 \underline{F}_{uu} + u_1 v_1 \underline{F}_{uv} + \frac{1}{2} v_1^2 \underline{F}_{vv}) \\ &+ \epsilon^3 (M \underline{u}_3 + u_1 u_2 \underline{F}_{uu} + (u_1 v_2 + u_2 v_1) \underline{F}_{uv} + v_1 v_2 \underline{F}_{vv} \\ &+ \frac{1}{6} u_1^3 \underline{F}_{uuu} + \frac{1}{2} u_1^2 v_1 \underline{F}_{uuv} + \frac{1}{2} u_1 v_1^2 \underline{F}_{uvv} + \frac{1}{6} v_1^3 \underline{F}_{vvv}) + O(\epsilon^4) \end{aligned} \tag{2.34}$$

where all the partial derivatives are evaluated at $\underline{u}_0$. In this particular case,

using the Schnackenberg kinetics, we have

$$\underline{F}_{uu} = \begin{pmatrix} 2v_0 \\ -2v_0 \end{pmatrix} \quad \underline{F}_{uv} = \begin{pmatrix} 2u_0 \\ -2u_0 \end{pmatrix} \quad \underline{F}_{vv} = \begin{pmatrix} 0 \\ 0 \end{pmatrix} \quad \underline{F}_{uuv} = \begin{pmatrix} 2 \\ -2 \end{pmatrix} \tag{2.35}$$

and all the remaining third derivatives are identically zero. Now set

$$z = \epsilon y \quad \Rightarrow \underline{u}_{yy} = \epsilon^2 \underline{u}_{zz} \quad \text{and note that} \quad \frac{\partial}{\partial t} = \frac{\partial}{\partial t^*} + \epsilon^2 \frac{\partial}{\partial \tau}. \tag{2.36}$$

From now on we replace t^* by t for notational convenience. Equating powers of ϵ in (2.29) leads to

$$O(1) \qquad 0 = \underline{F}(\underline{a}, \underline{u}_0) \tag{2.37}$$

$$O(\epsilon) \qquad \frac{\partial \underline{u}_1}{\partial t} = L\underline{u}_1 \tag{2.38}$$

$$O(\epsilon^2) \qquad \frac{\partial \underline{u}_2}{\partial t} = L\underline{u}_2 + u_1 v_1 \underline{F}_{uv} + \frac{1}{2} u_1^2 \underline{F}_{uu} \tag{2.39}$$

$$O(\epsilon^3) \qquad \frac{\partial \underline{u}_3}{\partial t} = L\underline{u}_3 + u_1 u_2 \underline{F}_{uu} + (u_1 v_2 + u_2 v_1)\underline{F}_{uv} + \frac{1}{2} u_1^2 v_1 \underline{F}_{uuv}$$

$$- \frac{\partial \underline{u}_1}{\partial \tau} + \begin{pmatrix} 0 & 0 \\ 0 & 1 \end{pmatrix} (\underline{u}_1)_{xx} + \begin{pmatrix} d_2 & 0 \\ 0 & d_4 \end{pmatrix} (\underline{u}_1)_{zz} \tag{2.40}$$

where

$$L = M + \begin{pmatrix} 1 & 0 \\ 0 & d_c \end{pmatrix} \frac{\partial^2}{\partial x^2}. \tag{2.41}$$

Equation (2.37) simply states that $\underline{u}_0$ is the solution of the steady state problem. The general solution of (2.38), the linearised form of the problem neglecting diffusion in the y direction, is

$$\underline{u}_1(x, z, \tau, t) = \int_k e^{\lambda_k^+ t} \begin{pmatrix} 1 \\ M_k^+ \end{pmatrix} (c_k^+(\tau, z)\cos(kx) + d_k^+(\tau, z)\sin(kx))$$

$$+ \int_k e^{\lambda_k^- t} \begin{pmatrix} 1 \\ M_k^- \end{pmatrix} (c_k^-(\tau, z)\cos(kx) + d_k^-(\tau, z)\sin(kx)) \tag{2.42}$$

where

$$\lambda_k^+, \lambda_k^- \quad \text{are the eigenvalues of} \quad M - k^2 \begin{pmatrix} 1 & 0 \\ 0 & d_c \end{pmatrix} = N_k \tag{2.43}$$

with corresponding eigenvectors $\begin{pmatrix} 1 \\ M_k^+ \end{pmatrix}, \begin{pmatrix} 1 \\ M_k^- \end{pmatrix}$.

At the onset of diffusion driven instability we have $\lambda_p^+ = 0$ for some p while $\Re(\lambda_k^+) < 0$ for $k \neq p$ and $\Re(\lambda_k^-) < 0$ for all k. Thus for t large

$$\underline{u}_1 \sim \begin{pmatrix} 1 \\ M_p^+ \end{pmatrix} (c_p^+(\tau, z)\cos(px) + d_p^+(\tau, z)\sin(px)) \quad + e.d. \tag{2.44}$$

where $e.d.$ denotes exponentially decreasing terms.

Now from Section 1.2 the critical mode is given by

$$p^2 = \frac{d_c f_u + g_v}{2d_c}. \tag{2.45}$$

Since $\lambda_p^+ = 0$ we obtain

$$M_p^+ = \frac{p^2 - f_u}{f_v} = \frac{g_u}{d_c p^2 - g_v}. \tag{2.46}$$

Substituting for $\underline{u}_1$ in (2.39) gives

$$\frac{\partial \underline{u}_2}{\partial t} - L\underline{u}_2 = (v_0 + 2u_0 M_p^+)(c_p \cos(px) + d_p \sin(px))^2 \begin{pmatrix} 1 \\ -1 \end{pmatrix}. \tag{2.47}$$

[As $t \to \infty$ the effects of the exponentially decreasing terms can be neglected. In (2.42) the right hand side is the integral of terms of the form $\exp(\mu t)\sin(kx)\underline{c}$ and $\exp(\mu t)\cos(kx)\ \underline{c}$ where $\Re(\mu) < 0$ and $\underline{c}$ is a constant vector. As the equation is linear each term can be treated separately. Consider the terms with $\Re(\mu) < 0$:

$$-\frac{\partial \underline{u}}{\partial t} + L\underline{u} = e^{\mu t}\sin(kx)\underline{c}. \tag{2.48}$$

Suppose $\mu \neq \lambda_n^{\pm}$ where $\lambda_n^{\pm}$ are the eigenvalues of N_n defined in (2.43). The solution of (2.48) in this case is

$$\underline{u} = e^{\mu t} \sin(kx)\underline{v} \tag{2.49}$$

where

$$(N_n - \mu I)\underline{v} = \underline{c} \tag{2.50}$$

and the solution itself is exponentially decreasing, so the effects of the exponentially decreasing terms can be ignored as $t \to \infty$. If $\mu = \lambda_n^{\pm}$ then the same result is obtained after using the Fredholm Alternative: see Baldwin (1984) for full details.]

The solution of (2.47) is

$$\underline{u}_2 = \int_k e^{\lambda_k^{\pm}} \begin{pmatrix} 1 \\ M_k^{\pm} \end{pmatrix} (\overline{c}_k^{\pm} \cos(kx) + \overline{d}_k^{\pm} \sin(kx)) - \underline{u}^* \tag{2.51}$$

where

$$L\underline{u}^* = (v_0 + 2u_0 M_p^+)(c_p^+ \cos(px) + d_p^+ \sin(px))^2 \begin{pmatrix} 1 \\ -1 \end{pmatrix}. \tag{2.52}$$

Now

$$(c_p \cos(px) + d_p \sin(px))^2 = \frac{1}{2}(c_p^2 + d_p^2) + c_p d_p \sin(2px) + \frac{1}{2}(c_p^2 - d_p^2)\cos(2px) \tag{2.53}$$

so no secular terms appear in (2.51). Let

$$r = v_0 + 2u_0 M_p \qquad \text{and} \qquad \underline{u}^* = \underline{w}_1 + \sin(2px)\underline{w}_2 + \cos(2px)\underline{w}_3. \tag{2.54}$$

Substituting for $\underline{u}^*$ in (2.52) gives

$$M\underline{w}_1 = \frac{r}{2}(c_p^2 + d_p^2) \begin{pmatrix} 1 \\ -1 \end{pmatrix} \qquad N_{2p}\underline{w}_2 = r c_p d_p \begin{pmatrix} 1 \\ -1 \end{pmatrix}$$

$$N_{2p}\underline{w}_3 = \frac{r}{2}(c_p^2 - d_p^2) \begin{pmatrix} 1 \\ -1 \end{pmatrix} \tag{2.55}$$

where N_{2p} is defined by (2.43). Letting

$$\Delta = \det M \qquad\qquad \Delta_2 = \det N_{2p} \tag{2.56}$$

we solve for $\underline{w}_i$ to give

$$\begin{aligned}
\underline{w}_1 &= \frac{r(c_p^2 + d_p^2)}{2\Delta} \begin{pmatrix} f_v + g_v \\ -f_u - g_u \end{pmatrix} \\
\underline{w}_2 &= \frac{r c_p d_p}{\Delta_2} \begin{pmatrix} f_v + g_v - 4p^2 d_c \\ -f_u - g_u + 4p^2 \end{pmatrix} \\
\underline{w}_3 &= \frac{r(c_p^2 - d_p^2)}{2\Delta_2} \begin{pmatrix} f_v + g_v - 4p^2 d_c \\ -f_u - g_u + 4p^2 \end{pmatrix} .
\end{aligned} \tag{2.57}$$

So the full solution of (2.47) as t $\to \infty$ is

$$\underline{u}_2 = -\underline{w}_1 - \sin(2px)\underline{w}_2 - \cos(2px)\underline{w}_3 + (\overline{c}_p(\tau, z)\cos(px) + \overline{d}_p(\tau, z)\sin(px)) \begin{pmatrix} 1 \\ M_p^+ \end{pmatrix} . \tag{2.58}$$

Now consider (2.40), which is of the form

$$\frac{\partial \underline{u}_3}{\partial t} - L\underline{u}_3 = \underline{J}(\underline{u}_1, \underline{u}_2) \tag{2.59}$$

where

$$\begin{aligned}
\underline{J}(\underline{u}_1, \underline{u}_2) = \; & -\frac{\partial \underline{u}_1}{\partial \tau} + \begin{pmatrix} 0 & 0 \\ 0 & 1 \end{pmatrix} (\underline{u}_1)_{xx} + \begin{pmatrix} d_2 & 0 \\ 0 & d_4 \end{pmatrix} (\underline{u}_1)_{zz} \\
+ \; & u_1 u_2 \underline{F}_{uu} + (u_1 v_2 + u_2 v_1)\underline{F}_{uv} + \tfrac{1}{2} u_1^2 v_1 \underline{F}_{uuv} \quad .
\end{aligned} \tag{2.60}$$

Secular terms can occur at this stage. They are suppressed (using the Fredholm Alternative) by making $\underline{J}$ orthogonal to the bounded solutions of the homogeneous adjoint equation

$$\frac{\partial \underline{u}}{\partial t} + \left(M^T + \begin{pmatrix} 1 & 0 \\ 0 & d_c \end{pmatrix} \frac{\partial^2}{\partial x^2} \right) \underline{u} = 0 \tag{2.61}$$

with inner product defined by

$$\underline{u}.\underline{v} = \lim_{T_1 \to \infty} \frac{1}{T_1} \int_0^{T_1} \int_0^{2\pi/p} \underline{u}^T \underline{v} dx dt. \tag{2.62}$$

The only two bounded solutions of (2.61) are

$$\underline{\varphi}_1 = \begin{pmatrix} 1 \\ S_p \end{pmatrix} \sin(px) \qquad \underline{\varphi}_2 = \begin{pmatrix} 1 \\ S_p \end{pmatrix} \cos(px) \tag{2.63}$$

where

$$\left(M^T - p^2 \begin{pmatrix} 1 & 0 \\ 0 & d_c \end{pmatrix} \right) \begin{pmatrix} 1 \\ S_p \end{pmatrix} = 0 \tag{2.64}$$

which gives

$$S_p = \frac{p^2 - f_u}{g_u} = \frac{f_v}{d_c p^2 - g_v}. \tag{2.65}$$

In the calculation of the inner product, terms of the form $\sin^2(px), \cos^2(px)$ and $\sin(px)\cos(px)$ in $\underline{J}$ do not contribute. Thus we need only examine the contribution to the inner product of the following terms in $\underline{u}_2$

$$\begin{aligned} u_2 &= \alpha_2(c_p^2 + d_p^2) + \alpha_3 c_p d_p \sin(2px) + \frac{\alpha_3}{2}(c_p^2 - d_p^2)\cos(2px) \\ v_2 &= \beta_2(c_p^2 + d_p^2) + \beta_3 c_p d_p \sin(2px) + \frac{\beta_3}{2}(c_p^2 - d_p^2)\cos(2px) \end{aligned} \tag{2.66}$$

where

$$\begin{aligned} \alpha_2 &= \frac{-r(f_v + g_v)}{2\Delta} & \alpha_3 &= \frac{-r(f_v + g_v - 4p^2 d_c)}{\Delta_2} \\ \beta_2 &= \frac{r(f_u + g_u)}{2\Delta} & \beta_3 &= \frac{r(f_u + g_u - 4p^2)}{\Delta_2}. \end{aligned} \tag{2.67}$$

Let us consider the contribution of each term in $\underline{J}$ to the inner product $\underline{J}.\underline{\varphi}_1$.

Letting $q^2 = c_p^2 + d_p^2$ we obtain

$$\begin{array}{ll}
-\frac{\partial \underline{u}_1}{\partial \tau} & -(1+M_pS_p)\frac{\pi}{p}\frac{\partial d_p}{\partial \tau} \\
\begin{pmatrix} 0 & 0 \\ 0 & 1 \end{pmatrix}(\underline{u}_1)_{xx} & -S_pM_pd_pp^2\frac{\pi}{p} \\
\begin{pmatrix} d_2 & 0 \\ 0 & d_4 \end{pmatrix}(\underline{u}_1)_{zz} & (d_2+d_4s_pM_p)\frac{\pi}{p}\frac{\partial^2 d_p}{\partial z^2} \\
u_1u_2\underline{F}_{uu} & 2v_0(1-S_p)\frac{\pi}{p}d_pq^2(\alpha_2+\frac{\alpha_3}{4}) \\
u_1v_2\underline{F}_{uv} & 2u_0(1-S_p)\frac{\pi}{p}d_pq^2(\beta_2+\frac{\beta_3}{4}) \\
u_2v_1\underline{F}_{uv} & 2u_0M_p(1-S_p)\frac{\pi}{p}d_pq^2(\alpha_2+\frac{\alpha_3}{4}) \\
\frac{1}{2}u_1^2v_1\underline{F}_{uuv} & 2M_p(1-S_p)\frac{\pi}{p}d_pq^2\frac{3}{8}.
\end{array} \tag{2.68}$$

So

$$\underline{J}.\underline{\varphi}_1 = \frac{\pi}{p}\left[-(1+M_pS_p)\frac{\partial d_p}{\partial \tau} + (d_2+d_4S_pM_p)\frac{\partial^2 d_p}{\partial z^2} + \gamma_2 d_p q^2 + \gamma_1 d_p\right] \tag{2.69}$$

where

$$\begin{aligned}
\gamma_1 &= -S_pM_pp^2 \\
\gamma_2 &= 2(1-S_p)((v_0+u_0M_p)(\alpha_2+\frac{\alpha_3}{4}) + u_0(\beta_2+\frac{\beta_3}{4}).
\end{aligned} \tag{2.70}$$

Note 2: $\quad 1 + S_pM_p > 0$

since $\quad S_pM_p = \dfrac{p^2 - f_u}{d_cp^2 - g_v} = \dfrac{\frac{-f_u}{2} + \frac{g_v}{2d_c}}{\frac{d_cf_u}{2} - \frac{g_v}{2}} = -\dfrac{1}{d_c}$

and so $\quad 1 + S_pM_p = \dfrac{d_c - 1}{d_c} > 0 \quad$ as $\quad d_c > 1.$

Note 3: $d_2 + d_4 S_p M_p > 0$

since $d_2 + d_4 S_p M_p = d_2 - \frac{d_4}{d_c}$ but $\frac{d_4}{d_2} < d_c$

and so $d_2 + d_4 S_p M_p > 0.$

Note 4: $1 - S_p > 0$

since $1 - S_p = 1 - \frac{f_v}{d_c p^2 - g_v} = \frac{d_c p^2}{d_c p^2 + u_0^2} > 0$

as in this case $f_v = u_0^2 \qquad g_v = -u_0^2$

Note 5: $M_p < 0$

since $M_p = \frac{g_u}{d_c p^2 - g_v}$ but $g_u = -2u_0 v_0 \qquad g_v = -u_0^2$

$M_p = \frac{-2u_0 v_0}{d_c p^2 + u_0^2} < 0.$

This gives us the condition for the suppression of secular terms as

$$\gamma_4 \frac{\partial d_p}{\partial \tau} = d_p(\gamma_1 + \gamma_2 q^2) + \gamma_3 \frac{\partial^2 d_p}{\partial z^2} \tag{2.71}$$

where

$$\gamma_1 > 0 \qquad \gamma_3 = d_2 + d_4 S_p M_p > 0 \qquad \gamma_4 = 1 + S_p M_p > 0. \tag{2.72}$$

Similarly from $\underline{J}.\underline{\varphi}_2$ we obtain

$$\gamma_4 \frac{\partial c_p}{\partial \tau} = c_p(\gamma_1 + \gamma_2 q^2) + \gamma_3 \frac{\partial^2 c_p}{\partial z^2} \tag{2.73}$$

to give us the simultaneous differential equations

$$\begin{aligned} \frac{\partial c_p}{\partial \tau} &= c_p(\mu + \lambda q^2) + \delta_1 \frac{\partial^2 c_p}{\partial z^2} \\ \frac{\partial d_p}{\partial \tau} &= d_p(\mu + \lambda q^2) + \delta_1 \frac{\partial^2 d_p}{\partial z^2} \end{aligned} \tag{2.74}$$

where

$$\mu = \frac{\gamma_1}{\gamma_4} > 0 \qquad \lambda = \frac{\gamma_2}{\gamma_4} \qquad \delta_1 = \frac{\gamma_3}{\gamma_4} > 0. \tag{2.75}$$

The curve $\lambda = 0$ is shown in Figure 2.4.

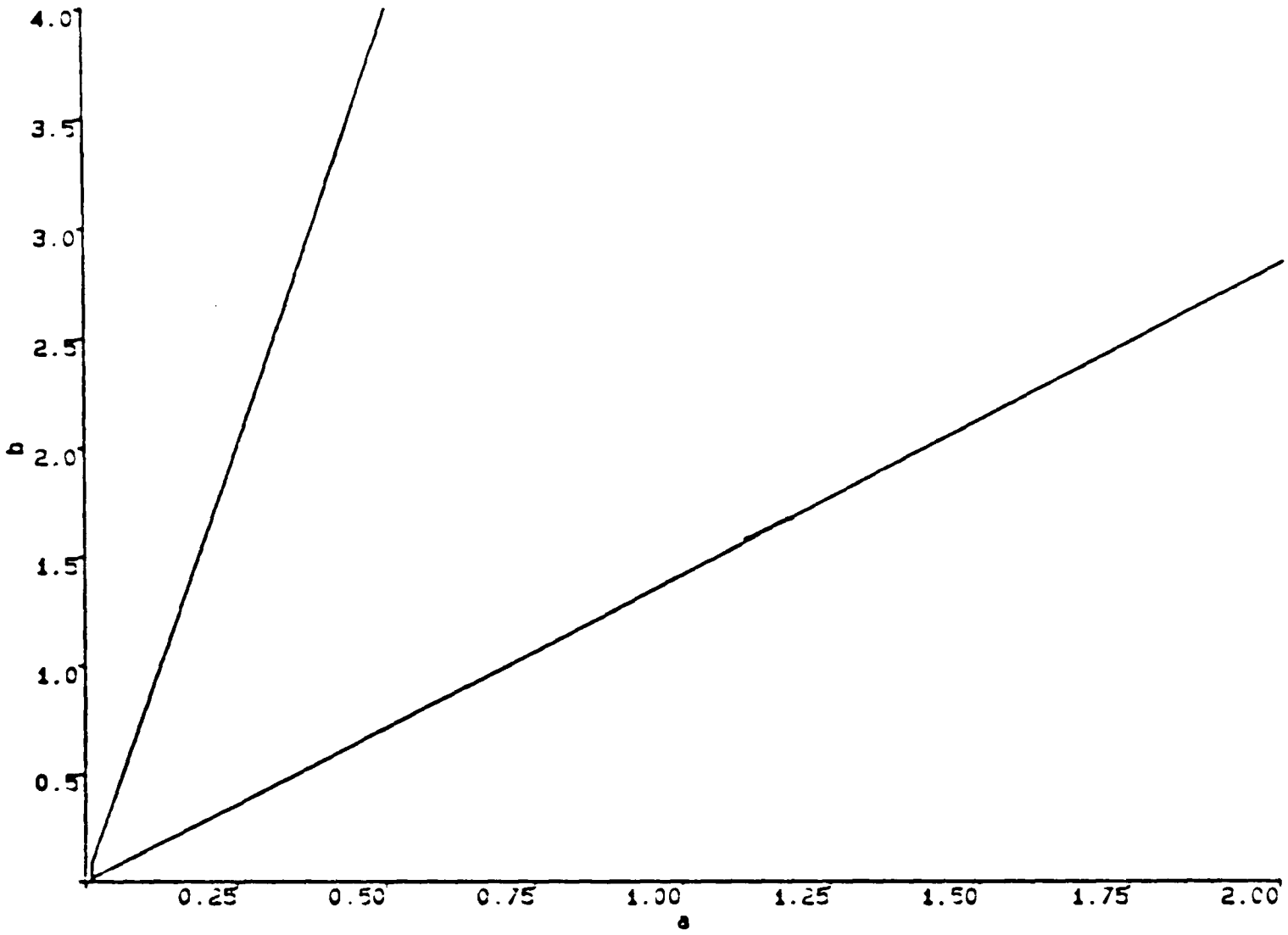

Figure 2.4: The curve $\lambda = 0$ where λ is defined by (2.70) and (2.75). The region between the curves is where $\lambda < 0$.

To solve this system we let

$$e = c_p + id_p \tag{2.76}$$

to give the single equation for the complex quantity e as

$$\frac{\partial e}{\partial \tau} = e(\mu + \lambda e\bar{e}) + \delta_1 e_{zz}. \tag{2.77}$$

We look for solutions to (2.77) of the form

$$e(\tau, z) = l_1(\tau)e^{isz} \tag{2.78}$$

which gives us the following equation for l_1

$$\frac{dl_1}{d\tau} = l_1(\lambda l_1^2 + \mu - \delta_1 s^2). \tag{2.79}$$

Figure 2.5 shows $\frac{dl_1}{d\tau}$ against l_1 for the various parameter cases a) $\mu - \delta_1 s^2 > 0$, $\lambda < 0$; b) $\mu - \delta_1 s^2 < 0$, $\lambda < 0$; c) $\mu - \delta_1 s^2 > 0$, $\lambda > 0$; d) $\mu - \delta_1 s^2 < 0$, $\lambda > 0$; leading to the conclusion that for a stable positive solution we need

$$\lambda < 0 \qquad -\sqrt{\frac{\mu}{\delta_1}} < s < \sqrt{\frac{\mu}{\delta_1}}. \tag{2.80}$$

Solving (2.79) for parameter values resulting in Figure 2.5a) gives us

$$l_1(\tau) = \left[\frac{(\mu - \delta_1 s^2) H e^{2\tau(\mu - \delta_1 s^2)}}{1 - \lambda H e^{2\tau(\mu - \delta_1 s^2)}}\right]^{1/2} \tag{2.81}$$

where H is an arbitary constant. As $\tau \to \infty$

$$l_1(\tau) \to \left(\frac{\mu - \delta_1 s^2}{-\lambda}\right)^{1/2}. \tag{2.82}$$

This tells us that as $\tau \to \infty$

$$\begin{aligned} c_p(\tau, z) &\to \int_{-\sqrt{\frac{\mu}{\delta_1}}}^{\sqrt{\frac{\mu}{\delta_1}}} \left(\frac{\mu - \delta_1 s^2}{-\lambda}\right)^{1/2} \cos(sz) ds \\ d_p(\tau, z) &\to \int_{-\sqrt{\frac{\mu}{\delta_1}}}^{\sqrt{\frac{\mu}{\delta_1}}} \left(\frac{\mu - \delta_1 s^2}{-\lambda}\right)^{1/2} \sin(sz) ds \quad = 0. \end{aligned} \tag{2.83}$$

The first integral in (2.83) cannot be evaluated analytically so we solve it numerically for a range of values of $z{=}\epsilon y$. For small values of γ, the size parameter taken to be 1 in the analysis for analytical convenience, we find that the integral is always positive so the predicted pattern will be the same as the pattern found by numerical simulation. However the numerical solution shows no y dependence at all whereas the analytical result does predict a slow

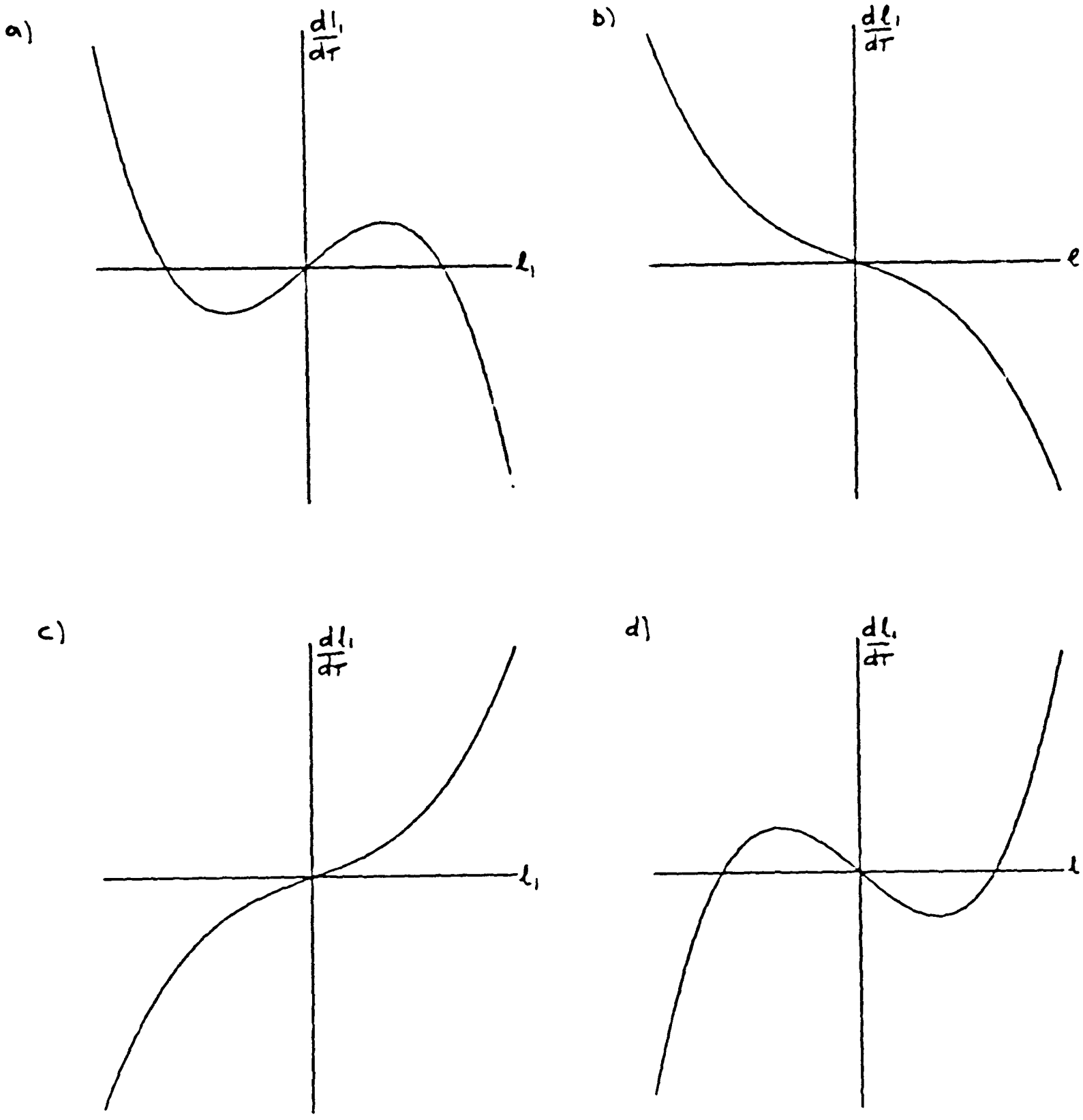

Figure 2.5: Diagram of $\frac{dl_1}{d\tau}$ vs. l_1 from (2.79)

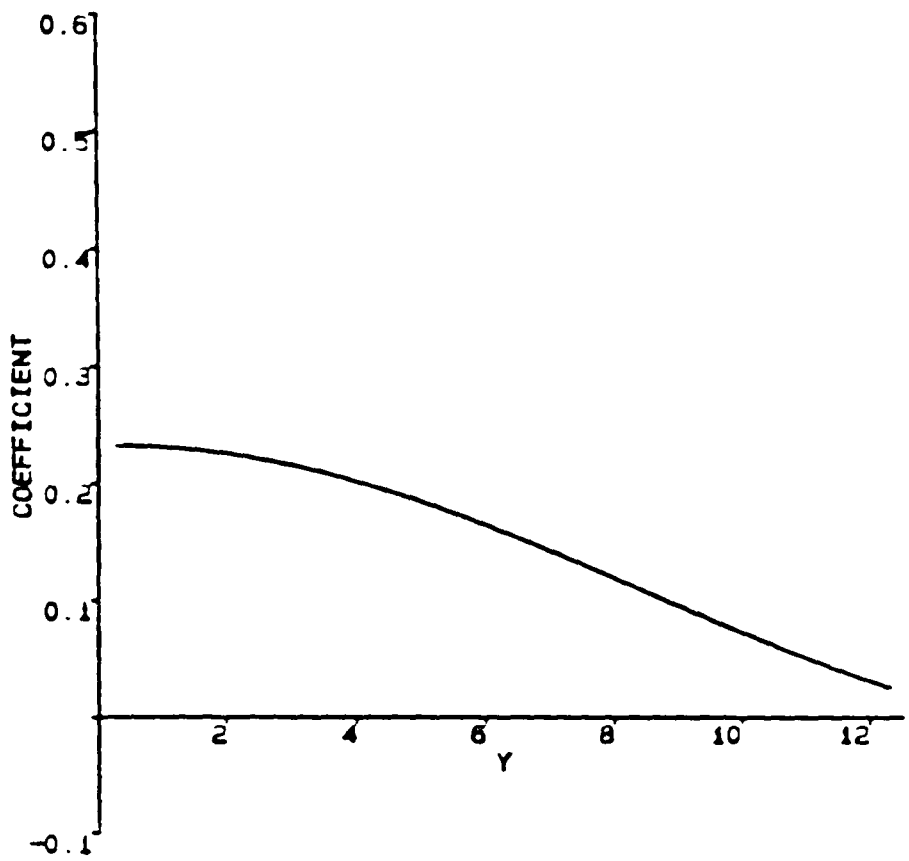

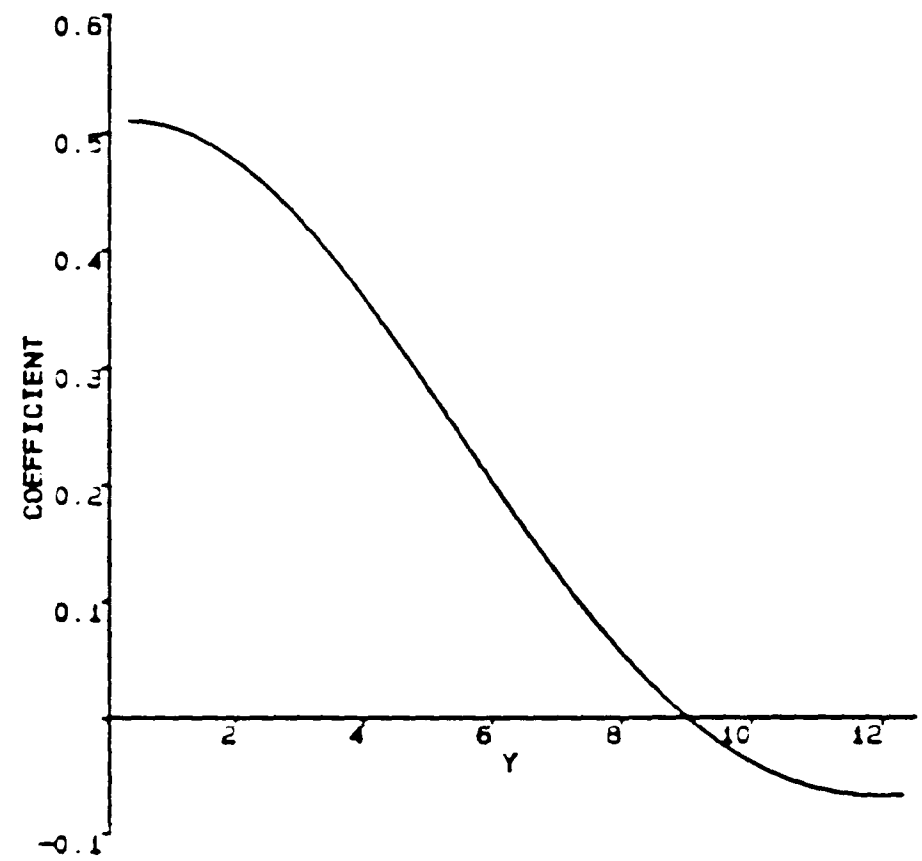

Figure 2.6: y dependence of the coefficient of $\cos(px)$ evaluated from (2.84) for the cases $D = 9$, $d_2 = 1$, a) $d_4 = 3$, $\gamma = 3$; b) $d_4 = 4$, $\gamma = 6$.

variance with respect to y. For larger values of γ, the value of the coefficient becomes negative for large enough values of y thus predicting that a fully two dimensional pattern will form. The numerical solution on the other hand is again purely one dimensional. Figure 2.6 shows the dependence of the integral (2.83) upon y for the two cases $D = 9$ $d_2 = 1$ and a) $d_4 = 3$, $\gamma = 3$; b) $d_4 = 4$, $\gamma = 6$. Figure 2.7 shows the predicted and the numerically obtained patterns for these cases.

The predicted pattern for the solution of the system as $\tau \to \infty$ (and so

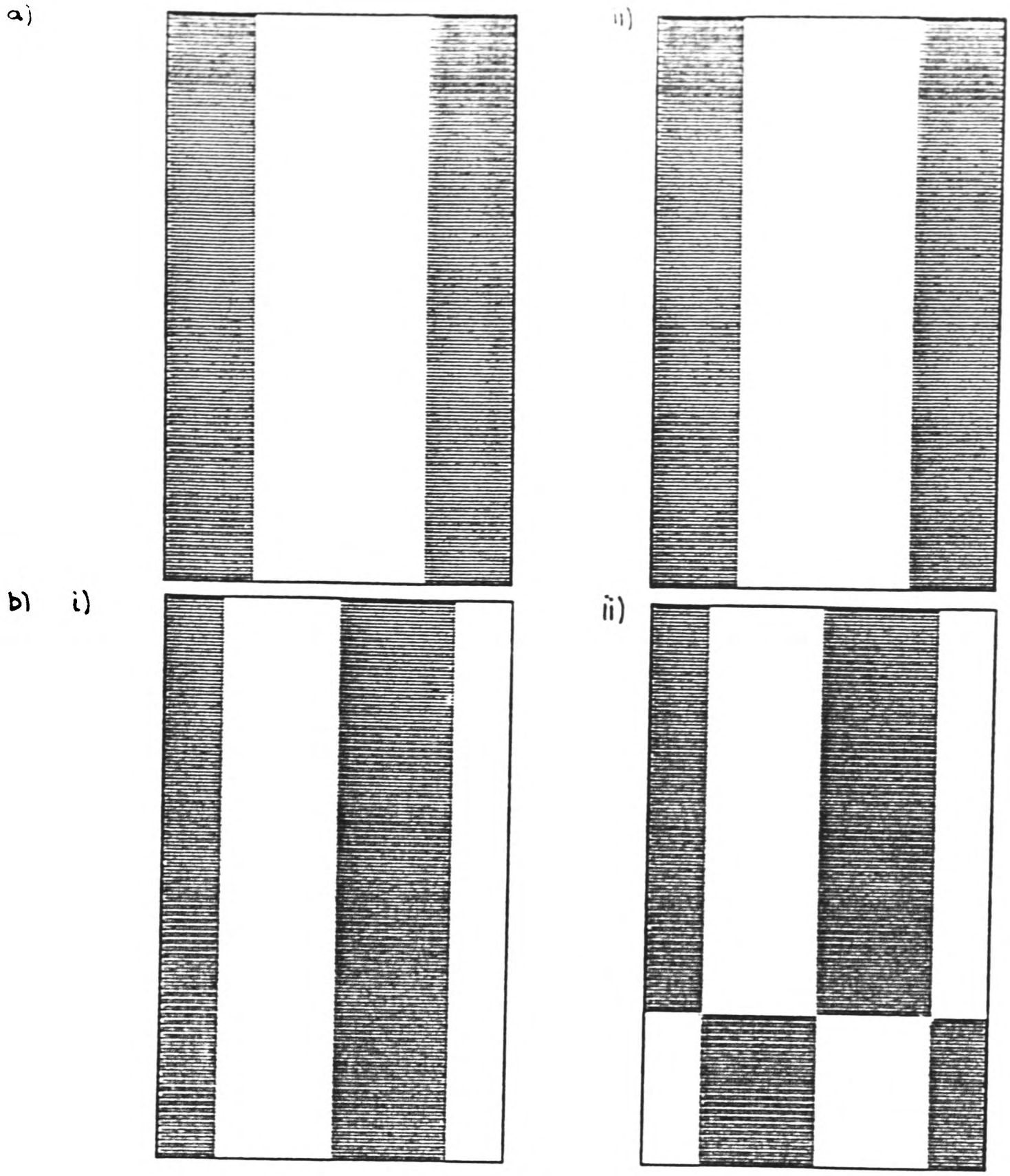

Figure 2.7: i) Numerical and ii) predicted solutions for the pattern formed using the parameter values in Figure 2.6a) and b).

$t \to \infty$) is of the form

$$\underline{u} \to \underline{u}_0 + (D - d_c)^{\frac{1}{2}} \begin{pmatrix} 1 \\ M_p \end{pmatrix} \left[\int_{-\sqrt{\frac{\mu}{\delta_1}}}^{\sqrt{\frac{\mu}{\delta_1}}} \left(\frac{\mu - \delta_1 s^2}{-\lambda} \right)^{\frac{1}{2}} \cos(\epsilon y s) ds \right] \cos(px) \tag{2.84}$$

whereas the numerical solution seems to be of the form

$$\underline{u} = \underline{u}_0 + (D - d_c)^{\frac{1}{2}} \begin{pmatrix} 1 \\ M_p \end{pmatrix} Q \cos(px) \tag{2.85}$$

for some constant Q.

Anisotropic models of the form considered in this section do not seem to

be very good at producing true two dimensional pattern. This is intuitively clear because a large ratio of diffusion coefficients in one direction will lead to this direction dominating the pattern and so a quasi one dimensional pattern will form. A mathematical explanation for this is that the shape of the curves H = constant lead to the minima of H in the positive quadrant lying on the boundary of the region and so leading to one dimensional dominant modes as opposed to the isotropic case which can lead to the minimum value of H at a truly two dimensional mode.

Patterns of this form where a stripe runs lengthways along the domain are found on certain species of snake such as the San Francisco Garter Snake (*Thamnophis sirtalis tetrataenia*). To use a rectangle with zero flux boundary conditions along the sides to model the roughly cylindrical surface of a snake is acceptable because of the unpatterned underbelly possessed by most species which can be considered as a region into which the chemical producing the pattern does not diffuse. Figure 2.8 shows a naturally occuring example of this type of pattern and a two threshold numerical pattern as comparison.

To obtain two dimensional pattern from a model with anisotropic diffusion we must consider both diffusion ratios to be greater than the critical value. This is the case we examine in the next section.

Figure 2.8: a) San Francisco Garter Snake (taken from Mehrtens (1987)). b) Two threshold numerical pattern using the same parameter values as in Figure 2.6a.

2.4 Nonlinear Analysis (ii).

In this section we consider the case when both diffusion coefficient ratios are greater than the critical value. We see that when this is the case a specific pattern is produced if certain constraints on the parameters hold. The model we study in this section is the Schnackenberg system with anisotropic diffusion in two spatial dimensions, namely

$$u_t = a_1 - u + u^2 v + u_{xx} + u_{yy}$$

$$v_t = b_1 - u^2 v + D v_{xx} + \overline{D} v_{yy}. \tag{2.86}$$

In the analysis we proceed by extending the method of Section 2.3. Let

$$D = d_c + \epsilon^2 \qquad \overline{D} = d_c + A\epsilon^2 \qquad \tau = \epsilon^2 t \qquad t^* = t \tag{2.87}$$

and look for solutions of the form

$$\underline{u} = \underline{u}_0 + \sum_j \epsilon^j \underline{u}_j(x, y, \tau, t^*). \tag{2.88}$$

Note here that the sign and magnitude of A is important. The following cases must be distinguished.

i)	$A < 0$	This is, in effect, the case considered in the preceding section.
ii)	$0 < A < 1$	This leads to dominant diffusion in the x-direction.
iii)	$A = 1$	This is the isotropic case already discussed by many others *eg.* Lara-Ochoa and Murray (1983).
iv)	$A > 1$	This leads to dominant diffusion in the y-direction.

Figure 2.9 shows the shape of $H(k_x^2, k_y^2)$ from (2.7) in these cases where $d_1 = d_2 = 1$, $d_3 = d_c + \epsilon^2$ and $d_4 = d_c + A\epsilon^2$.

Expanding $\underline{F}(\underline{a}, \underline{u}) = \begin{pmatrix} a_1 - u + u^2 v \\ b_1 - u^2 v \end{pmatrix}$ in a Taylor series to $O(\epsilon^3)$ we again obtain (2.34). Equating powers of ϵ we find the same expressions for $O(1)$, $O(\epsilon)$ and $O(\epsilon^2)$ where now

$$L = M + \begin{pmatrix} 1 & 0 \\ 0 & d_c \end{pmatrix} \nabla^2 \tag{2.89}$$

replacing the expression for L given in (2.41). The $O(\epsilon^3)$ equation is different to (2.40) and is

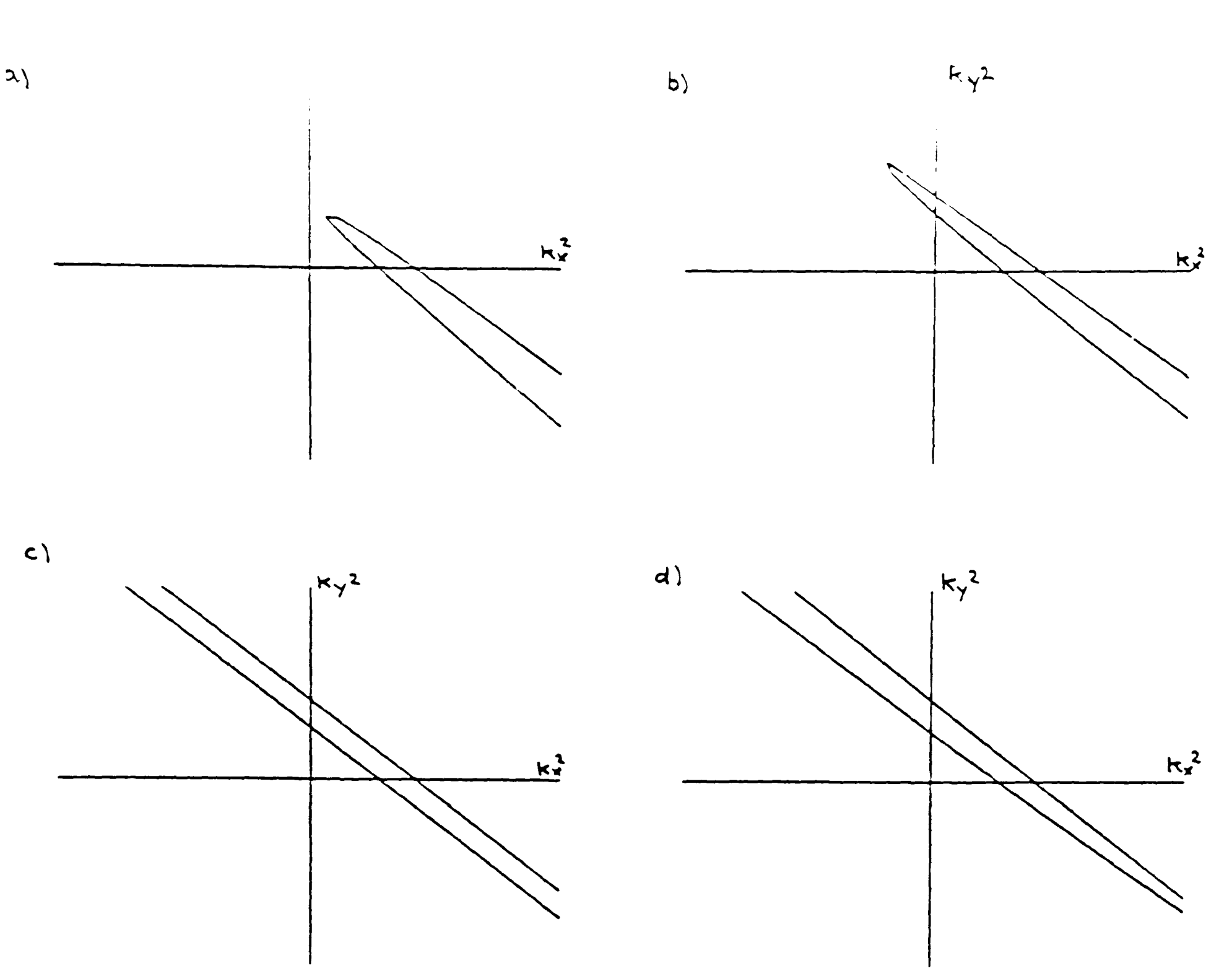

Figure 2.9: The curve $H(k_x^2, k_y^2) = 0$ as defined in (2.7) using the expressions (2.86), (2.87) for the cases i) $A < 0$, ii) $0 < A < 1$, iii) $A = 1$ and iv) $A > 1$.

$$\begin{aligned} \frac{\partial \underline{u}_3}{\partial t} &= L\underline{u}_3 + u_1 u_2 \underline{F}_{uu} + (u_1 v_2 + u_2 v_1)\underline{F}_{uv} + \frac{1}{2} u_1^2 v_1 \underline{F}_{uuv} \\ &- \frac{\partial \underline{u}_1}{\partial \tau} + \begin{pmatrix} 0 & 0 \\ 0 & 1 \end{pmatrix} (\underline{u}_1)_{xx} + \begin{pmatrix} 0 & 0 \\ 0 & A \end{pmatrix} (\underline{u}_1)_{yy}. \end{aligned} \tag{2.90}$$

The general solution of the $O(\epsilon)$ equation, which is the linearised form of the isotropic problem, namely

$$\begin{pmatrix} u_1 \\ v_1 \end{pmatrix}_t = \begin{pmatrix} f_u & f_v \\ g_u & g_v \end{pmatrix} \begin{pmatrix} u_1 \\ v_1 \end{pmatrix} + \begin{pmatrix} 1 & 0 \\ 0 & d_c \end{pmatrix} \left[\begin{pmatrix} u_1 \\ v_1 \end{pmatrix}_{xx} + \begin{pmatrix} u_1 \\ v_1 \end{pmatrix}_{yy} \right] \tag{2.91}$$

is

$$\begin{aligned}
\underline{u}_1 = \int_k e^{\lambda_k^+ t} \begin{pmatrix} 1 \\ M_k^+ \end{pmatrix} \sum_{k_x,k_y} \quad & (a_{k_x}^+(\tau)\cos k_x x + b_{k_x}^+(\tau)\sin k_x x) \\
& (c_{k_y}^+(\tau)\cos k_y y + d_{k_y}^+(\tau)\sin k_y y) \\
+ \int_k e^{\lambda_k^- t} \begin{pmatrix} 1 \\ M_k^- \end{pmatrix} \sum_{k_x,k_y} \quad & (a_{k_x}^-(\tau)\cos k_x x + b_{k_x}^-(\tau)\sin k_x x) \\
& (c_{k_y}^-(\tau)\cos k_y y + d_{k_y}^-(\tau)\sin k_y y) \qquad (2.92)
\end{aligned}$$

where

$$\sum_{k_x,k_y} \text{ is over } k_x, k_y \text{ such that } \quad k_x^2 + k_y^2 = k^2$$

and $\lambda_k^{\pm}$ are as defined in (2.43). In this analysis we aim to produce 'curved stripes' so we consider the case when the only contributions to the sum are $k_x = k, k_y = 0$ and $k_x = 0, k_y = k$. Renaming the coefficients of $\cos kx$, *etc.* using $a_k^+(\tau)c_0^+(\tau) = a_k^+(\tau)$ *etc.* the expression for $\underline{u}_1$ reduces to

$$\begin{aligned}
\underline{u}_1 \quad = \int_k e^{\lambda_k^+ t} \begin{pmatrix} 1 \\ M_k^+ \end{pmatrix} & (a_k^+(\tau)\cos kx + b_k^+(\tau)\sin kx + c_k^+(\tau)\cos ky + d_k^+(\tau)\sin ky) \\
+ \quad \int_k e^{\lambda_k^- t} \begin{pmatrix} 1 \\ M_k^- \end{pmatrix} & (a_k^-(\tau)\cos kx + b_k^-(\tau)\sin kx + c_k^-(\tau)\cos ky + d_k^-(\tau)\sin ky).
\end{aligned} \qquad (2.93)$$

At the onset of diffusion driven instability $\lambda_p^+ = 0$ for some p, $\Re(\lambda_k^+) < 0$ for $k \neq p$ and $\Re(\lambda_k^-) < 0$ for all k. So as $t \to \infty$

$$\underline{u}_1 \sim \begin{pmatrix} 1 \\ M_p^+ \end{pmatrix} (a_p(\tau)\cos(px) + b_p(\tau)\sin(px) + c_p(\tau)\cos(py) + d_p(\tau)\sin(py)). \qquad (2.94)$$

From the analysis in the preceding sections we have

$$p^2 = \frac{d_c f_u + g_v}{2d_c} \qquad \text{and} \qquad M_p^+ = \frac{p^2 - f_u}{f_v} \quad = \quad \frac{g_u}{d_c p^2 - g_v}. \qquad (2.95)$$

Substituting for $\underline{u}_1$ in (2.39), the equation for $\underline{u}_2$, gives

$$\begin{aligned}\frac{\partial \underline{u}_2}{\partial t} - L\underline{u}_2 &= u_1 v_1 \underline{F}_{uv} + \tfrac{1}{2} u_1^2 \underline{F}_{uu} \\ &= (v_0 + 2u_0 M_p^+)(a_p \cos px + b_p \sin px + c_p \cos py + d_p \sin py)^2 \begin{pmatrix} 1 \\ -1 \end{pmatrix}\end{aligned} \tag{2.96}$$

with solution

$$\begin{aligned}\underline{u}_2 = \int_k e^{\lambda_k^{\pm} t} \begin{pmatrix} 1 \\ M_k^{\pm} \end{pmatrix} \sum_{k_x, k_y} \quad & (\overline{a}_{k_x}^{\pm}(\tau) \cos k_x x + \overline{b}_{k_x}^{\pm} \sin k_x x \\ & + \overline{c}_{k_y}^{\pm} \cos k_y y + \overline{d}_{k_y}^{\pm} \sin k_y y) \quad - \underline{u}^*\end{aligned} \tag{2.97}$$

where

$$L\underline{u}^* = (v_0 + 2u_0 M_p^+)(a_p \cos(px) + b_p \sin(px) + c_p \cos(py) + d_p \sin(py))^2 \begin{pmatrix} 1 \\ -1 \end{pmatrix}. \tag{2.98}$$

Now

$$\begin{aligned}& (a_p \cos px + b_p \sin px + c_p \cos py + d_p \sin py)^2 \\ = \; & \tfrac{1}{2}(a_p^2 + b_p^2 + c_p^2 + d_p^2) + a_p b_p \sin(2px) + \tfrac{1}{2}(a_p^2 - b_p^2) \cos(2px) \\ + \; & c_p d_p \sin(2py) + \tfrac{1}{2}(c_p^2 - d_p^2) \cos(2py) + 2a_p c_p \cos(px) \cos(py) \\ + \; & 2b_p c_p \sin(px) \cos(py) + 2a_p d_p \cos(px) \sin(py) + 2b_p d_p \sin(px) \sin(py).\end{aligned} \tag{2.99}$$

Let $r = (v_0 + 2u_0 M_p^+)$ and set

$$\begin{aligned}\underline{u}^* &= \underline{w}_1 + \underline{w}_2 \sin 2px + \underline{w}_3 \cos 2px + \underline{w}_4 \sin 2py + \underline{w}_5 \cos 2py \\ &+ \underline{w}_6 \cos px \cos py + \underline{w}_7 \sin px \cos py + \underline{w}_8 \cos px \sin py \\ &+ \underline{w}_9 \sin px \sin py.\end{aligned} \tag{2.100}$$

Now let

$$\Delta = \det M \qquad \Delta_1 = \det N_{\sqrt{2}p} \qquad \Delta_2 = \det N_{2p} \tag{2.101}$$

and substitute for $\underline{u}^*$ in (2.97) to obtain

$$M\underline{w}_1 = \frac{r}{2}(a_p^2+b_p^2+c_p^2+d_p^2)\begin{pmatrix}1\\-1\end{pmatrix} \qquad \underline{w}_1 = \frac{r}{2\Delta}(a_p^2+b_p^2+c_p^2+d_p^2)\begin{pmatrix}f_v+g_v\\-f_u-g_u\end{pmatrix}$$

$$N_{2p}\underline{w}_2 = ra_pb_p\begin{pmatrix}1\\-1\end{pmatrix} \qquad \underline{w}_2 = \frac{r}{\Delta_2}a_pb_p\begin{pmatrix}f_v+g_v-4p^2d_c\\-f_u-g_u+4p^2\end{pmatrix}$$

$$N_{2p}\underline{w}_3 = \frac{r}{2}(a_p^2-b_p^2)\begin{pmatrix}1\\-1\end{pmatrix} \qquad \underline{w}_3 = \frac{r}{2\Delta_2}(a_p^2-b_p^2)\begin{pmatrix}f_v+g_v-4p^2d_c\\-f_u-g_u+4p^2\end{pmatrix}$$

$$N_{2p}\underline{w}_4 = rc_pd_p\begin{pmatrix}1\\-1\end{pmatrix} \qquad \underline{w}_4 = \frac{r}{\Delta_2}c_pd_p\begin{pmatrix}f_v+g_v-4p^2d_c\\-f_u-g_u+4p^2\end{pmatrix}$$

$$N_{2p}\underline{w}_5 = \frac{r}{2}(c_p^2-d_p^2)\begin{pmatrix}1\\-1\end{pmatrix} \qquad \underline{w}_5 = \frac{r}{2\Delta_2}(c_p^2-d_p^2)\begin{pmatrix}f_v+g_v-4p^2d_c\\-f_u-g_u+4p^2\end{pmatrix}$$

$$N_{\sqrt{2}p}\underline{w}_6 = 2ra_pc_p\begin{pmatrix}1\\-1\end{pmatrix} \qquad \underline{w}_6 = \frac{2r}{\Delta_1}a_pc_p\begin{pmatrix}f_v+g_v-2p^2d_c\\-f_u-g_u+2p^2\end{pmatrix}$$

$$N_{\sqrt{2}p}\underline{w}_7 = 2rb_pc_p\begin{pmatrix}1\\-1\end{pmatrix} \qquad \underline{w}_7 = \frac{2r}{\Delta_1}b_pc_p\begin{pmatrix}f_v+g_v-2p^2d_c\\-f_u-g_u+2p^2\end{pmatrix}$$

$$N_{\sqrt{2}p}\underline{w}_8 = 2ra_pd_p\begin{pmatrix}1\\-1\end{pmatrix} \qquad \underline{w}_8 = \frac{2r}{\Delta_1}a_pd_p\begin{pmatrix}f_v+g_v-2p^2d_c\\-f_u-g_u+2p^2\end{pmatrix}$$

$$N_{\sqrt{2}p}\underline{w}_9 = 2rb_pd_p\begin{pmatrix}1\\-1\end{pmatrix} \qquad \underline{w}_9 = \frac{2r}{\Delta_1}b_pd_p\begin{pmatrix}f_v+g_v-2p^2d_c\\-f_u-g_u+2p^2\end{pmatrix}. \tag{2.102}$$

Now for t large we obtain, by the same reasoning as above,

$$\underline{u}_2 = \begin{pmatrix}1\\M_p^+\end{pmatrix}(\overline{a}_p\cos px+\overline{b}_p\sin px+\overline{c}_p\cos py+\overline{d}_p\sin py) \tag{2.103}$$

$$- \ \underline{w}_1-\underline{w}_2\sin 2px-\underline{w}_3\cos 2px-\underline{w}_4\sin 2py-\underline{w}_5\cos 2py$$

$$- \ \underline{w}_6\cos px\cos py-\underline{w}_7\sin px\cos py-\underline{w}_8\cos px\sin py-\underline{w}_9\sin px\sin py.$$

Using the solutions $\underline{u}_1$ and $\underline{u}_2$ just calculated, we now consider the $O(\epsilon^3)$ equation, namely

$$\frac{\partial\underline{u}_3}{\partial t}-L\underline{u}_3 = -\frac{\partial\underline{u}_1}{\partial\tau}+\begin{pmatrix}0&0\\0&1\end{pmatrix}[(\underline{u}_1)_{xx}+A(\underline{u}_1)_{yy}]+u_1u_2\underline{F}_{uu}$$

$$+ \ (u_1v_2+u_2v_1)\underline{F}_{uv}+\frac{1}{2}u_1^2v_1\underline{F}_{uuv} = \underline{J}(\underline{u}_1,\underline{u}_2). \tag{2.104}$$

The general solution of this equation involves secular terms. In the usual way these are suppressed by requiring $\underline{J}(\underline{u}_1, \underline{u}_2)$ to be orthogonal to the bounded solutions of the homogeneous adjoint equation

$$\frac{\partial \underline{u}}{\partial t} + \left[M^T + \begin{pmatrix} 1 & 0 \\ 0 & d_c \end{pmatrix} \nabla^2 \right] \underline{u} = 0 \tag{2.105}$$

with inner product defined by

$$\underline{u}.\underline{v} = \lim_{T_1 \to \infty} \frac{1}{T_1} \int_0^{T_1} \int_0^{2\pi/p} \int_0^{2\pi/p} \underline{u}^T \underline{v} dx dy dt. \tag{2.106}$$

The bounded solutions of the homogeneous adjoint equation are

$$\begin{pmatrix} 1 \\ S_p \end{pmatrix} \sum (\cos k_x x + \sin k_x x)(\cos k_y y + \sin k_y y) \tag{2.107}$$

where the sum is over k_x, k_y such that $k_x^2 + k_y^2 = p^2$ and S_p is given by (2.64). The key point of this analysis is the following: as we are restricted to lie in the range of the parameter space where (2.92) only has solutions with k_x or $k_y = 0$, we can make the same restrictions on the solutions of the adjoint equation. Thus the solutions of the adjoint equation are

$$\begin{aligned} \underline{\varphi}_1 &= \begin{pmatrix} 1 \\ S_p \end{pmatrix} \cos px, & \underline{\varphi}_2 &= \begin{pmatrix} 1 \\ S_p \end{pmatrix} \sin px, \\ \underline{\varphi}_3 &= \begin{pmatrix} 1 \\ S_p \end{pmatrix} \cos py, & \underline{\varphi}_4 &= \begin{pmatrix} 1 \\ S_p \end{pmatrix} \sin py. \end{aligned} \tag{2.108}$$

Again by a similar reasoning to that in the preceding section, to calculate the inner product we need only consider terms in $\underline{u}_2$ of the form

$$\begin{aligned} \underline{u}_2 = \quad & -\underline{w}_1 - \underline{w}_2 \sin 2px - \underline{w}_3 \cos 2px - \underline{w}_4 \sin 2py - \underline{w}_5 \cos 2py \\ & -\underline{w}_6 \cos px \cos py - \underline{w}_7 \sin px \cos py - \underline{w}_8 \cos px \sin py \\ & -\underline{w}_9 \sin px \sin py. \end{aligned} \tag{2.109}$$

Consider the contributions of each term in $\underline{J}$ to the inner product $\underline{J}.\underline{\varphi}_1$: these are

$$
\begin{array}{ll}
-\dfrac{\partial \underline{u}_1}{\partial \tau} & -(1+M_pS_p)\dfrac{2\pi^2}{p^2}\dfrac{da_p}{d\tau} \\
\begin{pmatrix} 0 & 0 \\ 0 & 1 \end{pmatrix}(\underline{u}_1)_{xx} & -S_pM_p\dfrac{2\pi^2}{p^2}p^2a_p \\
\begin{pmatrix} 0 & 0 \\ 0 & A \end{pmatrix}(\underline{u}_1)_{yy} & 0 \\
u_2u_1\underline{F}_{uu} & 2v_0(1-S_p)\dfrac{2\pi^2}{p^2}a_p\left[\alpha_1(q^2+s^2)+\dfrac{\alpha_2}{4}q^2+\dfrac{\alpha_3}{2}s^2\right] \\
u_1v_2\underline{F}_{uv} & 2u_0(1-S_p)\dfrac{2\pi^2}{p^2}a_p\left[\beta_1(q^2+s^2)+\dfrac{\beta_2}{4}q^2+\dfrac{\beta_3}{2}s^2\right] \\
u_2v_1\underline{F}_{uv} & 2u_0M_p(1-S_p)\dfrac{2\pi^2}{p^2}a_p\left[\alpha_1(q^2+s^2)+\dfrac{\alpha_2}{4}q^2+\dfrac{\alpha_3}{2}s^2\right] \\
\frac{1}{2}u_1^2v_1\underline{F}_{uuv} & 2M_p(1-S_p)\dfrac{2\pi^2}{p^2}a_p\left[\dfrac{3}{8}(q^2+s^2)+\dfrac{7}{8}s^2\right]
\end{array}
\tag{2.110}
$$

where

$$q^2 = a_p^2 + b_p^2 \qquad s^2 = c_p^2 + d_p^2 \tag{2.111}$$

$$\alpha_1 = \frac{-r(f_v+g_v)}{2\Delta} \qquad \alpha_2 = \frac{-r(f_v+g_v-4p^2d_c)}{\Delta_2} \qquad \alpha_3 = \frac{-2r(f_v+g_v-2p^2d_c)}{\Delta_1}$$

$$\beta_1 = \frac{r(f_u+g_u)}{2\Delta} \qquad \beta_2 = \frac{r(f_u+g_u-4p^2)}{\Delta_2} \qquad \beta_3 = \frac{2r(f_u+g_u-2p^2)}{\Delta_1}. \tag{2.112}$$

So

$$\underline{J}.\underline{\varphi_1} = \frac{2\pi^2}{p^2}\left[-\gamma_5\frac{da_p}{d\tau}+\gamma_1a_p+\gamma_2a_p(q^2+s^2)+\gamma_3a_pq^2+\gamma_4a_ps^2\right] \tag{2.113}$$

where

$$
\begin{aligned}
\gamma_1 &= -S_pM_pp^2 \\
\gamma_2 &= 2(1-S_p)[(v_0+u_0M_p)\alpha_1+u_0\beta_1+\tfrac{3}{8}M_p] \\
\gamma_3 &= 2(1-S_p)[(v_0+u_0M_p)\tfrac{\alpha_2}{4}+u_0\tfrac{\beta_2}{4}] \\
\gamma_4 &= 2(1-S_p)[(v_0+u_0M_p)\tfrac{\alpha_3}{2}+u_0\tfrac{\beta_3}{2}+\tfrac{7}{8}M_p] \\
\gamma_5 &= 1+S_pM_p.
\end{aligned}
\tag{2.114}
$$

For $\underline{J}$ to be orthogonal to $\underline{\varphi}_1$ we require $\underline{J}.\underline{\varphi}_1 = 0$, that is

$$\gamma_5\frac{da_p}{d\tau} = [\gamma_1+(\gamma_2+\gamma_3)q^2+(\gamma_2+\gamma_4)s^2]a_p. \tag{2.115}$$

Similarly, by symmetry, we have

$$\begin{aligned}
\underline{J}.\underline{\varphi}_2 = 0 \quad &\Rightarrow \quad \gamma_5 \frac{db_p}{d\tau} = [\gamma_1 + (\gamma_2+\gamma_3)q^2 + (\gamma_2+\gamma_4)s^2]b_p \\
\underline{J}.\underline{\varphi}_3 = 0 \quad &\Rightarrow \quad \gamma_5 \frac{dc_p}{d\tau} = [A\gamma_1 + (\gamma_2+\gamma_4)q^2 + (\gamma_2+\gamma_3)s^2]c_p \\
\underline{J}.\underline{\varphi}_4 = 0 \quad &\Rightarrow \quad \gamma_5 \frac{dd_p}{d\tau} = [A\gamma_1 + (\gamma_2+\gamma_4)q^2 + (\gamma_2+\gamma_3)s^2]d_p.
\end{aligned} \tag{2.116}$$

Let

$$\lambda_1 = \frac{\gamma_2+\gamma_3}{\gamma_5} \qquad \lambda_2 = \frac{\gamma_2+\gamma_4}{\gamma_5} \qquad \mu = \frac{\gamma_1}{\gamma_5} > 0. \tag{2.117}$$

This gives four simultaneous ordinary differential equations for the four coefficients $a_p(\tau)$, *etc.* These equations cannot be solved exactly so, after reducing the system, we consider a phase plane analysis of the new system to see what values can occur as $\tau \to \infty$.

$$\begin{aligned}
\frac{da_p}{d\tau} &= [\mu + \lambda_1 q^2 + \lambda_2 s^2]a_p \\
\frac{db_p}{d\tau} &= [\mu + \lambda_1 q^2 + \lambda_2 s^2]b_p \\
\frac{dc_p}{d\tau} &= [A\mu + \lambda_2 q^2 + \lambda_1 s^2]c_p \\
\frac{dd_p}{d\tau} &= [A\mu + \lambda_2 q^2 + \lambda_1 s^2]d_p.
\end{aligned} \tag{2.118}$$

Let

$$f_1 = a_p + ib_p \qquad e_1 = c_p + id_p. \tag{2.119}$$

This gives the reduced system

$$\begin{aligned}
\frac{df_1}{d\tau} &= [\mu + \lambda_1 f_1\overline{f}_1 + \lambda_2 e_1\overline{e}_1]f_1 \\
\frac{de_1}{d\tau} &= [A\mu + \lambda_2 f_1\overline{f}_1 + \lambda_1 e_1\overline{e}_1]e_1.
\end{aligned} \tag{2.120}$$

However this system cannot be easily analysed as it stands so we set $E = e_1\overline{e}_1$, $F = f_1\overline{f}_1$. As μ, λ_1 and λ_2 are real constants we have

$$\begin{aligned}
\frac{dF}{d\tau} &= f_1\frac{d\overline{f}_1}{d\tau} + \overline{f}_1\frac{df_1}{d\tau} = 2[\mu + \lambda_1 F + \lambda_2 E]F = m(F,E) \\
\frac{dE}{d\tau} &= 2[A\mu + \lambda_2 F + \lambda_1 E]E = n(F,E).
\end{aligned} \tag{2.121}$$

Now $F = a_p^2 + b_p^2$ and $E = c_p^2 + d_p^2$ so we are only interested in the solutions (E, F) lying in the first quadrant. The steady states of (2.121) are

$$\begin{aligned} &F = 0 && E = 0 \\ &F = 0 && E = \frac{A\mu}{-\lambda_1} \\ &F = \frac{\mu}{-\lambda_1} && E = 0 \\ &F = \frac{\mu(\lambda_2 A - \lambda_1)}{\lambda_1^2 - \lambda_2^2} && E = \frac{\mu(\lambda_2 - \lambda_1 A)}{\lambda_1^2 - \lambda_2^2}. \end{aligned} \tag{2.122}$$

To consider the stability of these steady states we consider the partial derivatives

$$\begin{aligned} &m_F = 2[\mu + 2\lambda_1 F + \lambda_2 E] && m_E = 2\lambda_2 F \\ &n_F = 2\lambda_2 E && n_E = 2[A\mu + 2\lambda_1 E + \lambda_2 F]. \end{aligned} \tag{2.123}$$

$(0,0)$: $m_F = 2\mu \quad m_E = 0 \quad n_F = 0 \quad n_E = 2A\mu.$

The eigenvalues are $2\mu, \quad 2A\mu.$

The eigenvectors are $\begin{pmatrix} 1 \\ 0 \end{pmatrix} \quad \begin{pmatrix} 0 \\ 1 \end{pmatrix}.$

Now $A \neq 1$, $A > 0$ so (0,0) is an unstable node .

$\left(\frac{\mu}{-\lambda_1}, 0\right)$: This steady state exists only if $\lambda_1 < 0$. Here

$m_F = -2\mu \quad m_E = -2\mu\frac{\lambda_2}{\lambda_1} \quad n_F = 0 \quad n_E = 2\mu\left[A - \frac{\lambda_2}{\lambda_1}\right].$

Eigenvalues are $-2\mu, \quad 2\mu\left[A - \frac{\lambda_2}{\lambda_1}\right].$

Eigenvectors are $\begin{pmatrix} 1 \\ 0 \end{pmatrix}, \quad \begin{pmatrix} 1 \\ 1 - (A+1)\frac{\lambda_1}{\lambda_2} \end{pmatrix}.$

$\Rightarrow$ $\left(\frac{\mu}{-\lambda_1}, 0\right)$ is $\begin{cases} \text{a saddle point if } A\lambda_1 - \lambda_2 < 0. \\ \text{a stable node if } A\lambda_1 - \lambda_2 > 0. \end{cases}$

$\left(0, \frac{A\mu}{-\lambda_1}\right)$: This steady state exists only if $\lambda_1 < 0$. Now

$m_F = 2\mu\left[1 - A\frac{\lambda_2}{\lambda_1}\right] \quad m_E = 0 \quad n_F = -2A\mu\frac{\lambda_2}{\lambda_1} \quad n_E = -2A\mu.$

Eigenvalues are $-2A\mu, \quad 2\mu\left[1 - A\frac{\lambda_2}{\lambda_1}\right].$

Eigenvectors are $\begin{pmatrix} 0 \\ 1 \end{pmatrix} \quad \begin{pmatrix} 1 - (A+1)\frac{\lambda_1}{\lambda_2 A} \\ 1 \end{pmatrix}.$

$\Rightarrow$ $\left(0, \frac{A\mu}{-\lambda_1}\right)$ is $\begin{cases} \text{a saddle point if } \lambda_1 - \lambda_2 A < 0. \\ \text{a stable node if } \lambda_1 - \lambda_2 A > 0. \end{cases}$

$\left(\frac{\mu(\lambda_2 A - \lambda_1)}{\lambda_1^2 - \lambda_2^2}, \frac{\mu(\lambda_2 - \lambda_1 A)}{\lambda_1^2 - \lambda_2^2}\right)$:

This steady state exists only if $\lambda_2 - \lambda_1 A > 0, \quad \lambda_2 A - \lambda_1 > 0, \quad \lambda_1^2 - \lambda_2^2 > 0$ or

$\lambda_2 - \lambda_1 A < 0, \quad \lambda_2 A - \lambda_1 < 0, \quad \lambda_1^2 - \lambda_2^2 < 0$

$$m_F = \frac{2\mu\lambda_1(\lambda_2 A - \lambda_1)}{\lambda_1^2 - \lambda_2^2} \quad m_E = \frac{2\mu\lambda_2(\lambda_2 A - \lambda_1)}{\lambda_1^2 - \lambda_2^2}$$

$$n_F = \frac{2\mu\lambda_2(\lambda_2 - \lambda_1 A)}{\lambda_1^2 - \lambda_2^2)} \quad n_E = \frac{2\mu\lambda_1(\lambda_2 - \lambda_1 A)}{\lambda_1^2 - \lambda_2^2}.$$

The eigenvalues are given by

$$\sigma = \frac{(m_F + n_E) \pm \sqrt{(m_F - n_E)^2 + 4 m_E n_F}}{2}.$$

σ is real if $(m_F - n_E)^2 > -4 m_E n_F$ which is satisfied automatically if $m_E n_F > 0$.

$$m_E n_F = \frac{4\mu^2\lambda_2^2(\lambda_2 A - \lambda_1)(\lambda_2 - \lambda_1 A)}{(\lambda_1^2 - \lambda_2^2)^2} \tag{2.124}$$

so if $(\lambda_2 A - \lambda_1)(\lambda_2 - \lambda_1 A) > 0$ then σ is automatically real. That is, if the steady state exists then it has entirely real eigenvalues. Stability depends on the sign of

$$m_F n_E - m_E n_F = \frac{4\mu^2(\lambda_2 A - \lambda_1)(\lambda_2 - \lambda_1 A)}{\lambda_1^2 - \lambda_2^2} \tag{2.125}$$

and the sign of

$$m_F + n_E = \frac{2\mu\lambda_1(A+1)(\lambda_2 - \lambda_1)}{\lambda_1^2 - \lambda_2^2}. \tag{2.126}$$

$\left(\frac{\mu(\lambda_2 A - \lambda_1)}{\lambda_1^2 - \lambda_2^2}, \frac{\mu(\lambda_2 - \lambda_1 A)}{\lambda_1^2 - \lambda_2^2}\right)$ is $\begin{cases} \text{a saddle point if } \frac{(\lambda_2 A - \lambda_1)(\lambda_2 - \lambda_1 A)}{\lambda_1^2 - \lambda_2^2} < 0 \\ \text{a node if } \frac{(\lambda_2 A - \lambda_1)(\lambda_2 - \lambda_1 A)}{\lambda_1^2 - \lambda_2^2} > 0 \\ \qquad \text{stable if } \frac{\lambda_1}{\lambda_1 + \lambda_2} > 0 \\ \qquad \text{unstable if } \frac{\lambda_1}{\lambda_1 + \lambda_2} < 0 \end{cases}$

Let us now consider the various possibilities for the signs of λ_1 and λ_2:

1. $\lambda_1 > 0 \qquad \lambda_2 > 0$

   $(0,0)$ is an unstable node.

   The other steady states do not lie in the positive quadrant and as noted we are only considering this quadrant so they are not of interest.

2. $\lambda_1 > 0 \qquad \lambda_2 < 0$

   From Figure 2.10 we can see that the region $\lambda_2 < 0$ in the (a_1, b_1) parameter space lies entirely within the region $\lambda_1 < 0$ so this case is not possible.

3. $\lambda_1 < 0 \qquad \lambda_2 > 0$

   $(0,0)$ is an unstable node.

   $\left(\frac{\mu}{-\lambda_1}, 0\right)$ is a saddle point.

   $\left(0, \frac{A\mu}{-\lambda_1}\right)$ is a saddle point.

   $\left(\frac{\mu(\lambda_2 A - \lambda_1)}{\lambda_1^2 - \lambda_2^2}, \frac{\mu(\lambda_2 - \lambda_1 A)}{\lambda_1^2 - \lambda_2^2}\right)$ is $\begin{cases} \text{a stable node if } \lambda_1 + \lambda_2 < 0. \\ \text{does not 'exist' if } \lambda_1 + \lambda_2 > 0. \end{cases}$

4. $\lambda_1 < 0 \qquad \lambda_2 < 0$

   $(0,0)$ is an unstable node.

   $\left(\frac{\mu}{-\lambda_1}, 0\right)$ is $\begin{cases} \text{a stable node if} & \lambda_2 - \lambda_1 A < 0 \\ \text{a saddle point if} & \lambda_2 - \lambda_1 A > 0 \end{cases}$

   $\left(0, \frac{A\mu}{-\lambda_1}\right)$ is $\begin{cases} \text{a stable node if} & \lambda_2 A - \lambda_1 < 0 \\ \text{a saddle point if} & \lambda_2 A - \lambda_1 > 0 \end{cases}$

   $\left(\frac{\mu(\lambda_2 A - \lambda_1)}{\lambda_1^2 - \lambda_2^2}, \quad \frac{\mu(\lambda_2 - \lambda_1 A)}{\lambda_1^2 - \lambda_2^2}\right)$ is $\begin{cases} \text{a stable node if both other non-zero steady states are saddles and } \lambda_1 - \lambda_2 < 0. \\ \text{a saddle point if both other non-zero steady states are stable and } \lambda_1 - \lambda_2 > 0. \\ \text{does not exist otherwise} \end{cases}$

If we view these results relative to the regions marked on Figure 2.10 we

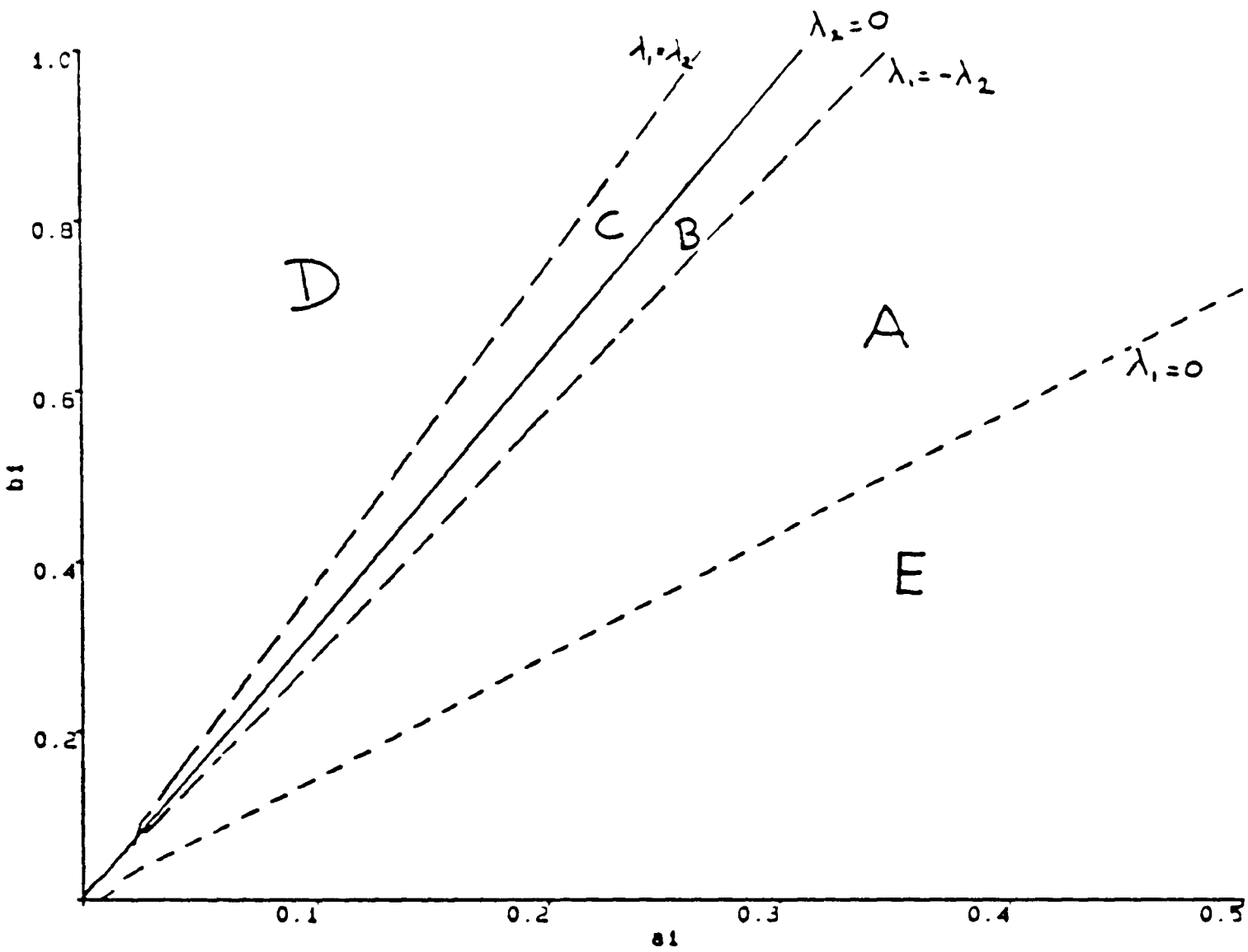

Figure 2.10: Diagram in the (a_1, b_1) parameter space showing the curves $\lambda_1 = 0$, $\lambda_2 = 0$, $\lambda_1^2 = \lambda_2^2$ from (2.114) and (2.117). ($\lambda_i < 0$ to the left of $\lambda_i = 0$)

see that in :

Region E, Only (0,0) exists so we cannot have pattern formed in this region of the parameter space.

Region A, $(0,0)$ is an unstable node, $\left(\frac{\mu}{-\lambda_1}, 0\right), \left(0, \frac{A\mu}{-\lambda_1}\right)$ are saddle points and $\left(\frac{\mu(\lambda_2 A - \lambda_1)}{\lambda_1^2 - \lambda_2^2}, \frac{\mu(\lambda_2 - \lambda_1 A)}{\lambda_1^2 - \lambda_2^2}\right)$ is not realistic.

Region B, $(0,0)$ is an unstable node, $\left(\frac{\mu}{-\lambda_1}, 0\right), \left(0, \frac{A\mu}{-\lambda_1}\right)$ are saddle points and $\left(\frac{\mu(\lambda_2 A - \lambda_1)}{\lambda_1^2 - \lambda_2^2}, \frac{\mu(\lambda_2 - \lambda_1 A)}{\lambda_1^2 - \lambda_2^2}\right)$ is a stable node.

Region C, $(0,0)$ is an unstable node,

$$\left(\frac{\mu}{-\lambda_1},0\right) \text{ is a } \begin{cases} \text{stable node if} & \lambda_2-\lambda_1 A<0 & A<\dfrac{|\lambda_2|}{|\lambda_1|} \\ \text{saddle point if} & \lambda_2-\lambda_1 A>0 & A>\dfrac{|\lambda_2|}{|\lambda_1|} \end{cases}$$

$$\left(0,\frac{A\mu}{-\lambda_1}\right) \text{ is a } \begin{cases} \text{stable node if} & \lambda_2 A-\lambda_1<0 & A>\dfrac{|\lambda_1|}{|\lambda_2|} \\ \text{saddle point if} & \lambda_2 A-\lambda_1>0 & A<\dfrac{|\lambda_1|}{|\lambda_2|} \end{cases}$$

$$\left(\frac{\mu(\lambda_2 A-\lambda_1)}{\lambda_1^2-\lambda_2^2},\frac{\mu(\lambda_2-\lambda_1 A)}{\lambda_1^2-\lambda_2^2}\right) \text{ is } \begin{cases} \text{a stable node if } \dfrac{|\lambda_2|}{|\lambda_1|}<A<\dfrac{|\lambda_1|}{|\lambda_2|} \\ \text{else it is not realistic.} \end{cases}$$

Region D,

$(0,0)$ is an unstable node.

$$\left(\frac{\mu}{-\lambda_1},0\right) \text{ is a } \begin{cases} \text{stable node if} & \lambda_2-\lambda_1 A<0 & A<\dfrac{|\lambda_2|}{|\lambda_1|} \\ \text{saddle point if} & \lambda_2-\lambda_1 A>0 & A>\dfrac{|\lambda_2|}{|\lambda_1|} \end{cases}$$

$$\left(0,\frac{A\mu}{-\lambda_1}\right) \text{ is a } \begin{cases} \text{stable node if} & \lambda_2 A-\lambda_1<0 & A>\dfrac{|\lambda_1|}{|\lambda_2|} \\ \text{saddle point if} & \lambda_2 A-\lambda_1>0 & A<\dfrac{|\lambda_1|}{|\lambda_2|} \end{cases}$$

$$\left(\frac{\mu(\lambda_2 A-\lambda_1)}{\lambda_1^2-\lambda_2^2},\frac{\mu(\lambda_2-\lambda_1 A)}{\lambda_1^2-\lambda_2^2}\right) \text{ is } \begin{cases} \text{a saddle point if } \dfrac{|\lambda_1|}{|\lambda_2|}<A<\dfrac{|\lambda_2|}{|\lambda_1|} \\ \text{else it does not exist.} \end{cases}$$

Figure 2.11 shows the phase plane diagrams for the above regions.

To obtain curved stripes we require both E and F to be non-zero. This implies that the regions of interest are B and C. In Region B

$$(F,E) \quad \rightarrow \quad \left(\frac{\mu(\lambda_2 A-\lambda_1)}{\lambda_1^2-\lambda_2^2},\frac{\mu(\lambda_2-\lambda_1 A)}{\lambda_1^2-\lambda_2^2}\right) \qquad \text{as } \tau\rightarrow\infty \qquad (2.127)$$

so the solution $\underline{u}$ tends to

$$\underline{u}_0+\begin{pmatrix} 1 \\ M_p^+ \end{pmatrix}\left(\sqrt{\frac{\mu(\lambda_2 A-\lambda_1)}{\lambda_1^2-\lambda_2^2}}\cos(px-\theta)+\sqrt{\frac{\mu(\lambda_2-\lambda_1 A)}{\lambda_1^2-\lambda_2^2}}\cos(py-\psi)\right)\epsilon+O(\epsilon^2) \qquad (2.128)$$

where θ and ψ are chosen so that

$$\begin{aligned} a_p(\tau) &\rightarrow \sqrt{\frac{\mu(\lambda_2 A-\lambda_1)}{\lambda_1^2-\lambda_2^2}}\cos\theta \qquad & b_p(\tau) &\rightarrow \sqrt{\frac{\mu(\lambda_2 A-\lambda_1)}{\lambda_1^2-\lambda_2^2}}\sin\theta \\ c_p(\tau) &\rightarrow \sqrt{\frac{\mu(\lambda_2-\lambda_1 A)}{\lambda_1^2-\lambda_2^2}}\cos\psi \qquad & d_p(\tau) &\rightarrow \sqrt{\frac{\mu(\lambda_2-\lambda_1 A)}{\lambda_1^2-\lambda_2^2}}\sin\psi \end{aligned} \qquad (2.129)$$

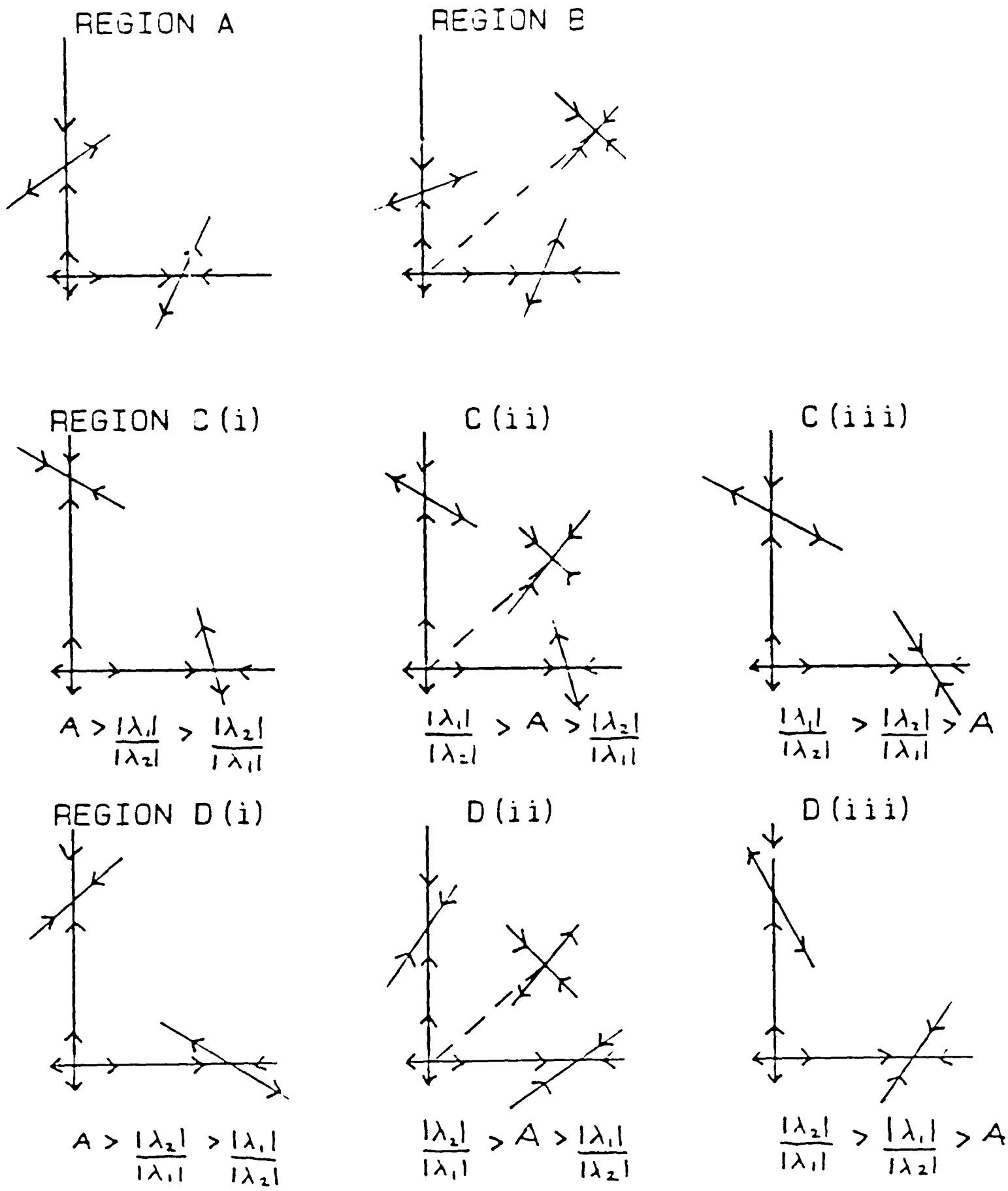

Figure 2.11: Phase plane diagrams for the above regions. The dashed lines are hypothetical separatrices.

and are determined by the initial and boundary conditions.

In Region C

$$(F,E) \rightarrow \left(\frac{\mu(\lambda_2 A - \lambda_1)}{\lambda_1^2 - \lambda_2^2}, \frac{\mu(\lambda_2 - \lambda_1 A)}{\lambda_1^2 - \lambda_2^2} \right) \quad \text{as } \tau \rightarrow \infty \text{ if } \frac{|\lambda_2|}{|\lambda_1|} < A < \frac{|\lambda_1|}{|\lambda_2|} \tag{2.130}$$

and the solution $\underline{u}$ tends to the same as for Region B.

For curved stripes we require the coefficient in one spatial direction to be significantly greater than that in the other. For Region B this leads to the intuitively obvious result that, for an x-dominated pattern we require $A \ll 1$ and for a y-dominated pattern we require $A \gg 1$. In Region C we obtain the same result but as we already have a restriction on the range of A we will require parameter values so that $\frac{|\lambda_2|}{|\lambda_1|} \ll 1$ and $A \approx \frac{|\lambda_2|}{|\lambda_1|}$ for an x-dominated pattern and $\frac{|\lambda_1|}{|\lambda_2|} \gg 1$ and $A \approx \frac{|\lambda_1|}{|\lambda_2|}$ for a y dominated pattern.

Numerical simulations of the model with parameter values lying in Region C give good agreement with the analytically predicted solutions. However the numerical solutions although stable for long periods of time eventually change to a slightly different steady state. This pattern is inherently the same except the variation in the non-dominant spatial direction has become more pronounced. This is probably due to the effect of higher order terms for large time. Figure 2.12 shows *i*) the predicted, *ii*) the intermediate and *iii*) the final numerical patterns for parameter values $a_1 = 0.225$ $b_1 = 0.775$ $D = 16.9$ $\overline{D} = 16.78$ and γ the 'size' parameter =4 for a) a 6×6 and b) a 6×9 domain.

The fact that the curved stripe pattern does not remain indefinitely does

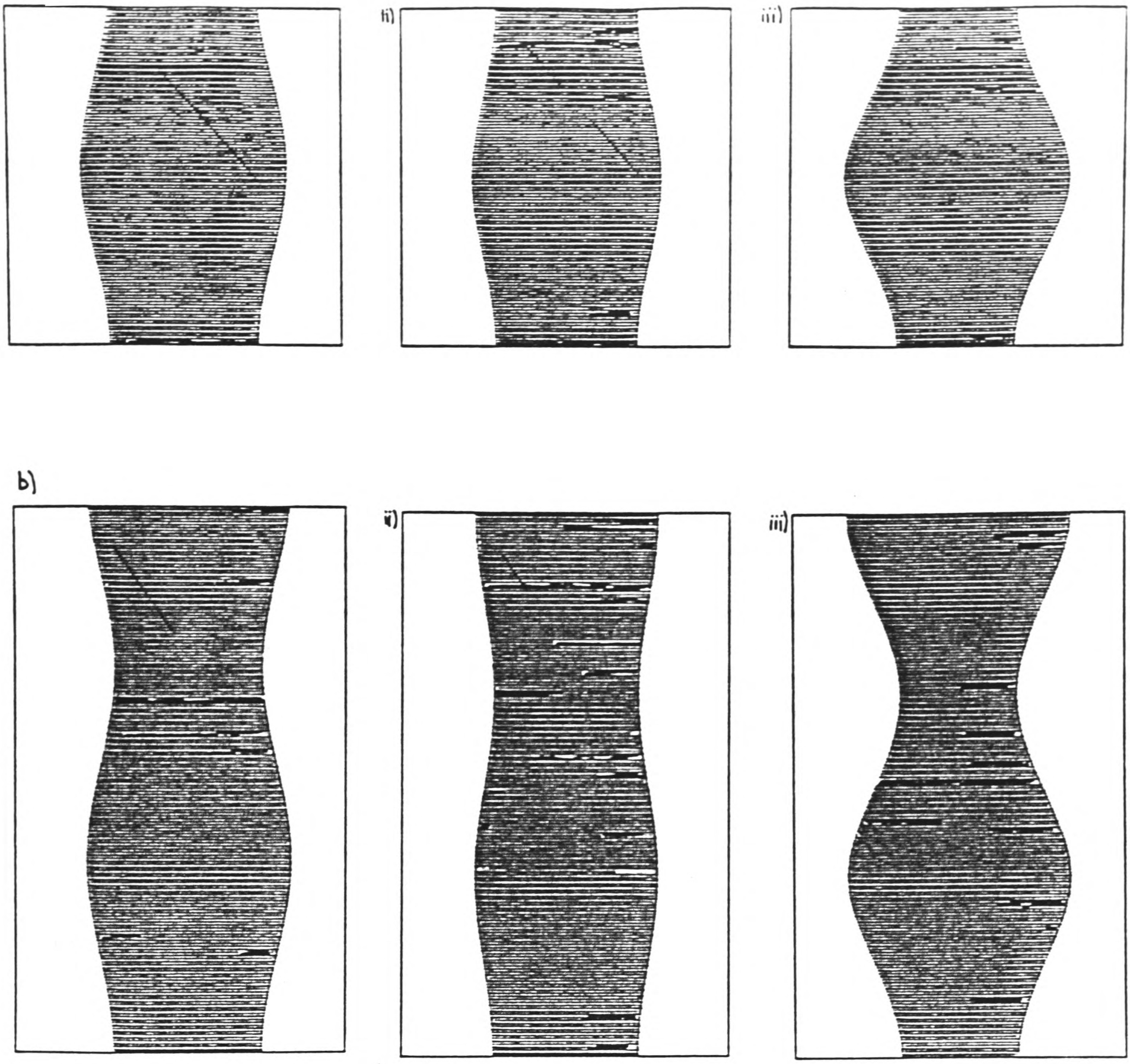

Figure 2.12: *i*) Predicted, *ii*) intermediate and *iii*) final curved stripe patterns formed with parameter values $a_1 = 0.225$, $b_1 = 0.775$, $D = 16.9$, $\overline{D} = 16.78$, $\gamma = 4$ on a) a 6×6 and b) a 6×9 domain.

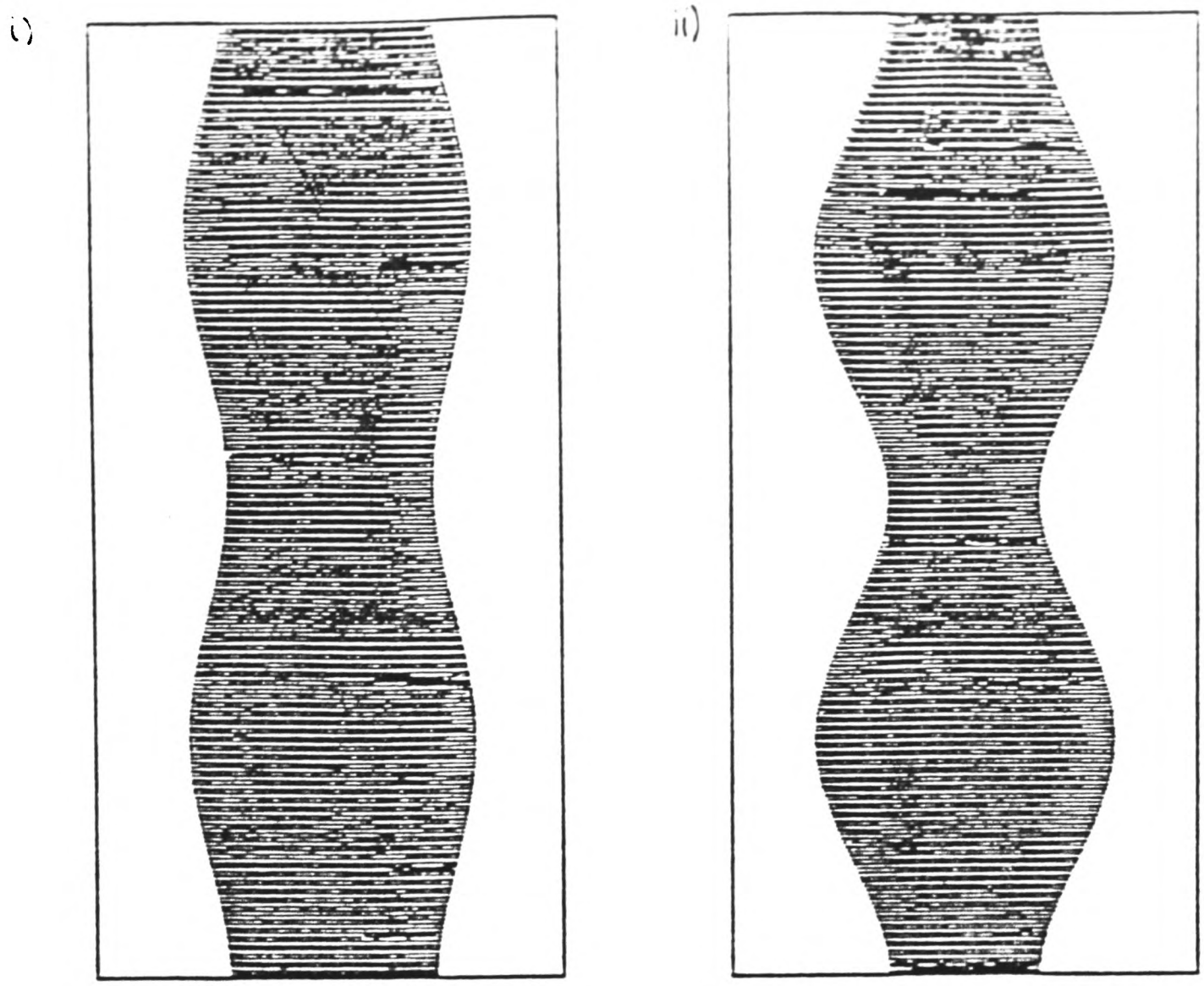

Figure 2.13: *i*) Predicted and *ii*) numerical patterns formed on a 6×12 rectangle using the same parameters as in Figure 2.12.

not necessarily mean that the model cannot be of the type which forms curved stripes in nature. The pattern remains constant for a long time as it gradually increases in magnitude and it could be that it has already become fixed upon the cells, which may be receptive to a chemical pre-pattern for only a limited time, in other words before any significant change in the shape of the pattern occurs. The restriction on the model that only modes with $k_x = 0$ or $k_y = 0$ is very sensitive and it becomes very difficult to produce a pattern with more curves on the stripe. Figure 2.13 shows a pattern where a double curve has been obtained. For any further extension of the pattern we need to join 'cells' together to obtain it. An example of this is shown in Figure 2.14.

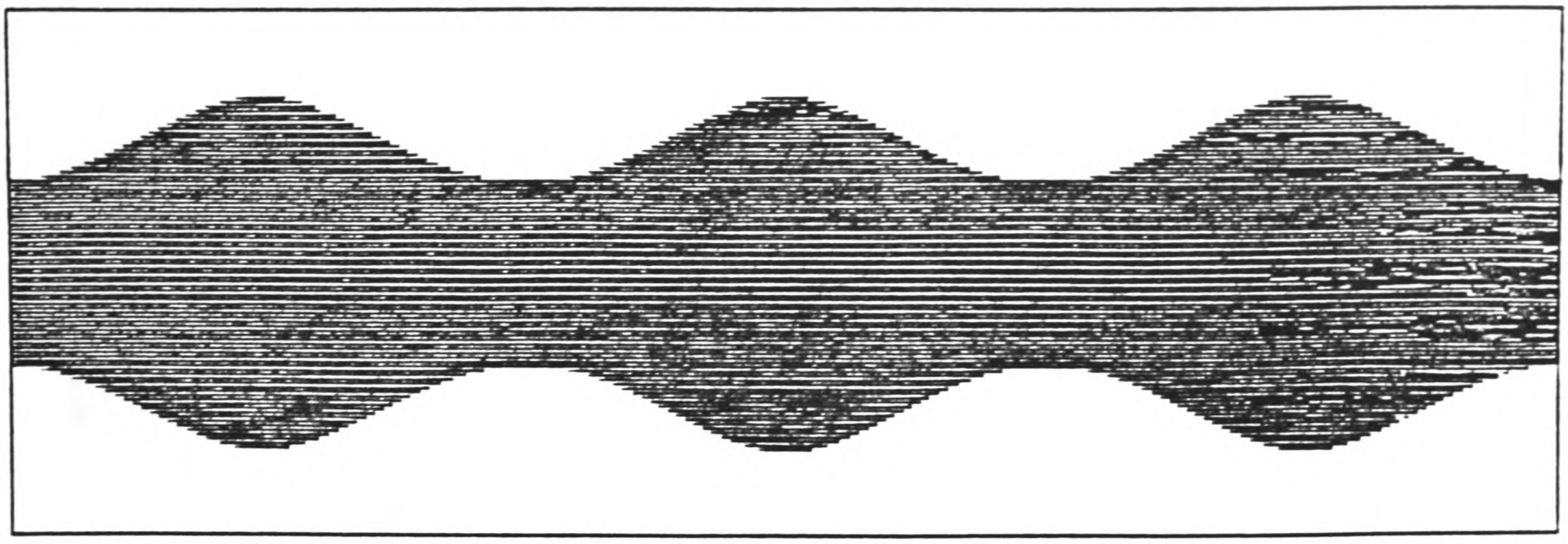

Figure 2.14: Pattern formed by fitting 3 6×6 rectangles together.

These types of patterns are similar to those found on certain species of viper such as the Adder or Crossed Viper (*Vipera berus berus*) shown in two of its colour phases in Figure 2.15. If we consider a slightly higher threshold value for the chemical we can obtain patterns similar to the characteristic diamond pattern common to many species of rattlesnake. Figure 2.16 shows an example of such a naturally occuring pattern in the markings of the Eastern Diamondback Rattlesnake (*Crotalus adamanteus*) and the result of taking a higher threshold value in a numerical simulation using the same parameters as in Figure 2.13.

In the next chapter we consider a model suggested by Nagorcka (1988) used to explain the segmentation sequence in the embryo of *Drosophila* using an asymmetric reaction diffusion scheme with the diffusion coefficients depending upon the density of the nuclei on the surface of the embryo.

a)

b)

Figure 2.15: The Adder (from Mehrtens (1987)) in a) normal colouration and b) brown colour phase.

a)

b)

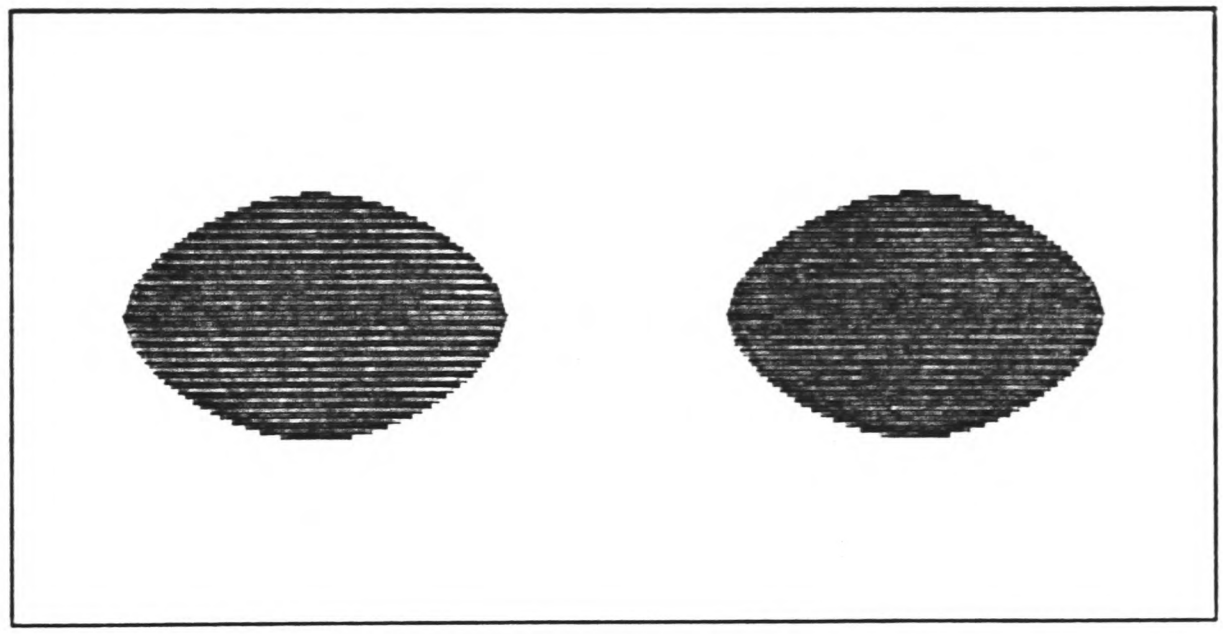

Figure 2.16: a) Eastern Diamondback Rattlesnake (from Mehrtens (1987)).
b) Numerical simulation showing a similar pattern.

Chapter 3

Analysis of a Model for Stripe Formation.

3.1 Introduction.

In this chapter we consider the problem of segmentation sequences in the early embryogenesis of the fruit fly *Drosophila Melanogaster* and analyse in detail a reaction diffusion mechanism for producing this sequence suggested by Nagorcka (1988). We examine the hypothesis he puts forward concerning the form of the reaction kinetics necessary for the required type of pattern.

Experimental work upon the embryo, such as that considered in Vogel (1977), has given rise to the hypothesis that the segmentation process occurs in a sequence of steps. It has been seen that several genes, known collectively as segmentation genes, are expressed in a sequence of banded patterns following fertilization of the egg. In the fertilized embryo the nuclei divide simultaneously enabling us to consider the development in stages called division cycles. Figure 3.1, from Foe and Alberts (1983), shows a diagramatic representation of the distribution of the nuclei during division cycles 7-14. As we can see, after the 7th division cycle the majority of the nuclei migrate

Figure 3.1: Cross-sectional diagram showing the distribution of the nuclei within the embryo. Taken from Foe and Alberts (1983).

to the surface of the egg to form a layer known as the presumptive syncytial blastoderm. During cycles 8 and 9 the size of the embryo increases while the nuclear density and the shape, generally assumed to be a prolate spheroid, remain constant. At the end of cycle 9 no further increase in size is possible, so in each cycle that follows the density of the nuclei on the surface will double. It is the effect of this density doubling upon the segmentation gene patterns that we analyse in this chapter. In the last ten years various possible mechanisms have been proposed to produce these sequential patterns using reaction diffusion systems.

Kauffman, Shymko and Trabert (1978) used a linear approximation to a

reaction diffusion system of the form

$$\begin{aligned} u_t = & \quad -Au + \frac{Bv^n}{1+v^n} & +d_1\nabla^2 u \\ v_t = & \quad -Cu + \frac{D(v^n+b)}{1+v^n} & +d_2\nabla^2 v \end{aligned} \tag{3.1}$$

to obtain a sequence of patterns which can be used as a basis to divide the blastoderm into sections. However when Bunow, Kernevez, Joly and Thomas (1980) solved a particular, more experimental, reaction diffusion mechanism of the form

$$\begin{aligned} u_t = & \quad \gamma(u_0 - u - \frac{\rho uv}{1+u+ku^2}) & +\nabla^2 u \\ v_t = & \quad \gamma(\alpha(v_0 - v) - \frac{\rho uv}{1+u+ku^2}) & +\beta\nabla^2 v \end{aligned} \tag{3.2}$$

on more accurate representations of the blastoderm, they were unable to produce the patterns predicted. In fact they indicated that a banded pattern along the anterior-posterior axis of a prolate spheroid is a very unlikely stable solution of a reaction diffusion system.

Meinhardt (1986) used a 2-component reaction diffusion system to set up a simple anterior-posterior gradient in the embryo. Using this gradient and a set of four threshold values, he divides the blastoderm into five "cardinal regions". Further division is obtained using a 4-component system or two linked 2-component systems. Another suggestion by Russell (1985) used two independent reaction diffusion systems and an undefined mechanism to interpret the phase angle between the independent wave-like patterns produced by the systems as the basis for a segmentation process.

Nagorcka (1988) suggested that there is at least one class of reaction diffusion systems which can produce a pre-pattern sequence controlling the cell differentiation within the embryo. The mechanism he suggests does not

encounter the problems of Bunow *et al.* (1980) and does produce a sequence of banded patterns. The mechanism also displays a frequency doubling effect which is common in the sequential development of segmentation genes. In the rest of this chapter we analyse this mechanism using the same techniques as in the previous chapter. We then make certain alterations to the mechanism to test whether his hypothesis is the likely cause of the preference for banded patterns.

In Section 3.2 we carry out a linear analysis to establish any parameter restrictions that are necessary for a linear prediction of pattern formation potential. In Section 3.3 we use a nonlinear bifurcation analysis to try and justify the preference for stripes. In Section 3.4 we consider the solution of the system in terms of regular tesselations of the plane to see if this can explain the preference any further. In Section 3.5 we use the same analytical techniques on slightly modified versions of the original model to test the hypothesis that it is the asymmetry of the equations that is the main cause of the striped pattern. In Section 3.6 we consider a general system and establish a condition upon the form of the system which we consider to be the true reason why the Nagorcka system demonstrates a preference for striped patterns. In Section 3.7 we briefly discuss an application of the theory of Kurata *et al.* (1989) to demonstrate that a reaction diffusion system, solved on the surface of a cylinder with sufficiently small radius, will give rise to a circumferentially homogeneous solution. Throughout these sections numerical simulations are presented to back up the analytical results.

3.2 Linear Analysis.

The Nagorcka system which we investigate in this chapter is of the form

$$\begin{aligned} U_t &= n(-AU + B(1 + \tanh(s(V - V_0)))) + n^{-1} d_u \nabla^2 U \\ V_t &= n(-CU + D(1 + \alpha \tanh(s(V - V_0)))) + n^{-1} d_v \nabla^2 V \end{aligned} \tag{3.3}$$

where n is the nuclear density, V_0 the arbitary steady state of V and A, B, C, D, α and s are positive parameters. Nagorcka (1988) suggests that it is the asymmetry of these reaction kinetics with respect to a sign change in both $u = U - U_0$ and $v = V - V_0$

$$i.e. \quad f(-(U - U_0), -(V - V_0)) = -f(U - U_0, V - V_0) \tag{3.4}$$

which is the cause of this model's preference for striped patterns. The diffusion coefficients depend inversely on n as it is likely that as the cell membranes form and separate nuclei, resistance to the diffusion increases and so the effective diffusion coefficients are made smaller. This has the effect, if the ratio of the diffusion coefficients remains the same, of shortening the unstable wavelength. Mathematically that is the same as allowing the domain to grow for fixed diffusion coefficients and unstable wavelengths so a succession of different patterns fit onto the egg at a discrete succession of allowable wavelengths (Kauffman *et al.* (1978)). For mathematical simplicity in the analysis to follow the *Drosophila* blastoderm will be considered to be cylindrical in shape instead of the more realistic prolate spheroid. (In fact when solving the system we will use a rectangle with periodic boundary conditions along two opposite sides to mimic a cylinder).

Let us now consider a linear analysis of (3.3). A homogeneous steady state (U_0, V_0) is only possible if

$$\frac{B}{A} = \frac{D}{C} = U_0. \tag{3.5}$$

Let

$$\beta = \frac{C}{A} = \frac{D}{B} \quad \underline{x} = \underline{x} d_v^{\frac{1}{2}} \quad d = \frac{d_u}{d_v} \quad u = U - U_0 \quad v = V - V_0. \tag{3.6}$$

This gives rise to the system

$$\begin{aligned} u_t &= -nAu + Bn\tanh sv + n^{-1}d\nabla^2 u &&= nf(u,v) + n^{-1}d\nabla^2 u \\ v_t &= -n\beta Au + Bn\beta\alpha\tanh sv + n^{-1}\nabla^2 v &&= ng(u,v) + n^{-1}\nabla^2 v. \end{aligned} \tag{3.7}$$

The nullclines of this system are shown in Figure 3.2. Proceeding with the linear analysis in the normal way we require the steady state to be stable in the absence of diffusion. This gives rise to the parameter conditions

$$\begin{aligned} &i) \quad A - B\beta\alpha s > 0. \\ &ii) \quad AB\beta s(1-\alpha) > 0 \quad \Rightarrow \alpha < 1. \end{aligned} \tag{3.8}$$

We now require the steady state to be unstable in the presence of diffusion. This gives rise to the following parameter conditions

$$\begin{aligned} &iii) \quad A - B\beta\alpha sd < 0 \quad \Rightarrow d > 1. \\ &iv) \quad (A - B\beta\alpha sd)^2 - 4dAB\beta s(1-\alpha) > 0 \\ &\qquad \Rightarrow d > d_c = \frac{A(2 - \alpha + 2\sqrt{1-\alpha})}{B\beta s\alpha^2}. \end{aligned} \tag{3.9}$$

This establishes the basic parameter restrictions for the possibility of forming spatial patterns. In the next section we carry out a nonlinear bifurcation analysis to try and determine why this mechanism has a preference for stripes.

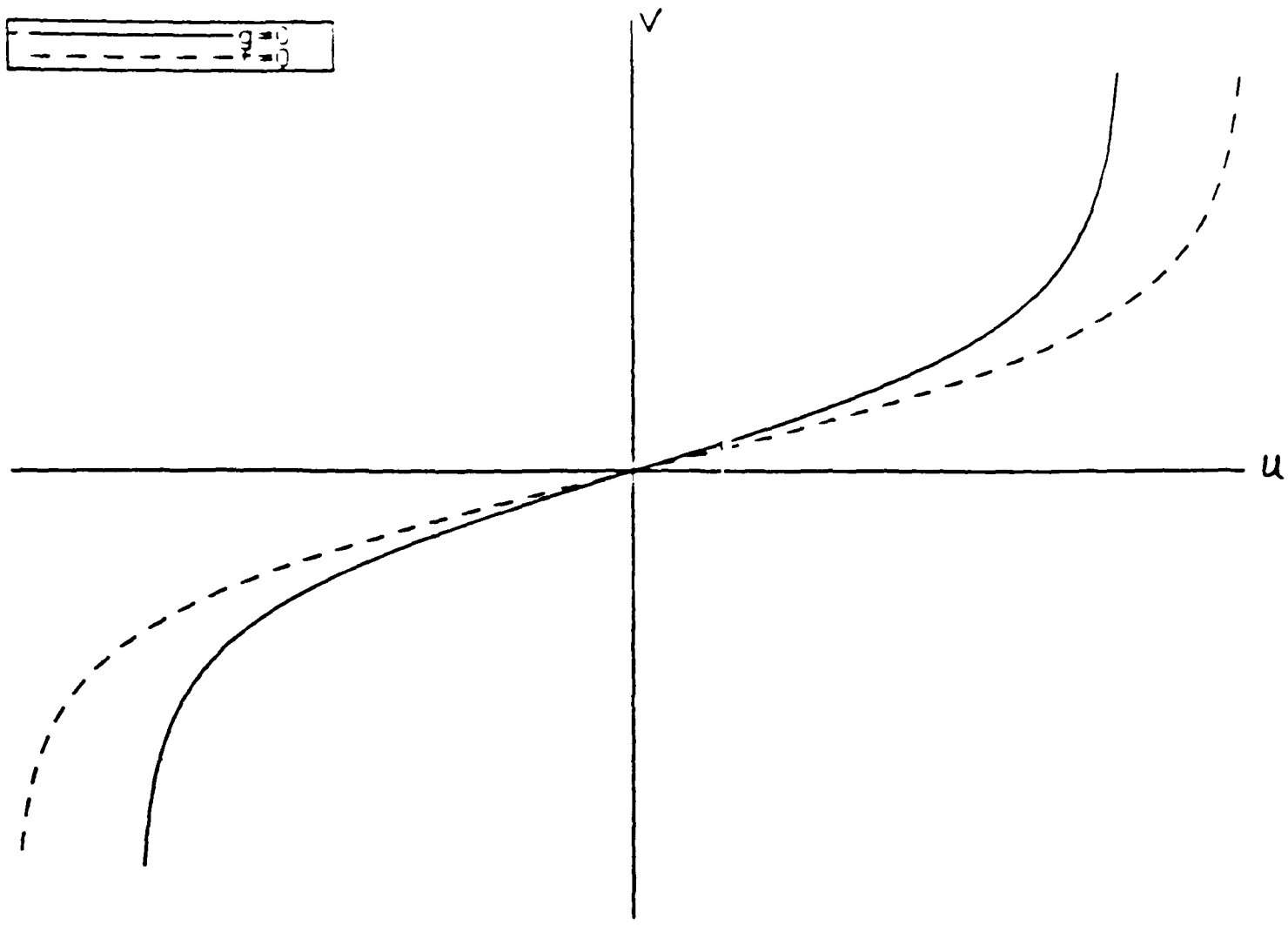

Figure 3.2: The nullclines of (3.7) drawn for $A = B$, $\alpha < 1$.

3.3 Nonlinear Analysis.

In this section we use a singular perturbation technique to solve (3.7) repeated here for completeness

$$\begin{aligned} u_t &= -nAu + nB\tanh sv + n^{-1}d\nabla^2 u \quad = nf(u,v) + n^{-1}d\nabla^2 u \\ v_t &= -n\beta Au + nB\beta\alpha\tanh sv + n^{-1}\nabla^2 v \quad = ng(u,v) + n^{-1}\nabla^2 v. \end{aligned} \tag{3.10}$$

As before we examine the behaviour of this system when d is in the vicinity of d_c. Define a small parameter ϵ $(0 < \epsilon \ll 1)$ by

$$d = d_c + \epsilon^2 \tag{3.11}$$

and slow and fast time variables τ and t^* by

$$\tau = \epsilon^2 t \qquad t^* = t \tag{3.12}$$

and look for solutions of the form

$$\underline{u} = \sum_{j=1} \epsilon^j \underline{u}_j(x, y, \tau, t^*). \tag{3.13}$$

For notational convenience in the analysis to follow we replace t^* by t. Equating powers of ϵ in (3.10) leads to the following equations

$$O(\epsilon) \qquad (\underline{u}_1)_t - nM\underline{u}_1 - n^{-1}D_1\nabla^2\underline{u}_1 = 0 \tag{3.14}$$

$$O(\epsilon^2) \qquad (\underline{u}_2)_t - nM\underline{u}_2 - n^{-1}D_1\nabla^2\underline{u}_2 = 0 \tag{3.15}$$

$$O(\epsilon^3) \qquad (\underline{u}_3)_t - nM\underline{u}_3 - n^{-1}D_1\nabla^2\underline{u}_3 = -\frac{\partial \underline{u}_1}{\partial \tau} + n^{-1}Q\nabla^2\underline{u}_1 - \frac{1}{3}s^3Bnv_1^3Z \tag{3.16}$$

$$O(\epsilon^4) \qquad (\underline{u}_4)_t - nM\underline{u}_4 - n^{-1}D_1\nabla^2\underline{u}_4 = -\frac{\partial \underline{u}_2}{\partial \tau} + n^{-1}Q\nabla^2\underline{u}_2 - s^3Bnv_1^2v_2Z \tag{3.17}$$

where

$$M = \begin{pmatrix} f_u & f_v \\ g_u & g_v \end{pmatrix} \quad D_1 = \begin{pmatrix} d_c & 0 \\ 0 & 1 \end{pmatrix} \quad Q = \begin{pmatrix} 1 & 0 \\ 0 & 0 \end{pmatrix} \quad Z = \begin{pmatrix} 1 \\ \beta\alpha \end{pmatrix}. \tag{3.18}$$

The solution to (3.14) is

$$\underline{u}_1 = \int_k e^{\lambda_k^{\pm} t} \begin{pmatrix} 1 \\ M_k^{\pm} \end{pmatrix} \sum (a_{k_x}^{\pm}(\tau)\cos k_x x + b_{k_x}^{\pm}(\tau)\sin k_x x)(c_{k_y}^{\pm}\cos k_y y + d_{k_y}^{\pm}\sin k_y y) \tag{3.19}$$

where the sum is over k_x, k_y such that $k_x^2 + k_y^2 = k^2$ and $\lambda_k^{\pm}$ are the eigenvalues of $M - k^2 D_1$ with corresponding eigenvectors $\begin{pmatrix} 1 \\ M_k^{\pm} \end{pmatrix}$. At the onset of

diffusion driven instability we have $\lambda_p^+ = 0$ for some p, $\Re(\lambda_k^+) < 0$ for $k \neq p$ and $\Re(\lambda_k^-) < 0$ for all k. Thus as $t \to \infty$ we obtain the solution

$$\underline{u}_1 = \begin{pmatrix} 1 \\ M_p^+ \end{pmatrix} (a_{p_x} \cos p_x x + b_{p_x} \sin p_x x)(c_{p_y} \cos p_y y + d_{p_y} \sin p_y y) \qquad (3.20)$$

where

$$p^2 = \frac{n^2(d_c g_v + f_u)}{2d_c} \qquad M_p^+ = \frac{n^{-2}p^2 d_c - f_u}{f_v} = \frac{g_u}{n^{-2}p^2 - g_v}. \qquad (3.21)$$

Note 1.

$$f_v > 0, f_u < 0 \quad \Rightarrow M_p^+ > 0.$$

At this point we have a choice as to how to proceed. We can either look for solutions in regular tesselations of the plane or keep the form of the solutions as general as possible but make another restriction to enable us to solve the system. We deal with the case of regular tesselations in the next section.

To apply the analysis to the *Drosophila* embryo we consider the boundary conditions to be

$$\begin{aligned} &\text{zero flux on } y = 0,\ y = b \ \Rightarrow \ d_{p_y} = 0, \quad p_y = \frac{m_y \pi}{b} \\ &\text{periodic on } x = 0,\ x = a \ \Rightarrow \ p_x = \frac{m_x \pi}{a}, \quad m_x \text{ even} \end{aligned} \qquad (3.22)$$

In fact when Nagorcka simulated his equations numerically he used fixed boundary conditions for both u and v, fixed at $0.7U_0$ and $0.7V_0$ respectively, on $y = 0, b$ to force the minimum to occur at the domain ends. This case cannot be dealt with analytically as we are considering small perturbations about the steady state and so need the boundary conditions to be close to the steady state if fixed conditions are required. In this analysis we consider zero flux conditions which will give a better indication of the true pattern forming potential of the model rather than inducing a pattern from the boundary

conditions which is implied by the conditions used by Nagorcka. These conditions give

$$\underline{u}_1 = \begin{pmatrix} 1 \\ M_p \end{pmatrix} \sum (\overline{a}_p \cos \frac{m_x \pi x}{a} + \overline{b}_p \sin \frac{m_x \pi x}{a}) \cos \frac{m_y \pi y}{b} \quad \text{as } t \to \infty. \quad (3.23)$$

To proceed we consider the case when there is only one possible combination m_x, m_y such that

$$\frac{m_x^2}{a^2} + \frac{m_y^2}{b^2} = \frac{p^2}{\pi^2} \quad \text{and } m_x \text{ is even.} \quad (3.24)$$

By a similar argument at $O(\epsilon^2)$ we obtain the solution

$$\underline{u}_2 = \begin{pmatrix} 1 \\ M_p \end{pmatrix} (\overline{a_1}_p \cos \frac{m_x \pi x}{a} + \overline{b_1}_p \sin \frac{m_x \pi x}{a}) \cos \frac{m_y \pi y}{b} \quad \text{as } t \to \infty. \quad (3.25)$$

At $O(\epsilon^3)$ we obtain secular terms. These are suppressed in the normal way by making

$$\underline{J}(\underline{u}_1, \underline{u}_2) = -\frac{\partial \underline{u}_1}{\partial \tau} + n^{-1} Q \nabla^2 \underline{u}_1 - \frac{1}{3} B n s^3 v_1^3 Z \quad (3.26)$$

orthogonal to the bounded solutions of the homogeneous adjoint equation, namely

$$\begin{pmatrix} 1 \\ S_p \end{pmatrix} \cos \frac{m_x \pi x}{a} \cos \frac{m_y \pi y}{b} \qquad \begin{pmatrix} 1 \\ S_p \end{pmatrix} \sin \frac{m_x \pi x}{a} \cos \frac{m_y \pi y}{b} \quad (3.27)$$

where the inner product is defined as

$$\underline{w}.\underline{z} = \lim_{T_1 \to \infty} \frac{1}{T_1} \int_0^{T_1} \int_0^{\frac{2a}{m_x}} \int_0^{\frac{2b}{m_y}} w^T z \, dy dx dt. \quad (3.28)$$

This leads to the following simultaneous ordinary differential equations for the amplitudes:

$$\begin{aligned} (1 + S_p M_p) \frac{d\overline{a}}{d\tau} &= -n^{-1} p^2 \overline{a} - \frac{3}{16} B n s^3 (1 + \alpha \beta S_p) M_p^3 \overline{a} (\overline{a}^2 + \overline{b}^2) \\ (1 + S_p M_p) \frac{d\overline{b}}{d\tau} &= -n^{-1} p^2 \overline{b} - \frac{3}{16} B n s^3 (1 + \alpha \beta S_p) M_p^3 \overline{b} (\overline{a}^2 + \overline{b}^2). \end{aligned} \quad (3.29)$$

Note 2.

$$1 + S_p M_p = 1 + \frac{n^{-2}p^2 d_c - f_u}{n^{-2}p^2 - g_v} = 1 + \frac{d_c g_v - f_u}{f_u d_c^{-1} - g_v} = 1 - d_c < 0.$$

Note 3.

$$\begin{aligned} 1 + \alpha\beta S_p &= 1 + \alpha\beta\left(\frac{d_c g_v - f_u}{2g_u}\right) = 1 - \alpha\frac{\left(\frac{A}{B\beta s}\left[\frac{2-\alpha+2\sqrt{1-\alpha}}{\alpha^2}\right] Bn\beta\alpha s + An\right)}{2An} \\ &= 1 - \frac{\alpha(1+\sqrt{1-\alpha})}{\alpha} = -\sqrt{1-\alpha} < 0. \end{aligned}$$

Let $R = \overline{a}^2 + \overline{b}^2$. Multiplying the first equation in (3.29) by $\overline{a}$, the second by $\overline{b}$ and adding we obtain

$$\frac{dR}{d\tau} = -\frac{2n^{-1}p^2}{1 + S_p M_p} R - \frac{3Bn(1+\alpha\beta S_p)s^3 M_p^3}{8(1+S_p M_p)} R^2 \tag{3.30}$$

$$\frac{dR}{d\tau} = \mu R + \eta R^2 \qquad \mu > 0, \eta < 0 \quad \mu, \eta = O(n). \tag{3.31}$$

Solving this equation we obtain the following solutions for the amplitudes $\overline{a}, \overline{b}$

$$\begin{aligned} \overline{a} &= \left(\frac{\mu\theta e^{\mu\tau}}{1 - \eta\theta e^{\mu\tau}}\right)^{\frac{1}{2}} \cos\psi \;\rightarrow\; \left(\frac{\mu}{-\eta}\right)^{\frac{1}{2}} \cos\psi \quad \text{as } \tau \rightarrow \infty \\ \overline{b} &= \left(\frac{\mu\theta e^{\mu\tau}}{1 - \eta\theta e^{\mu\tau}}\right)^{\frac{1}{2}} \sin\psi \;\rightarrow\; \left(\frac{\mu}{-\eta}\right)^{\frac{1}{2}} \sin\psi \quad \text{as } \tau \rightarrow \infty \end{aligned} \tag{3.32}$$

for some constants ψ,θ. Therefore as $t \rightarrow \infty$, $\tau \rightarrow \infty$ the heterogeneous steady state is of the form

$$\underline{u}_1 = \begin{pmatrix} 1 \\ M_p \end{pmatrix} \left(\frac{\mu}{-\eta}\right)^{\frac{1}{2}} \cos\left(\frac{m_x \pi x}{a} - \psi\right) \cos\frac{m_y \pi y}{b}. \tag{3.33}$$

Because of the form of equation (3.17) we can obtain equations for the τ dependence of $\underline{u}_2$ by suppressing secular terms at $O(\epsilon^4)$. This leads to the simultaneous ordinary differential equations

$$\begin{aligned} \frac{d\overline{a}_1}{d\tau} &= \frac{\mu}{2}\overline{a}_1 + \frac{\eta}{2}[\overline{a}_1(\overline{a}^2 + \overline{b}^2) + 2\overline{a}_1\overline{a}^2 + 2\overline{a}\overline{b}\overline{b}_1] \\ \frac{d\overline{b}_1}{d\tau} &= \frac{\mu}{2}\overline{b}_1 + \frac{\eta}{2}[\overline{b}_1(\overline{a}^2 + \overline{b}^2) + 2\overline{b}_1\overline{b}^2 + 2\overline{a}\overline{b}\overline{a}_1]. \end{aligned} \tag{3.34}$$

In matrix form this can be written as

$$\begin{pmatrix} \overline{a}_1 \\ \overline{b}_1 \end{pmatrix}_\tau = \begin{pmatrix} f_1(\tau,\psi) & g_1(\tau,\psi) \\ g_1(\tau,\psi) & h_1(\tau,\psi) \end{pmatrix} \begin{pmatrix} \overline{a}_1 \\ \overline{b}_1 \end{pmatrix} \tag{3.35}$$

where

$$\begin{aligned} f_1(\tau,\psi) &= \frac{\mu}{2}\left[1 + \frac{\mu\theta e^{\mu\tau}}{1-\eta\theta e^{\mu\tau}} + \frac{2\eta\theta e^{\mu\tau}}{1-\eta\theta e^{\mu\tau}}\cos^2\psi\right] \\ g_1(\tau,\psi) &= \frac{\mu\eta\theta e^{\mu\tau}}{1-\eta\theta e^{\mu\tau}}\sin\psi\cos\psi \\ h_1(\tau,\psi) &= \frac{\mu}{2}\left[1 + \frac{\eta\theta e^{\mu\tau}}{1-\eta\theta e^{\mu\tau}} + \frac{2\eta\theta e^{\mu\tau}}{1-\eta\theta e^{\mu\tau}}\sin^2\psi\right]. \end{aligned} \tag{3.36}$$

We can solve this system explicitly by setting $x = -\eta\theta e^{\mu\tau}$ to give

$$\begin{aligned} \frac{d\overline{a}_1}{dx} &= \frac{1-2rx}{2x(1+x)}\overline{a}_1 - \frac{q}{1+x}\overline{b}_1, \qquad p = \sin^2\psi \quad r = \cos^2\psi \\ \frac{d\overline{b}_1}{dx} &= \frac{-q}{1+x}\overline{a}_1 + \frac{1-2px}{2x(1+x)}\overline{b}_1, \qquad q = \sin\psi\cos\psi. \end{aligned} \tag{3.37}$$

Reducing this system to one equation, for $\overline{a}_1$ say, we obtain

$$\frac{d^2\overline{a}_1}{dx^2} + \frac{2x-1}{x(1+x)}\frac{d\overline{a}_1}{dx} + \frac{3}{4x^2(1+x)^2}\overline{a}_1 = 0 \qquad (\text{if } q \neq 0). \tag{3.38}$$

Now we are interested in the behaviour of the solution as $x \to \infty$, that is $\tau \to \infty$. We transform the equation by setting $x = \frac{1}{t_1}$ and study the behaviour of the solution as $t_1 \to 0$. This transformation results in the equation

$$\frac{d^2\overline{a}_1}{dt_1^2} + \frac{3}{t_1+1}\frac{d\overline{a}_1}{dt_1} + \frac{3}{4(t_1+1)^2}\overline{a}_1 = 0. \tag{3.39}$$

We look for solutions to (3.39) of the form

$$\overline{a}_1(t_1) = t_1^c(d_0 + d_1t_1 + d_2t_1^2 + d_3t_1^3 + \ldots). \tag{3.40}$$

The solutions of the indicial equation resulting from this differ by an integer and we find that for $c = 0$ (one of the solutions of the indicial equation) the

constant d_1 is indeterminate. This gives us our solution with two arbitary constants, namely

$$\begin{aligned}\overline{a}_1(t_1) &= d_0\left(1-\frac{3}{8}t_1^2+\ldots+\frac{(-1)^{n+1}(2n-1)!}{2^{2n}n!(n-2)!}t_1^n+\ldots\right)\\ &+ d_1t_1\left(1-\frac{3}{2}t_1+\ldots+\frac{(-1)^{n+1}(2n-1)!}{2^{2n-2}((n-1)!)^2}t_1^n+\ldots\right).\end{aligned} \tag{3.41}$$

Now from (3.37)

$$\overline{b}_1=\frac{1-2rx}{2qx}\overline{a}_1-\frac{1+x}{q}\frac{d\overline{a}_1}{dx}=\frac{t_1-2r}{2q}\overline{a}_1+\frac{t_1(t_1+1)}{q}\frac{d\overline{a}_1}{dt_1}. \tag{3.42}$$

As $t_1\to 0$, $\overline{a}_1(t_1)\to d_0$ and $\frac{d\overline{a}_1}{dt_1}\to d_1$. So as $t_1\to 0$, $\overline{b}_1\to -\frac{r}{q}\overline{a}_1=-\frac{\cos\psi}{\sin\psi}d_0$ and so

$$\underline{u}_2\to -\begin{pmatrix}1\\ M_p\end{pmatrix}\frac{d_0}{\sin\psi}\sin\left(\frac{m_x\pi x}{a}-\psi\right)\cos\frac{m_y\pi y}{b}\quad\text{as }\tau\to\infty, t\to\infty. \tag{3.43}$$

These result in an expression for the first two terms of the solution $\underline{u}$ as $\tau\to\infty, t\to\infty$, specifically

$$\underline{u}=\epsilon\begin{pmatrix}1\\ M_p\end{pmatrix}\cos\frac{m_y\pi y}{b}\left[\left(\frac{\mu}{-\eta}\right)^{\frac{1}{2}}\cos\left(\frac{m_x\pi x}{a}-\psi\right)-\frac{\epsilon d_0}{\sin\psi}\sin\left(\frac{m_x\pi x}{a}-\psi\right)\right] \tag{3.44}$$

where ψ and d_0 are determined from the initial conditions. This analysis for the τ dependence of $\underline{u}_2$ is only valid for $q=\sin\psi\cos\psi\neq 0$. If $q=0$, with $\sin\psi=0$ say, then we obtain the result that, as $\tau\to\infty$

$$\overline{a}\to\left(\frac{\mu}{-\eta}\right)^{\frac{1}{2}}\quad\overline{b}=0\quad\overline{a}_1\to 0\quad\overline{b}_1=\phi\quad\text{for some constant }\phi\neq 0.$$

This analysis, as it stands, indicates no concrete preference for stripes. Stripes will form if the only possible combination of m_x, m_y satisfying (3.24) has $m_y=0$. However this would seem to depend upon the choice of parameters and the initial and boundary conditions. Figure 3.3 shows a specific

pattern sequence, using zero flux boundary conditions at the ends and using the preceding pattern as the initial conditions for the next stage, where a striped pattern does form. This sequence is an attempt to produce the patterns of *ftz* expression during cycles 8 to 12. The parameter values used are $A = B = 23.1$, $\beta = 0.0563$, $\alpha = 0.8$, $s = 3.0$ and $d = 20$. For the first two in the sequence the nuclear density n remains constant ($n = 1$) while the size of the rectangle increases from 2.1×3.15 to 4.2×6.3 and for the remainder of the sequence the size remains fixed and the nuclear density doubles at each stage. Figure 3.4 illustrates the dependency of the model upon the initial conditions as it is formed by taking random perturbations about the steady state as its initial conditions for the same parameter values as the third of the pictures in Figure 3.3. In the next section we consider a regular tesselation analysis of the model to see if this is where the preference for stripes originates.

3.4 Regular Tesselation Analysis.

In this section we consider the time independent solutions of (3.14) which form regular tesselations of the plane. The only possibilities are rolls (stripes), hexagons (triangles) and rhombi (squares). With this in mind we look for solutions of the form

$$\underline{u}_1 = \begin{pmatrix} 1 \\ M_p \end{pmatrix} (a_2(\tau)\cos kx \cos ly + b_2(\tau)\cos 2ly) \tag{3.45}$$

where

$$k^2 + l^2 = p^2 \qquad 4l^2 = p^2. \tag{3.46}$$

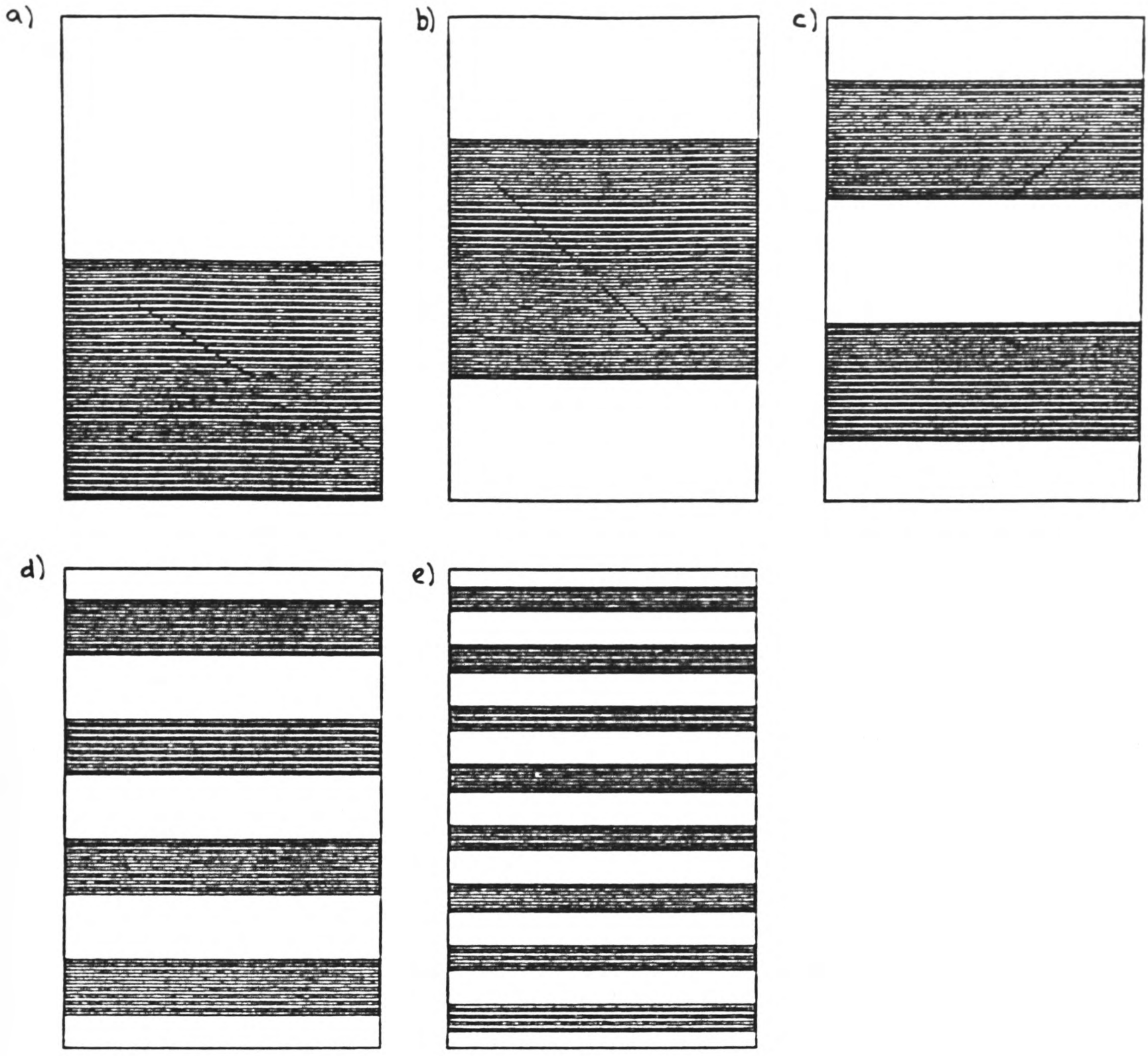

Figure 3.3: Pattern formation sequence using the Nagorcka kinetics (3.7) and parameter values $A = B = 23.1$, $\beta = 0.0563$, $\alpha = 0.8$, $s = 3.0$, $d = 20$ with a) $n = 1$ size $=2.1 \times 3.15$; b) size $=4.2 \times 6.3$; c) $n = 2$; d) $n = 4$; e) $n = 8$.

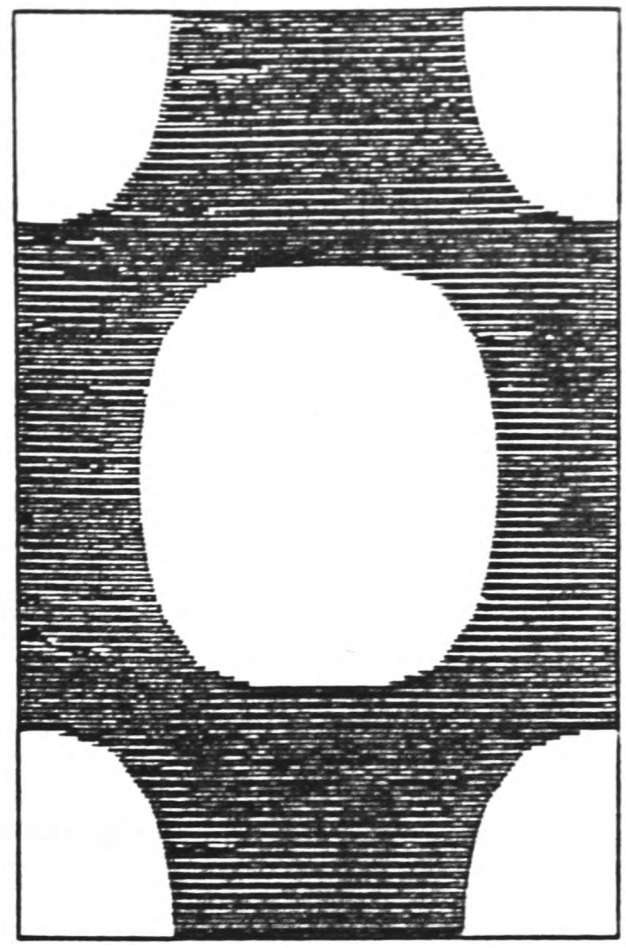

Figure 3.4: Pattern formed using random initial conditions for the same parameter values as Figure 3.3c).

This solution will give rolls, hexagons or rhombi to $O(\epsilon)$ depending on the values of $a_2(\tau)$ and $b_2(\tau)$.

$$\begin{aligned}
&\text{If } a_2 = 0 \quad \underline{u}_1 = \begin{pmatrix} 1 \\ M_p \end{pmatrix} b_2(\tau)\cos 2ly && \text{(a)}\\
&\text{If } b_2 = 0 \quad \underline{u}_1 = \begin{pmatrix} 1 \\ M_p \end{pmatrix} a_2(\tau)\cos kx\cos ly && \text{(b)}\\
&\text{If } a_2 = 2b_2 \quad \underline{u}_1 = \begin{pmatrix} 1 \\ M_p \end{pmatrix} b_2(\tau)(\cos(kx+ly)+\cos(kx-ly)+\cos 2ly) && \text{(c)}
\end{aligned} \tag{3.47}$$

where (a) is a roll pattern, (b) is a rhombic pattern and (c) is a hexagonal pattern. Using (3.45) we now continue as in Section 3.3 and try to suppress the secular terms at $O(\epsilon^3)$. This means we must make (3.26) orthogonal to the bounded solutions of the adjoint equation in regular tesselations of the

plane. This leads to the simultaneous ordinary differential equations

$$\begin{aligned} \frac{da_2}{d\tau} &= \mu_1 a_2 + \eta_1 a_2(3a_2^2 + 8b_2^2) \\ \frac{db_2}{d\tau} &= \mu_1 b_2 + 4\eta_1 b_2(a_2^2 + b_2^2) \end{aligned} \tag{3.48}$$

where

$$\mu_1 = \frac{-n^{-1}p^2}{1 + S_p M_p} > 0 \qquad \eta_1 = \frac{-Bns^3 M_p^3(1 + \alpha\beta S_p)}{16(1 + S_p M_p)} < 0. \tag{3.49}$$

The behaviour of this system is given by a phase plane analysis.

The steady states are given by the solutions of

$$\begin{aligned} 0 &= (\mu_1 + 3\eta_1 a_2^2 + 8\eta_1 b_2^2)a_2 \\ 0 &= (\mu_1 + 4\eta_1 a_2^2 + 4\eta_1 b_2^2)b_2 \end{aligned} \tag{3.50}$$

which gives

$$(0,0), \left(0, \left(\frac{\mu_1}{-4\eta_1}\right)^{\frac{1}{2}}\right), \left(\left(\frac{\mu_1}{-3\eta_1}\right)^{\frac{1}{2}}, 0\right), \left(\left(\frac{\mu_1}{-5\eta_1}\right)^{\frac{1}{2}}, \frac{1}{2}\left(\frac{\mu_1}{-5\eta_1}\right)^{\frac{1}{2}}\right) \tag{3.51}$$

and correspond to 1) homogeneous pattern, 2) roll pattern, 3) rhombic pattern and 4) hexagonal pattern. We now consider the stability of these steady states with respect to τ. Let

$$\begin{aligned} F(a_2, b_2) &= a_2(\mu_1 + 3\eta_1 a_2^2 + 8\eta_1 b_2^2) \\ G(a_2, b_2) &= b_2(\mu_1 + 4\eta_1 a_2^2 + 4\eta_1 b_2^2) \end{aligned} \tag{3.52}$$

which give partial derivatives evaluated at the steady states, namely

$$\begin{aligned} F_{a_2} &= \mu_1 + 9\eta_1 a_2^2 + 8\eta_1 b_2^2 & F_{b_2} &= 16\eta_1 a_2 b_2 \\ G_{a_2} &= 8\eta_1 a_2 b_2 & G_{b_2} &= \mu_1 + 4\eta_1 a_2^2 + 12\eta_1 b_2^2. \end{aligned} \tag{3.53}$$

We consider each steady state in turn and look for solutions proportional to $e^{\lambda\tau}$ in the usual way.

$$\text{At } (0,0) \quad F_{a_2} = G_{b_2} = \mu_1 \quad F_{b_2} = G_{a_2} = 0$$
$$\begin{vmatrix} \mu_1 - \lambda & 0 \\ 0 & \mu_1 - \lambda \end{vmatrix} = 0 \quad \Rightarrow \lambda = \mu_1, \mu_1 \tag{3.54}$$
so $(0,0)$ is an unstable type *II* node.

$$\text{At } \left(0, \left(\frac{\mu_1}{-4\eta_1}\right)^{\frac{1}{2}}\right) \quad F_{a_2} = -\mu_1 \quad G_{b_2} = -2\mu_1 \quad F_{b_2} = G_{a_2} = 0$$
$$\begin{vmatrix} -\mu_1 - \lambda & 0 \\ 0 & -2\mu_1 - \lambda \end{vmatrix} = 0 \quad \Rightarrow \lambda = -\mu_1, -2\mu_1$$
so $\left(0, \left(\frac{\mu_1}{-4\eta_1}\right)^{\frac{1}{2}}\right)$ is a stable node with eigenvectors $\begin{pmatrix} 1 \\ 0 \end{pmatrix}$ and $\begin{pmatrix} 0 \\ 1 \end{pmatrix}$. (3.55)

$$\text{At } \left(\left(\frac{\mu_1}{-3\eta_1}\right)^{\frac{1}{2}}, 0\right) \quad F_{a_2} = -2\mu_1 \quad G_{b_2} = -\frac{\mu_1}{3} \quad F_{b_2} = G_{a_2} = 0$$
$$\begin{vmatrix} -2\mu_1 - \lambda & 0 \\ 0 & -\frac{\mu_1}{3} - \lambda \end{vmatrix} = 0 \quad \Rightarrow \lambda = -2\mu_1, -\frac{\mu_1}{3}$$
so $\left(\left(\frac{\mu_1}{-3\eta_1}\right)^{\frac{1}{2}}, 0\right)$ is a stable node with eigenvectors $\begin{pmatrix} 1 \\ 0 \end{pmatrix}$ and $\begin{pmatrix} 0 \\ 1 \end{pmatrix}$. (3.56)

$$\text{At } \left(\left(\frac{\mu_1}{-5\eta_1}\right)^{\frac{1}{2}}, \frac{1}{2}\left(\frac{\mu_1}{-5\eta_1}\right)^{\frac{1}{2}}\right) \quad F_{a_2} = \frac{-6\mu_1}{5}, G_{b_2} = \frac{-2\mu_1}{5}, F_{b_2} = \frac{-8\mu_1}{5}, G_{a_2} = \frac{-4\mu_1}{5}$$
$$\begin{vmatrix} \frac{-6\mu_1}{5} - \lambda & \frac{-8\mu_1}{5} \\ \frac{-4\mu_1}{5} & \frac{-2\mu_1}{5} - \lambda \end{vmatrix} = 0 \quad \Rightarrow \lambda = -2\mu_1, \frac{2\mu_1}{5}$$
so $\left(\left(\frac{\mu_1}{-5\eta_1}\right)^{\frac{1}{2}}, \frac{1}{2}\left(\frac{\mu_1}{-5\eta_1}\right)^{\frac{1}{2}}\right)$ is a saddle point with eigenvectors $\begin{pmatrix} 2 \\ 1 \end{pmatrix}, \begin{pmatrix} 1 \\ -1 \end{pmatrix}$. (3.57)

The phase plane configuration is shown in Figure 3.5. As the stable steady states are the ones with either a_2 or b_2 equal to zero this would seem to imply that as $t, \tau \to \infty$ the solution $\underline{u}_1$ is of the form

$$\underline{u}_1 = \begin{pmatrix} 1 \\ M_p \end{pmatrix} \left(\frac{\mu_1}{-3\eta_1}\right)^{\frac{1}{2}} \cos\left(\frac{\sqrt{3}px}{2}\right) \cos\left(\frac{py}{2}\right)$$
or
$$\underline{u}_1 = \begin{pmatrix} 1 \\ M_p \end{pmatrix} \left(\frac{\mu_1}{-4\eta_1}\right)^{\frac{1}{2}} \cos(py) \tag{3.58}$$

depending upon the initial conditions. For a sequence of numerical simulations as described in Figure 3.3 the first two patterns that form are the only

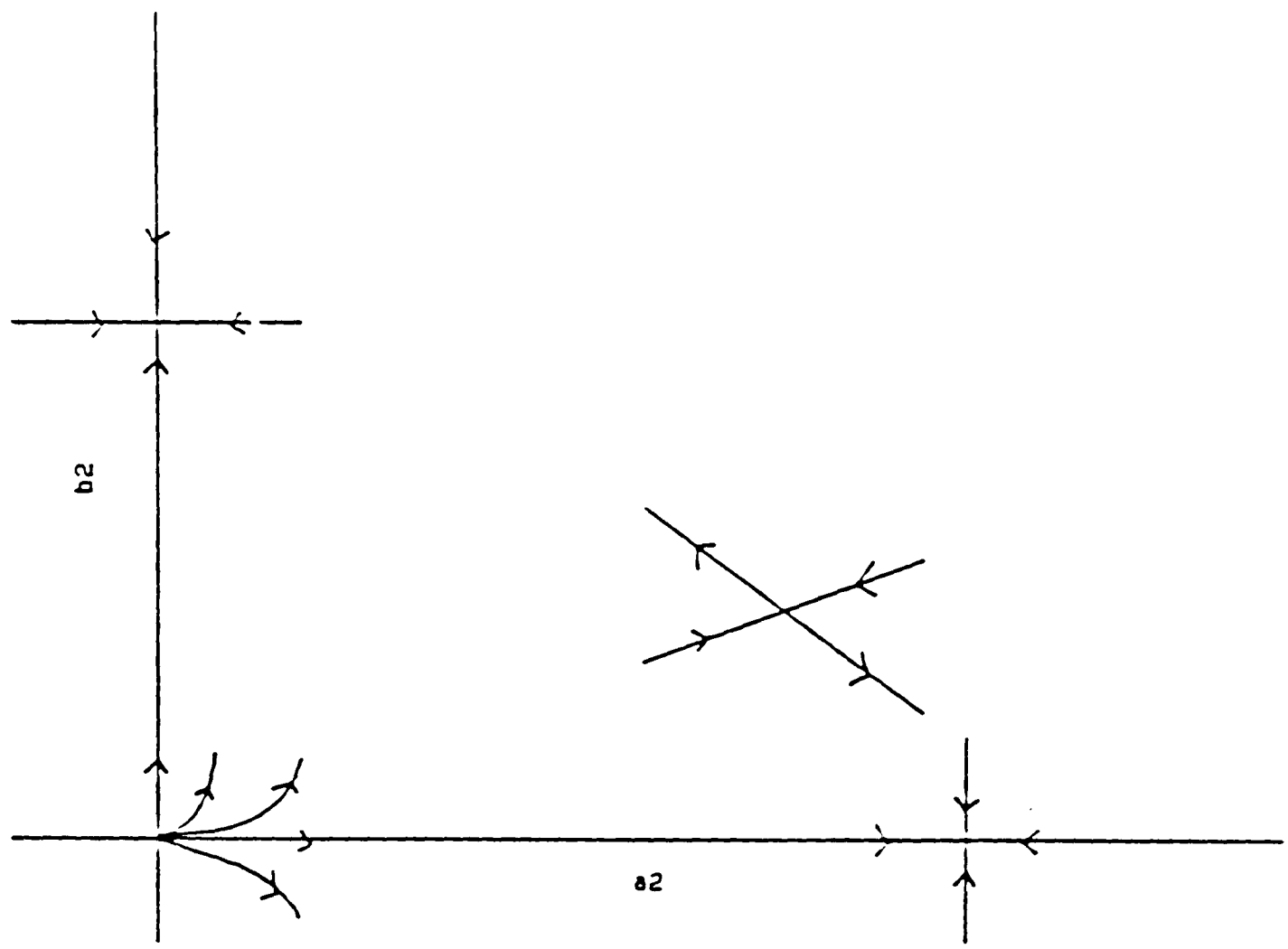

Figure 3.5: a_2, b_2 phase plane for (3.48).

unstable modes and as these are stripe patterns it would not be surprising if, when the pattern from the preceding stage is used as the initial condition, at the next stage a purely one dimensional pattern formed. In Figure 3.6 the patterns formed with a) $n = 4$ and b) $n = 8$ on a wider rectangle are shown to illustrate this. In Figure 3.7 the same type of pattern sequence as in Figure 3.3 is shown where now we are considering the boundary conditions at the ends of the rectangle to be fixed at $0.7\times(U_0, V_0)$ except in the first picture where we allow zero flux conditions else no pattern would form. In the next section we examine slightly modified versions of the Nagorcka model

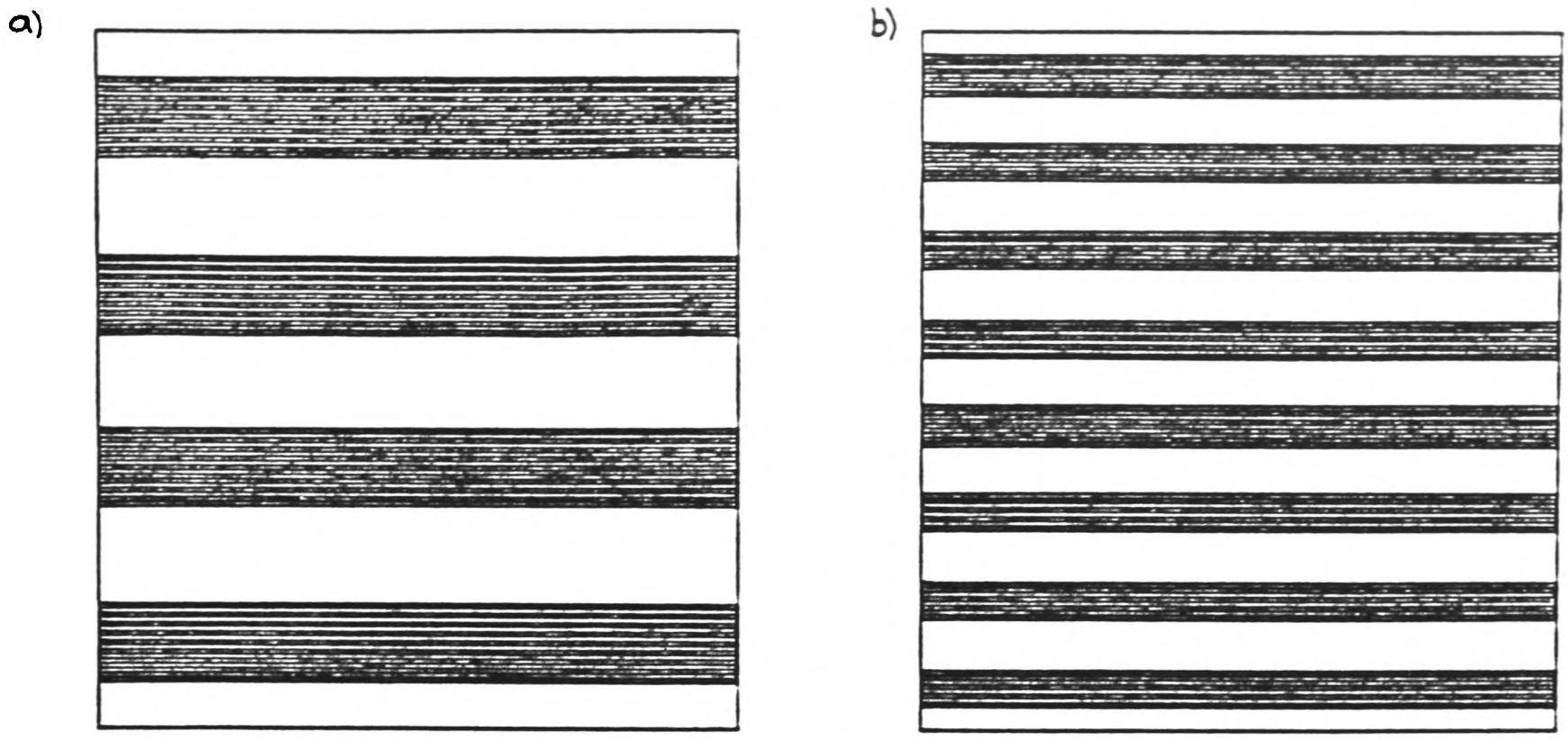

Figure 3.6: Pattern formed on a 20×21 grid with parameter values as in Figure 3.3 d) and e).

to see if we can determine the reason for the preference for stripes.

3.5 Modified Nagorcka Kinetics.

The Nagorcka reaction kinetics we have been considering up to now do not have any terms involving products of u and v and it could be this rather than the assumption of asymmetry that gives rise to the preference for striped patterns. To examine this posibility we consider the system

$$\begin{aligned} u_t &= n(-Au + B(\tanh sv + \frac{E}{B}u^2v)) + n^{-1}d\nabla^2 u \\ v_t &= n(-Cu + D(\tanh sv + \frac{E}{B}u^2v)) + n^{-1}\nabla^2 v. \end{aligned} \tag{3.59}$$

This is equivalent to (3.10), is asymmetric and, to a linear approximation about (0,0), is the same as (3.10) if we set $C = A\beta$, $D = B\beta\alpha$. The system (3.59) has only one steady state $u = v = 0$ as required if and only if

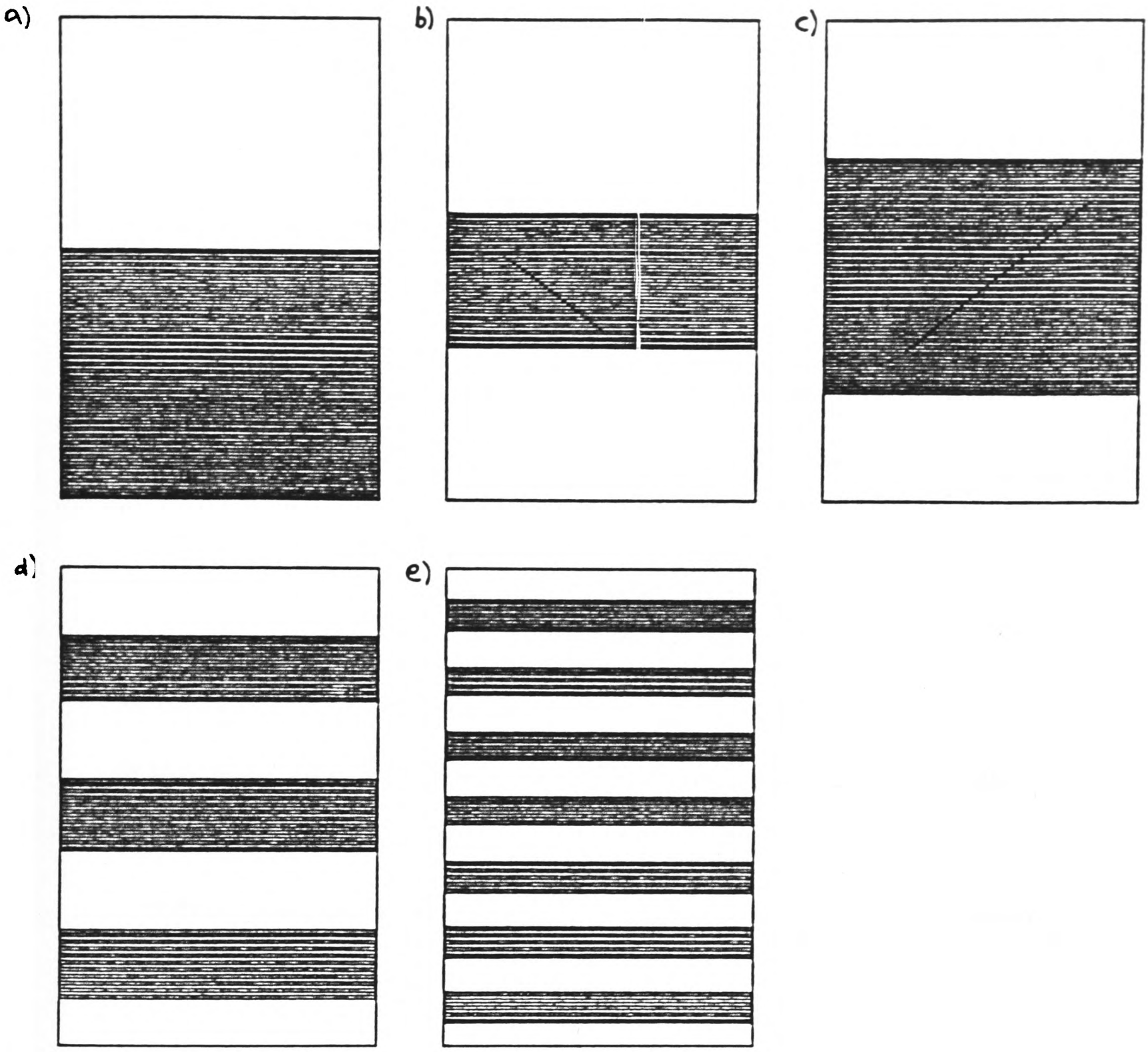

Figure 3.7: Pattern sequence on a 14×20 grid using fixed boundary conditions at the ends of the rectangle and parameter values as in Figure 3.3.

$AD - BC \neq 0$. If we apply a linear analysis to (3.59) we find that diffusion driven instability is possible if (*cf.* (3.8), (3.9)).

$$\begin{aligned} &i) \quad A - Ds > 0 \\ &ii) \quad BC - AD > 0 \\ &iii) \quad A - Dds < 0 \quad \Rightarrow d > 1 \\ &iv) \quad (A - Dds)^2 - 4ds(BC - AD) > 0 \\ &\qquad \Rightarrow d > d_c = \frac{2BC - AD + 2\sqrt{BC(BC - AD)}}{D^2 s}. \end{aligned} \tag{3.60}$$

A nonlinear bifurcation analysis in terms of regular tesselations of the plane as in Section 3.4 is then carried out. The analysis carries through exactly as before except at (3.49) where η_1, one of the coefficients arising from the suppression of secular terms, is now

$$\eta_1 = \frac{-(Bs^3 M_p^2 - 3E) n M_p (1 + \alpha\beta S_p)}{16(1 + S_p M_p)}. \tag{3.61}$$

So the same results would apply if $s^3 M_p^2 B - 3E > 0$. Numerical simulations of this model give similar results for the patterns, although in shape rather than size, to the original Nagorcka model (see Figure 3.3).

Let us now consider another model which has the same linear behaviour as (3.10) but is not asymmetric, such as

$$\begin{aligned} u_t &= n(-Au + B(\tanh sv + \frac{E}{B} u^2 v^2)) + n^{-1} d \nabla^2 u \\ v_t &= n(-Cu + D(\tanh sv + \frac{E}{B} u^2 v^2)) + n^{-1} \nabla^2 v. \end{aligned} \tag{3.62}$$

This model results in the same equations to $O(\epsilon^3)$ as the original Nagorcka model (if we set $C = A\beta$ and $D = B\beta\alpha$) and so its solutions to $O(\epsilon)$ are the same. This result seems to imply that asymmetry in the reaction kinetics is

not the essential prerequisite for sequential stripe formation. However when this model is simulated numerically, using random initial conditions at each stage, a different result to the normal horizontal stripes is obtained at certain stages. Figure 3.8 illustrates this different pattern.

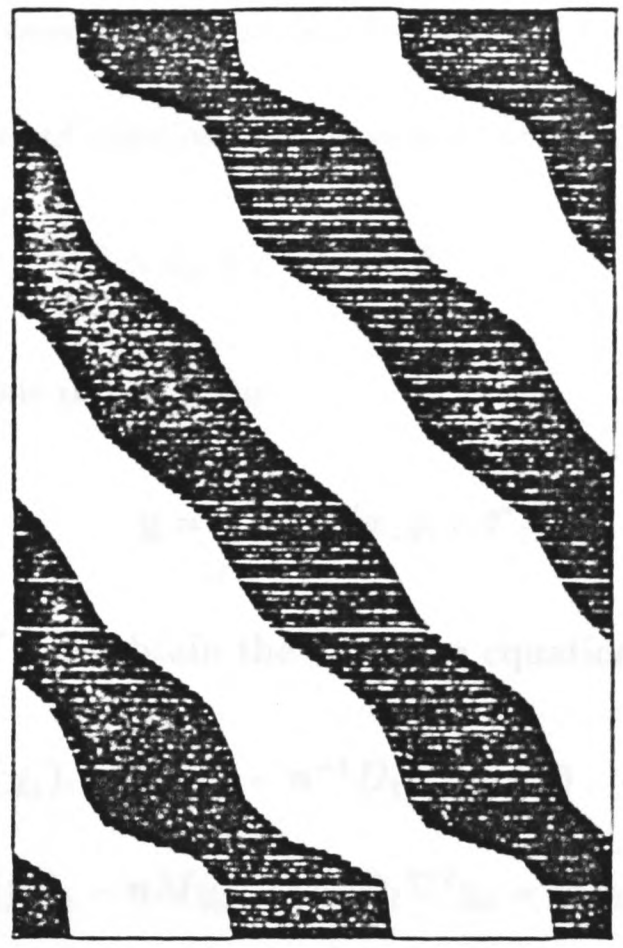

Figure 3.8: Pattern formed using random initial conditions for (3.62) on a 14 $\times$21 grid with parameter values $A = B = 23.1$, $C = 1.3$, $D = 1.04$, $d = 20$, $E = 20$, $n = 4$ and $\Delta x = \Delta y = 0.3$.

Apart from being identical from a linear point of view, what all three models considered so far have in common is that they all have their second derivatives, when evaluated at the steady state, identically equal to zero. So, let us now consider a model where at least one of the second derivatives is non-zero but is still identical from a linear viewpoint with the original

Nagorcka model, namely

$$\begin{aligned} u_t &= n(-Au + B(\tanh sv + \frac{E}{B}uv)) + n^{-1}d\nabla^2 u \\ v_t &= n(-Cu + D(\tanh sv + \frac{E}{B}uv)) + n^{-1}\nabla^2 v. \end{aligned} \tag{3.63}$$

Now we consider a nonlinear bifurcation analysis of this model and look for solutions in the form of regular tesselations of the plane. As before we let

$$d = d_c + \epsilon^2 \quad \tau = \epsilon^2 t \quad t^* = t \tag{3.64}$$

and look for solutions of the form

$$\underline{u} = \sum_{j=1} \epsilon^j \underline{u}_j(x, y, \tau, t^*). \tag{3.65}$$

Equating powers of ϵ we obtain the following equations

$$O(\epsilon) \qquad (\underline{u}_1)_t - nM\underline{u}_1 - n^{-1}D_1\nabla^2\underline{u}_1 = 0 \tag{3.66}$$

$$O(\epsilon^2) \qquad (\underline{u}_2)_t - nM\underline{u}_2 - n^{-1}D_1\nabla^2\underline{u}_2 = u_1 v_1 \frac{En}{B}\begin{pmatrix} B \\ D \end{pmatrix} \tag{3.67}$$

$$\begin{aligned} O(\epsilon^3) \qquad (\underline{u}_3)_t - nM\underline{u}_3 - n^{-1}D_1\nabla^2\underline{u}_3 &= -\frac{\partial \underline{u}_1}{\partial \tau} + n^{-1}Q\nabla^2\underline{u}_1 \\ &\quad -\frac{s^3 n v_1^3}{3}\begin{pmatrix} B \\ D \end{pmatrix} + \frac{En}{B}(u_1 v_2 + u_2 v_1)\begin{pmatrix} B \\ D \end{pmatrix}. \end{aligned} \tag{3.68}$$

Regular tesselation solutions of the plane as $t \to \infty$ are

$$\underline{u}_1 = \begin{pmatrix} 1 \\ M_p \end{pmatrix}(a(\tau)\cos kx \cos ly + b(\tau)\cos 2ly). \tag{3.69}$$

The solution to the $O(\epsilon^2)$ equation (3.67) is

$$\underline{u}_2 = \begin{pmatrix} 1 \\ M_p \end{pmatrix}(a_1(\tau)\cos kx \cos ly + b_1(\tau)\cos 2ly) - \underline{u}^* \tag{3.70}$$

where

$$L\underline{u}^* = M_p \frac{En}{B}(a(\tau)\cos kx \cos ly + b(\tau)\cos 2ly)^2 \begin{pmatrix} B \\ D \end{pmatrix}. \tag{3.71}$$

We note that

$$\begin{aligned}(a\cos kx\cos ly + b\cos 2ly)^2 &= \frac{a^2+2b^2}{4} + \frac{a^2}{4}\cos 2kx + \frac{a^2}{4}\cos 2ly \\ &+ \frac{a^2}{4}\cos 2kx\cos 2ly + \frac{b^2}{2}\cos 4ly \qquad (3.72)\\ &+ 4ab\cos^3 kx\cos ly - 2ab\cos kx\cos ly.\end{aligned}$$

The third and the last terms on the right hand side of (3.72) are of the same form as the original solution and so give rise to secular terms if we attempt to solve for $\underline{u}^*$. The only way we can avoid this is to use a different scaling for d and τ as compared with (3.64) and suppress secular terms at $O(\epsilon^2)$. We do this by replacing ϵ^2 with ϵ in (3.64) and considering solutions of the same form as (3.65).

The $O(\epsilon)$ equation arising from this and its solution in regular tesselations of the plane are identical to (3.14) and (3.45) respectively. However secular terms arise at $O(\epsilon^2)$ and can now be suppressed. The equivalent equation to (3.15) arising at $O(\epsilon^2)$ is

$$(\underline{u}_2)_t - nM\underline{u}_2 - n^{-1}D_1\nabla^2\underline{u}_2 = -\frac{\partial \underline{u}_1}{\partial\tau} + n^{-1}Q\nabla^2\underline{u}_1 + u_1v_1\frac{En}{B}\begin{pmatrix} B \\ D\end{pmatrix}. \quad (3.73)$$

The secular terms are suppressed in the normal way by making the right hand side of (3.73) orthogonal to

$$\begin{pmatrix} 1 \\ S_p\end{pmatrix}\cos kx\cos ly \quad \text{and} \quad \begin{pmatrix} 1 \\ S_p\end{pmatrix}\cos 2ly, \qquad (3.74)$$

the bounded solutions of the homogeneous adjoint equation. This leads to the simultaneous ordinary differential equations

$$\begin{aligned}\frac{da}{d\tau} &= \mu a + \eta ab \qquad & \mu &= \frac{-n^{-1}p^2}{1+S_pM_p} > 0\\ \frac{db}{d\tau} &= \mu b + \eta\frac{a^2}{4} \qquad & \eta &= \frac{EnM_p(B+DS_p)}{1+S_pM_p}.\end{aligned} \qquad (3.75)$$

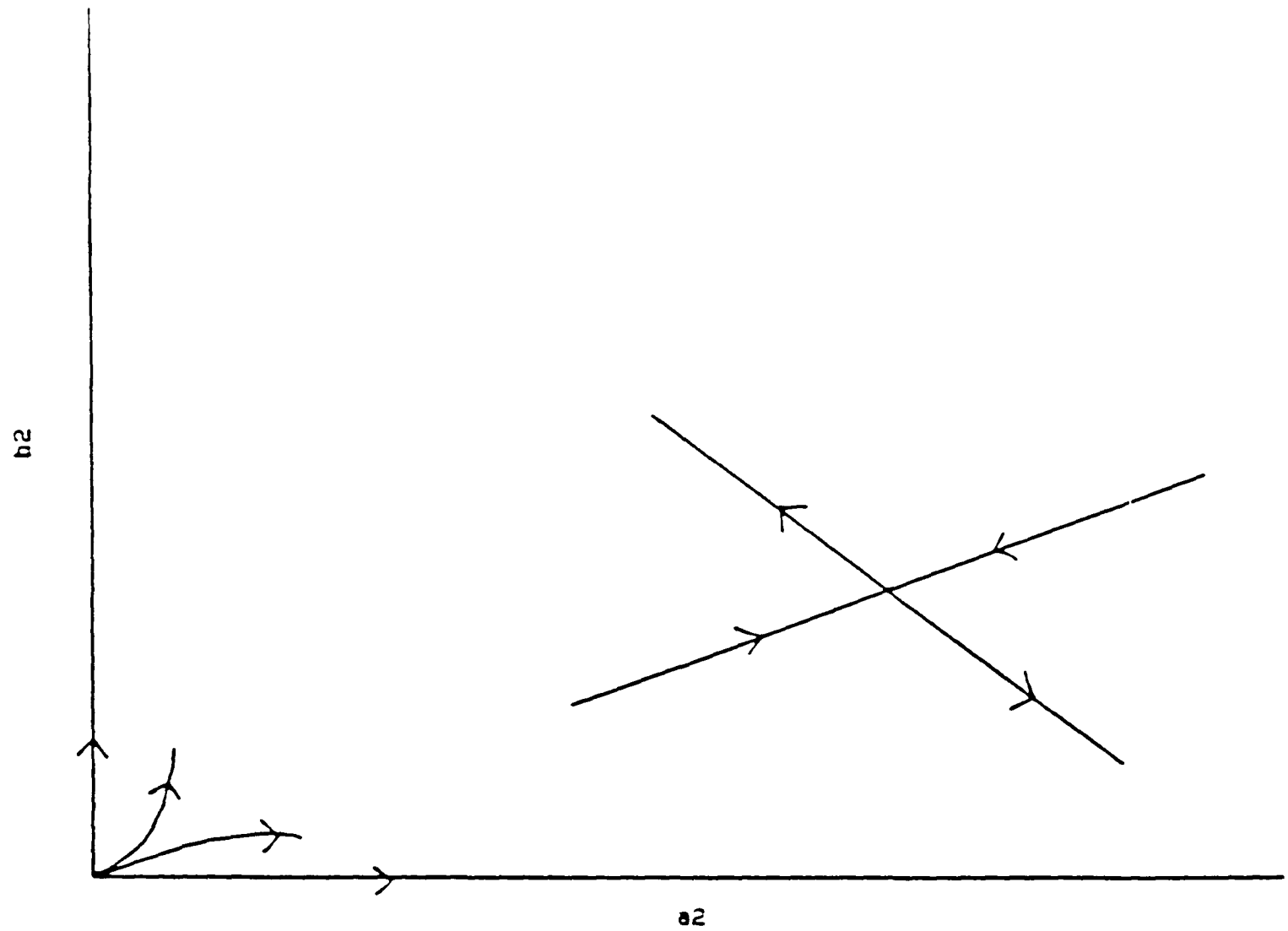

Figure 3.9: a, b phase plane for (3.75), drawn for $\eta < 0$.

A phase plane analysis on this system gives the following steady states and their stability :

$(0,0)$ is an unstable type *II* node.

$\left(2\left(\frac{\mu}{-\eta}\right), \left(\frac{\mu}{-\eta}\right)\right)$ is a saddle point with eigenvalues 2μ, $-\mu$ and corresponding eigenvectors $\begin{pmatrix} 1 \\ -1 \end{pmatrix}, \begin{pmatrix} 2 \\ 1 \end{pmatrix}$.

The phase plane for this system is shown in Figure 3.9. So for a model like this, solutions in regular tesselations of the plane are unstable when we consider both a and b to be non zero. If we consider a purely one-dimensional solution, namely

$$\underline{u}_1 = \begin{pmatrix} 1 \\ M_p \end{pmatrix} b(\tau) \cos 2ly \tag{3.76}$$

we can return to (3.64) as the scaling for d and τ and continue as normal.

The solution at $O(\epsilon^2)$ is

$$\underline{u}_2 = \begin{pmatrix} 1 \\ M_p \end{pmatrix} b_1(\tau)\cos 2ly - \underline{u}^* \tag{3.77}$$

where

$$L\underline{u}^* = \frac{EnM_p}{2B} b^2(\tau) \begin{pmatrix} B \\ D \end{pmatrix} (1+\cos 4ly). \tag{3.78}$$

If we look for solutions $\underline{u}^*$ of the form

$$\underline{u}^* = \underline{w}_1 + \underline{w}_2 \cos 4ly \tag{3.79}$$

we obtain

$$\underline{w}_1 = \frac{EM_p}{2B\Delta} \begin{pmatrix} Bg_v - Df_v \\ Df_u - Bg_u \end{pmatrix} \quad \underline{w}_2 = \frac{EnM_p}{2B\Delta_1} \begin{pmatrix} B(ng_v - 16n^{-1}l^2) - Dnf_v \\ D(nf_u - 16n^{-1}d_c l^2) - Bng_u \end{pmatrix} \tag{3.80}$$

where

$$\Delta = \begin{vmatrix} f_u & f_v \\ g_u & g_v \end{vmatrix} \quad \Delta_1 = \begin{vmatrix} nf_u - 16n^{-1}d_c l^2 & nf_v \\ ng_u & ng_v - 16n^{-1}l^2 \end{vmatrix} = 9n^2\Delta \tag{3.81}$$

and for ease of notation we are using the general forms f and g for the reaction kinetics. At $O(\epsilon^3)$ secular terms can arise. Suppressing these leads to the (Landau) equation

$$\frac{db}{d\tau} = \mu b + \eta b^3 \qquad \mu = \frac{-n^{-1}p^2}{1+S_pM_p} > 0 \tag{3.82}$$

$$\begin{aligned} \eta \; &= \frac{(B+DS_p)M_p n}{1+S_pM_p} \left[-\frac{s^3M_p^2}{4} + \frac{E^2}{2B^2\Delta}\left[-Df_u + M_pDf_v - M_pBg_v + Bg_u\right] \right. \\ &\left. + \frac{E^2}{18B^2n\Delta}\left[-D(nf_u - 16n^{-1}d_cl^2) + M_pDnf_v - M_pB(ng_v - 16n^{-1}l^2) + BNg_u\right] \right] \end{aligned}$$

which has a stable solution

$$b = \pm\left(\frac{\mu}{-\eta}\right)^{\frac{1}{2}}, \quad \text{if } \eta < 0. \tag{3.83}$$

This gives the following condition on E necessary for a stable one dimensional pattern to form (on substituting the values of f_u *etc.*), namely

$$E^2 < \frac{9s^2(P_1 + \sqrt{P_1Q_1})^2 Q_1(P_1 + Q_1 + 2\sqrt{P_1Q_1})}{D^2(4(Q_1 + \sqrt{P_1Q_1})(2P_1 + Q_1 + 3\sqrt{P_1Q_1}) - 10Q_1(P_1 + Q_1 + 2\sqrt{P_1Q_1}))} \tag{3.84}$$

where

$$P_1 = BC \quad Q_1 = BC - AD.$$

Considering solutions with b =0 we run into the same problems as before as terms like cos2ly appear at O(ϵ^2) and since this is a solution of the original equation (3.66) it gives rise to secular terms. In fact if we consider a general reaction diffusion system we will obtain the same result unless a specific condition is satisfied. This condition, which we derive in the next section is

$$\frac{\underline{F}_{uu}}{2} + M_p\underline{F}_{uv} + \frac{M_p^2\underline{F}_{vv}}{2} = 0 \tag{3.85}$$

where the partial derivatives are evaluated at the steady state and is automatically satisfied by any asymmetric reaction kinetics as they must have $\underline{F}_{uu} = \underline{F}_{uv} = \underline{F}_{vv} = 0$. In Figure 3.10 we show that (3.63) cannot have a stable solution in truly two dimensional tesselations of the plane. Figure 3.10a) is obtained from a linear analysis to discover what modes are unstable and will lead to pattern. This is used as the initial conditions for a numerical simulation using the same parameter values as for Figure 3.8. Although the initial pattern is a valid solution of the problem it does not remain and gives way to the numerically stable one dimensional pattern shown in Figure 3.10b).

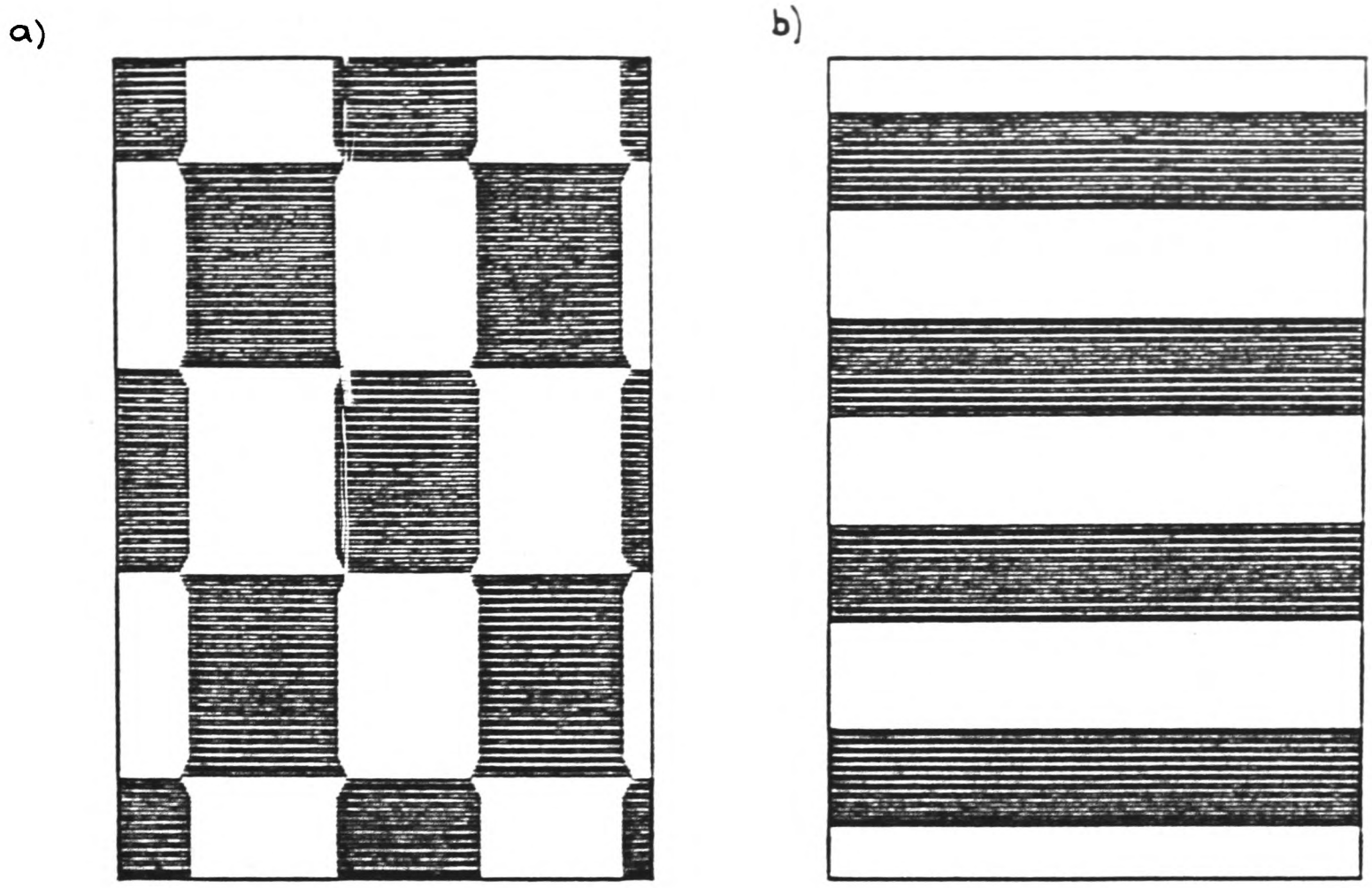

Figure 3.10: Numerical stability of a) two dimensional tesselations vs. b) one dimensional tesselations (3.63) solved on a 14×21 grid with parameters as in Figure 3.8.

3.6 Analysis of a general system.

In this section we consider the analysis of a general reaction diffusion system for heterogeneous spatial pattern in terms of regular tesselations of the plane.

Consider the system

$$\begin{aligned} u_t &= nf(u,v) + n^{-1}\nabla^2 u \\ v_t &= ng(u,v) + n^{-1}d\nabla^2 v. \end{aligned} \tag{3.86}$$

If we consider the scaling (3.64) and look for a solution of the form

$$\underline{u} = \underline{u}_0 + \sum_{j=1} \epsilon^j(x,y,\tau,t^*) \tag{3.87}$$

we obtain the following equations on equating powers of ϵ.

$$\begin{aligned} O(1) \qquad 0 &= nf(u_0, v_0) \\ 0 &= ng(u_0, v_0) \end{aligned} \tag{3.88}$$

$$O(\epsilon) \qquad (\underline{u}_1)_t \quad -nM\underline{u}_1 - n^{-1}D_2\nabla^2\underline{u}_1 = 0 \tag{3.89}$$

$$O(\epsilon^2) \qquad (\underline{u}_2)_t \quad -nM\underline{u}_2 - n^{-1}D_2\nabla^2\underline{u}_2 = \frac{\underline{F}_{uu}}{2}u_1^2 + \underline{F}_{uv}u_1v_1 + \frac{\underline{F}_{vv}}{2}v_1^2 \tag{3.90}$$

where

$$D_2 = \begin{pmatrix} 1 & 0 \\ 0 & d_c \end{pmatrix}.$$

If we look for solutions to (3.89) in terms of regular tesselations of the plane we obtain, as $t \to \infty$

$$\underline{u}_1 = \begin{pmatrix} 1 \\ M_p \end{pmatrix} (a(\tau)\cos kx \cos ly + b(\tau)\cos 2ly). \tag{3.91}$$

At $O(\epsilon^2)$ the solution is of the form

$$\underline{u}_2 = \begin{pmatrix} 1 \\ M_p \end{pmatrix} (a_1(\tau)\cos kx \cos ly + b_1(\tau)\cos 2ly) - \underline{u}^* \tag{3.92}$$

where

$$L\underline{u}^* = (a(\tau)\cos kx \cos ly + b(\tau)\cos 2ly)^2 \left[\frac{\underline{F}_{uu}}{2} + M_p\underline{F}_{uv} + \frac{M_p^2\underline{F}_{vv}}{2}\right]. \tag{3.93}$$

Now as

$$(\cos kx \cos ly)^2 = \frac{1}{4}(1 + \cos 2kx + \cos 2ly + \cos 2kx \cos 2ly) \tag{3.94}$$

we obtain secular terms at this stage unless

$$L\underline{u}^* = 0 \qquad ie. \quad \frac{\underline{F}_{uu}}{2} + M_p\underline{F}_{uv} + \frac{M_p^2\underline{F}_{vv}}{2} = 0. \tag{3.95}$$

Using the scaling (3.64) we cannot suppress these terms at this stage so we must use the scaling $d = d_c + \epsilon$, $\tau = \epsilon t$ which gives the following expression at $O(\epsilon^2)$

$$(\underline{u}_2)_t - nM\underline{u}_2 - n^{-1}D_2\nabla^2\underline{u}_2 = -\frac{\partial \underline{u}_1}{\partial \tau} + B_1\nabla^2\underline{u}_1 + \frac{\underline{F}_{uu}}{2}u_1^2 + \underline{F}_{uv}u_1v_1 + \frac{\underline{F}_{vv}}{2}v_1^2 \tag{3.96}$$

where

$$B_1 = \begin{pmatrix} 0 & 0 \\ 0 & 1 \end{pmatrix}.$$

We suppress the secular terms that arise here by making the right hand side of (3.96) orthogonal to $\begin{pmatrix} 1 \\ S_p \end{pmatrix} \cos kx \cos ly$ and $\begin{pmatrix} 1 \\ S_p \end{pmatrix} \cos 2ly$. This leads to the simultaneous ordinary differential equations

$$\begin{aligned} \frac{da}{d\tau} &= \mu a + \eta ab \qquad & \mu &= \frac{-n^{-1}p^2 M_p S_p}{1 + S_p M_p} \\ \frac{db}{d\tau} &= \mu b + \eta \frac{a^2}{4} \qquad & \eta &= \frac{n(f_{uu} + 2f_{uv} + f_{vv}) + nS_p(g_{uu} + 2g_{uv} + g_{vv})}{1 + S_p M_p}. \end{aligned} \tag{3.97}$$

Now

$$M_p S_p = -\frac{1}{d_c} \qquad 1 + S_p M_p = \frac{d_c - 1}{d_c}$$

so if

$$d_c \gtrless 1 \qquad 1 + S_p M_p \gtrless 0 \quad \Rightarrow \mu \gtrless 0.$$

A phase plane analysis of (3.97) shows that

$(0,0)$ is a $\left.\begin{matrix} \text{stable} \\ \text{unstable} \end{matrix}\right\}$ type *II* node depending upon $\mu \gtrless 0$.

$\left(2\left(\frac{\mu}{-\eta}\right), \left(\frac{\mu}{-\eta}\right)\right)$ is a saddle point with eigenvalues 2μ and $-\mu$ and corresponding eigenvectors $\begin{pmatrix} 1 \\ -1 \end{pmatrix}$ and $\begin{pmatrix} 2 \\ 1 \end{pmatrix}$.

The phase plane of this is the same as Figure 3.9. This result tells us that irrespective of the signs of μ, η no heterogeneous pattern in regular

tesselations of the plane are possible which are truly two-dimensional unless (3.95) is satisfied. Figure 3.11 shows a pattern formation sequence for the Schnackenberg system (1.32) which has been extensively used in the previous chapters. The parameter values used are $a = 0.25$, $b = 0.75$, $d_u = 0.227$ and $d_v = 5$. The third and fourth patterns in the sequence, although regular to some extent, do not satisfy the expressions given in (3.47) and so are not true tesselations of the plane. The only patterns which are regular are the striped patterns of the first and second pictures. In the next section we present some analysis which may begin to give some insight upon the formation of stripes on the surface of a cylindrical body.

3.7 Circumferential Homogeneity.

In this section we present an application of the theory of Kurata, Kishimoto and Yanagida (1989) to show that for a reaction diffusion system solved on the surface of a cylinder with sufficiently small radius, a banded pattern along the cylinder will occur. The method we consider requires reaction kinetics for which an invariant region exists. The system they analyse is written as (using the notation as in the paper)

$$\frac{\partial u(x,y,t)}{\partial t} = D\Delta u(x,y,t) + f(u(x,y,t)) \quad u \in \Re^2 \tag{3.98}$$

$$(x,y) \in \Omega \subset \Re^2, \quad t > 0, \quad u(x,y,0) = u_0(x,y), \quad \Omega = \Omega_1 \times \Omega_2.$$

The boundary conditions we consider here are written

$$\frac{\partial u(x,y,t)}{\partial n} = 0 \quad \text{on } \partial\Omega_1 \quad \Omega_1 = [0,a], \quad \Omega_2 = [0,l] \tag{3.99}$$

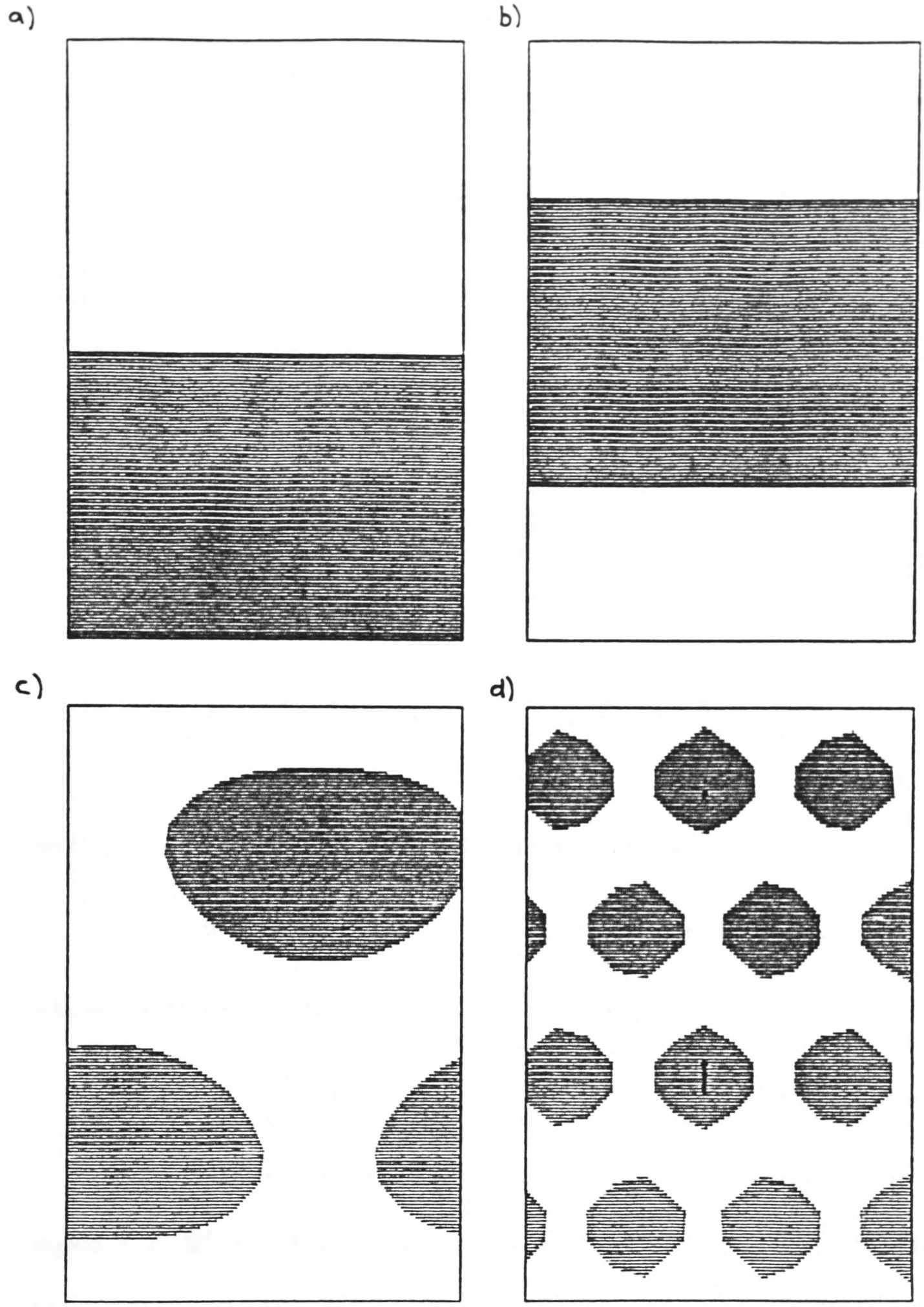

Figure 3.11: Pattern formation sequence using the Schnackenberg reaction kinetics on a 14×21 grid. Values of n and Δx, Δy are as for Figure 3.3 a)-d).

$$u(x,0,t) = u(x,l,t) \qquad \frac{\partial u(x,0,t)}{\partial n} = \frac{\partial u(x,l,t)}{\partial n}.$$

Introduce the notation

$$\nabla_x u = \left(\frac{\partial u}{\partial x}, 0\right) \quad \nabla_y u = \left(0, \frac{\partial u}{\partial y}\right) \quad \nabla u = \nabla_x u + \nabla_y u \quad \Delta_y u = \frac{\partial^2 u}{\partial y^2}. \tag{3.100}$$

$V(t)$, a measure of the inhomogeneity of u in the circumferential direction, is defined by

$$V(t) = \frac{1}{2}\int_0^l \int_0^a < \nabla_y u, \nabla_y u > dxdy \quad = \int_0^a U(x,t)dx \tag{3.101}$$

where

$$U(x,t) = \frac{1}{2}\int_0^l < \nabla_y u, \nabla_y u > dy \qquad < \nabla_y u, \nabla_y u >= \sum_{j=1}^{2} \left(\frac{\partial u_j}{\partial y}\right)\left(\frac{\partial v_j}{\partial y}\right) \tag{3.102}$$

and u_j, v_j are the jth components of u and v respectively.

$$V(t) = 0 \quad \Rightarrow u(x,y,t) = \overline{u}(x,t) \text{ holds for } (x,y) \in [0,a] \times [0,l]$$

where $\overline{u}(x,t)$ denotes the spatial average of $u(x,y,t)$ over Ω_2, namely

$$\overline{u}(x,t) = \frac{1}{l}\int_0^l u(x,y,t)dy. \tag{3.103}$$

Now we need the assumption that the system admits a compact invariant region $\Sigma \subset \Re^2$, *ie.* there exists a region Σ such that $u_0(x,y) \in \Sigma$ for all $(x,y) \in \Omega_1 \times \Omega_2$ implies that $u(x,y,t) \in \Sigma$ for all $(x,y) \in \Omega_1 \times \Omega_2$ and $t > 0$. This guarantees that the solution never diverges to infinity.

Let $d > 0$ be the smallest diagonal element of D,
let M_1 be defined by $M_1 = \max\{|df(u)| : u \in \Sigma\}$ and
let λ_1 be the smallest eigenvalue of $-\Delta_y$ on Ω with the given boundary conditions.

Now λ_1 is inversely proportional to the square of the length of Ω_2 $\left(\lambda_1 = \frac{4\pi^2}{l^2}\right)$ so we can take $\delta_1 = d\lambda_1 - M_1$ arbitarily large if we consider l sufficiently small. As we are considering the system equivalent to a cylinder $l = 2\pi r_1$ so $\lambda_1 = r_1^{-2}$. We denote the L^2 norm of a function v over Ω by

$$||v||_{L^2(\Omega)} = \int_0^l \int_0^a (v_1^2 + v_2^2) dx dy. \tag{3.104}$$

The result is formulated as follows. Assume that

i) $\delta_1 > 0$,

ii) $u_0(x,y) \in \Sigma \quad \forall (x,y) \in [0,a] \times [0,l]$,

iii) u is a solution of the system.

Then, $\exists$ a constant $c > 0$ such that $||u(x,y,t) - \overline{u}(x,t)||_{L^2(\Omega)} \leq ce^{-\delta_1 t}$.

Proof.

$$\begin{aligned}
\frac{\partial U}{\partial t} &= \int_0^l < \nabla_y u, \frac{\partial \nabla_y u}{\partial t} > dy \\
&= \int_0^l \{ < \nabla_y u, \nabla_y D\Delta u > + < \nabla_y u, \nabla_y f(u) > \} dy \\
&+ \left[\frac{\partial u_1}{\partial y} d_1 \Delta u_1 + \frac{\partial u_2}{\partial y} d_2 \Delta u_2 \right]_0^l \\
&= \int_0^l \{ - < \Delta_y u, D\Delta u > + < \nabla_y u, \nabla_y f(u) > \} dy \\
&+ \left[d_1 \frac{\partial u_1}{\partial y} \Delta u_1 + d_2 \frac{\partial u_2}{\partial y} \Delta u_2 \right]_0^l \\
&- \int_0^l < \Delta_y u, D\Delta_x u > dy \\
&\equiv K_1 + Z_1 - K_2.
\end{aligned} \tag{3.105}$$

Conway *et al.* (1978) showed that $K_1 \leq -2\delta_1 U(x,t)$. We now consider Z_1

$$Z_1 = \left[d_1 \frac{\partial u_1}{\partial y} \Delta u_1 + d_2 \frac{\partial u_2}{\partial y} \Delta u_2 \right]_0^l = \left[\frac{\partial u_1}{\partial y} (-f_1(u) + \frac{\partial u_1}{\partial t}) + \frac{\partial u_2}{\partial y} (-f_2(u) + \frac{\partial u_2}{\partial t}) \right]_0^l \tag{3.106}$$

$$\text{but} \quad \left. \frac{\partial u_i}{\partial y} \right|_{y=0} = \left. \frac{\partial u_i}{\partial y} \right|_{y=l} \qquad u_i|_{y=0} = u_i|_{y=l}\,.$$

$$\Rightarrow Z_1 = 0. \tag{3.107}$$

Let (.,.) denote the two dimensional inner product. The most technical point of the proof is to notice the following inequality:

$$\begin{aligned}
\int_0^a K_2 dx &= \int_0^l \int_0^a (\Delta_x u, D\Delta_y u) dx dy \\
&= \int_0^a \left\{ \left[d_1 \frac{\partial u_1}{\partial y} \frac{\partial^2 u_1}{\partial x^2} + d_2 \frac{\partial u_2}{\partial y} \frac{\partial^2 u_2}{\partial x^2} \right]_0^l \right\} dx \\
&- \int_0^a \int_0^l < \nabla_y u, \nabla_y D\Delta u > dy dx \\
&= \alpha_1 - \int_0^a \int_0^l < \nabla_y u, \nabla_y D\Delta u > dy dx \\
&= \alpha_1 - \int_0^l \left\{ \left[d_1 \frac{\partial u_1}{\partial y} \frac{\partial^2 u_1}{\partial x \partial y} + d_2 \frac{\partial u_2}{\partial y} \frac{\partial^2 u_2}{\partial x \partial y} \right]_0^a \right\} dy \\
&+ \int_0^l \int_0^a < \nabla_x \nabla_y u, D\nabla_y \nabla_x u > dx dy \\
&= \alpha_1 + \beta_1 + \int_0^l \int_0^a \left\{ d_1 \left(\frac{\partial^2 u_1}{\partial x \partial y} \right)^2 + d_2 \left(\frac{\partial^2 u_2}{\partial x \partial y} \right)^2 \right\} dx dy.
\end{aligned} \tag{3.108}$$

Now

$$\alpha_1 = \int_0^a \left\{ \left[d_1 \frac{\partial u_1}{\partial y} \frac{\partial^2 u_1}{\partial x^2} + d_2 \frac{\partial u_2}{\partial y} \frac{\partial^2 u_2}{\partial x^2} \right]_0^l \right\} dx$$

$$\text{but } u_i|_{y=0} = u_i|_{y=l} \quad \left. \frac{\partial u_i}{\partial y} \right|_{y=0} = \left. \frac{\partial u_i}{\partial y} \right|_{y=l} \Rightarrow \alpha_1 = 0.$$

$$\beta_1 = \int_0^l \left\{ \left[d_1 \frac{\partial u_1}{\partial y} \frac{\partial^2 u_1}{\partial x \partial y} + d_2 \frac{\partial u_2}{\partial y} \frac{\partial^2 u_2}{\partial x \partial y} \right]_0^a \right\} dy$$

$$\text{but } \left. \frac{\partial u_i}{\partial x} \right|_{x=0,a} \quad \forall y \quad \Rightarrow \beta_1 = 0$$

$$\Rightarrow \quad \int_0^a K_2 dx \geq 0.$$

Thus we have

$$\frac{dV(t)}{dt} = \frac{1}{2} \int_0^a (K_1 - K_2) dx \quad \leq -\delta_1 V(t) \tag{3.109}$$

$$\Rightarrow V(t) \leq c e^{-\delta_1 t}.$$

The result follows directly from this inequality and Lemma A.2 of Conway *et al.* (1978) which says

$$\lambda_1 \left| \left| u(x,y,t) - \overline{u}(x,t) \right| \right|_{L^2(\Omega)} \leq \left| \left| \nabla_y u(x,y,t) \right| \right|_{L^2(\Omega)}.$$

This concludes the proof.

The above analysis shows that periodic patterns will not occur in the circumferential direction for cylinders with sufficiently small radii. The analysis requires that the reaction kinetics admit a compact invariant region, and whilst it is possible to construct invariant regions for both the Nagorcka (3.3) and the Schnackenberg (1.32) kinetics, as shown here in Figures 3.12 and 3.13, they are only invariant for the diffusionless problem. When diffusion is added to the system, a necessary condition (Grindrod pers. comm.) for the region to still be invariant is that the normal vectors to the boundary, at every point of the boundary, must be left eigenvectors of the diffusion matrix. For the type of problem we are dealing with this implies that the boundary must be rectangular as the normals must be either $\begin{pmatrix} 1 \\ 0 \end{pmatrix}$ or $\begin{pmatrix} 0 \\ 1 \end{pmatrix}$. Thus we cannot apply the theory of this section directly to the problem we have been considering in the rest of the chapter. However, in most cases, when the full system is solved numerically, the solutions do not "blow-up" but remain relatively near the steady state and so can be considered to be confined in a non-rigorous sense. We can then use the theory of Kurata *et al.* (1989) to begin to explain mathematically why stripes will form along the cylinder.

3.8 Conclusion.

The work we have presented in this chapter seems to indicate that while asymmetry in the reaction kinetics may have a strong effect on stripe formation it is not essential. The major cause of the sequential appearance of

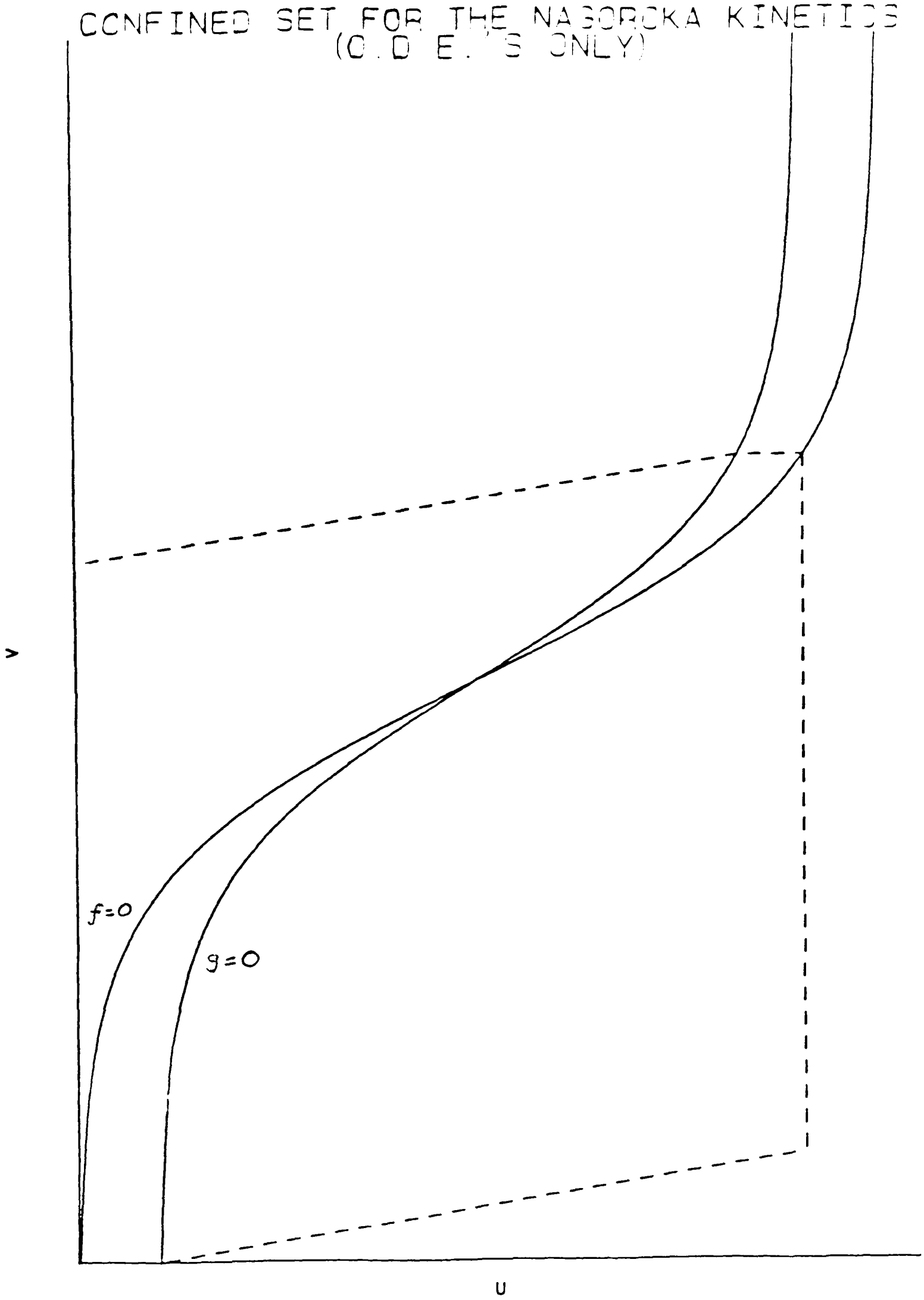

Figure 3.12: An invariant region for the diffusionless problem for the Nagorcka kinetics (3.3).

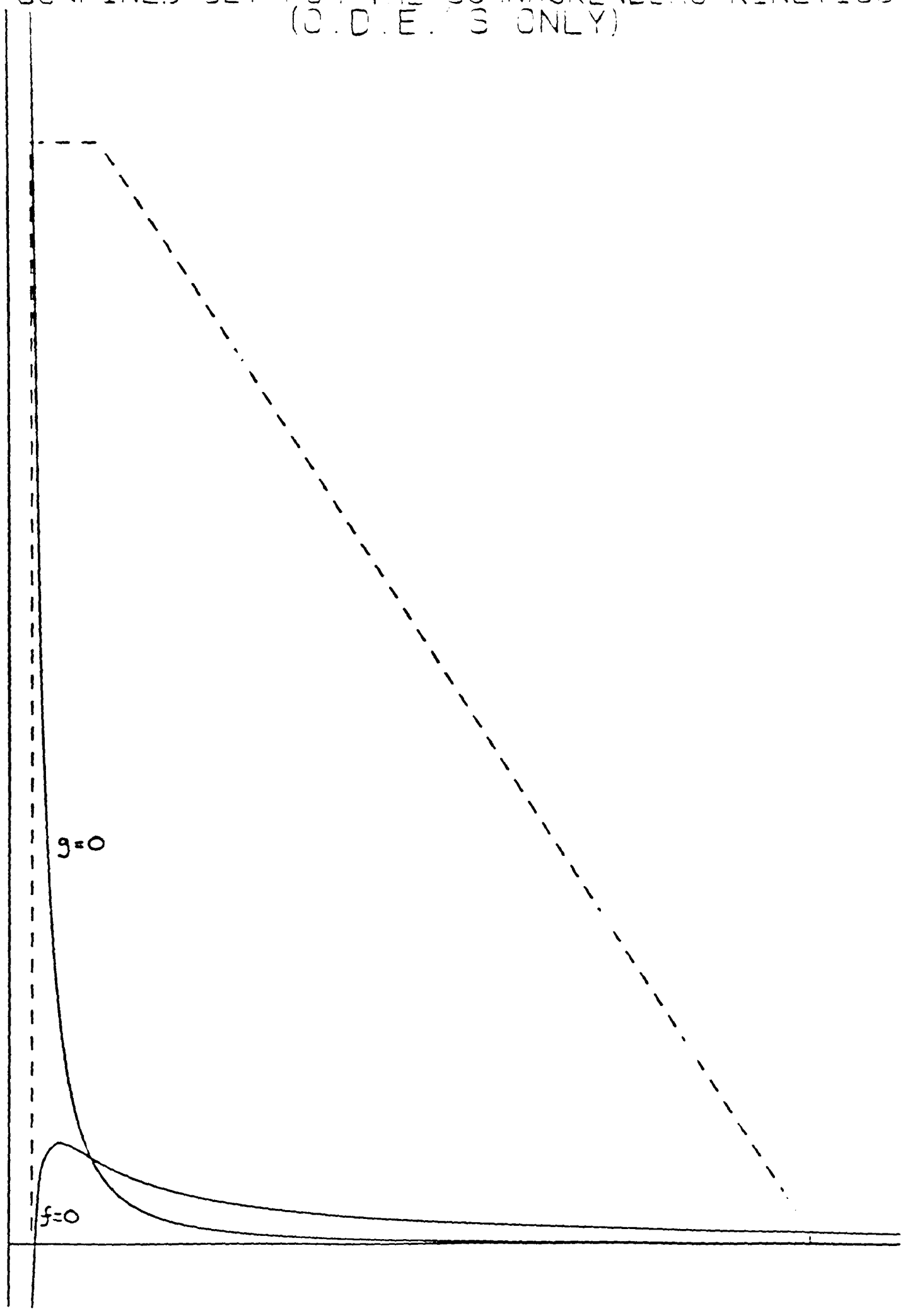

Figure 3.13: An invariant region for the diffusionless problem for the Schnackenberg kinetics (1.32).

striped patterns using these reaction kinetics appears to be the fixed boundary conditions at the ends of the cylinder and the fact that at each stage the initial conditions are taken to be invariant in the circumferential direction. Figure 3.11 shows that this cannot explain matters entirely or the Schnackenberg kinetics would also produce a striped pattern sequence. The Nagorcka model is quite robust with respect to changes in the parameter values and will still produce the same pattern sequence on a 14×21 grid, for example, when a 10% change in the parameter values is made, both when each value is changed individually or when all are changed at once.

An alternative mechanism has been suggested by Lacalli, Wilkinson and Harrison (1988) to produce the final seven stripe pattern exhibited in the gene expression of *fushi tarazu* in the *Drosophila* embryo. While they do not claim their mechanism to be exceptionally realistic, they illustrate, by means of numerical simulations, that a spatial gradient in some of the reaction parameters can give rise to a striped pattern perpendicular to the gradient. In the next chapter we examine briefly this and other types of model with spatially varying parameters to see if they can produce any types of pattern which have proved impossible to produce using reaction diffusion systems with spatially constant parameters.

Chapter 4

Reaction Diffusion Systems with Space Varying Parameters.

4.1 Introduction.

In this chapter we consider reaction diffusion systems with spatial variation in the model parameters to see if any different patterns can be obtained. Very little work has been carried out on models of this type. Most recently Almirantis and Nicolis (1987) have applied a nonlinear bifurcation analysis to a one dimensional system with zero-flux boundary conditions and a small gradient in one of the reaction parameters. We review this work in Section 4.2. Lacalli, Wilkinson and Harrison (1988) have numerically solved a variant of the Brusselator mechanism with spatial gradients in the reaction parameters to examine what effects this can have. They relate their results to some of the data available on stripe formation and expression of a segmentation gene like *fushi tarazu (ftz)* in the *Drosophila* embryo. We examine this and another type of model on a cylindrical domain in Section 4.3. Finally in Section 4.4 we examine the effects of space varying diffusion coefficients both

on domains with zero-flux boundary conditions all round and on domains modelling the *Drosophila* blastoderm.

4.2 Gradients in Reaction Parameters (i).

In this section we first review the analytical work of Almirantis and Nicolis (1987) who showed, via a bifurcation analysis, that a slight asymmetry in the system could give rise to a marked asymmetry in the resulting dissipative structures. Their analysis was carried out on a general one dimensional system and then extended to three dimensions. They relate their results to the problem of chirality and the fundamental asymmetry of the arrangement of the internal organs in vertabrates, known as *situs rectus*. We then present an analysis of the Schnackenberg system in two space dimensions and show that a one dimensional spatial gradient in one of the reaction parameters has no effect on the pattern produced. This is fully in line with the findings of Almirantis and Nicolis (1987).

The general system they considered is of the form

$$\begin{aligned} \frac{\partial U}{\partial t} &= A + f(U,V,\lambda) + D_u \frac{\partial^2 U}{\partial x^2} \\ \frac{\partial V}{\partial t} &= g(U,V,\lambda) + D_v \frac{\partial^2 V}{\partial x^2} \qquad (4.1) \\ \left.\frac{\partial U}{\partial x}\right|_{0,L} &= \left.\frac{\partial V}{\partial x}\right|_{0,L} = 0 \\ A > 0 \qquad f(0,0) &= g(0,0) = 0 \qquad 0 \le x \le L \end{aligned}$$

where it is assumed that the system (4.1), when operating in a uniform enviroment, will produce a stable spatial pattern by diffusion driven instability

when the parameter λ exceeds λ_c. The precursor A is assumed to have the form of a shallow gradient.

$$A = A_0 + ex. \tag{4.2}$$

The problem is then scaled by letting

$$\begin{aligned} u &= U - U_0 & v &= V - V_0 \\ u &= \epsilon u_1 + \epsilon^2 u_2 + \ldots & v &= \epsilon v_1 + \epsilon^2 v_2 + \ldots \\ \lambda - \lambda_c &= \epsilon\gamma_1 + \epsilon^2\gamma_2 + \ldots & e &= \epsilon^3\overline{e}. \end{aligned} \tag{4.3}$$

The choice of e to be $O(\epsilon^3)$ is inherent in the form of the equations with the boundary conditions. In fact, if lower order terms are used in the expression for e then to solve the system these terms must vanish, a something we prove in the second half of this section. If, however, terms of higher order than $O(\epsilon^3)$ are considered these make no contribution to the leading order terms of u and v. At $O(\epsilon)$ we have

$$L_c \begin{pmatrix} u_1 \\ v_1 \end{pmatrix} = 0 \qquad L_c = L(\lambda_c) \tag{4.4}$$

where

$$L(\lambda) = \begin{pmatrix} \frac{\partial f}{\partial U} + D_u \frac{\partial^2}{\partial x^2} & \frac{\partial f}{\partial V} \\ \frac{\partial g}{\partial U} & \frac{\partial g}{\partial V} + D_v \frac{\partial^2}{\partial x^2} \end{pmatrix}. \tag{4.5}$$

Because of the form of the boundary conditions the solution may be written as

$$\begin{pmatrix} u_1 \\ v_1 \end{pmatrix} = J\underline{\omega}\cos(k_c x) \qquad k_c = \frac{m\pi}{L} \tag{4.6}$$

where J is an as yet undetermined constant, k_c is the critical wavenumber corresponding to the bifurcation occuring at $\lambda = \lambda_c$ and $\underline{\omega}$ is a normalised

eigenvector of $\hat{L}(\lambda_c)$ (=$L(\lambda_c)$ with $-k_c^2$ replacing $\frac{\partial^2}{\partial x^2}$). At $O(\epsilon^2)$ the equation is

$$-L_c \begin{pmatrix} u_2 \\ v_2 \end{pmatrix} = \gamma_1 \left(\frac{\partial L}{\partial \lambda}\right)_{\lambda=\lambda_c} \begin{pmatrix} u_1 \\ v_1 \end{pmatrix} + \begin{pmatrix} h_{u_2} \\ h_{v_2} \end{pmatrix} \tag{4.7}$$

where h_{u_2},h_{v_2} are the quadratic nonlinearities of the functions f and g. By invoking symmetry arguments the following solution to (4.7) is obtained as γ_1 is found to be zero:

$$\begin{pmatrix} u_2 \\ v_2 \end{pmatrix} = J^2 \left(\underline{q}_0 + \underline{q}_{2k_c} \cos(2k_c x)\right). \tag{4.8}$$

Here $\underline{q}_0$ and $\underline{q}_{2k_c}$ depend upon the specific forms of f and g. At $O(\epsilon^3)$ the effect of the gradient first becomes relevant.

$$-L_c \begin{pmatrix} u_3 \\ v_3 \end{pmatrix} = \gamma_2 \left(\frac{\partial L}{\partial \lambda}\right)_{\lambda=\lambda_c} \begin{pmatrix} u_2 \\ v_2 \end{pmatrix} + \begin{pmatrix} \overline{e}x \\ 0 \end{pmatrix} + \begin{pmatrix} h_{u_3} \\ h_{v_3} \end{pmatrix} \tag{4.9}$$

where h_{u_3}, h_{v_3} involve the cubic nonlinearities and products of the quadratic and linear terms. To obtain a solution to this multiply both sides of (4.9) by $\underline{\omega}^* \cos(k_c x)$, the eigenvector of the adjoint of L_c, and integrate over space. This gives

$$\begin{aligned} \gamma_2 J \int_0^L \underline{\omega}^* \left(\frac{\partial L}{\partial \lambda}\right)_{\lambda=\lambda_c} \underline{\omega} \cos^2 k_c x dx \quad &+ \int_0^L \underline{\omega}^* \cos(k_c x) \underline{h}_3 dx \\ &+ \overline{e}\underline{\omega}^* \int_0^L x \cos(k_c x) dx \quad = 0. \end{aligned} \tag{4.10}$$

The third term in this equation is non-zero if $k_c L/\pi = m$ is odd. Assuming this to be the case (4.10) can then be written as

$$ed + (\lambda - \lambda_c) P_1 z + P_3 z^3 = 0 \tag{4.11}$$

where $z = \epsilon J$, the equivalent, using this method of bifurcation analysis, of the Landau equation. Here d,P_1,P_3 are system dependent parameters.

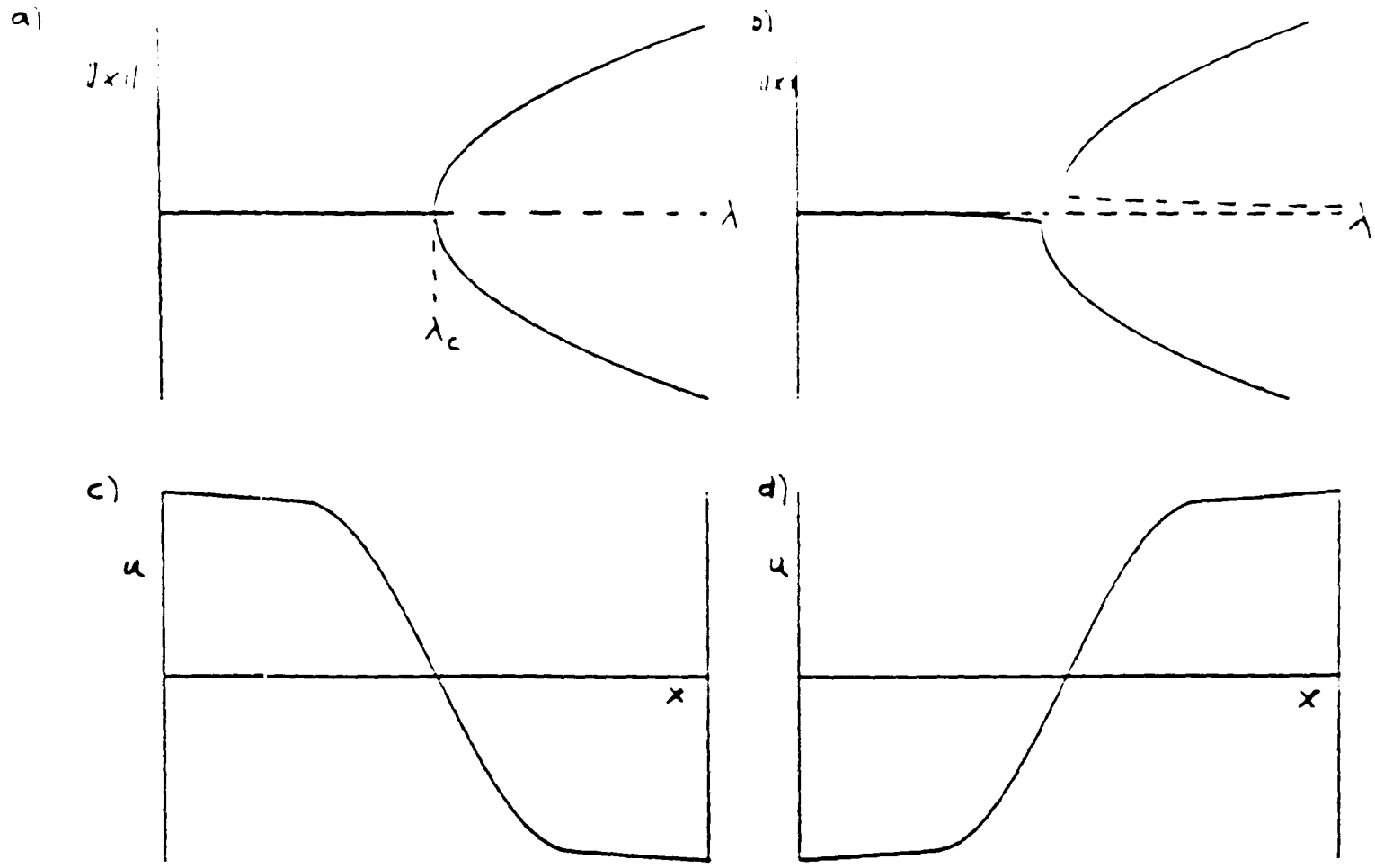

Figure 4.1: Bifurcation diagram for (4.1) with a) $e = 0$, b) $e \neq 0$. Pictures c) and d) show the resulting dissipative structures, both of wavenumber one, with opposite polarities corresponding to the two different branches in b).

Solving this it is seen that the amplitude of the pattern to dominant order of perturbation theory is $e^{1/3}$. This is a tremendous amplification of the original asymmetry. Figure 4.1 (Almirantis and Nicolis (1987) Figures 4+5) shows the bifurcation diagram for such a system with and without the gradient. The gradient has induced a choice between the two solution branches which, because of the assumption that m is odd, are polar patterns of opposite polarity. The analysis is then extended to three spatial dimensions where the variation of A is taken to be of the form

$$A(x, y, z) = A_0 + e\alpha(x, y, z) \tag{4.12}$$

It is established that the spatial variation will only make a contribution to

the bifurcation analysis if a certain condition is satisfied by the variation, namely

$$\int_0^{L_x}\int_0^{L_y}\int_0^{L_z} \alpha(x,y,z)\cos(k_c z)\cos(k_c y)\cos(k_c x)dzdydx \neq 0. \qquad (4.13)$$

We now consider an analysis of the Schnackenberg system, which does not have quite the same form as (4.1), under the same type of boundary conditions on a two dimensional domain. The system we consider is of the form

$$\begin{aligned} u_t &= \gamma(a_0 + \epsilon^n a_1 \frac{x}{r} + u^2 v - u) + \nabla^2 u \\ v_t &= \gamma(b - u^2 v) + d\nabla^2 v. \end{aligned} \qquad (4.14)$$

For convenience in the analysis to follow we take $\gamma = 1$. For $n \geq 2$ the gradient term $\epsilon^n a_1 \frac{x}{r}$ does not contribute to the linear analysis and we find that the normal parameter conditions (1.10), (1.18) and (1.22) for diffusion driven instability, as discussed in Chapter One, will apply. We now consider a bifurcation analysis in the usual way using the scaling as in (3.64). Equating powers of ϵ we obtain

$$O(\epsilon) \qquad \frac{\partial}{\partial t}\begin{pmatrix} u_1 \\ v_1 \end{pmatrix} - \begin{pmatrix} f_u & f_v \\ g_u & g_v \end{pmatrix}\begin{pmatrix} u_1 \\ v_1 \end{pmatrix} - \begin{pmatrix} 1 & 0 \\ 0 & d_c \end{pmatrix}\nabla^2\begin{pmatrix} u_1 \\ v_1 \end{pmatrix} = \frac{\delta}{r}\begin{pmatrix} a_1 x \\ 0 \end{pmatrix} \qquad (4.15)$$

where

$$\delta = 1 \quad \text{if} \quad n = 1 \qquad\qquad \delta = 0 \quad \text{if} \quad n \geq 2.$$

If we try to solve this we obtain as $t \to \infty$

$$\begin{pmatrix} u_1 \\ v_1 \end{pmatrix} = \begin{pmatrix} \overline{u}_1 \\ \overline{v}_1 \end{pmatrix} + \frac{\delta a_1 x}{r(f_u g_v - f_v g_u)}\begin{pmatrix} -g_v \\ g_u \end{pmatrix} \qquad (4.16)$$

where

$$\begin{pmatrix} \overline{u}_1 \\ \overline{v}_1 \end{pmatrix}_t - \begin{pmatrix} f_u & f_v \\ g_u & g_v \end{pmatrix} \begin{pmatrix} \overline{u}_1 \\ \overline{v}_1 \end{pmatrix} - \begin{pmatrix} 1 & 0 \\ 0 & d_c \end{pmatrix} \nabla^2 \begin{pmatrix} \overline{u}_1 \\ \overline{v}_1 \end{pmatrix} = 0. \qquad (4.17)$$

When we attempt to solve this with zero-flux boundary conditions on an $r \times s$ rectangle we find that this is not possible.

Proof.

$$\begin{pmatrix} u_1 \\ v_1 \end{pmatrix} = \begin{pmatrix} 1 \\ M_p \end{pmatrix} \sum \; (a_{p_x} \cos(p_x x) + b_{p_x} \sin(p_x x))(c_{p_y} \cos(p_y y) + d_{p_y} \sin(p_y y)) + \frac{\delta a_1 x}{r(f_u g_v - f_v g_u)} \begin{pmatrix} -g_v \\ g_u \end{pmatrix} \qquad (4.18)$$

as $t \to \infty$. For zero-flux in the y direction we require

$$d_{p_y} = 0 \qquad p_y = \frac{n_y \pi}{s}. \qquad (4.19)$$

For zero-flux in the x direction we require

$$\begin{pmatrix} 1 \\ M_p \end{pmatrix} \sum p_x \; (-a_{p_x} \sin(p_x x) + b_{p_x} \cos(p_x x)) c_{p_y} \cos(p_y y) + \frac{\delta a_1 / r}{f_u g_v - f_v g_u} \begin{pmatrix} -g_u \\ g_v \end{pmatrix} = 0 \qquad (4.20)$$

on $x = 0,r \; \forall$y. If n_y is odd we consider $y{=}s/2 \Rightarrow \delta = 0$. If n_y is even, *i.e.* $n_y = 2^j w$ where w is odd, we consider $y = s/2^{(j+1)} \Rightarrow \delta = 0$. Thus no solution with $\delta \neq 0$ is possible so we need $n \geq 2$. Now the zero-flux boundary conditions tell us that

$$b_{p_x} = 0 \qquad p_x = \frac{n_x \pi}{r}. \qquad (4.21)$$

At $O(\epsilon^2)$ we have

$$\frac{\partial}{\partial t} \begin{pmatrix} u_2 \\ v_2 \end{pmatrix} - \begin{pmatrix} f_u & f_v \\ g_u & g_v \end{pmatrix} \begin{pmatrix} u_2 \\ v_2 \end{pmatrix} - \begin{pmatrix} 1 & 0 \\ 0 & d_c \end{pmatrix} \nabla^2 \begin{pmatrix} u_2 \\ v_2 \end{pmatrix} = (2u_0 v_1 u_1 + v_0 u_1^2) \begin{pmatrix} 1 \\ -1 \end{pmatrix} + \frac{\delta_1 a_1}{\mathrm{r}} \begin{pmatrix} x \\ 0 \end{pmatrix} \qquad (4.22)$$

where

$$\delta_1 = 1 \quad \text{if} \quad n = 2 \qquad\qquad \delta_1 = 0 \quad \text{if} \quad n \geq 3.$$

A similar argument at this stage tells us that $n \geq 3$. If we consider $n \geq 4$ then the first order terms can be evaluated fully without involving the gradient. Hence we must consider $n = 3$. The equation at $O(\epsilon^3)$ is

$$\begin{aligned} \frac{\partial}{\partial t}\begin{pmatrix} u_3 \\ v_3 \end{pmatrix} &- \begin{pmatrix} f_u & f_v \\ g_u & g_v \end{pmatrix}\begin{pmatrix} u_3 \\ v_3 \end{pmatrix} - \begin{pmatrix} 1 & 0 \\ 0 & d_c \end{pmatrix}\nabla^2\begin{pmatrix} u_3 \\ v_3 \end{pmatrix} \\ &= (2u_0(u_1v_2 + u_2v_1) + u_1^2v_1 + 2v_0u_1u_2)\begin{pmatrix} 1 \\ -1 \end{pmatrix} \\ &+ \begin{pmatrix} 0 & 0 \\ 0 & 1 \end{pmatrix}\nabla^2\begin{pmatrix} u_1 \\ v_1 \end{pmatrix} - \frac{\partial}{\partial \tau}\begin{pmatrix} u_1 \\ v_1 \end{pmatrix} + \frac{a_1}{\mathrm{r}}\begin{pmatrix} x \\ 0 \end{pmatrix}. \end{aligned} \tag{4.23}$$

Secular terms can occur at this stage. They are suppressed by making the right hand side of (4.23) orthogonal to $\begin{pmatrix} 1 \\ S_p \end{pmatrix}\cos(p_x x)\cos(p_y y)$. The term involving the gradient makes a contribution of

$$\int_0^r \int_0^s a_1 x \cos\left(\frac{n_x \pi x}{r}\right)\cos\left(\frac{n_y \pi y}{s}\right) dydx = 0. \tag{4.24}$$

This tells us that in two space dimensions with zero-flux boundary conditions and $a = a_0 + \epsilon^2\beta(x, y)$, we need

$$\int_0^r \int_0^s \beta(x, y)\cos\left(\frac{n_x \pi x}{r}\right)\cos\left(\frac{n_y \pi y}{s}\right) dydx \neq 0 \tag{4.25}$$

or the analysis indicates that the first order terms can be evaluated without involving the gradient. This generalises the work of Almirantis and Nicolis (1987) to two dimensions. However it may be the case that $O(1)$ gradients in the reaction parameters, whilst being impossible to deal with analytically, can have some effect on the pattern formed by a system as compared with the pattern from a system with spatially uniform parameters. We examine

this possibility briefly from a numerical point of view at the end of Section 4.4.

4.3 Gradients in Reaction Parameters (ii).

In this section we consider a reaction diffusion system solved on a rectangular domain with zero-flux boundary conditions along the ends and periodic boundary conditions along the sides, thus mimicking a cylinder. The gradient in the reaction parameter is taken to be along the cylinder. We relate this analysis to the work of Lacalli, Wilkinson and Harrison (1988) who consider a variant of the Brusselator model which they solve numerically, then use the results to suggest the possibility of this kind of model being applied to produce the striped pattern of segmentation genes such as *fushi tarazu* found in the *Drosophila* embryo.

We first consider the system, (similar to (4.14))

$$\begin{aligned} u_t &= \gamma(a - u + u^2 v) + \nabla^2 u \\ v_t &= \gamma(b_0 + \epsilon^n b_1 \frac{x}{r} - u^2 v) + d\nabla^2 v. \end{aligned} \tag{4.26}$$

Again we consider $\gamma = 1$ for analytical convenience. As in Section 4.2 the linear analysis carries through as normal if $n \geq 2$ with no contribution from the gradient. A bifurcation analysis with the scaling as in (3.64) leads to the following equations:

$$\begin{aligned} O(\epsilon) \qquad \frac{\partial}{\partial t}\begin{pmatrix} u_1 \\ v_1 \end{pmatrix} - \begin{pmatrix} f_u & f_v \\ g_u & g_v \end{pmatrix}\begin{pmatrix} u_1 \\ v_1 \end{pmatrix} - \begin{pmatrix} 1 & 0 \\ 0 & d_c \end{pmatrix}\nabla^2\begin{pmatrix} u_1 \\ v_1 \end{pmatrix} \\ = \frac{\delta}{\mathrm{r}}\begin{pmatrix} 0 \\ b_1 x \end{pmatrix} \end{aligned} \tag{4.27}$$

$$
\begin{aligned}
O(\epsilon^2) \qquad \frac{\partial}{\partial t}\begin{pmatrix} u_2 \\ v_2 \end{pmatrix} &- \begin{pmatrix} f_u & f_v \\ g_u & g_v \end{pmatrix}\begin{pmatrix} u_2 \\ v_2 \end{pmatrix} - \begin{pmatrix} 1 & 0 \\ 0 & d_c \end{pmatrix}\nabla^2\begin{pmatrix} u_2 \\ v_2 \end{pmatrix} \\
&= (2u_0u_1v_1 + v_0u_1^2)\begin{pmatrix} 1 \\ -1 \end{pmatrix} + \frac{\delta_1}{\mathrm{r}}\begin{pmatrix} 0 \\ b_1x \end{pmatrix} \qquad (4.28)
\end{aligned}
$$

$$
\begin{aligned}
O(\epsilon^3) \qquad \frac{\partial}{\partial t}\begin{pmatrix} u_3 \\ v_3 \end{pmatrix} &- \begin{pmatrix} f_u & f_v \\ g_u & g_v \end{pmatrix}\begin{pmatrix} u_3 \\ v_3 \end{pmatrix} - \begin{pmatrix} 1 & 0 \\ 0 & d_c \end{pmatrix}\nabla^2\begin{pmatrix} u_3 \\ v_3 \end{pmatrix} \\
&= \left[2u_0(u_2v_1 + u_1v_2) + u_1^2v_1 + 2v_0u_1u_2\right]\begin{pmatrix} 1 \\ -1 \end{pmatrix} + \frac{\delta_2}{r}\begin{pmatrix} 0 \\ b_1x \end{pmatrix} \\
&+ \begin{pmatrix} 1 & 0 \\ 0 & 1 \end{pmatrix}\nabla^2\begin{pmatrix} u_1 \\ v_1 \end{pmatrix} - \frac{\partial}{\partial\tau}\begin{pmatrix} u_1 \\ v_1 \end{pmatrix} \qquad (4.29)
\end{aligned}
$$

where

$$
\begin{array}{lll}
\delta = 1 \quad \text{if } n = 1 & \delta_1 = 1 \quad \text{if } n = 2 & \delta_2 = 1 \quad \text{if } n = 3 \\
\delta = 0 \quad \text{if } n \geq 2 & \delta_1 = 0 \quad \text{if } n \geq 3 & \delta_2 = 0 \quad \text{if } n \geq 4.
\end{array}
$$

The solution to the O(ϵ) equation as $t \to \infty$ is

$$
\begin{aligned}
\begin{pmatrix} u_1 \\ v_1 \end{pmatrix} &= \begin{pmatrix} 1 \\ M_p \end{pmatrix}\sum(a(\tau)\cos(k_xx) + b(\tau)\sin(k_xx))(c(\tau)\cos(k_yy) + d(\tau)\sin(k_yy)) \\
&+ \frac{\delta b_1x}{\mathrm{r}\Delta}\begin{pmatrix} -f_v \\ f_u \end{pmatrix} \qquad (4.30)
\end{aligned}
$$

where

$$\Delta = f_ug_v - g_uf_v.$$

We consider the system with zero-flux boundary conditions on $x = 0, r$ and periodic boundary conditions on $y = 0, s$. This tells us, by a similar argument to that employed in Section 4.2 that

$$b(\tau) = 0 \qquad k_y = \frac{n_y\pi}{s} \quad n_y \text{ is even} \qquad k_x = \frac{n_x\pi}{r} \qquad \delta = 0. \qquad (4.31)$$

Similarly if we consider the O(ϵ^2) equation, no solution satisfying the boundary conditions is possible unless $\delta_1 = 0$. Now we consider $n = 3$, *i.e.* $\delta_2 = 1$. Secular terms can occur at this stage. They are suppressed by making the

right hand side of (4.29) orthogonal to the bounded solutions of the homogeneous adjoint equation, namely $\begin{pmatrix} 1 \\ S_p \end{pmatrix} \sin(k_y y)\cos(k_x x)$, $\begin{pmatrix} 1 \\ S_p \end{pmatrix} \cos(k_y y)\cos(k_x x)$. The gradient term makes a contribution of :

$$\left.\begin{array}{cc} \frac{b_1 S_p 2sr}{n_x^2 \pi^2} & \text{if } n_x \text{ is odd, } n_y = 0 \\ 0 & \text{otherwise} \end{array}\right\} \quad \begin{array}{c} \text{to the inner product with} \\ \begin{pmatrix} 1 \\ S_p \end{pmatrix} \cos(k_x x)\cos(k_y y). \end{array} \tag{4.32}$$

$$\left.\begin{array}{cc} \frac{-4 b_1 S_p rs}{n_x^2 n_y^2 \pi^3} & n_x, n_y \text{ odd} \\ \frac{-b_1 S_p rs}{n_y \pi} & n_x = 0,\ n_y \text{ is odd} \\ 0 & \text{otherwise} \end{array}\right\} \quad \begin{array}{c} \text{to the inner product with} \\ \begin{pmatrix} 1 \\ S_p \end{pmatrix} \cos(k_x x)\sin(k_y y). \end{array} \tag{4.33}$$

But we already know that n_y must be even so the only possibility for a non-zero contribution from the gradient is if $n_y = 0$, n_x is odd, *ie.* stripes perpendicular to the gradient. This tells us that the gradient will enhance the pattern forming potential of stripe modes.

This would seem to agree with the numerical findings of Lacalli, Wilkinson and Harrison (1988) who discovered that a gradient in the reaction parameters could force a model to produce stripes when it would not ordinarily do so if its parameters were optimised for stripe production. This would be the case when a number of modes were unstable and so interacted to produce the pattern which could not be predicted from a linear analysis with a stripe mode as the dominant one. The system they used is of the form

$$\begin{aligned} u_t &= a - (b+e)u - cu^2 v + D_u \nabla^2 u \\ v_t &= bu + cu^2 v - dv + D_v \nabla^2 v \end{aligned} \tag{4.34}$$

with spatial gradients in c and e. They do not put forward this model as being an accurate representation of the stripe forming mechanism for

ftz genes in *Drosophila* but merely as an example of what gradients can do to a model. The careful adjustment of parameters needed to produce stripes which would be a drawback in the physical sciences need not be in biology. Life depends upon metabolic reactions that have evolved, by natural selection, to operate in a highly structured enviroment at rates kept within narrow ranges. It would be unreasonable to assume that the rate processes involved in biological pattern formation have not been subject to the same stringent selection or the same high degree of control.

In the *Drosophila* embryo *ftz* stripes develop in a heterogeneous system where larger scale patterns are already well established. Genes such as *caudal* (Macdonald and Struhl (1986)) and segmentation genes of the gap class (Tautz *et al.* (1987)) form gradients which could influence *ftz* expression. Regulatory effects on *ftz* pattern have been demonstrated for several genes (Carroll and Scott (1986)) by means as yet unknown. If these gene products were to act as templates for the reaction parameters this would be control of one pattern by another of an indirect form. Figure 4.2 (from Lacalli *et al.* (1988)) shows the type of pattern that (4.34) can produce.

4.4 Spatially Dependent Diffusion Coefficients.

In this section we examine the effect a spatial gradient in the diffusion coefficient of a reaction diffusion system has upon the pattern forming potential of the model. Because of the method of derivation of the diffusion term we

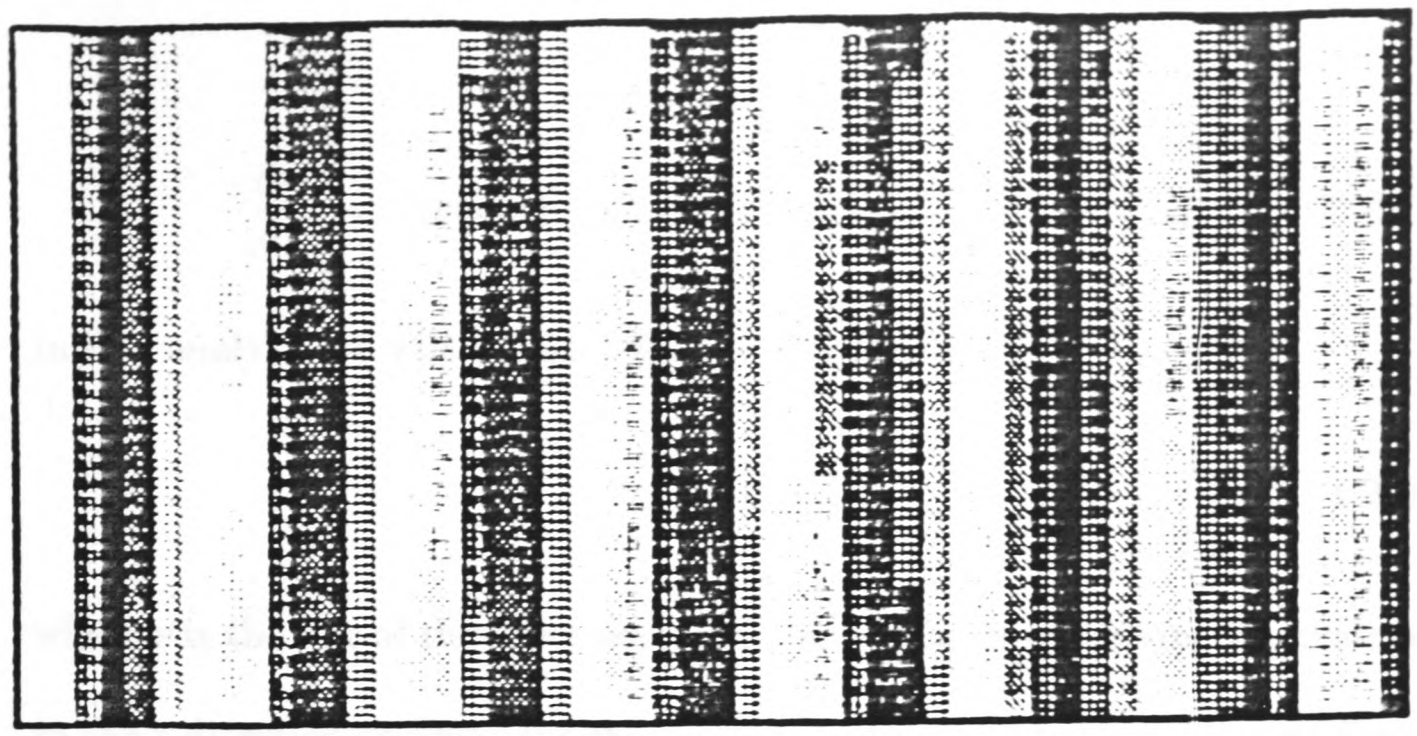

Figure 4.2: 7 stripe pattern typical of *ftz* expression in *Drosophila*. Produced from equations (4.34) with parameter values $a = 0.0175$, $b = 0.001$, $d = 0.1$, $D_u = 0.18$, $D_v = 0.004$. The gradient along the rectangle is in c (0.02 to 0.04) and e (0.015 to 0.025).

cannot simply write the system as

$$\begin{aligned} u_t &= \gamma f(u,v) + (1+h(x))u_{xx} + u_{yy} \\ v_t &= \gamma g(u,v) + d(1+h(x))v_{xx} + dv_{yy}. \end{aligned} \tag{4.35}$$

Instead we need to return to the derivation of the diffusion term (*cf.* Cohen and Murray (1981)).

$$\begin{aligned} \frac{\partial u}{\partial t} &= \gamma f(u,v) - \nabla.\underline{J}_1 & \underline{J}_1 &= -\begin{pmatrix} 1+h(x) & 0 \\ 0 & 1 \end{pmatrix} \nabla u \\ \frac{\partial v}{\partial t} &= \gamma g(u,v) - \nabla.\underline{J}_2 & \underline{J}_2 &= -d\begin{pmatrix} 1+h(x) & 0 \\ 0 & 1 \end{pmatrix} \nabla v. \end{aligned} \tag{4.36}$$

This gives us

$$\begin{aligned} -\nabla.\underline{J}_1 &= h'(x)u_x + (1+h(x))u_{xx} + u_{yy} \\ -\nabla.\underline{J}_2 &= dh'(x)v_x + d(1+h(x))v_{xx} + dv_{yy}. \end{aligned} \tag{4.37}$$

The full system now reads

$$\frac{\partial u}{\partial t} = \gamma f(u,v) + h'(x)u_x + (1+h(x))u_{xx} + u_{yy}$$

$$\frac{\partial v}{\partial t} = \gamma g(u,v) + dh'(x)v_x + d(1+h(x))v_{xx} + dv_{yy}. \qquad (4.38)$$

In this analysis we will consider $h(x)$ to have the form

$$h(x) = \epsilon^2 \frac{a_1 x}{r} \qquad (4.39)$$

where r is the size of the finite domain upon which we are solving the system in the x direction and we have chosen ϵ^2 so as the contribution of the gradient becomes apparent at $O(\epsilon^3)$ in the bifurcation analysis. By way of an example we will consider the Schnackenberg system on a bounded $r \times s$ domain with zero flux boundary conditions and $\gamma = 1$ for analytical convenience. We use the normal scaling (3.64) and obtain, on equating powers of ϵ,

$$O(\epsilon) \quad \begin{pmatrix} u_1 \\ v_1 \end{pmatrix}_t - \begin{pmatrix} f_u & f_v \\ g_u & g_v \end{pmatrix} \begin{pmatrix} u_1 \\ v_1 \end{pmatrix} - \begin{pmatrix} 1 & 0 \\ 0 & d_c \end{pmatrix} \nabla^2 \begin{pmatrix} u_1 \\ v_1 \end{pmatrix} = 0. \qquad (4.40)$$

The solution of this as $t \to \infty$ with zero flux boundary conditions is

$$\begin{pmatrix} u_1 \\ v_1 \end{pmatrix} = \begin{pmatrix} 1 \\ M_p \end{pmatrix} a(\tau)\cos(k_x x)\cos(k_y y) \quad k_x = \frac{n_x \pi}{r}, \quad k_y = \frac{n_y \pi}{s} \qquad (4.41)$$

where we have assumed that there exists only one mode (n_x, n_y) such that $k_x^2 + k_y^2 = p^2$. At $O(\epsilon^2)$ we have

$$\begin{aligned} \begin{pmatrix} u_2 \\ v_2 \end{pmatrix}_t - \begin{pmatrix} f_u & f_v \\ g_u & g_v \end{pmatrix} \begin{pmatrix} u_2 \\ v_2 \end{pmatrix} - \begin{pmatrix} 1 & 0 \\ 0 & d_c \end{pmatrix} \nabla^2 \begin{pmatrix} u_2 \\ v_2 \end{pmatrix} \\ = \frac{1}{2} u_1^2 \underline{F}_{uu} + u_1 v_1 \underline{F}_{uv} \end{aligned} \qquad (4.42)$$

with solution

$$\begin{aligned} \underline{u}_2 = \begin{pmatrix} 1 \\ M_p \end{pmatrix} a_1(\tau)\cos(k_x x)\cos(k_y y) &- \underline{w}_1 - \underline{w}_2 \cos(2k_x x) - \underline{w}_3 \cos(2k_y y) \\ &- \underline{w}_4 \cos(2k_x x)\cos(2k_y y) \end{aligned} \qquad (4.43)$$

as $t \to \infty$, where

$$\underline{w}_1 = \frac{\mathrm{R}a^2(\tau)}{4\,\Delta}\begin{pmatrix} g_v + f_v \\ -g_u - f_u \end{pmatrix} \qquad R = v_0 + 2u_0 M_p \quad \Delta = f_u g_v - f_v g_u$$

$$\underline{w}_2 = \frac{\mathrm{R}a^2(\tau)}{4\Delta_1}\begin{pmatrix} g_v - 4k_x^2 d_c + f_v \\ -g_u - f_u + 4k_x^2 \end{pmatrix} \quad \Delta_1 = \begin{vmatrix} f_u - 4k_x^2 & f_v \\ g_u & g_v - 4k_x^2 d_c \end{vmatrix}$$

$$\underline{w}_3 = \frac{\mathrm{R}a^2(\tau)}{4\Delta_2}\begin{pmatrix} g_v - 4k_y^2 d_c + f_v \\ -g_u - f_u + 4k_y^2 \end{pmatrix} \quad \Delta_2 = \begin{vmatrix} f_u - 4k_y^2 & f_v \\ g_u & g_v - 4k_y^2 d_c \end{vmatrix}$$

$$\underline{w}_4 = \frac{\mathrm{R}a^2(\tau)}{4\Delta_3}\begin{pmatrix} g_v - 4p^2 d_c + f_v \\ -g_u - f_u + 4p^2 \end{pmatrix} \quad \Delta_3 = \begin{vmatrix} f_u - 4p^2 & f_v \\ g_u & g_v - 4p^2 d_c \end{vmatrix} = 9\Delta. \tag{4.44}$$

At $\mathrm{O}(\epsilon^3)$ we have the equation

$$\begin{pmatrix} u_3 \\ v_3 \end{pmatrix}_t - \begin{pmatrix} f_u & f_v \\ g_u & g_v \end{pmatrix}\begin{pmatrix} u_3 \\ v_3 \end{pmatrix} - \begin{pmatrix} 1 & 0 \\ 0 & d_c \end{pmatrix}\nabla^2\begin{pmatrix} u_3 \\ v_3 \end{pmatrix} \tag{4.45}$$

$$= u_1 u_2 \underline{F}_{uu} + (u_1 v_2 + u_2 v_1)\underline{F}_{uv} + \frac{1}{2}u_1^2 v_1 \underline{F}_{uuv} - \frac{\partial}{\partial \tau}\begin{pmatrix} u_1 \\ v_1 \end{pmatrix}$$

$$+ \begin{pmatrix} 0 & 0 \\ 0 & 1 \end{pmatrix}\nabla^2\begin{pmatrix} u_1 \\ v_1 \end{pmatrix} + \frac{a_1 x}{\mathrm{r}}\begin{pmatrix} u_1 \\ d_c v_1 \end{pmatrix}_{xx} + \frac{a_1}{\mathrm{r}}\begin{pmatrix} u_1 \\ d_c v_1 \end{pmatrix}_x .$$

Secular terms can appear at this stage. They are suppressed in the usual way by making the right hand side of (4.45) orthogonal to $\begin{pmatrix} 1 \\ S_p \end{pmatrix}\cos(k_x x)\cos(k_y y)$.

This gives rise to the following equation (Landau equation):

$$\frac{da}{d\tau} = \mu a + \eta a^3 \tag{4.46}$$

where

$$\mu = \frac{-S_p M_p p^2}{1 + S_p M_p} \tag{4.47}$$

$$+ \frac{1 + d_c S_p M_p}{1 + S_p M_p}\frac{k_x a_1}{\mathrm{r}}\left[\frac{k_x \int_0^r x\cos^2(k_x x)dx \quad + \int_0^r \cos(k_x x)\sin(k_x x)dx}{\int_0^r \cos^2(k_x x)dx}\right]$$

and η does not involve the gradient term. Now

$$S_p M_p = -\frac{1}{d_c} \quad \text{giving} \quad 1 + d_c S_p M_p = 0 \tag{4.48}$$

and so the gradient in the diffusion coefficient is making no contribution to the solution of the model at first order. If we consider the same model but now with periodic boundary conditions as in Section 4.3 we find that the same result occurs. The analysis presented in this chapter seems to show that gradients of a size which makes an analysis possible do not, in the main, give rise to specific changes in the expected patterns when we are dealing with a two dimensional domain and a one dimensional gradient. As mentioned at the end of Section 4.2, it may be the case that O(1) gradients, whilst being impossible to deal with analytically, can give rise to significantly different patterns when compared with the case when no gradient is present. It would not be surprising if, when using a large one dimensional gradient in one of the reaction parameters, we found that the resulting steady state patterns were predominantly one dimensional even though the patterns formed in the absence of a gradient were two dimensional. This is indeed the case as we can see from Figure 4.3 which shows the results of some simulations using O(1) gradients.

This completes our work on reaction diffusion systems. In the next two chapters we consider different types of pattern forming models - a mechanical type model suggested by Goldwasser, Maini and Murray (1989) used to model the branching process in bryozoans in Chapter 5 and a gene switch mechanism suggested by Murray (1981) to model pattern formation of certain pattern elements on butterfly wings in Chapter 6.

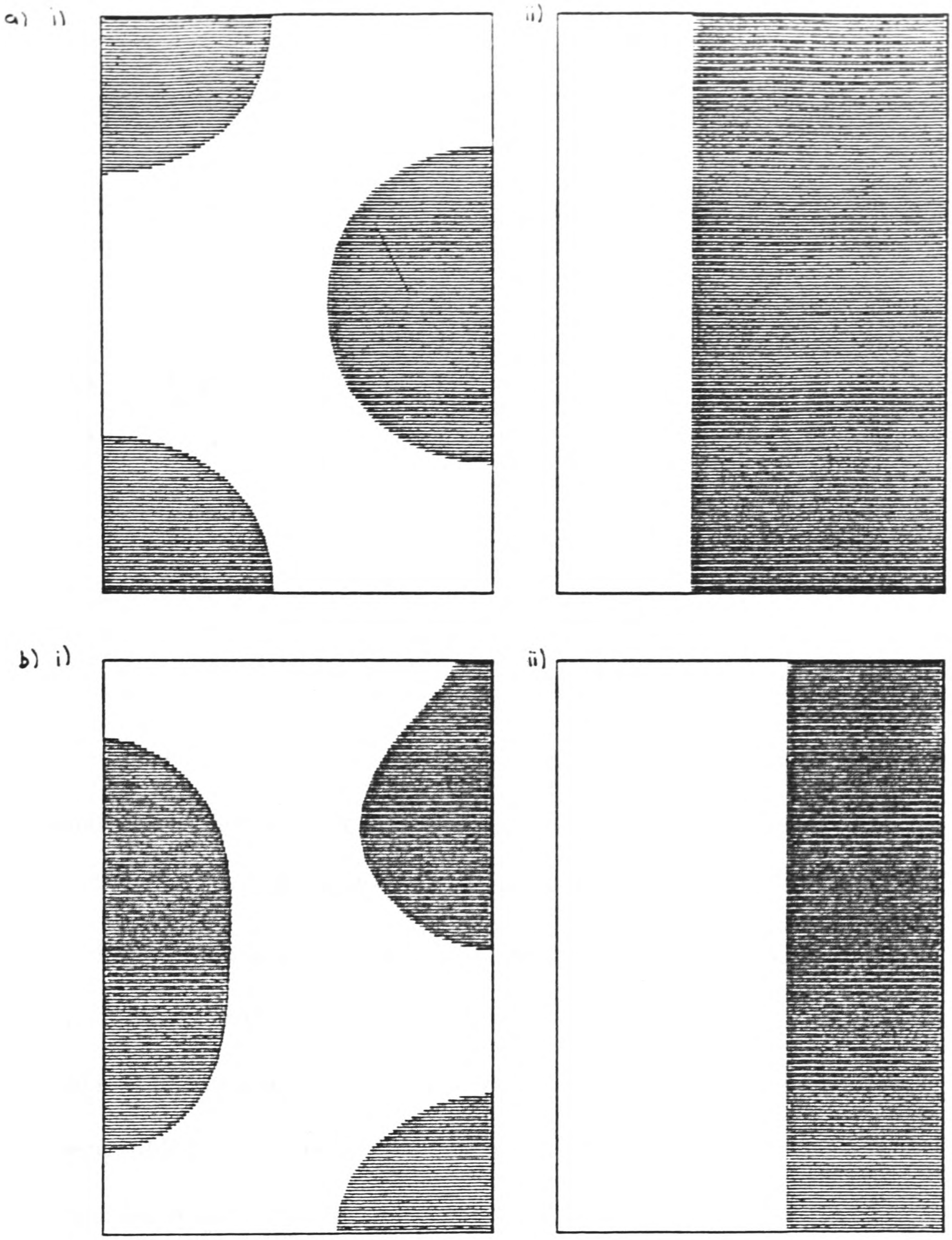

Figure 4.3: Patterns formed from a) (4.14) with parameter values $a_0 = 0.2$, b=0.9, r=3.9, s=6.0, d=20, n=0, $\gamma = 6$ and i) a_1=0, ii) $a_1 = a_0$; b) (4.35) with the same parameter values as in a) except $\gamma = 8$ and ii) $a_1 = 1$.

Chapter 5

Branching Patterns in Bryozoans.

5.1 Background.

In this chapter we analyse in detail a cell mechanical model proposed by Goldwasser, Maini and Murray (1989). By means of nonlinear bifurcation analysis we show that, under certain constraints on the model parameters, both stationary and standing wave type solutions are possible.

Figure 5.1 is a diagram of an arborescent bryozoan colony such as *Bugula sp.* (from Goldwasser *et al.* (1989)). It shows that the basic growth behaviour of bryozoans is distal (growing at the tip) with new units (zooids) being added to the tips of the branches irrespective of whether splitting has occurred or not. The right hand branch has begun to split and two daughter branches are starting to form. The model we consider here specifically considers the questions posed in one of the few studies of growing tips in Bryozoans by Schneider (1963). He says, of a group of cells observed in *Bugula* which exhibit striking behaviour; *"While there is limited random movement of the individual cells, the degree of cell co-ordination is remarkable. All these*

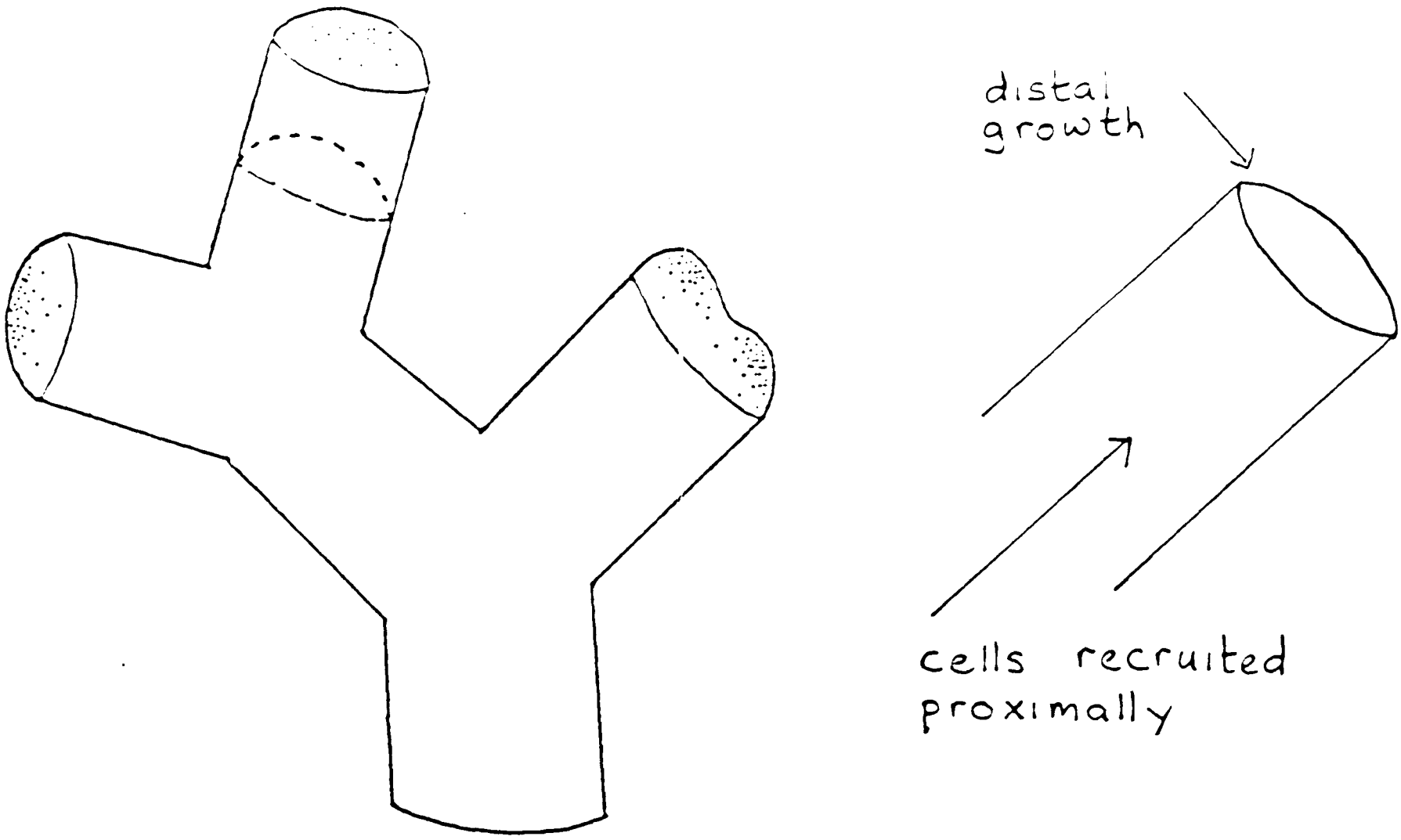

Figure 5.1: a) Diagram of an arborescent bryozoan colony. b) Diagram explaining distal and proximal growth through cell recruitment.

cells are somehow oriented to the centre of the cell plate, which is rhythmically expanding or contracting or even twisting", and concludes: "*How this locomotive activity and co-ordination is brought about is quite unknown*". These cells lie on the inner, dome-shaped, surface of a growing tip where they secrete cuticle, or cell matrix, as the branch grows (Taverner-Smith and Williams (1972)). Figure 5.2 is a diagramatic cross section of a bryozoan branch laid flat (taken from Goldwasser *et al.* (1989)). It indicates how the cuticle secreted is inserted into the existing cuticle which then spreads out carrying the cells and adhesive sites with it. As the older cuticle reaches the edge of the dome it calcifies and gets pushed outward to form part of the cylinder of the branch behind the growing tip. The direction of the branch

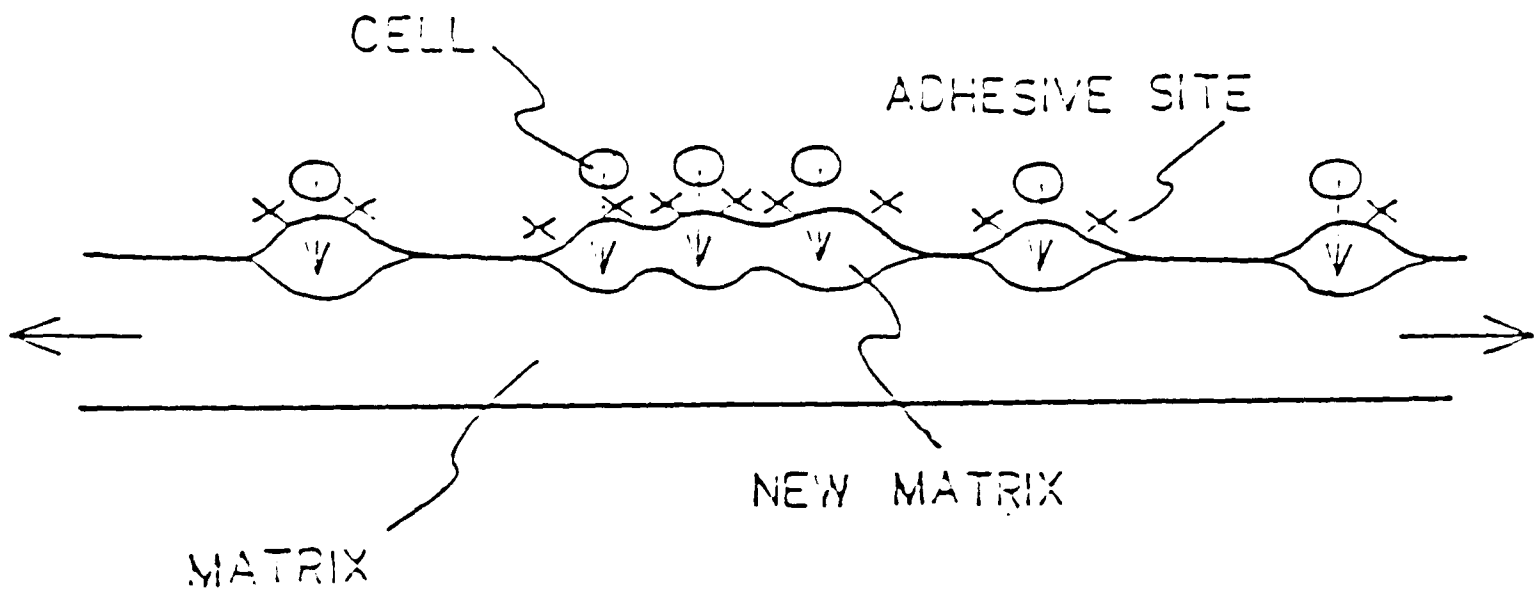

Figure 5.2: Diagramatic cross section through the cuticle at the tip of a bryozoan branch.

elongation depends upon the location of the cells within the tip. A few other details are known about these cells. They do not reproduce, new cells are recruited proximally (from within the parent branch) (Schneider (1963)) and their motion is rapid on the time scale of branch growth (Goldwasser pers. comm.).

The process of branching in bryozoans (and other structures such as corals and trees) is created by the iteration of two separate events; the growth of the branch and its subsequent splitting. The multitude of different branching patterns found in nature occur because the location and timing of the splitting varies. This can be modelled phenomenologically by constructing rules based on the angles of rotation from the main branch, the length of

the tip and the time of branching and then examining the resulting patterns (for example, Bell (1976),(1986); Goldwasser (1988); Edelstein-Keshet and Ermentrout (1989)). However models such as these do not consider the biological processes that actually cause the events. Reaction diffusion systems depending upon an as yet undiscovered morphogen to establish the branching have also been widely considered (for example, Lacalli and Harrison (1987), Harrison and Kolař (1988)). Numerical simulations of these, under appropriate parameter restrictions, give rise to branching patterns. Figure 5.3, taken from Lacalli and Harrison (1987), shows the formation of a branch, with pattern scale decreasing relative to system size, using a variant of the Brusselator reaction kinetics which routinely produces branches of this type. The surface is of morphogen concentration.

In this chapter we consider an alternative model based mainly on cellular behaviour known to occur in both branch growth and splitting. Models of cellular mechanics (Murray and Oster (1984a,b)) usually consider the initial formation of spatial pattern from deviations about a homogeneous steady state. In the case of bryozoan growth what is required is the splitting of one cell cluster into two (Schneider (1963)) and a linear stability analysis, which is usually carried out to predict the formation of a heterogeneous pattern, is rarely possible about an initial non-uniform state. In Section 5.2 we present the model and carry out a linear analysis about a uniform steady state and consider various possible configurations for the dispersion relation. In Section 5.3 we attempt a nonlinear analysis to demonstrate the initial

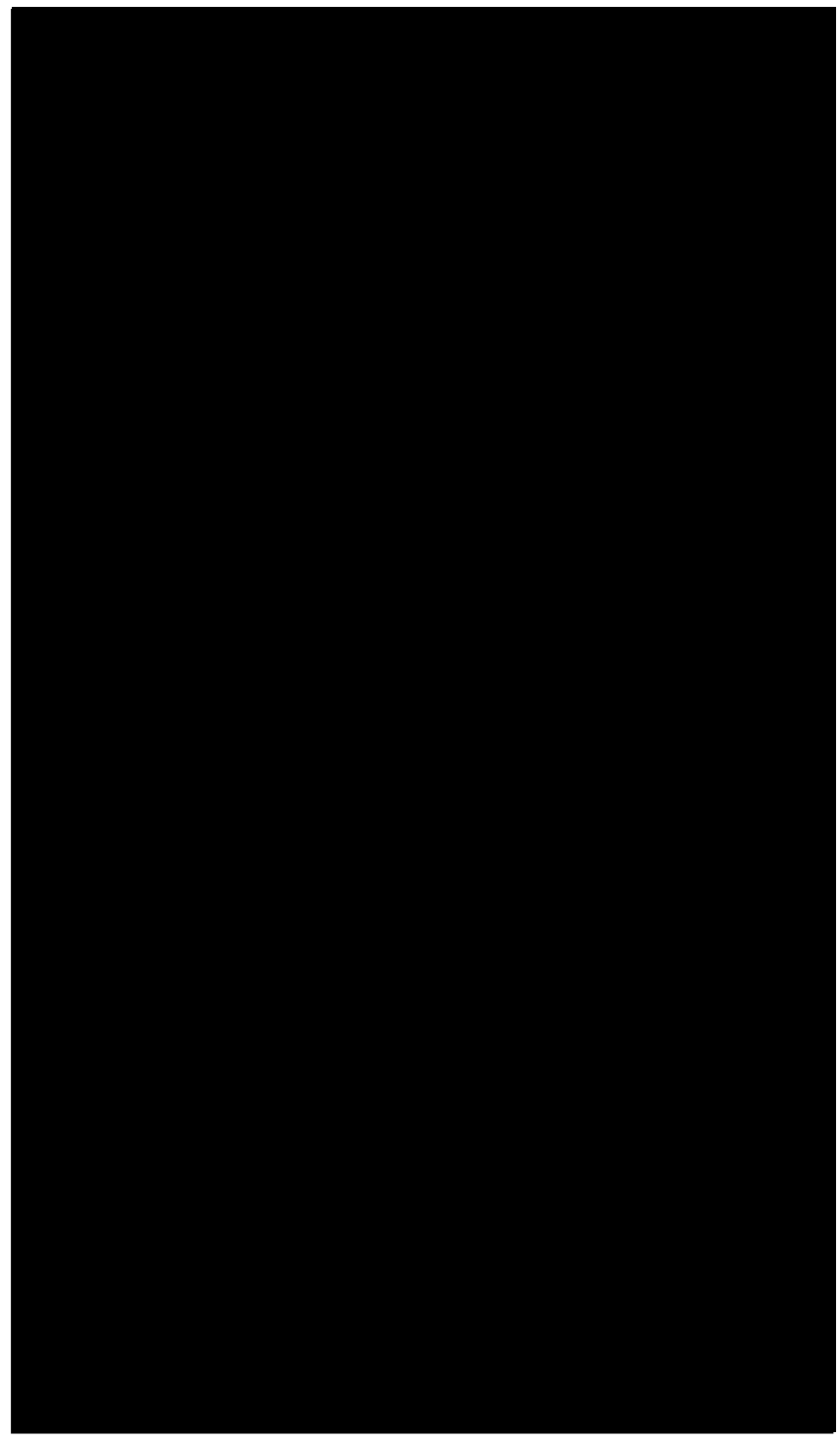

Figure 5.3: Branch formation using a reaction diffusion system. Figure 1 from Lacalli and Harrison (1987).

formation of one cell cluster. In Section 5.4 we examine the possibility of standing wave solutions and discuss the possibility of combining solutions of these two types to give branching and oscillations in the cell distribution as have been observed.

5.2 The Model and a Linear Analysis.

For ease in analysis, the model is constructed on a one dimensional domain, so as to focus on what happens to the clusters of cells, rather than the more realistic but more complicated dome shaped tips. The basic model is of the

form

$$\begin{array}{rcccccc} r_t & = & \xi n & - & \lambda r & + & c(rr_x)_x \\ & & \text{secretion} & & \text{calcification} & & \text{convection} \\ a_t & = & bn & - & \mu a & + & c(ar_x)_x \\ & & \text{secretion} & & \text{decay} & & \text{convection} \\ n_t & = & dn_{xx} & - & h(na_x)_x & + & c(nr_x)_x \\ & & \text{diffusion} & & \text{haptotaxis} & & \text{convection} \end{array} \tag{5.1}$$

where

$r(x,t)$ denotes the density of the matrix or cuticle.

$a(x,t)$ denotes the density of the adhesive sites.

$n(x,t)$ denotes the density of the cells.

The adhesive sites are only postulated to exist but they are necessary to act as an attractive entity for producing the spatial pattern. By itself the convection term tends to break up the pattern as the cells are carried out of the domain. The model is essentially based upon two processes; the matrix spreading and carrying the cells and adhesive sites with it and the secretion by the cells of the matrix and the adhesive sites. The cells move up a gradient in the adhesive sites, a process known as haptotaxis (as described by Harris (1983) for chick limb cells), of their own creation as they are carried along by the matrix. A diffusion term is included for the cells alone as they are the only motile element. The secretion, calcification and decay terms have been chosen to be linear for simplicity.

We first nondimensionalise the model using N as the mean cell density throughout the domain, L_0 as the original length of the domain and L as the

current length. Let

$$\begin{aligned} n^* &= \frac{n}{N} \quad a^* = \frac{ah}{\mu L_0^2} \quad r^* = \frac{rc}{\mu L_0^2} \quad x^* = \frac{x}{L} \quad t^* = \frac{t\mu L_0^2}{L^2} \\ \gamma &= \frac{L^2}{L_0^2} \quad \xi^* = \frac{cN\xi}{\mu^2 L_0^2} \quad d^* = \frac{d}{\mu L_0^2} \quad \lambda^* = \frac{\lambda}{\mu} \quad b^* = \frac{bhN}{\mu^2 L_0^2} \end{aligned} \tag{5.2}$$

to give, on dropping the asterisks for notational convenience,

$$\begin{aligned} r_t &= \gamma(\xi n - \lambda r) &+ (rr_x)_x \\ a_t &= \gamma(bn - a) &+ (ar_x)_x \\ n_t &= dn_{xx} - (na_x)_x &+ (nr_x)_x. \end{aligned} \tag{5.3}$$

From the nondimensionalisation, if n is constant over the domain then $n = 1$.

The uniform steady states for (r, a, n) are

$$(\tilde{r}, \tilde{a}, \tilde{n}) = (0, 0, 0), \left(\frac{\xi}{\lambda}, b, 1\right) \tag{5.4}$$

of which the second is the biologically relevant one.

Linearise about this steady state and look for solutions of the form

$$\begin{pmatrix} r - \frac{\xi}{\lambda} \\ a - b \\ n - 1 \end{pmatrix} \propto e^{\sigma t + ikx}. \tag{5.5}$$

This gives the dispersion relation between k, the wavenumber, and σ, the growth rate of perturbation as a function of the wavenumber k, as

$$\begin{aligned} \sigma^3 &+ [(d + \frac{\xi}{\lambda})k^2 + \gamma(\lambda + 1)]\sigma^2 + [\frac{d\xi}{\lambda}k^4 + k^2\gamma(\frac{\xi}{\lambda} + d\lambda + d + \xi - b) + \gamma^2\lambda]\sigma \\ &+ k^2\gamma[\frac{k^2\xi}{\lambda}(d + b(\lambda - 1)) + \gamma((d - b)\lambda + \xi)] = 0 \end{aligned} \tag{5.6}$$

or

$$\sigma^3 + A_1(k^2)\sigma^2 + B_1(k^2)\sigma + C_1(k^2) = 0. \tag{5.7}$$

In the absence of any spatial variation the dispersion equation reduces to

$$\sigma^3 + \gamma(\lambda + 1)\sigma^2 + \gamma^2\lambda\sigma = 0 \tag{5.8}$$

with solutions

$$\sigma = 0, \quad \sigma = -\gamma\lambda, \quad \sigma = -\gamma. \tag{5.9}$$

As these are all non-positive the system is stable in the spatially homogeneous case. The fact that the dispersion relation passes through the origin in the $\sigma - k^2$ plane for all values of the model parameters is due to the lack of mitosis among the tip cells as pointed out by Taverner-Smith and Williams (1972). When $k \neq 0$ the dispersion equation has either three real roots or one real root and two complex conjugate roots. As can be seen from the dispersion equation (if $d + b(\lambda - 1) > 0$) all wavenumbers k satisfying

$$0 < k^2 < \frac{\gamma\lambda[(b-d)\lambda - \xi]}{\xi[d + b(\lambda - 1)]} \tag{5.10}$$

are unstable. This means that it is impossible to isolate a single value of k for growth unless specific boundary conditions are used. This is the type of argument we use in the next section. Figure 5.4 shows some possibilities for the form of the dispersion relation, the feasibility of which we examine below.

Let the solutions to the dispersion equation (5.6) be $\sigma_1(k^2), \sigma_R(k^2) \pm i\sigma_I(k^2)$ so

$$(\sigma - \sigma_1)(\sigma - (\sigma_R + i\sigma_I))(\sigma - (\sigma_R - i\sigma_I)) = 0 \tag{5.11}$$

giving

$$\begin{aligned} -\sigma_1 - 2\sigma_R &= A_1(k^2) \\ \sigma_R^2 + \sigma_I^2 + 2\sigma_1\sigma_R &= B_1(k^2) \\ -\sigma_1(\sigma_R^2 + \sigma_I^2) &= C_1(k^2). \end{aligned} \tag{5.12}$$

Note that $A_1(k^2) > 0 \; \forall k^2$ so we cannot have σ_1 and σ_R both positive for any value of k^2. This tells us that case d) in Figure 5.4 cannot occur.

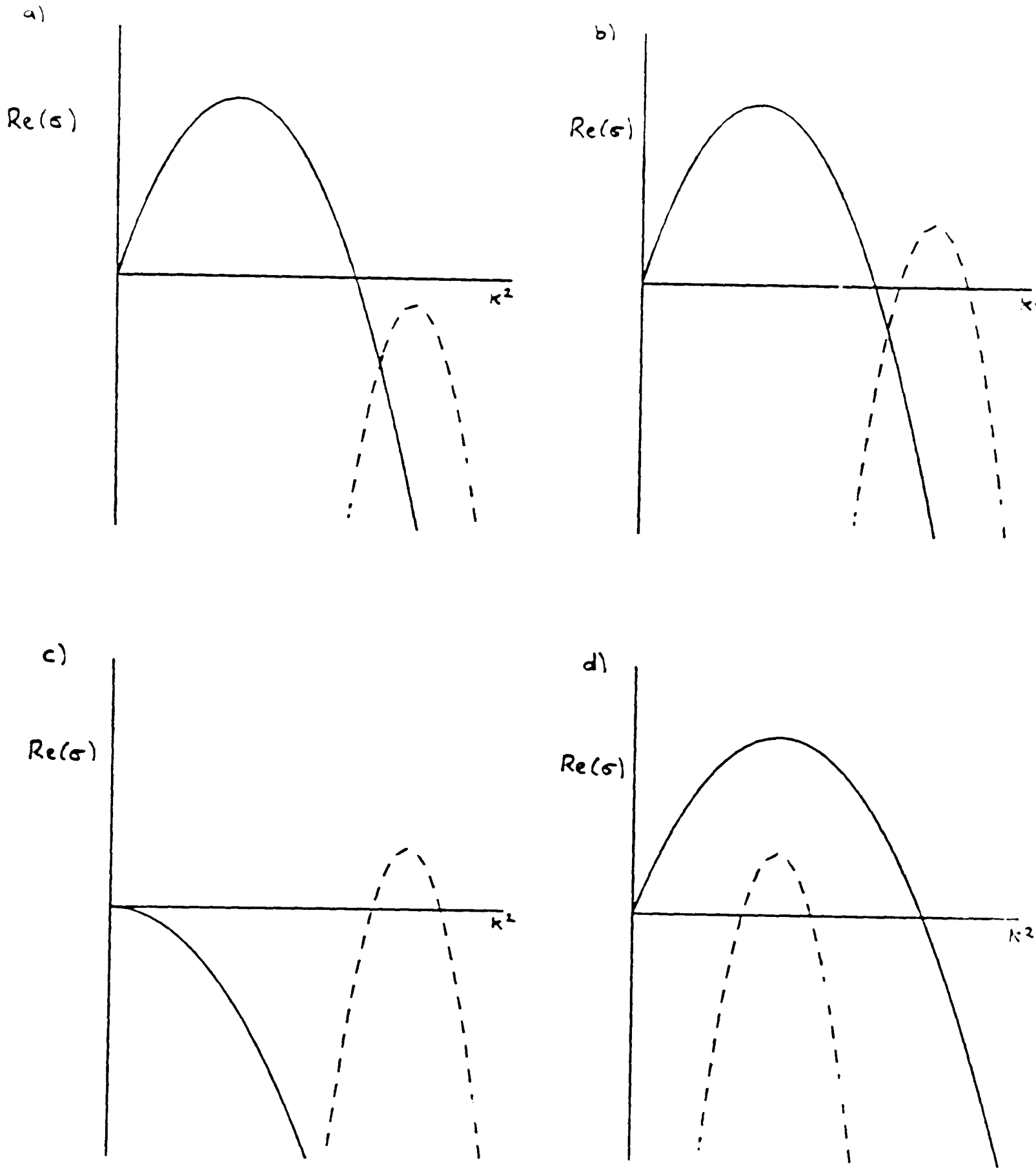

Figure 5.4: Possible forms for the dispersion obtained by solving (5.6), with the solid line representing the real solution and the broken line line representing the real part of a complex solution.

If $C_1(k^2) > 0\ \forall k^2$, as in the case in Fig. 5.4c), then the only way a root of the dispersion equation can have a positive real part (using the Routh-Hurwitz criteria) is if $A_1(k^2)B_1(k^2) - C_1(k^2) < 0$ for some value of k^2. We have

$$C_1(k^2) > 0 \Rightarrow d + b(\lambda - 1) > 0, \quad (d - b)\lambda + \xi = \psi > 0. \tag{5.13}$$

$$\begin{aligned} A_1B_1 - C_1 &= k^6 \frac{d\xi}{\lambda}\left(d + \frac{\xi}{\lambda}\right) \\ &+ k^4\left[\frac{\gamma d\xi}{\lambda}(\lambda + 1) + \gamma\left(d + \frac{\xi}{\lambda}\right)\left(d\lambda + d + \xi + \frac{\xi}{\lambda} - b\right) - \frac{\gamma\xi}{\lambda}(d + b(\lambda - 1)\right] \\ &+ k^2\left[\gamma^2(\lambda + 1)\left(\xi + d\lambda + d + \frac{\xi}{\lambda} - b\right) + \gamma^2\lambda b\right] + \gamma^3\lambda(\lambda + 1). \end{aligned} \tag{5.14}$$

Consider the coefficient of k^4:

$$\begin{aligned} &\gamma d\xi + d\gamma\left(\xi + d\lambda + \frac{\psi}{\lambda}\right) + \frac{\gamma\xi}{\lambda}\left(d\lambda + d + \xi + \frac{\xi}{\lambda}\right) - \gamma\xi b \\ &= \gamma\xi(d - b) + d\gamma\left(\xi + d\lambda + \frac{\psi}{\lambda}\right) + \frac{\gamma\xi}{\lambda}\left(d\lambda + d + \frac{\xi}{\lambda}\right) + \frac{\gamma\xi^2}{\lambda} \\ &= \frac{\gamma\xi\psi}{\lambda} + d\gamma\left(\xi + d\lambda + \frac{\psi}{\lambda}\right) + \frac{\gamma\xi}{\lambda}\left(d\lambda + d + \frac{\psi}{\lambda}\right) > 0. \end{aligned} \tag{5.15}$$

Consider now the coefficient of k^2:

$$\begin{aligned} &\gamma^2(\lambda + 1)\left(\xi + d\lambda + d + \frac{\xi}{\lambda}\right) - \gamma^2 b \\ &= \gamma^2(\lambda + 1)(d\lambda + \xi) + \gamma^2 d\lambda + \gamma^2(d - b) + \frac{\gamma^2\xi}{\lambda} + \gamma^2\xi \\ &= \gamma^2(\lambda + 2)(d\lambda + \xi) + \frac{\gamma^2\psi}{\lambda} > 0. \end{aligned} \tag{5.16}$$

So with $C_1(k^2) > 0\ \forall k^2$ we have $A_1(k^2)B_1(k^2) - C_1(k^2) > 0\ \forall k^2$, which shows that Fig. 5.4c) cannot occur.

For case a) in Figure 5.4 we have $C_1(k^2) < 0$ for $k^2 < k_c^2$ so by the Routh-Hurwitz criteria we can have a positive root for $k < k_c$. This tells us that

this case can occur. We examine the pattern formation potential of this case in Section 5.3.

For case b) in Figure 5.4 we require $A_1 B_1 - C_1 < 0$ for some $k^2 \in (k_c^2, \infty)$ where $A_1(k^2), C_1(k^2) > 0$ for $k^2 \in (k_c^2, \infty)$. A sufficient (but not necessary) condition for this to occur is for $B_1(k^2) < 0$.

$$B_1(k^2) = \frac{d\xi}{\lambda} k^4 + k^2 \gamma \left(d\lambda + d + \frac{\xi}{\lambda} + \xi - b \right) + \gamma^2 \lambda. \tag{5.17}$$

The minimum value occurs when

$$k^2 = \frac{\gamma \lambda}{2d\xi} \left(b - \left(d + \frac{\xi}{\lambda} \right) (\lambda + 1) \right) \tag{5.18}$$

so the first sufficient condition (to make the value of k^2 positive) is

$$b > (\lambda + 1) \left(d + \frac{\xi}{\lambda} \right). \tag{5.19}$$

The minimum value of $B_1(k^2)$ is

$$\frac{-\gamma^2 \lambda}{4d\xi} \left(b - (\lambda + 1) \left(d + \frac{\xi}{\lambda} \right) \right)^2 + \gamma^2 \lambda \tag{5.20}$$

so for this to be negative we require

$$\left(b - \left(d + \frac{\xi}{\lambda} \right) (\lambda + 1) \right)^2 > 4d\xi. \tag{5.21}$$

So for certain values of the parameters the case depicted in Figure 5.4b) can occur. We examine this case in detail in Section 5.4.

As we are primarily interested in the pattern formed by the cells we rearrange the order of the equations in (5.3) for the nonlinear analysis and consider the system as

$$\begin{aligned} n_t &= dn_{xx} - (na_x)_x + (nr_x)_x \\ r_t &= \gamma(\xi n - \lambda r) + (rr_x)_x \\ a_t &= \gamma(bn - a) + (ar_x)_x. \end{aligned} \tag{5.22}$$

In the next section we consider a nonlinear analysis for the model using parameters so as the dispersion curve is as illustrated in Figure 5.4a).

5.3 Nonlinear Analysis (i).

In this section the parameters are assumed to be such that the solutions to the dispersion equation (5.6) are of the form shown in Figure 5.4a). The entirely real solution cuts the k^2 axis at 0 and at k_c^2 where

$$k_c^2 = \frac{\gamma\lambda((b-d)\lambda - \xi)}{\xi(d + b(\lambda - 1))}. \tag{5.23}$$

These are the values of k^2 where $C_1(k^2) = 0$. For $k^2 > k_c^2$ there are no positive roots to the dispersion equation so using the Routh-Hurwitz criteria we can deduce that $C_1(k^2)$ is negative for $k^2 < k_c^2$ and positive for $k^2 > k_c^2$. This gives a first restriction on the parameters, namely

$$b > d + \frac{\xi}{\lambda} \quad \text{and} \quad b < \frac{d}{1-\lambda} \text{ if } \lambda < 1. \tag{5.24}$$

The expression for k_c^2 gives the critical value of d for each particular k_c^2,

$$d_c = \left(1 - \frac{\xi\lambda k_c^2}{\xi k_c^2 + \gamma\lambda^2}\right) b - \frac{\gamma\lambda\xi}{\xi k_c^2 + \gamma\lambda^2}. \tag{5.25}$$

For this analysis we wish to isolate the first mode only so we need to consider the model under suitable boundary conditions (such that it appears that the dispersion relation has a sharp peak at $k_c^2 = \pi^2$ and is zero everywhere else, as shown in Figure 5.5). The appropriate type of boundary conditions are periodic, zero-flux or fixed at the steady state.

To carry out the analysis we take

$$d = d_c + \epsilon^2\nu, \quad \nu = \pm 1, \quad 0 < \epsilon \ll 1, \quad \tau = \epsilon^2 t, \quad t^* = t \tag{5.26}$$

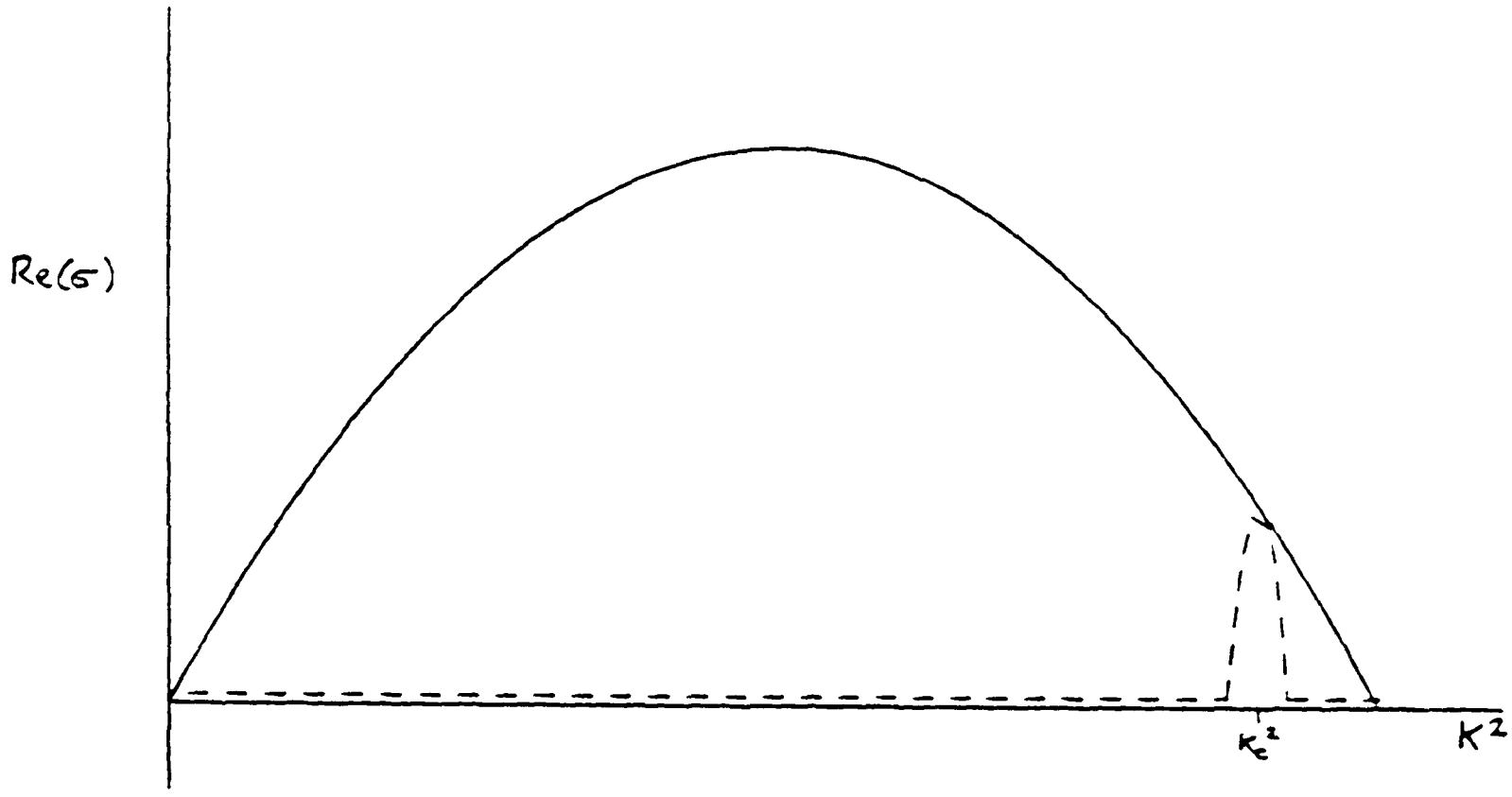

Figure 5.5: A 'peak' dispersion relation formed by considering the model under certain specific boundary conditions.

and look for solutions of the form

$$\underline{u} = \begin{pmatrix} n \\ r \\ a \end{pmatrix} = \underline{u}_0 + \sum_{j=1} \epsilon^j \underline{u}_j(x, \tau, t^*). \tag{5.27}$$

A Taylor expansion of σ about $(k_c^2; d_c)$ gives

$$\sigma(k_c^2; d) = \sigma(k_c^2; d_c) + \frac{\partial \sigma}{\partial d}(k_c^2; d_c)\epsilon^2 \nu + O(\epsilon^4). \tag{5.28}$$

Now

$$\frac{\partial \sigma}{\partial d}(k_c^2; d_c) = \frac{-k_c^2 \gamma(\gamma\lambda + k_c^2 \frac{\xi}{\lambda})}{B_1(k_c^2; d_c)}. \tag{5.29}$$

At $k_c^2 + \epsilon'$ all the roots of the dispersion equation have negative real parts so from the Routh-Hurwitz criteria (and noting that $A_1(k_c^2 + \epsilon')$, $C_1(k_c^2 + \epsilon')$ are positive $\forall \epsilon' > 0$) we have

$$A_1(k_c^2 + \epsilon')B_1(k_c^2 + \epsilon') - C_1(k_c^2 + \epsilon') > 0 \quad \forall \epsilon' > 0. \tag{5.30}$$

Thus $B_1(k_c^2; d_c) \geq 0$. Hence we must take $\nu = -1$ to have a positive exponential growth rate of $O(\epsilon^2 t)$.

Substituting for $\underline{u}$ from (5.27) in (5.22) and equating powers of ϵ gives, on dropping the asterisk for notational convenience,

$$O(\epsilon): \quad \frac{\partial \underline{u}_1}{\partial t} - L\underline{u}_1 = 0 \tag{5.31}$$

$$O(\epsilon^2): \quad \frac{\partial \underline{u}_2}{\partial t} - L\underline{u}_2 = \begin{pmatrix} n_{1x}(r_{1x} - a_{1x}) & + & n_1(r_{1xx} - a_{1xx}) \\ r_{1x}r_{1x} & + & r_1 r_{1xx} \\ a_{1x}r_{1x} & + & a_1 r_{1xx} \end{pmatrix} \tag{5.32}$$

$$\begin{aligned} O(\epsilon^3): \quad & \frac{\partial \underline{u}_3}{\partial t} - L\underline{u}_3 = -\frac{\partial \underline{u}_1}{\partial \tau} + \Psi \underline{u}_{1xx} \\ & + \begin{pmatrix} n_{2x}(r_{1x} - a_{1x}) & + & n_2(r_{1xx} - a_{1xx}) & + & n_{1x}(r_{2x} - a_{2x}) & + & n_1(r_{2xx} - a_{2xx} \\ r_{2x}r_{1x} & + & r_2 r_{1xx} & + & r_{1x}r_{2x} & + & r_1 r_{2xx} \\ a_{2x}r_{1x} & + & 2_2 r_{1xx} & + & a_{1x}r_{2x} & + & a_1 r_{2xx} \end{pmatrix} \\ & = \underline{J}_1(\underline{u}_1, \underline{u}_2) \end{aligned} \tag{5.33}$$

where

$$L = \gamma \begin{pmatrix} 0 & 0 & 0 \\ \xi & -\lambda & 0 \\ b & 0 & -1 \end{pmatrix} + \begin{pmatrix} d_c & 1 & -1 \\ 0 & \xi & 0 \\ 0 & \lambda & 0 \\ 0 & b & 0 \end{pmatrix} \frac{\partial^2}{\partial x^2} = M + D\frac{\partial^2}{\partial x^2} \tag{5.34}$$

$$\Psi = \begin{pmatrix} \nu & 0 & 0 \\ 0 & 0 & 0 \\ 0 & 0 & 0 \end{pmatrix}. \tag{5.35}$$

We ignore the fast time (t) dependence as the growth rate is $O(\epsilon^2)$ and so the pattern will develop over time τ (Matkowsky (1970a,b)). The solution to the $O(\epsilon)$ problem, under the suitable boundary conditions chosen to obtain the peak dispersion relation (for example, fixed at the steady state or zero-flux or periodic), is

$$\underline{u}_1 = \begin{pmatrix} 1 \\ P \\ R \end{pmatrix} (p(\tau)\cos \pi x + q(\tau) \sin \pi x) \tag{5.36}$$

where

$$\begin{pmatrix} -d_c\pi^2 & -\pi^2 & \pi^2 \\ \gamma\xi & -\gamma\lambda - \frac{\xi\pi^2}{\lambda} & 0 \\ \gamma b & -b\pi^2 & -\gamma \end{pmatrix} \begin{pmatrix} 1 \\ P \\ R \end{pmatrix} = 0 \tag{5.37}$$

giving

$$P = \frac{\gamma\xi\lambda}{\gamma\lambda^2 + \xi\pi^2} \qquad R = P + d_c. \tag{5.38}$$

The solution to the $O(\epsilon^2)$ problem is

$$\underline{u}_2 = \begin{pmatrix} 1 \\ P \\ R \end{pmatrix} (p_1(\tau)\cos\pi x + q_1(\tau)\sin\pi x) - \underline{u}^* \tag{5.39}$$

where

$$L\underline{u}^* = (q^2(\tau) - p^2(\tau))\cos 2\pi x \begin{pmatrix} (P-R)\pi^2 \\ P^2\pi^2 \\ RP\pi^2 \end{pmatrix} - 2p(\tau)q(\tau)\sin 2\pi x \begin{pmatrix} (P-R)\pi^2 \\ P^2\pi^2 \\ RP\pi^2 \end{pmatrix}. \tag{5.40}$$

Let

$$\underline{u}^* = \underline{w}_1 \cos 2\pi x + \underline{w}_2 \sin 2\pi x \tag{5.41}$$

which gives

$$\begin{aligned} \underline{w}_1 &= (q^2(\tau) - p^2(\tau))(N_{2\pi})^{-1} \begin{pmatrix} (P-R)\pi^2 \\ P^2\pi^2 \\ PR\pi^2 \end{pmatrix} \\ &= (q^2(\tau) - p^2(\tau) \begin{pmatrix} A \\ B \\ C \end{pmatrix} \qquad (5.42) \\ \underline{w}_2 &= -2p(\tau)q(\tau)(N_{2\pi})^{-1} \begin{pmatrix} (P-R)\pi^2 \\ P^2\pi^2 \\ PR\pi^2 \end{pmatrix} = -2p(\tau)q(\tau) \begin{pmatrix} A \\ B \\ C \end{pmatrix} \qquad (5.43) \end{aligned}$$

Now

$$N_{2\pi} = \begin{pmatrix} -4\pi^2 d_c & -4\pi^2 & 4\pi^2 \\ \gamma\xi & -\gamma\lambda - 4\frac{\xi\pi^2}{\lambda} & 0 \\ \gamma b & -4b\pi^2 & -\gamma \end{pmatrix} \tag{5.44}$$

and so

$$(N_{2\pi})^{-1} = \frac{K}{\Delta} \tag{5.45}$$

where

$$\Delta = 4\pi^2\gamma((b-d_c)(\gamma\lambda + 4\frac{\xi\pi^2}{\lambda}) - \xi(4\pi^2 b - \gamma)) \tag{5.46}$$

and

$$K = \begin{pmatrix} \gamma(\gamma\lambda + 4\frac{\xi\pi^2}{\lambda}) & \gamma^2\xi & \gamma b(\gamma\lambda + 4(1-\lambda)\frac{\xi\pi^2}{\lambda}) \\ -4\pi^2(4b\pi^2 + \gamma) & -4\pi^2\gamma(b-d_c) & -4\pi^2 b(4\pi^2 d_c + \gamma) \\ 4\pi^2(\gamma\lambda + 4\frac{\xi\pi^2}{\lambda}) & 4\pi^2\gamma\xi & 4\pi^2((\gamma\lambda + 4\frac{\xi\pi^2}{\lambda})d_c + \gamma^2\lambda \end{pmatrix} \tag{5.47}$$

giving

$$\begin{aligned} A &= \frac{\pi^2}{\Delta}\left[\gamma(P-R)(\gamma\lambda + 4\frac{\xi\pi^2}{\lambda}) + P^2\gamma^2\xi + PR\gamma(\gamma\lambda \right. \\ &\qquad \left. +4(1-\lambda)\frac{\xi\pi^2}{\lambda})\right] \qquad (5.48) \\ B &= \frac{-4\pi^4}{\Delta}[(P-R)(4b\pi^2+\gamma) + P^2\gamma(b-d_c) + PRb(4\pi^2 d_c + \gamma)] \qquad (5.49) \\ C &= \frac{4\pi^4}{\Delta}\left[(P-R)(\gamma\lambda + 4\frac{\xi\pi^2}{\lambda}) + P^2\gamma\xi + PR(d_c(\gamma\lambda \right. \\ &\qquad \left. +4\frac{\xi\pi^2}{\lambda}) + \gamma\xi)\right]. \qquad (5.50) \end{aligned}$$

At $O(\epsilon^3)$ secular terms can occur. These are suppressed in the usual way by making $J_1(\underline{u}_1, \underline{u}_2)$ orthogonal to the bounded solutions of the homogeneous adjoint equation with inner product

$$\underline{u}.\underline{v} = \lim_{T_1\to\infty}\frac{1}{T_1}\int_0^{T_1}\int_0^2 \underline{u}^T\underline{v}dxdt. \tag{5.51}$$

The bounded solutions are

$$\begin{pmatrix} 1 \\ X \\ Y \end{pmatrix}\sin\pi x \text{ and } \begin{pmatrix} 1 \\ X \\ Y \end{pmatrix}\cos\pi x \tag{5.52}$$

where

$$[M^T - \pi^2 D^T]\begin{pmatrix} 1 \\ X \\ Y \end{pmatrix} = 0 \tag{5.53}$$

giving

$$X = \frac{-\pi^2(b - d_c)}{\gamma\xi} \qquad Y = \frac{\pi^2}{\gamma}. \tag{5.54}$$

The terms in $\underline{u}_2$ involving $\sin \pi x$ and $\cos \pi x$ make no contribution to the inner product so we need only consider $\underline{u}_2 = -\underline{u}^*$. This gives rise to the following simultaneous ordinary differential equations for the amplitudes $p(\tau)$ and $q(\tau)$

$$\begin{aligned} \frac{dp}{d\tau} &= p(\alpha + \beta q^2 + \beta p^2) \\ \frac{dq}{d\tau} &= q(\alpha + \beta q^2 + \beta p^2) \end{aligned} \tag{5.55}$$

where

$$\alpha = \frac{-\pi^2\nu}{1 + XP + YR}, \quad \beta = \frac{(A(P - R) - 2(B - C) - XBP + Y(PC - 2RB))\pi^2}{2(1 + XP + YR)}. \tag{5.56}$$

These reduce to

$$\frac{dU}{d\tau} = 2U(\alpha + \beta U) \quad \text{where} \quad U = p^2 + q^2 \tag{5.57}$$

with solution

$$U = \frac{\alpha F e^{2\alpha\tau}}{1 - \beta F e^{2\alpha\tau}}, \quad F \text{ an arbitary constant.} \tag{5.58}$$

Thus as $\tau \to \infty$

$$U \to 0 \text{ if } \alpha < 0 \qquad U \to \frac{\alpha}{-\beta} \text{ if } \alpha > 0. \tag{5.59}$$

This last expression is only be realistic in terms of $p(\tau)$ and $q(\tau)$ if $\beta < 0$. So for a heterogeneous spatial pattern to form we must be in the region of the $(\xi, \lambda, b, \gamma)$ parameter space where $\alpha > 0$ and $\beta < 0$. This requires

$$1 + XP + YR > 0 \text{ and } A(P - R) - 2(B - C) - XBP + Y(PC - 2RB) < 0. \tag{5.60}$$

If this is the case then, as $t \to \infty$, $\tau \to \infty$, the solution $\underline{u}_1$ is of the form

$$\underline{u}_1 = \left(\frac{\alpha}{-\beta}\right)^{\frac{1}{2}} \begin{pmatrix} 1 \\ P \\ R \end{pmatrix} \sin(\pi x + \theta) \tag{5.61}$$

where θ is obtained from the boundary and initial conditions and is such that

$$p(\tau) \to \left(\frac{\alpha}{-\beta}\right)^{\frac{1}{2}} \sin\theta \qquad q(\tau) \to \left(\frac{\alpha}{-\beta}\right)^{\frac{1}{2}} \cos\theta \quad \text{as } \tau \to \infty. \tag{5.62}$$

Taking boundary conditions fixed at the steady state implies θ=0 and the analysis shows that we can obtain a stable one-humped pattern as shown in Figure 5.6. However this says nothing about the splitting from one hump to two required for branching or about the oscillations that have been observed. To see if we can explain this phenomena we now consider the case when the real part of the complex roots of the dispersion relation becomes positive.

5.4 Nonlinear Analysis (ii)

Let us assume (for the moment) that there exist parameters such that the dispersion relation is of the form shown in Figure 5.7. We assume that the real part of the complex solution just touches the k^2 axis at $k^2 = k_1^2$ ($k_1 = \pi, 2\pi, 3\pi, ...$). We also assume that the intersection of the real solution with the k^2 axis is at $k_c^2 < \pi^2$ so that when we consider the model under the boundary conditions which give the peak dipersion relation, the real solution will make no contribution. At $k^2 = k_1^2$, $\sigma(k_1^2) = \pm i\sqrt{B_1(k_1^2)}$ where $B_1(k_1^2)$ is the coefficient of σ in the dispersion equation (5.6). We now attempt another nonlinear analysis on the system (5.22). We look for solutions of the form

$$\underline{u} = \begin{pmatrix} n \\ r \\ a \end{pmatrix} = \underline{u}_0 + \sum_{j=1} \epsilon^j \underline{u}_j(x, \tau, t) \tag{5.63}$$

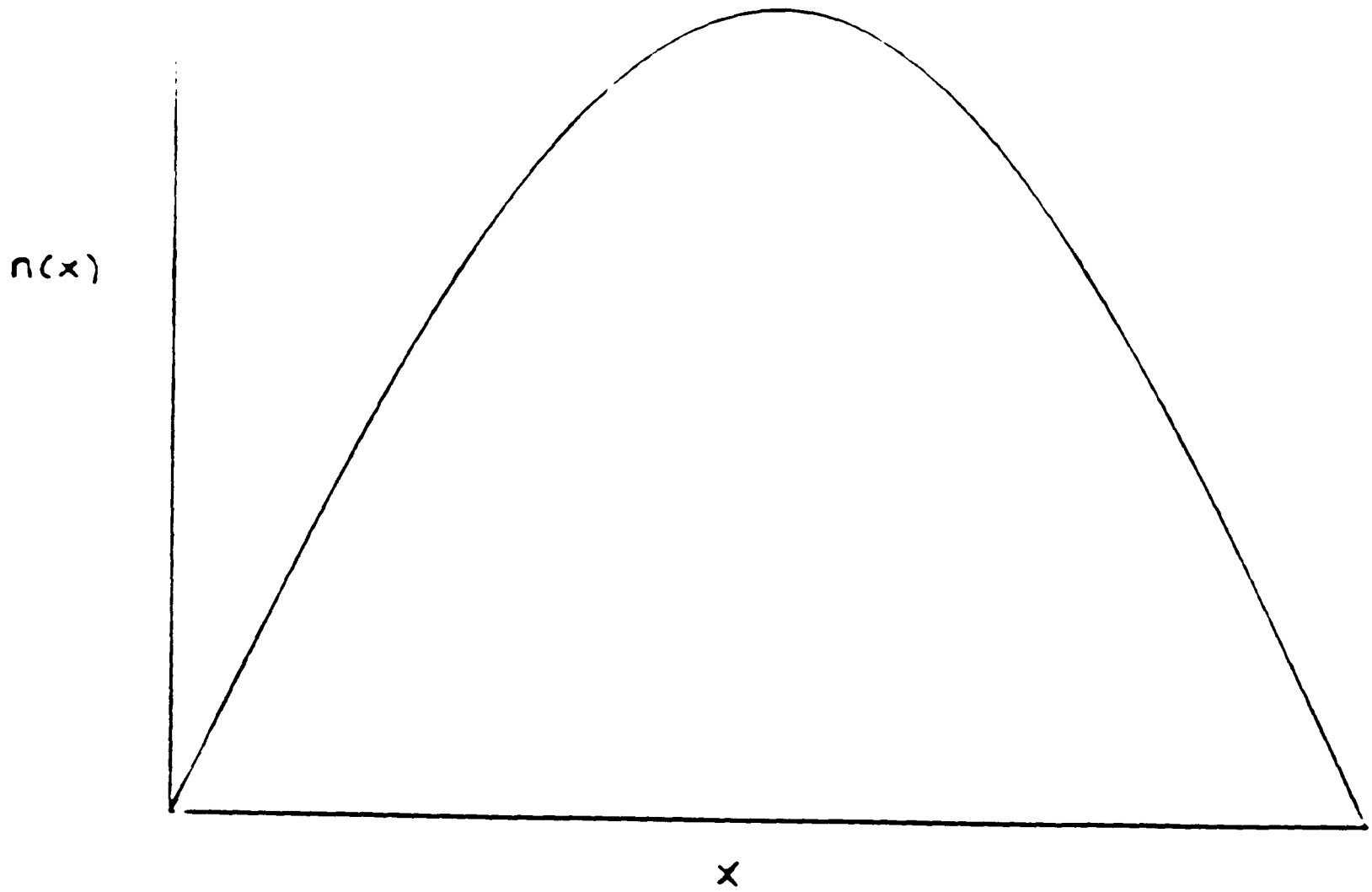

Figure 5.6: One-humped stationary pattern predicted by the nonlinear analysis.

where

$$\tau = \epsilon^2 t, \quad b = b_c + \epsilon^2. \tag{5.64}$$

Equating orders of ϵ we obtain the same equations at $O(\epsilon)$ and $O(\epsilon^2)$ as (5.31) and (5.32). At $O(\epsilon^3)$ we have a different equation to (5.33), namely

$$\begin{aligned}
&\frac{\partial \underline{u}_3}{\partial t} - L\underline{u}_3 = -\frac{\partial \underline{u}_1}{\partial \tau} + \Gamma \underline{u}_1 + Z\underline{u}_{1xx} \\
&+ \begin{pmatrix} n_1(r_{2xx} - a_{2xx}) & + & n_{1x}(r_{2x} - a_{2x}) & + & n_2(r_{1xx} - a_{1xx}) & + & n_{2x}(r_{1x} - a_{1x}) \\ r_1 r_{2xx} & + & r_{1x} r_{2x} & + & r_2 r_{1xx} & + & r_{2x} r_{1x} \\ a_1 r_{2xx} & + & a_{1x} r_{2x} & + & a_2 r_{1xx} & + & a_{2x} r_{1x} \end{pmatrix} \\
&= \underline{J}(\underline{u}_1, \underline{u}_2)
\end{aligned} \tag{5.65}$$

where L is given by (5.34) and

$$\Gamma = \begin{pmatrix} 0 & 0 & 0 \\ 0 & 0 & 0 \\ \gamma & 0 & 0 \end{pmatrix} \quad Z = \begin{pmatrix} 0 & 0 & 0 \\ 0 & 0 & 0 \\ 0 & 1 & 0 \end{pmatrix}. \tag{5.66}$$

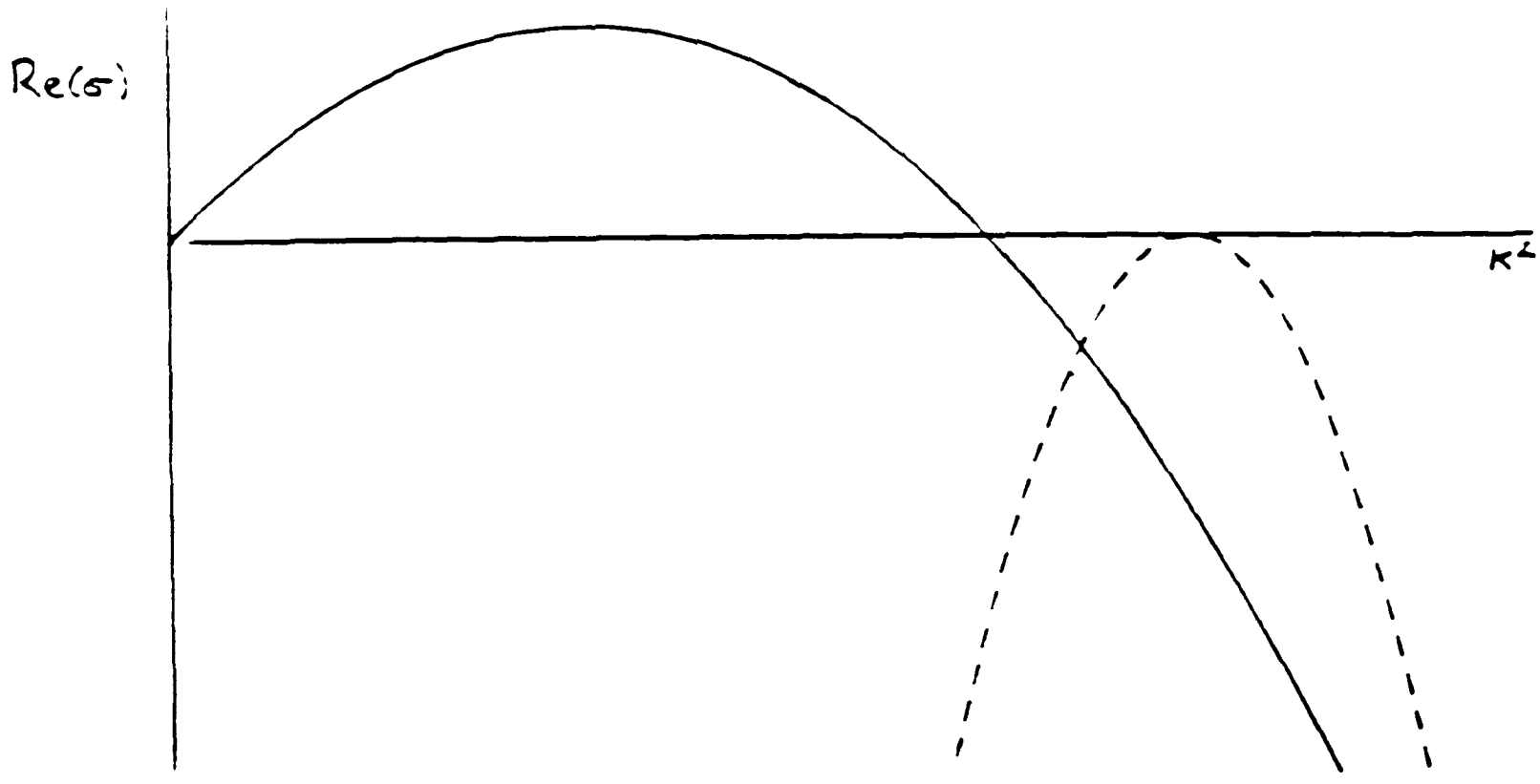

Figure 5.7: Solution to the dispersion equation (5.6) when the real part of the complex solution just touches the k^2 axis.

Consider the $O(\epsilon)$ equation. For $b = b_c + \epsilon^2$ the system has exponential growth rate $O(\epsilon^2 t)$ so we can incorporate this into the τ dependence of the model. At this stage a full analysis of this would look for dispersive waves, that is, a wave train of solutions giving rise to a group velocity with solutions of the form

$$\int \Omega(k) e^{i(\omega t - kx)} dk \quad \text{where } \sigma = \sigma_R + i\omega \tag{5.67}$$

and $\Omega(k)$ incorporates the e^{σ_R} dependence. To solve this type of problem we would use the method of stationary phase. However the problem we are considering makes this type of analysis very difficult so we restrict ourselves to looking at a particular monochromatic periodic solution - a standing wave solution satisfying boundary conditions fixed at the steady state. This gives the solution as

$$\underline{u}_1 = p(\tau) \sin k_1 x \left[\begin{pmatrix} 1 \\ P \\ R \end{pmatrix} \cos Qt + \begin{pmatrix} A \\ B \\ C \end{pmatrix} \sin Qt \right] \tag{5.68}$$

where

$$Q = \sqrt{B_1(k_1^2)}. \tag{5.69}$$

Note that because the real solution to the dispersion relation intersects at $k_c^2 < \pi^2$ there is no contribution to the resulting pattern from this term. Solutions of this form are possible iff

$$\begin{aligned} & p(\tau)\sin k_1 x \left[-\begin{pmatrix} 1 \\ P \\ R \end{pmatrix} Q \sin Qt + \begin{pmatrix} A \\ B \\ C \end{pmatrix} Q \cos Qt \right] \\ & = \begin{pmatrix} -dk_1^2 & -k_1^2 & k_1^2 \\ \gamma\xi & -\gamma\lambda - \frac{\xi k_1^2}{\lambda} & 0 \\ \gamma b_c & -b_c k_1^2 & -\gamma \end{pmatrix} \left[\begin{pmatrix} 1 \\ P \\ R \end{pmatrix} \cos Qt + \begin{pmatrix} A \\ B \\ C \end{pmatrix} \sin Qt \right] p(\tau)\sin k_1 x. \end{aligned} \tag{5.70}$$

To solve for the parameters P, R, A, B, C we equate the coefficients of $\sin Qt$ and $\cos Qt$ separately. Equating coefficients of $\sin Qt$ gives

$$-Q = k_1^2(C - B - Ad) \tag{5.71}$$

$$-PQ = \gamma\xi A - (\gamma\lambda + \frac{\xi k_1^2}{\lambda})B \tag{5.72}$$

$$-RQ = \gamma b_c A - b_c k_1^2 B - \gamma C \tag{5.73}$$

while equating coefficients of $\cos Qt$ gives

$$AQ = k_1^2(R - P - d) \tag{5.74}$$

$$BQ = \gamma\xi - (\gamma\lambda + \frac{\xi k_1^2}{\lambda})P \tag{5.75}$$

$$CQ = \gamma b_c - b_c k_1^2 P - \gamma R. \tag{5.76}$$

These are six simultaneous equations in five unknowns so the system is overdetermined. In the previous nonlinear analyses carried out we obtained three simultaneous equations in two unknowns at this stage but because of

the form of the dispersion relation these equations gave consistent solutions. This is not automatically true here so we obtain an extra restriction on the model parameters. From the coefficients of $\cos Qt$ we obtain

$$A = \frac{k_1^2}{Q}(R-P-d) \quad B = \frac{\gamma\xi - (\gamma\lambda + \frac{\xi k_1^2}{\lambda})P}{Q} \quad C = \frac{\gamma b_c - k_1^2 P - \gamma R}{Q}. \tag{5.77}$$

Substituting for A, B and C in (5.71) gives $R = XP + Y$ where

$$X = \frac{k_1^2(d - b_c + \frac{\xi}{\lambda}) + \gamma\lambda}{\gamma + k_1^2 d} \quad Y = \frac{\gamma k_1^2(b_c - \xi) + d^2 k_1^4 + Q^2}{\gamma + dk_1^2}. \tag{5.78}$$

Substituting this expression for R and the expressions for A, B, C into (5.72) gives

$$P = \frac{(\gamma\lambda + \frac{\xi k_1^2}{\lambda})\gamma\xi - Y\gamma\xi k_1^2 + \gamma\xi d k_1^2}{(\gamma\lambda + \frac{\xi k_1^2}{\lambda})^2 - \gamma\xi k_1^2(1 - X) + Q^2}. \tag{5.79}$$

So far we have not used (5.73). As before, substitute in the expressions for R, A, B and C to obtain

$$P = \frac{-Y(Q^2 + \gamma b_c k_1^2 + \gamma^2) + \gamma^2 b_c + \gamma b_c k_1^2(\xi + d)}{X(Q^2 + \gamma b_c k_1^2 + \gamma^2) + b_c k_1^2(\gamma\lambda + \frac{\xi k_1^2}{\lambda})}. \tag{5.80}$$

The extra parameter restriction comes from requiring these two values for P to be equal. With this expression for the $O(\epsilon)$ solution, the $O(\epsilon^2)$ equation (5.32) now reads

$$\begin{aligned}\frac{\partial \underline{u}_2}{\partial t} - L\underline{u}_2 &= \frac{p^2(\tau)k_1^2}{2}\cos 2k_1 x \left[\begin{pmatrix} (P-R) + A(B-C) \\ P^2 + B^2 \\ PR + BC \end{pmatrix} \right. \\ &\left. + \begin{pmatrix} A(P-R) + (B-C) \\ 2PB \\ BR + PC \end{pmatrix} \sin 2Qt + \begin{pmatrix} (P-R) - A(B-C) \\ P^2 - B^2 \\ PR - BC \end{pmatrix} \cos 2Qt \right] \\ &= \frac{p^2(\tau)k_1^2}{2}\cos 2k_1 x[\underline{v}_1 + \underline{v}_2 \sin 2Qt + \underline{v}_3 \cos 2Qt] = \underline{J}_1(\underline{u}_1).\end{aligned} \tag{5.81}$$

The solution to this is

$$\underline{u}_2 = p_1(\tau)\sin k_1 x \left[\begin{pmatrix} 1 \\ P \\ R \end{pmatrix} \cos Qt + \begin{pmatrix} A \\ B \\ C \end{pmatrix} \sin Qt \right] + \underline{u}^* \tag{5.82}$$

where

$$\frac{\partial \underline{u}^*}{\partial t} - L\underline{u}^* = \underline{J}_1. \tag{5.83}$$

Let

$$\underline{u}^* = [\underline{w}_1 + \underline{w}_2 \sin 2Qt + \underline{w}_3 \cos 2Qt] \cos 2k_1 x. \tag{5.84}$$

Solving for $\underline{w}_1$ *etc.* gives

$$\underline{w}_1 = \frac{p^2(\tau)k_1^2}{2} D_1^{-1}\underline{v}_1 \quad = p^2(\tau) \begin{pmatrix} W_{11} \\ W_{12} \\ W_{13} \end{pmatrix} \tag{5.85}$$

$$\begin{aligned} \underline{w}_2 &= \frac{p^2(\tau)k_1^2}{2} \left(2QD_1^{-1} + \frac{1}{2Q} D_1\right)^{-1} \left(D_1^{-1}\underline{v}_3 + \frac{1}{2Q}\underline{v}_2\right) \\ &= p^2(\tau) \begin{pmatrix} W_{21} \\ W_{22} \\ W_{23} \end{pmatrix} \end{aligned} \tag{5.86}$$

$$\begin{aligned} \underline{w}_3 &= \frac{p^2(\tau)k_1^2}{2} \left(2QD_1^{-1} + \frac{1}{2Q} D_1\right)^{-1} \left(\frac{1}{2Q}\underline{v}_3 - D_1^{-1}\underline{v}_2\right) \\ &= p^2(\tau) \begin{pmatrix} W_{31} \\ W_{32} \\ W_{33} \end{pmatrix} \end{aligned} \tag{5.87}$$

where

$$D_1 = \begin{pmatrix} 4k_1^2 d & 4k_1^2 & -4k_1^2 \\ -\gamma\xi & \gamma\lambda + \frac{\xi k_1^2}{\lambda} & 0 \\ -\gamma b_c & 4k_1^2 b_c & \gamma \end{pmatrix}. \tag{5.88}$$

At $O(\epsilon^3)$ secular terms can arise. These are suppressed in the usual manner by requiring $\underline{J}(\underline{u}_1, \underline{u}_2)$ to be orthogonal to the bounded solutions of the homogeneous adjoint equation. Terms in $\underline{u}_2$ of the form $\sin k_1 x f(t)$ make no contribution to the inner product so we consider $\underline{u}_2 = \underline{u}^*$. In this case

$$\begin{aligned} \underline{J}(\underline{u}_1, \underline{u}_2) &= -\frac{\partial \underline{u}_1}{\partial \tau} + \Gamma\underline{u}_1 + Z\underline{u}_{1xx} \\ &- 2k_1^2 p^3(\tau) \sin 2k_1 x \cos k_1 x (\underline{F}_1 \cos Qt + \underline{G}_1 \sin Qt + \underline{F}_2 \cos Qt \sin 2Qt \\ &+ \underline{G}_2 \sin Qt \sin 2Qt + \underline{F}_3 \cos Qt \cos 2Qt + \underline{G}_3 \sin Qt \cos 2Qt) \end{aligned} \tag{5.89}$$

$$- \quad k_1^2 p^3(\tau) \sin k_1 x \cos 2k_1 x (\underline{H}_1 \cos Qt + \underline{E}_1 \sin Qt + \underline{H}_2 \cos Qt \sin 2Qt$$

$$+ \quad \underline{E}_2 \sin Qt \sin 2Qt + \underline{H}_3 \cos Qt \cos 2Qt + \underline{E}_3 \sin Qt \cos 2Qt)$$

where

$$\underline{F}_i = \begin{pmatrix} (W_{i2} - W_{i3}) + W_{i1}(P - R) \\ 2PW_{i2} \\ PW_{i3} + RW_{i2} \end{pmatrix} \quad \underline{G}_i = \begin{pmatrix} A(W_{i2} - W_{i3}) + W_{i1}(B - C) \\ 2BW_{i2} \\ BW_{i3} + CW_{i2} \end{pmatrix} \tag{5.90}$$

$$\underline{H}_i = \begin{pmatrix} 4(W_{i2} - W_{i3}) + W_{i1}(P - R) \\ 5PW_{i2} \\ PW_{i3} + 4RW_{i2} \end{pmatrix} \quad \underline{E}_i = \begin{pmatrix} 4A(W_{i2} - W_{i3}) + W_{i1}(B - C) \\ 5BW_{i2} \\ BW_{i3} + 4CW_{i2} \end{pmatrix}. \tag{5.91}$$

For future use we define

$$\underline{F}_i = \begin{pmatrix} F_{i1} \\ F_{i2} \\ F_{i3} \end{pmatrix}, \quad etc. \tag{5.92}$$

The solution of the homogeneous adjoint equation is

$$\underline{\tilde{u}} = \sin k_1 x \left[\begin{pmatrix} 1 \\ X_1 \\ Y_1 \end{pmatrix} \cos Qt + \begin{pmatrix} S_1 \\ V_1 \\ Z_1 \end{pmatrix} \sin Qt \right] \tag{5.93}$$

where

$$\left[-\frac{\partial}{\partial t} - \gamma \begin{pmatrix} 0 & \xi & b_c \\ 0 & -\lambda & 0 \\ 0 & 0 & -1 \end{pmatrix} - \begin{pmatrix} d & 0 & 0 \\ 1 & \frac{\xi}{\lambda} & b_c \\ -1 & 0 & 0 \end{pmatrix} \frac{\partial^2}{\partial x^2} \right] \underline{\tilde{u}} = 0. \tag{5.94}$$

Again this gives six equations in five unknowns. As before we obtain a restriction on the parameters necessary for this type of solution to be valid.

Solving for these five unknowns S_1, V_1, Z_1, Y_1 and X_1 we obtain

$$S_1 = \frac{dk_1^2 - \gamma\xi X_1 - \gamma b_c Y_1}{Q} \quad V_1 = \frac{[k_1^2(1 + b_c Y_1) + (\gamma\lambda + \frac{\xi k_1^2}{\lambda})X_1]}{Q}, \tag{5.95}$$

$$Z_1 = \frac{\gamma Y_1 - k_1^2}{Q} \qquad Y_1 = \theta_1 X_1 + \phi_1 \tag{5.96}$$

where

$$\theta_1 = \frac{-\xi((\gamma\lambda + \frac{\xi k_1^2}{\lambda}) + dk_1^2)}{b_c(\gamma + \xi k_1^2 + dk_1^2)} \quad \phi_1 = \frac{\gamma b_c - \gamma\xi k_1^2 + d^2 k_1^2 + Q^2}{\gamma b_c(\gamma + \xi k_1^2 + dk_1^2)} \tag{5.97}$$

giving

$$X_1 = \frac{-\phi_1 b_c k_1^2(\gamma\lambda + \frac{\xi k_1^2}{\lambda}) - k_1^2[k_1^2(d - b_c) + (\gamma\lambda + \frac{\xi k_1^2}{\lambda})]}{(\gamma\lambda + \frac{\xi k_1^2}{\lambda})^2 - \gamma\xi k_1^2 + \theta_1(\gamma\lambda + \frac{\xi k_1^2}{\lambda})b_c k_1^2 + Q^2} \tag{5.98}$$

and

$$X_1 = \frac{-\phi_1(Q^2 + k_1^2\gamma b_c + \gamma^2) + k_1^2(dk_1^2 + \gamma)}{\theta_1(Q^2 + k_1^2\gamma b_c + \gamma^2) + \gamma\xi k_1^2}. \tag{5.99}$$

The extra parameter restriction comes from requiring these two values of X_1 to be equal.

Supression of secular terms requires

$$\int_0^{\frac{2\pi}{k_1}} \int_0^{\frac{2\pi}{Q}} [\underline{J}_1(\underline{u}_1, \underline{u}_2)]^T \underline{\tilde{u}} dt dx = 0. \tag{5.100}$$

This gives the Landau equation for the amplitude as

$$\delta \frac{dp}{d\tau} = \alpha_1 p - \beta_1 p^3 \tag{5.101}$$

or

$$\frac{dp}{d\tau} = \alpha p - \beta p^3 \qquad \alpha = \frac{\alpha_1}{\delta}, \quad \beta = \frac{\beta_1}{\delta} \tag{5.102}$$

where

$$\delta = (1 + PX_1 + RY_1) + (AS_1 + BV_1 + CZ_1) \tag{5.103}$$

$$\alpha_1 = Y_1(\gamma - k_1^2 P) + Z_1(\gamma A - k_1^2 B) \tag{5.104}$$

$$\begin{aligned} \beta_1 &= k_1^2[(F_{11} + F_{12}X_1 + F_{13}Y_1) + \frac{1}{2}(G_{21} + G_{22}X_1 + G_{23}Y_1) \\ &+ \frac{1}{2}(F_{31} + F_{32}X_1 + F_{33}Y_1) - \frac{1}{2}(H_{11} + H_{12}X_1 + H_{13}Y_1) \\ &- \frac{1}{4}(E_{21} + E_{22}X_1 + E_{23}Y_1) - \frac{1}{4}(H_{31} + H_{32}X_1 + H_{33}Y_1) \\ &+ (G_{11}S_1 + G_{12}V_1 + G_{13}Z_1) + \frac{1}{2}(F_{21}S_1 + F_{22}V_1 + F_{23}Z_1) \end{aligned} \tag{5.105}$$

$$- \frac{1}{2}(G_{31}S_1 + G_{32}V_1 + G_{33}Z_1) - \frac{1}{2}(E_{11}S_1 + E_{12}V_1 + E_{13}Z_1)$$
$$- \frac{1}{4}(H_{21}S_1 + H_{22}V_1 + H_{23}Z_1) + \frac{1}{4}(E_{31}S_1 + E_{32}V_1 + E_{33}Z_1)].$$

The solution to the Landau equation is

$$p(\tau) = \left(\frac{\frac{\alpha_1}{\delta} A_5 e^{2\frac{\alpha_1}{\delta}\tau}}{1 + \frac{\beta_1}{\delta} A_5 e^{2\frac{\alpha_1}{\delta}\tau}} \right)^{\frac{1}{2}} \quad \text{for some constant } A_5. \tag{5.106}$$

This shows that

$$\begin{array}{llllll} \text{if} & \frac{\alpha_1}{\delta} > 0, \ \frac{\beta_1}{\delta} > 0 & \text{then} & p(\tau) \to & \left(\frac{\alpha_1}{\beta_1}\right)^{\frac{1}{2}} & \text{as } \tau \to \infty \\ \text{if} & \frac{\alpha_1}{\delta} < 0, \ \frac{\beta_1}{\delta} < 0 & \text{then} & p(\tau) \to & 0 & \text{as } \tau \to \infty. \end{array} \tag{5.107}$$

For a heterogeneous spatial pattern to form we need $\frac{\alpha_1}{\delta} > 0$, $\frac{\beta_1}{\delta} > 0$. If we are in a region of the parameter space such that these conditions are satisfied then the solution $\underline{u}$ can be written as

$$\underline{u} = \underline{u}_0 + \epsilon \left(\frac{\alpha_1}{\beta_1}\right)^{\frac{1}{2}} \begin{pmatrix} X_3 \cos(Qt - \tan^{-1}\theta_3) \\ X_4 \cos(Qt - \tan^{-1}\theta_4) \\ X_5 \cos(Qt - \tan^{-1}\theta_5) \end{pmatrix} \sin k_1 x \quad \text{as } \tau \to \infty \tag{5.108}$$

where

$$\begin{array}{ll} X_3 = \sqrt{1 + A^2} & \theta_3 = A \\ X_4 = \sqrt{P^2 + B_2} & \theta_4 = \frac{B}{P} \\ X_5 = \sqrt{R^2 + C^2} & \theta_5 = \frac{C}{R}. \end{array} \tag{5.109}$$

In Figure 5.8 we illustrate the changing patterns for the cell densities that this analysis predicts as time increases for two specific values of k_1^2. We now examine whether it is possible to have the dispersion relation as drawn in Figure 5.7. Consider the behaviour of the dispersion equation (5.6) at $k^2 = k_1^2$. Assuming the real solution is negative, the roots can be written as

$$\sigma = -\sigma_1(k_1^2) \quad \sigma = \pm i\sigma_2(k_1^2) \quad \sigma_1, \sigma_2 > 0 \tag{5.110}$$

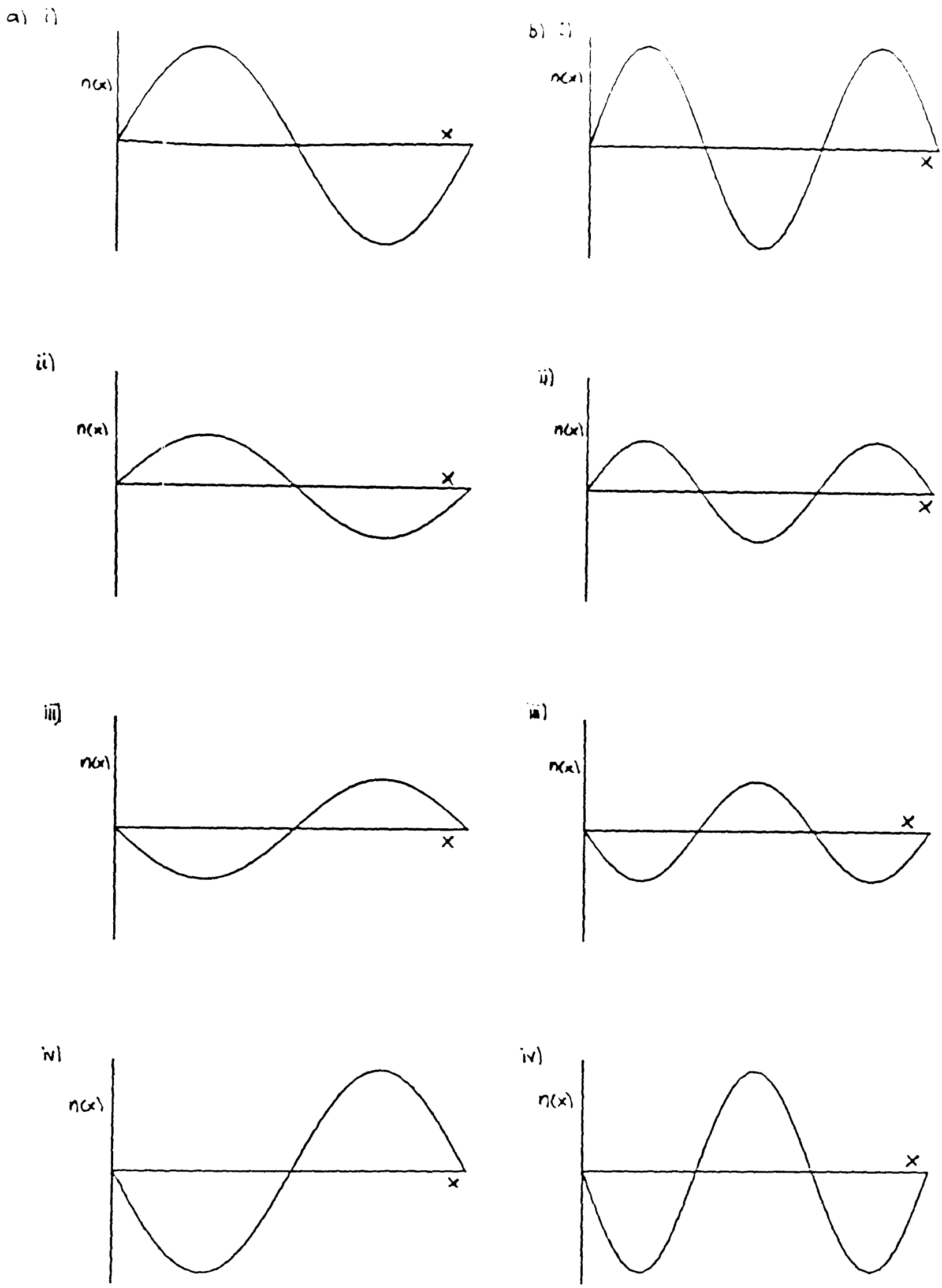

Figure 5.8: Standing wave patterns at varying times for the cell densities for two different values of k_1^2. a) $k_1^2 = 4\pi^2$,b) $k_1^2 = 9\pi^2$.

which gives

$$\sigma_1 = A_1(k_1^2) \quad \sigma_2^2 = B_1(k_1^2) \quad \sigma_1\sigma_2^2 = C_1(k_1^2) \tag{5.111}$$

so $\sigma_2 = \sqrt{B_1(k_1^2)}$. For this to be consistent we need $A_1(k_1^2)B_1(k_1^2) = C_1(k_1^2)$. From this relation we try to find a critical value for b.

For instability at that point only we know, by applying the Routh-Hurwitz criteria and noting that $A_1(k_1^2), C_1(k_1^2) > 0$, that $\forall k^2 \in (k_c^2, \infty)$, $A_1B_1 - C_1$ has a minimum value at $k^2 = k_1^2$ so we require

$$A_1B_1 - C_1 = 0 \qquad k^2 = k_1^2$$

$$A_1B_1 - C_1 > 0 \qquad k^2 \neq k_1^2 \quad k^2 \in (k_c^2, \infty) \tag{5.112}$$

$$i.e. \qquad \frac{\partial}{\partial k^2}(A_1B_1 - C_1) = 0 \qquad \text{at } k^2 = k_1^2. \tag{5.113}$$

As previously mentioned (*cf.* (5.13)) the conditions for $C_1(k_1^2)$ to be positive for $k > k_c$ and negative for $k < k_c$ are

$$b > d + \frac{\xi}{\lambda} \quad \text{and, if} \quad \lambda < 1 \quad b < \frac{d}{1-\lambda}. \tag{5.114}$$

$$A_1B_1 - C_1 = 0 \quad \Rightarrow \quad b_c = -\frac{k_1^2\gamma\left[\frac{d\xi k_1^2}{\lambda} + \gamma\lambda\left(d + \frac{\xi}{\lambda}\right)\right]}{k_1^2\gamma\left(k_1^2(\xi + d) + \gamma\right)}$$

$$+ \frac{\left[\left(d + \frac{\xi}{\lambda}\right)k_1^2 + \gamma(\lambda + 1)\right]\left[\frac{d\xi k_1^4}{\lambda} + k_1^2\gamma\left(d + \frac{\xi}{\lambda}\right)(\lambda + 1) + \gamma^2\lambda\right]}{k_1^2\gamma(k_1^2(\xi + d) + \gamma)}. \tag{5.115}$$

$$\frac{\partial}{\partial k^2}(A_1B_1 - C_1)\perp_{k_1^2} = 0 \qquad \Rightarrow b_c =$$

$$\frac{\frac{3d\xi}{\lambda}\left(d + \frac{\xi}{\lambda}\right)k_1^2 + 2\gamma k_1^2 + 2k_1^2\gamma\left[\left(d + \frac{\xi}{\lambda}\right)^2(\lambda + 1) - \frac{2d\xi}{\lambda}\right] + \gamma^2(\lambda + 1)^2\left(d + \frac{\xi}{\lambda}\right)}{2k_1^2\gamma(d + \xi) + \gamma^2}. \tag{5.116}$$

For the real part of the complex root to touch the k^2 axis at $k^2 = k_1^2$ we require these two values for b_c to be equal. Also for the real solution not

to give rise to any pattern when the model is considered with boundary conditions fixed at the steady state we require $d > d_c(\pi^2)$

$$i.e. \quad d > \left(1 - \frac{\lambda\xi\pi^2}{\gamma\lambda^2 + \xi\pi^2}\right) - \frac{\gamma\lambda\xi}{\gamma\lambda^2 + \xi\pi^2}. \tag{5.117}$$

All these conditions on the model parameters imply that the production of standing wave type patterns could be extremely sensitive. These standing wave patterns in themselves do not produce the branching or oscilating patterns required. In the next section we discuss how, by analytical manipulation, we can obtain the required patterns.

5.5 Discussion and Speculation

In this section we speculate as to how we could piece together the two solution types considered in the preceding two sections. Such manipulation is possible *if* we can find parameters such that the real part of the complex solution to the dispersion equation is just touching the k^2 axis at $k^2 = (2\pi)^2$ or $(3\pi)^2$ and the real solution is cutting the k^2 axis at $k^2 = \pi^2$. For parameter values satisfying these restrictions we could consider a solution of the form obtained by adding the solutions considered in the previous two sections to obtain a solution which displays the required properties. This composite solution (written for the cell density only) is of the form

$$n(x,t) \rightarrow A_1(\sin \pi x + A_2 \sin 2\pi x \cos(Qt - A_3)) \tag{5.118}$$

$$n(x,t) \rightarrow \tilde{A}_1(\sin \pi x + \tilde{A}_2 \sin 3\pi x \cos(Qt - \tilde{A}_3)) \tag{5.119}$$

for constants A_1, A_2, A_3 and $\tilde{A}_1, \tilde{A}_2, \tilde{A}_3$ determined by the analysis. Figures 5.9 and 5.10 show the behaviour of these for increasing values of t.

To analyse the model when we are considering a solution to the $O(\epsilon)$ problem of the form

$$\underline{u}_1 = \begin{pmatrix} 1 \\ P \\ R \end{pmatrix} p(\tau) \sin \pi x + q(\tau) \sin 3\pi x \left[\begin{pmatrix} 1 \\ X \\ Y \end{pmatrix} \cos Qt + \begin{pmatrix} A \\ B \\ C \end{pmatrix} \sin Qt \right] \tag{5.120}$$

has proved to be too complicated. To produce the patterns considered numerically will not require such stringent restrictions on the parameters as we do not need to consider the real part of the complex solution to the dispersion equation which just touches the k^2 axis at a particular value, only that the values of k^2 where the real part is positive contains $k^2 = (n\pi)^2$ for some values of n. This is the case considered numerically by Goldwasser *et al.* (1989) the results of which are shown in Figure 5.11. As we can see two humps form initially, then join and then split again. Another possibility for obtaining the branching behaviour (but not the oscillating behaviour) is to consider the real solution cutting the k^2 axis at some point $k_p^2 > (3\pi)^2$ so that the three possible growth modes can interact. It is not possible to consider this analytically as the growth rate at the modes would not be $O(\epsilon^2)$ which is necessary for this type of analysis.

The work presented in this chapter is theoretical and cannot be verified experimentally until the existence of the postulated adhesive sites is confirmed (or denied). The analysis serves only to show that such branching behaviour is possible from a model constructed from known cellular behaviour.

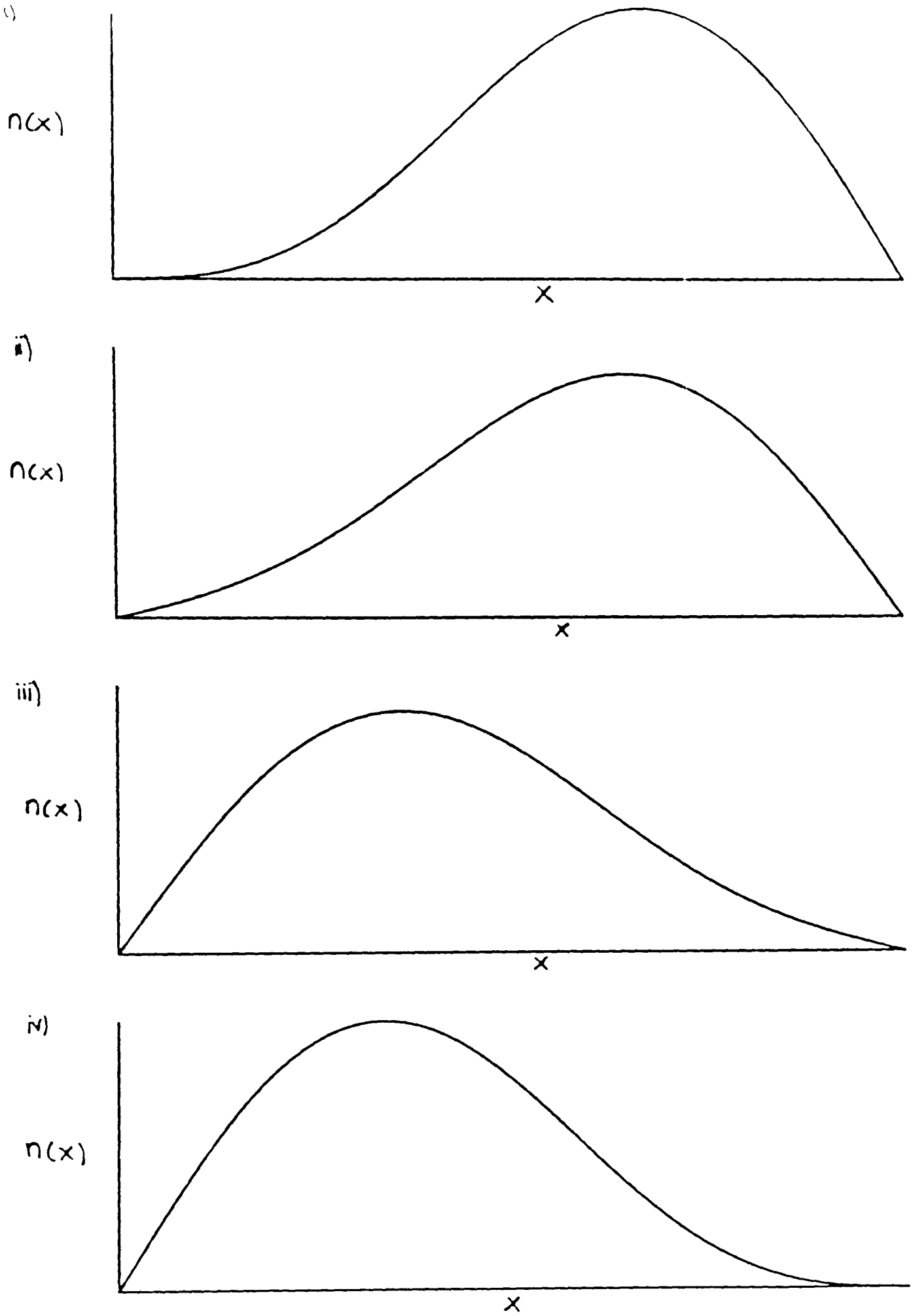

Figure 5.9: Oscillating pattern of cell density as time increases. Formed using the solution given in (5.118).

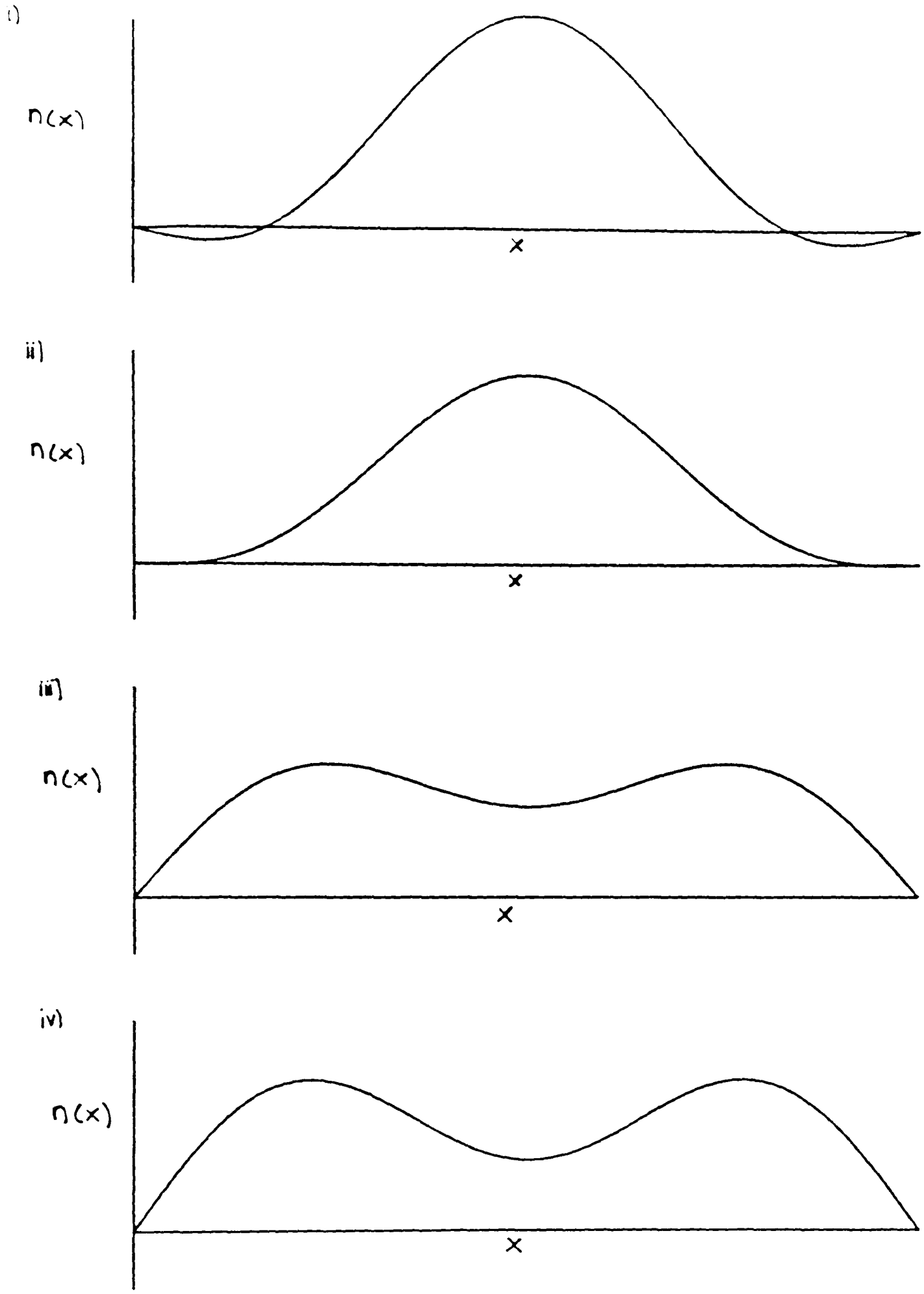

Figure 5.10: Branching patterns of cell density as time increases. Formed using the solution given in (5.119).

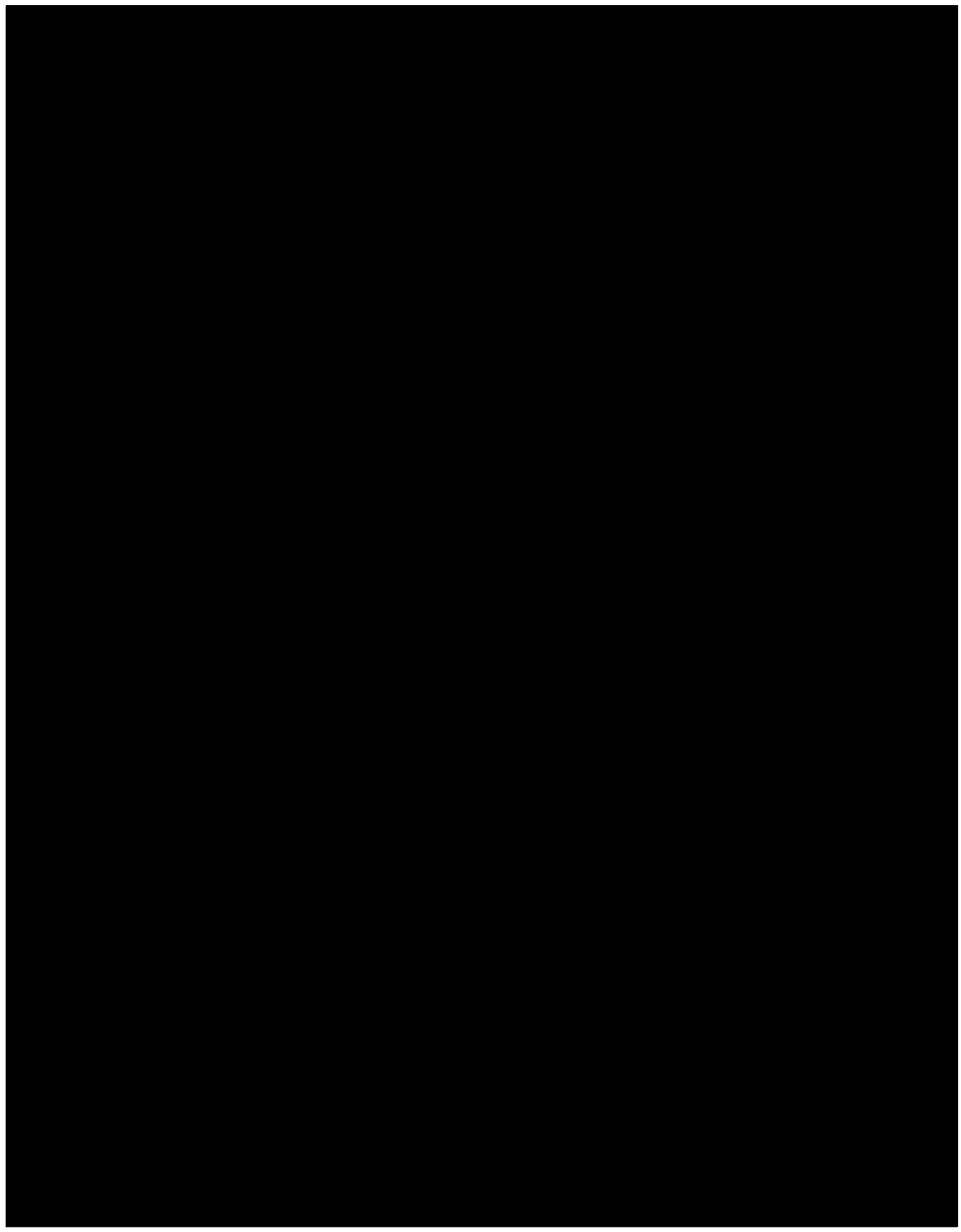

Figure 5.11: Numerical branching behaviour from Goldwasser *et al.* (1989).

Chapter 6

Development of an Eyespot on a Butterfly Wing under Coldshock.

6.1 Background.

In this chapter we examine the behaviour of a genetic switch model, suggested by Murray (1981b) to model pattern formation on lepidopteran wings, and attempt to incorporate the effect of a coldshock into the solution behaviour. A great deal of work has been carried out on the development of colour patterns on butterfly wings. The peak of activity was in the '20's and '30's when lepidopteran colour patterns were established as a tractable system to explore certain aspects of local control processes in development. The reviews by Sondhi (1963) and Nijhout (1978) give details of this work.

The reasons lepidopteran colour patterns are of such interest are twofold. Firstly there is a great diversity of patterns although the lepidoptera evolved only relatively recently, a fact reflected in the Nymphalid Groundplan (Schwanwitsch (1924)) which gives relationships among the various pattern elements. Secondly the patterns have a relatively simple structure. They are a two di-

mensional distribution of pigmented cells within a single layer. The cells do not move around so the observed pattern is an undistorted record of the pattern in which determination occured. Also the wings themselves are large (1-2cm) and are easily accessible to experimental manipulation and can tolerate considerable damage.

One of the most important elements in butterfly wing patterns are occelli (eyespots). Using Wolpert's (1969) theory of positional information, the simplest colour pattern that can be specified in a two dimensional system is a circle. All that is needed is a single point source for a positional signal and a homogeneous response threshold for the cells within the field of that signal. Nijhout (1978) suggests a gradient model based on a conical distribution with the apex as the reference point for positional information: the apex is considered to be the focus of the eyespot. Nijhout (1980) presents evidence that the foci of the eyespots are the influencing factors in surrounding pattern formation. He shows that the development of circular eyespots in the nymphalid butterfly *Precis coenia* is prevented when cautery, killing the cells at the presumptive focus, is carried out during the early part of pupal development. Furthermore when these presumptive foci are transplanted to a different part of the wing surface they were able to produce a circular pattern centered on the new location. The focus is assumed to generate a morphogen whose level activates a colour specific enzyme. This is the basis for Murray's (1981b) model which we analyse in later sections.

An alternative model, based on the existance of an underlying pre-pattern,

was proposed by Sibatani (1980). He suggests that the formation of an eyespot involves several interacting variables. These two models are not mutually exclusive since a model involving positional information relies on cells reacting in a specified manner to the level of some chemical: this could involve in Nijhout's (1978) gradient model the morphogen generated at the focus reacting to an underlying pattern.

There has been some work on the effect of cold and hot shocks during development and of thermal cautery, upon the wing patterns. The cautery work of Kühn and von Engelhardt (1933) on the wings of the moth *Ephestia kühniella* suggests that there are at least two mechanisms involved in the patterning as different effects are obtained depending upon the time after pupation cautery was carried out. They proposed a phenomenological model in which a 'determination stream' emanates from point sources on the anterior and posterior edges of the wing. However the more recent cautery experiments of Toussaint and French (1988) conclude that this theory is not valid as they do not observe the temporal sequence underlying the variability in the degree of global modification implied by the determination wave model. They suggest instead that the banded pattern on *Ephestia kühniella* could be caused by a line of foci acting as in Nijhout's (1978) model.

In Section 6.2 we describe the model and, using the simplest possible assumptions, show how an eyespot can be produced. In Section 6.3 we introduce a temperature variation (coldshock) by instantaneously changing the values of certain model parameters quantitatively in line with what might

be expected by a reduction in temperature and suggest how this could effect the growth of the eyespot. We then discuss the results obtained comparing them to experimental findings in Section 6.4.

6.2 A Model for Eyespot Development.

In this section we present a simple model mechanism, first suggested by Murray (1981b), involving a diffusing morphogen and a biochemically plausible gene or colour specific enzyme activation switch process capable of producing, amongst others, eyespot patterns. Nijhout (1980) suggests, after experimentation on the wings of *Precis coenia* that the foci of the eyespots are the influencing factor in their formation. The model, considered to act just after pupation, gives good results when compared with experiment.

We assume that the foci emits a pulse of morphogen S, of strength S_0, at a certain time after pupation, which then diffuses across the surface of the wing. We assume that, as it diffues, it also degrades linearly. The equation for the morphogen concentration $S(r,t)$ is then

$$\frac{\partial S}{\partial t} = D\left(\frac{\partial^2 S}{\partial r^2} + \frac{1}{r}\frac{\partial S}{\partial r}\right) - KS \tag{6.1}$$

where D ($\mathrm{cm^2 s^{-1}}$) is the diffusion coefficient and K ($\mathrm{s^{-1}}$) is the degredation rate constant. The value, at this stage, is purely speculative and is probably species dependent but a value of D of $\mathrm{O}(10^{-7}\ \mathrm{cm^2 s^{-1}})$ (Crick 1970) or smaller is reasonable.

As S diffuses across the wing surface, we assume that the cells respond to the local morphogen concentration and activate a gene G to produce a

product g. We assume that the gene product mechanism exhibits biological switch behaviour. The mechanism used by Murray (1981b) is the one used by Lewis *et al.* (1977), specifically

$$\frac{dg}{dt} = K_1 S + \frac{K_2 g^2}{(K_4 + g^2)} - K_3 g \tag{6.2}$$

for positive parameters K_i. Here g is activated linearly by the morphogen, from which it obtains its positional dependence, by its own product in a nonlinear negative feedback manner and is linearly degraded proportional to itself. Figure 6.1 shows the shape of this curve for different values of S. In

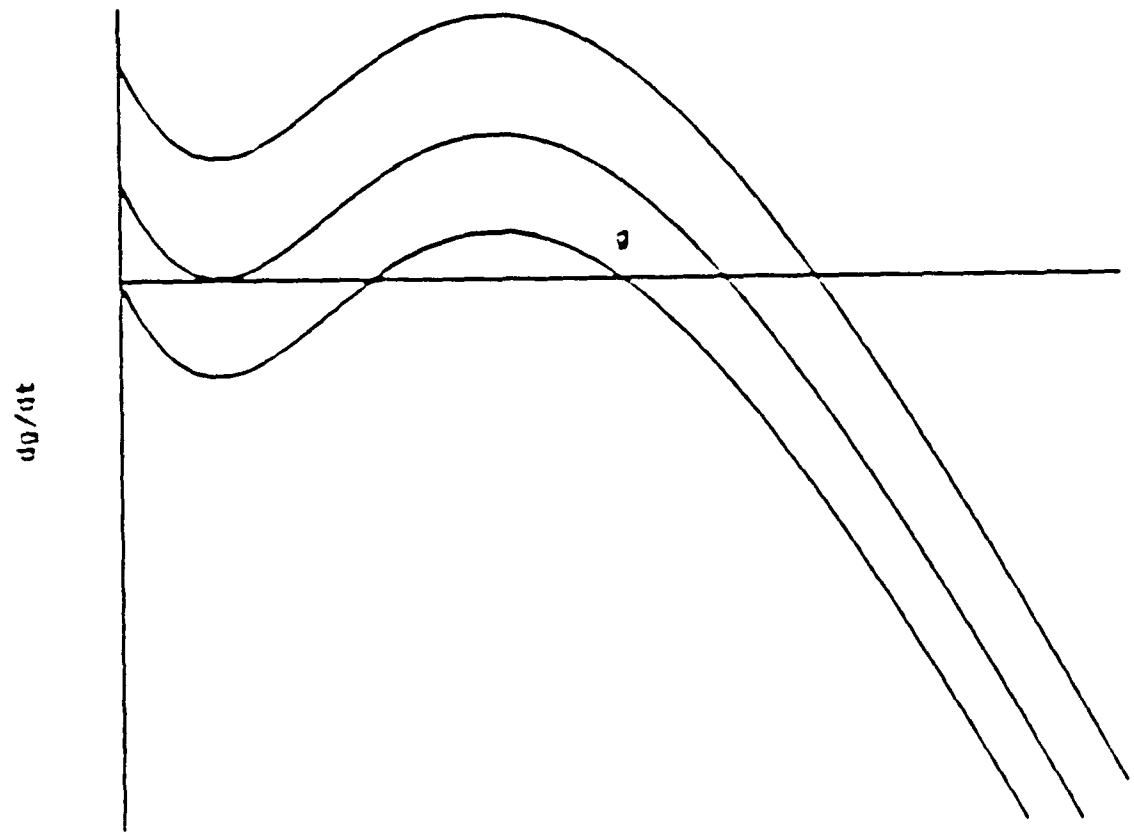

Figure 6.1: The curve g_t versus g from (6.2) for differing values of S.

fact, in this chapter, we consider an algebraically simpler switch mechanism, qualitatively similar to the original, namely

$$\frac{dg}{dt} = K_1 S + \alpha g(g - K_2)(g_c - g). \tag{6.3}$$

These equations (6.1) and (6.3) together with the conditions

$$S(r,0) = S_0\delta(r) \quad S(\infty,t) = 0 \tag{6.4}$$

form the model for the generation of eyespots.

So as to be able to obtain analytical results we assume that the gene product g is in equilibrium. A full analysis of the model when g is not in equilibrium, leading to a complex singular perturbation problem, is considered in Kath and Murray (1985). We nondimensionalise the system using

$$S^* = \frac{S}{S_0}, \quad g^* = \frac{g}{g_c}, \quad t^* = \frac{Dt}{a^2}, \quad r^* = \frac{r}{a}, \quad \gamma = \frac{a^2}{L^2} \tag{6.5}$$

where L (cm) is some standard reference length and a (cm) is a relevent length of interest in the wing, to give, on dropping the asterisks for notational convenience,

$$S_t = S_{rr} + r^{-1}S_r - \gamma kS \tag{6.6}$$

$$0 = k_1 S + g(g-k_2)(1-g) \tag{6.7}$$

$$S(r,0) = \delta(r), \quad S(\infty,r) = 0 \tag{6.8}$$

where

$$k = \frac{KL^2}{D}, \quad k_1 = \frac{K_1}{\alpha g_c^3 S_0}, \quad k_2 = \frac{K_2}{g_c}. \tag{6.9}$$

Initially all the gene product is assumed to be at state $g = 0$. As $S(r,t)$ increases, for each fixed r, the curve g_t is raised, as seen in Figure 6.1. If $S(r,t)$ exceeds S_c, the value of S where $g_t = 0$ has a double root, then the switch to the higher stable steady state will occur. Then, when $S(r,t)$ decreases again past S_c, the gene product will remain in the activated state.

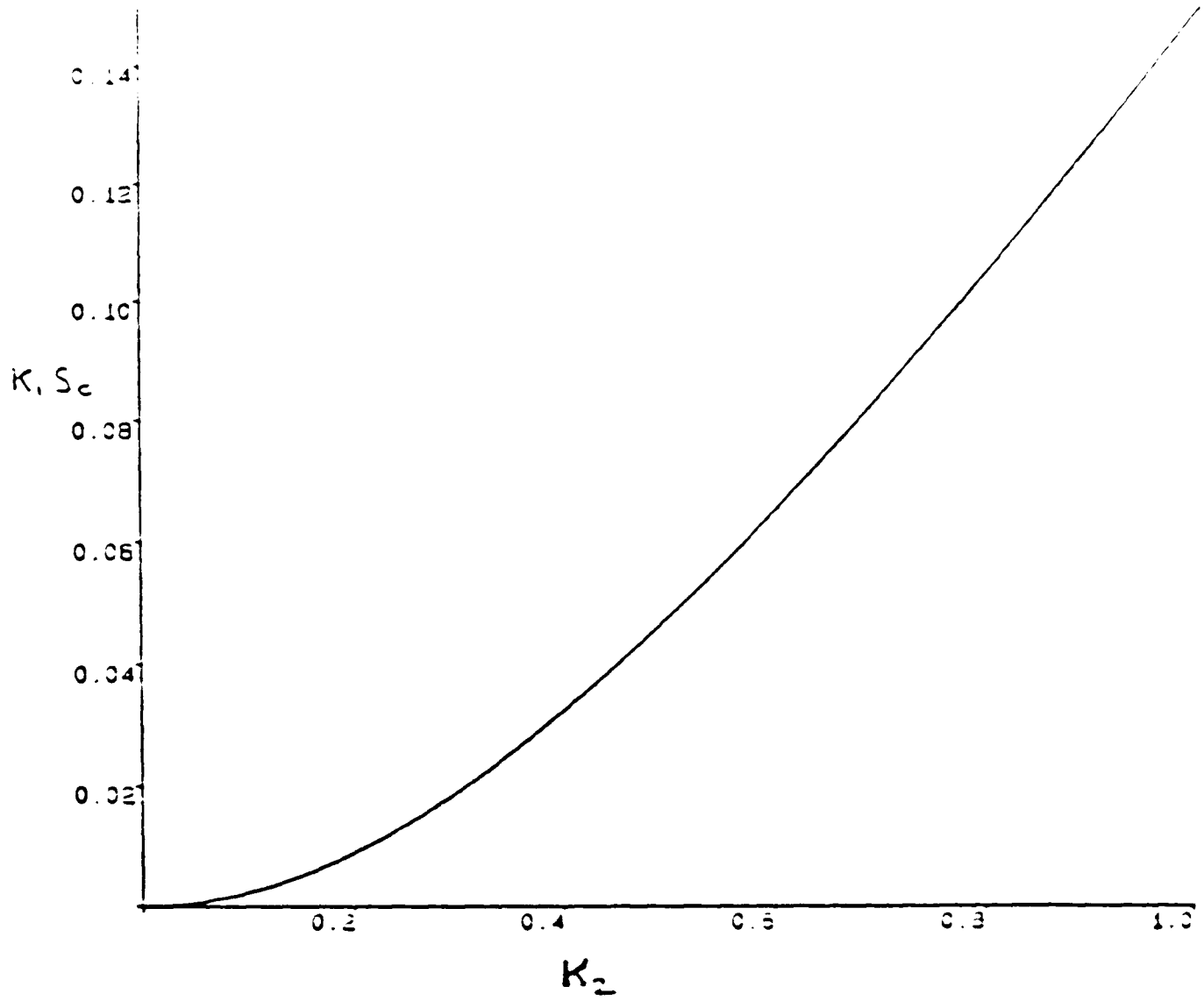

Figure 6.2: The critical value $k_1 S_c$ as a function of k_2 from (6.7).

Thus the problem of finding the size of the activated region is equivalent to finding the value of the radius where the maximum value achieved by the morphogen is S_c. By considering (6.7) to have a double root we find that S_c is given by

$$S_c = \frac{-(2 - 3k_2 - 3k_2^2 + 2k_2^3) + 2\sqrt{(1 - k_2 + k_2^2)}}{27k_1}. \tag{6.10}$$

Figure 6.2 shows the dependence of $k_1 S_c$ upon k_2. If we solve (6.6) with (6.8) we obtain

$$S(r,t) = \frac{1}{4\pi t} \exp\left[-\frac{r^2}{4t} - \gamma k t\right] \quad t > 0. \tag{6.11}$$

The maximum value of S ($=S_{\max}$), for a given r, is given by

$$S_{\max} = \left[\frac{\gamma k}{2\pi(z-1)}\right] e^{-z}, \quad z = (1 + \gamma k r^2)^{\frac{1}{2}}. \tag{6.12}$$

Thus the radius r_a of the activated domain where the gene switch has occured is given by

$$2\pi S_c(z_a - 1) - \gamma k e^{-z_a} = 0, \quad z_a = (1 + \gamma k r_a^2)^{\frac{1}{2}}. \tag{6.13}$$

To see how the radius of the activated domain grows in time we consider $R(t)$ to be the value of r such that $S = S_c$. This gives

$$R^2(t) = -4t[\gamma k t + \ln(4\pi t S_c)]. \tag{6.14}$$

Figure 6.3 shows the shape of the curve $R(t)$ for illustrative parameter values $k = 300$, $\gamma = 1$ and $S_c = 0.3$.

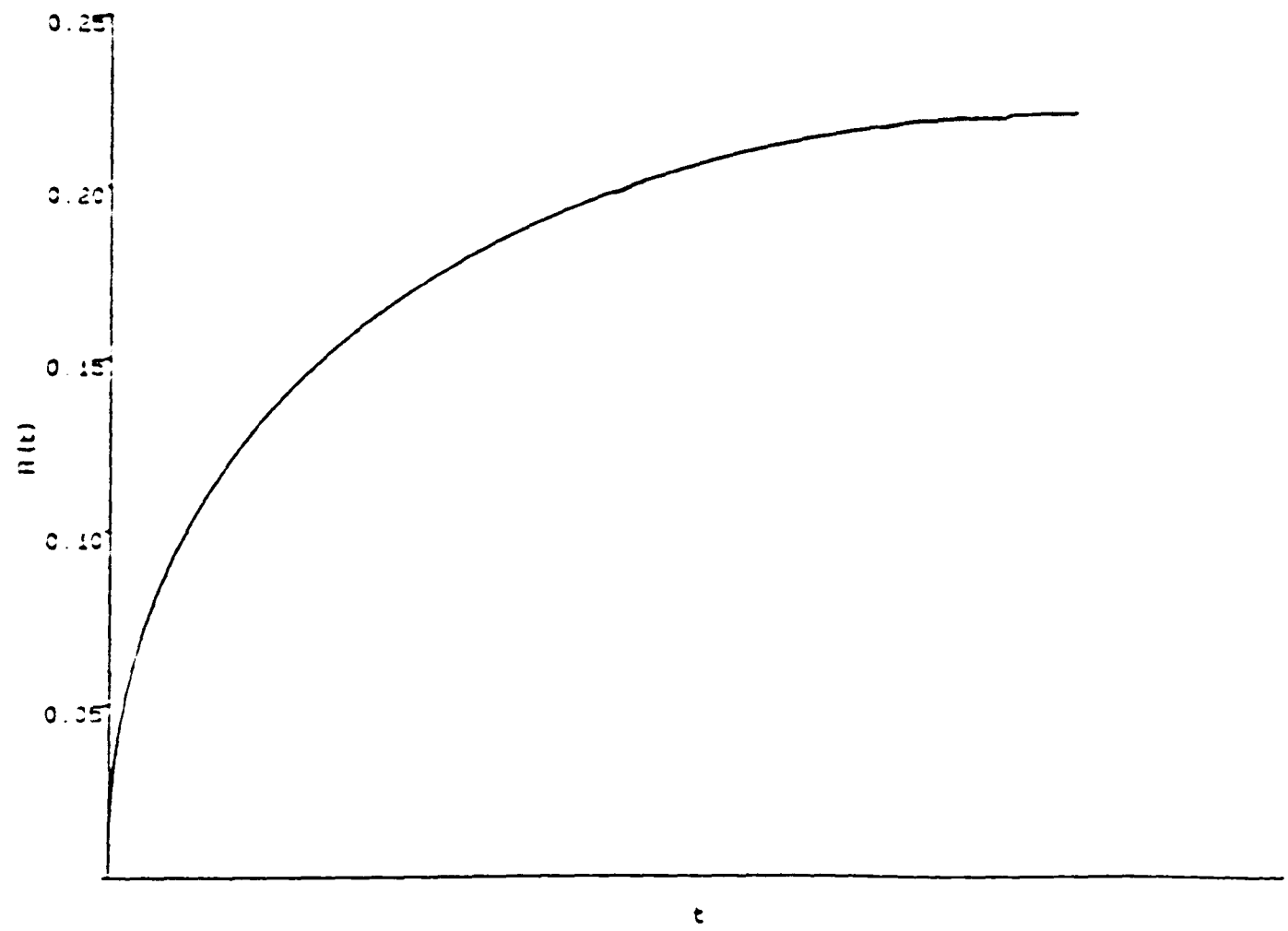

Figure 6.3: The radius $R(t)$ from (6.11) of the activated region as a function of time with parameter values $k = 300$, $\gamma = 1$ and $S_c = 0.3$.

This result can be compared with the experimental findings of Nijhout

(1980) if we convert this radius to the dimensional diameter d_1

$$d_1^2(t) = -16Dt[Kt + \ln t + C] \quad C = \ln\left[\frac{4\pi S_c D}{S_0 a^2}\right]. \tag{6.15}$$

The values of D, K and C can now be determined from a best fit analysis using (6.15) and the experimental points from Figure 6.4. As mentioned

Figure 6.4: Diameter of the developing eyespot at different temperatures, taken from Nijhout (1980) as compared with the analytical results from Murray (1989).

at the start of the section we have no information about the degredation rate constant of an unknown morphogen. We do, however, have information about how diffusion coefficients vary with temperature. The fitting process, carried out by Murray (1989), gave the values $D = 4 \times 10^{-9}\text{cm}^2\text{s}^{-1}$ at 29°C and $D = 6 \times 10^{-10}\text{cm}^2\ \text{s}^{-1}$ at 19°C. The velocity of spread of the eyespot,

$v(t) = \frac{d[d_1(t)]}{dt}$, from (6.15) is given by

$$v(t) = \frac{-2D([Kt + \ln t + C] + t[K + t^{-1}])}{(-Dt[Kt + \ln t + C])^{\frac{1}{2}}} \tag{6.16}$$

so

$$v(t) \sim 2(-Dt^{-1} \ln t)^{\frac{1}{2}} \quad \text{as } t \to 0. \tag{6.17}$$

The rate of growth of the eyespots was measured by Nijhout and found to be 0.27mm/day at 29^o and 0.12mm/day at 19^o. The estimated diffusion coefficients give the ratio of the initial wavespeeds to be $(D_{29}/D_{19})^{\frac{1}{2}}$ =2.58, which compares quite favourably with the experimental value of 0.27/0.12 = 2.25. In the next section we use these calculated values of the diffusion coefficients at different temperatures to model the growth of the eyespot when the wing is subjected to a coldshock.

6.3 The Effect of Coldshock upon Eyespot Formation.

In this section we consider the same gene switch and diffusible morphogen model, as in the previous section, in the case where the temperature of the wing is reduced for a period of time of length Q. Experimentally Q can be from hours to days. To simplify the analysis, as is reasonable experimentally as the wing is very thin, we assume that the wing responds instantaneously to the coldshock to give a wing temperature profile as shown in Figure 6.5. At $t = t_0$, the time of the shock, we assume that the change in temperature reduces (instantly) the dimensional parameters D and K to the values $\overline{D}$ and $\overline{K}$ respectively. At time $t = t_0 + Q$ the wing is returned to its original

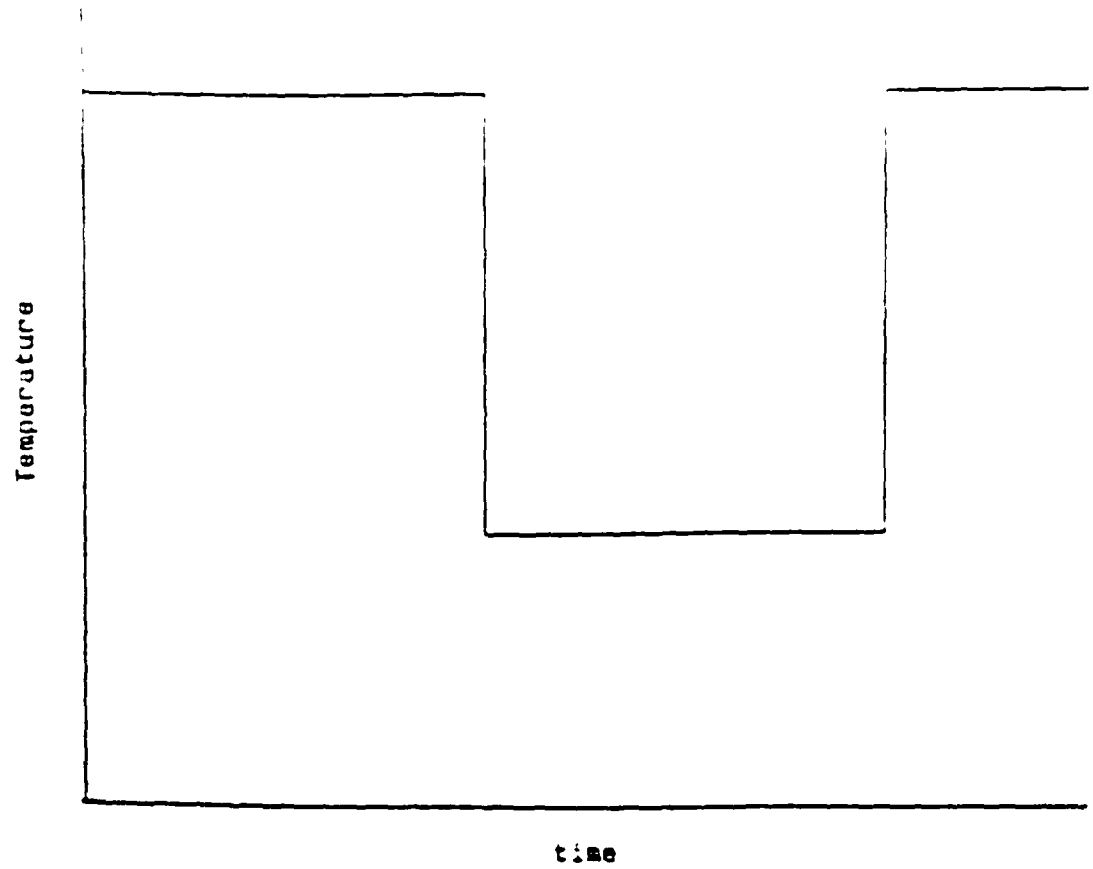

Figure 6.5: Temperature profile in the wing.

temperature thus restoring the diffusion coefficient and the degredation rate constant to their original values D and K.

Using the same nondimensionalisation (6.5) as in the previous section, the relevant equation for $S(r,t)$ in each time region is

$$\text{a) } t \in (0, t_0]: \qquad S_t = S_{rr} + r^{-1}S_r - \gamma k S \tag{6.18}$$

$$S(r,0) = \delta(r), \qquad S(\infty, t) = 0$$

$$\text{b) } t \in (t_0, t_0+Q]: \quad S_t = d(S_{rr} + r^{-1}S_r) - \gamma\lambda k S \tag{6.19}$$

$$\text{c) } t \in (t_0+Q, \infty): \quad S_t = S_{rr} + r^{-1}S_r - \gamma k S \tag{6.20}$$

where

$$d = \frac{\overline{D}}{D}, \quad \lambda = \frac{\overline{K}}{K}. \tag{6.21}$$

Solving these equations for S in the different time regions gives

$$\text{a) } S(r,t) = \frac{1}{4\pi t}\exp\left[-\frac{r^2}{4t} - \gamma k t\right] \tag{6.22}$$

$$\text{b) } S(r,t) = \frac{1}{4\pi[t_0 + d(t-t_0)]}\exp\left[\frac{-r^2}{4[t_0 + d(t-t_0)]} - \gamma\lambda k t - \gamma k t_0(1-\lambda)\right] \tag{6.23}$$

$$\text{c) } S(r,t) = \frac{1}{4\pi[t-Q(1-d)]}\exp\left[\frac{-r^2}{4[t-Q(1-d)]} - \gamma kt + \gamma Qk(1-\lambda)\right]. \tag{6.24}$$

We are interested in the spread of the eyespot, that is, how the radius of the region where $S(r,t) = S_c$ increases in time. From the above expressions for S we obtain

$$\text{a) } R(t) = 2\sqrt{-t[\gamma kt + \ln t + C_1]}, \qquad C_1 = \ln(4\pi S_c) \tag{6.25}$$

$$\text{b) } R(t) = 2\sqrt{-[t_0 + d(t-t_0)][\gamma\lambda kt + \ln[t_0 + d(t-t_0)] + C_1 + \gamma kt_0(1-\lambda)]} \tag{6.26}$$

$$\text{c) } R(t) = 2\sqrt{-[t-Q(1-d)][\gamma kt + \ln[t-Q(1-d)] + C_1 - \gamma Qk(1-\lambda)]}. \tag{6.27}$$

Figure 6.6 shows how the radius $R(t)$ varies for a fixed length coldshock Q and varying t_0. As can be seen the maximum value of $R(t)$ is the same in all cases. So a coldshock could result in a much smaller eyespot forming than would be the case on the untreated wing. Figure 6.7 shows a similar situation where now the length of the shock Q is varying and the time of shock t_0 is fixed. In this case the maximum radius decreases as the length of the shock increases.

We now consider this behaviour analytically. Make the assumption that the maximum radius $R_m(t)$ is reached after the wing has been returned to its original temperature. The maximum value in time region c) occurs at $t = \bar{t}_m$ where

$$2\gamma k\bar{t}_m + \ln[\bar{t}_m - Q(1-d)] = -1 - C_1 - \gamma kQ(\lambda + d - 2) \tag{6.28}$$

giving the maximum radius as

$$R_m(\bar{t}_m) = 2\sqrt{[\bar{t}_m - Q(1-d)][1 + \gamma k\bar{t}_m - \gamma Qk(1-d)]}. \tag{6.29}$$

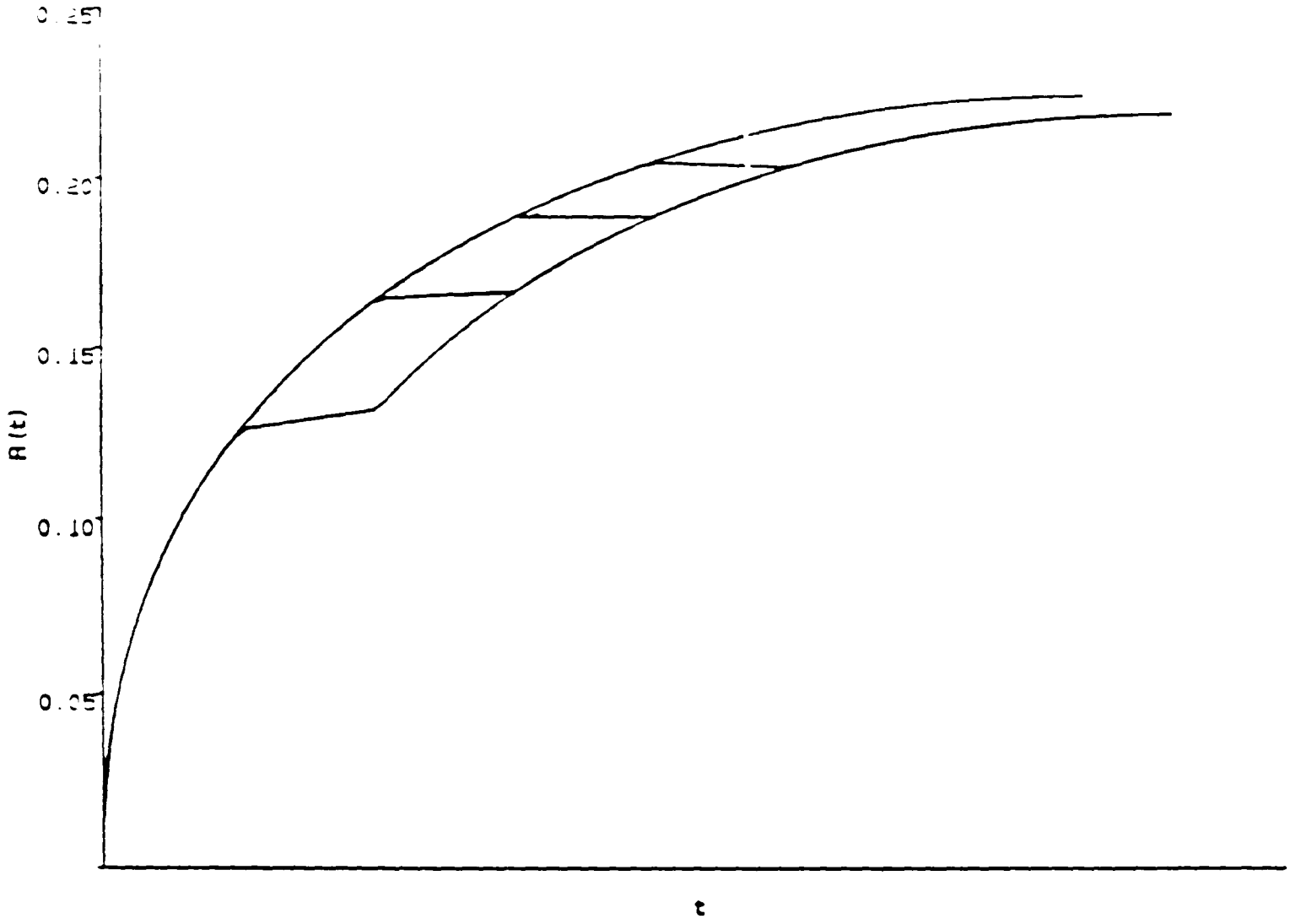

Figure 6.6: Growth of the eyespot for a 12 hr coldshock. Drawn for shocks after (t_0=) 12hrs, 24hrs, 36hrs and 48hrs.

This has no dependence upon t_0 so for a fixed length shock the maximum radius, and hence the size of the eyespot, will be the same for all t_0 satisfying the assumption above. Figure 6.8 shows the dependence of $R_m(\overline{t}_m)$ upon Q. As we can see it is a decreasing function which agrees with the claims made earlier. Throughout this section we have used the following parameter values for the graphical results:

$$D = 4 \times 10^{-9}, \quad \overline{D} = 6 \times 10^{-10}, \quad \Rightarrow d = 0.15, \quad L = a = 0.5\text{cm} \quad \Rightarrow \gamma = 1$$
$$S_c = 0.3, \quad \lambda = 0.7, \quad k = 300, \quad \Rightarrow K = 4.8 \times 10^{-6}, \quad \overline{K} = 3.36 \times 10^{-6}.$$

These parameter values are only estimates to give some pictorial representation of what is occuring. In the next section we discuss these results comparing them to specific coldshock experiments.

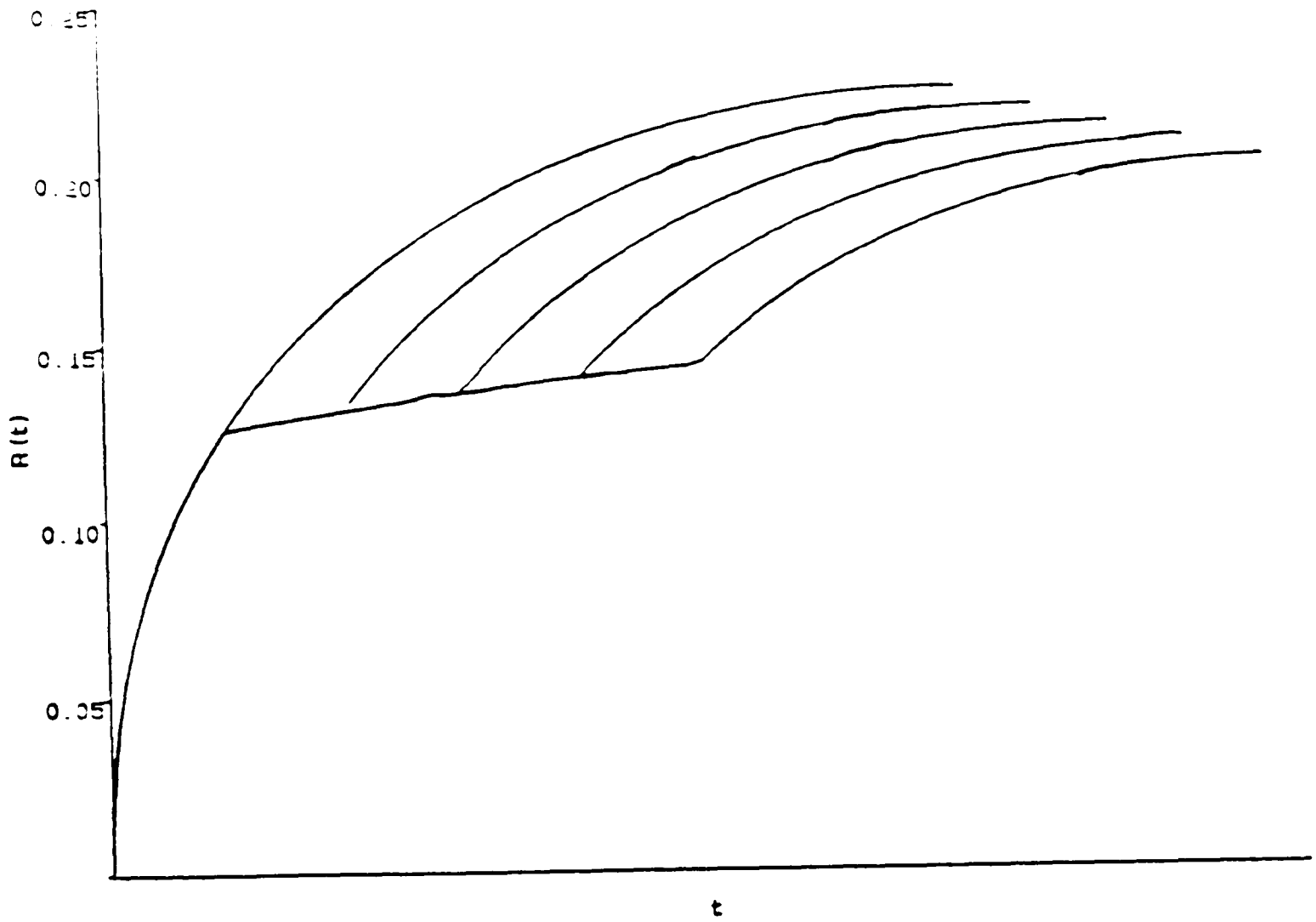

Figure 6.7: Growth of the eyespot for a coldshock after 12hrs. Drawn for shocks of length 12hrs, 24hrs, 36hrs and 48hrs.

6.4 Discussion.

We have shown in the preceeding section, using a model of the form (6.1), (6.3) and (6.4), that the size of the eyespot depends critically on the length of the coldshock and not on the time at which the shock is applied. If we compare this result with experimental findings we see that this is indeed the case, at least for certain species of butterfly. Nijhout (1984) says of the colour patterns formed after coldshock experiments on the butterfly *Vanessa cardui*: "*It should be noted that the types of pattern aberrations observed when 15-24hr old pupae were coldshocked were identical to those for 3-5hr pupae*". It is not the case, however, that a shock at a certain time during the pupal stage and of a certain length gives rise to a fixed pattern aberration. Generally

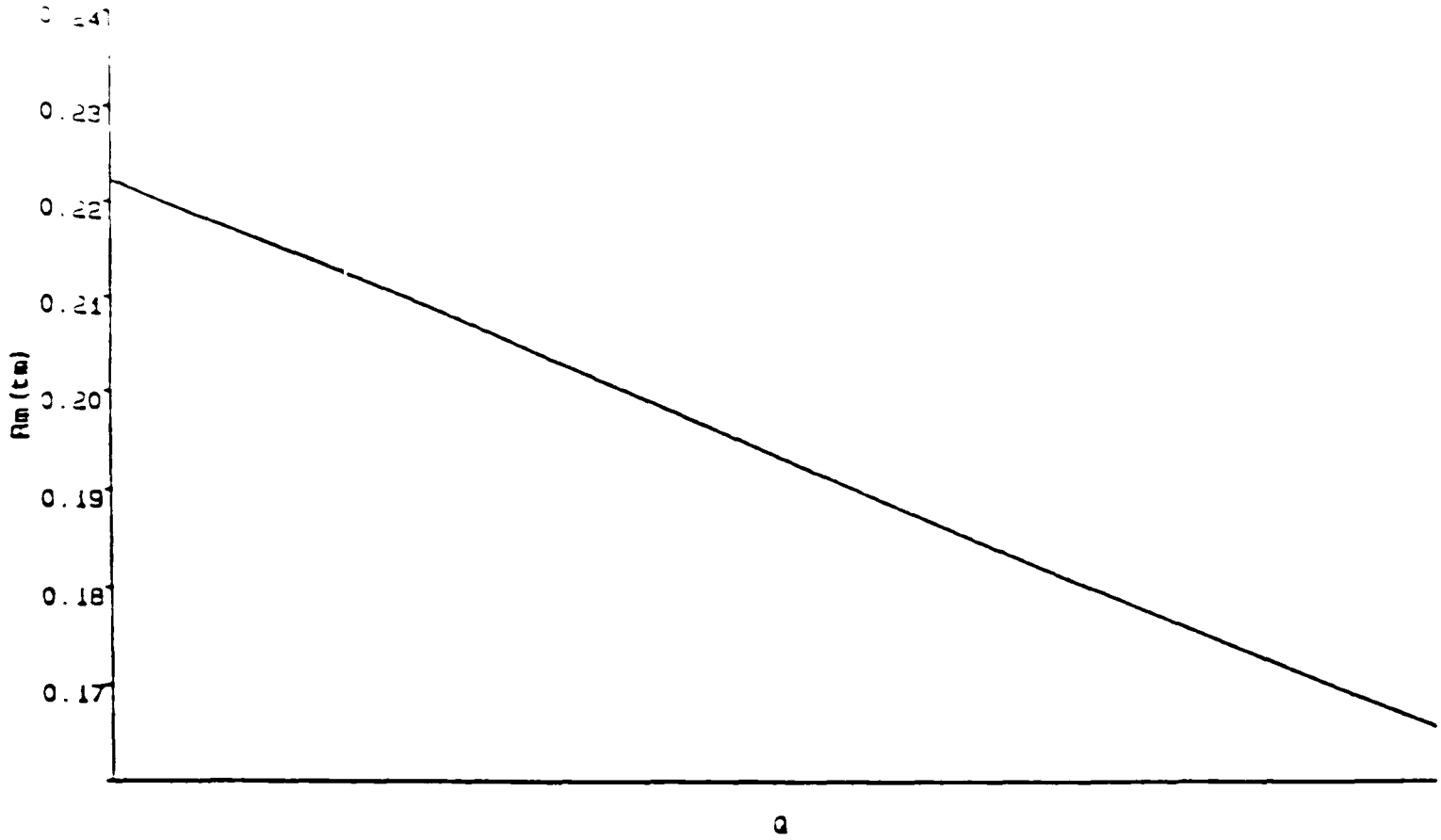

Figure 6.8: Dependence of $R_m(\bar{t}_m)$ upon Q from (6.27) and (6.28).

there is a morphocline (*i.e.* a sequence of graded aberrations) of patterns formed ranging from the almost unchanged to the almost unidentifiable. Another experimental observation from Nijhout (1984) which we have predicted analytically is that "*cold induced aberrations generally involve a diminution of pattern*". The fact that the predicted radius of the eyespot after coldshock is smaller than the unshocked is shown in Figure 6.7.

This analytical work cannot fully explain every aspect of eyespot formation as it leaves no room for natural variation in the wing tissue, a possible cause of the morphocline in coldshocked pattern. Other possible explanations of this pattern morphocline are that there is more than one mechanism at work within the wing or that the gene itself is affected by the change in temperature. Temperature induced aberrations, in some cases, show a remarkable resemblence to the patterns of a different geographic race of the

species. It could be the case that these aberrations have become fixed in the species by genetic assimilation. Shapiro (1983) has examined the ecological and evolutionary implications of such aberrations.

A full analysis of the model in the case where the gene switch does not occur instantly (Kath and Murray (1985)) and there is a period of cooling (and warming) in the wing on application (and removal) of the coldshock may be able to give better representations of the pattern morphocline. This is something that could warrant further research.

Conclusion.

In this thesis we have examined various types of mathematical systems which have been postulated as the possible governing equations for the behaviour of certain chemicals which are thought to be important in the production of biological pattern. The first system we analysed was a reaction diffusion system with anisotropic diffusion. We showed that anisotropy can be used to produce striped patterns on long rectangular domains and we compared these results with the pigmentation patterns found on certain species of snake. We also showed that anisotropic diffusion can produce modulated striped patterns, such as have been seen on some families of snakes, which have not been observed in the solutions of isotropic models.

Secondly we examined a specific reaction diffusion system proposed by Nagorcka (1988) as a possible mechanism for producing the sequences seen in the expression of certain genes in the early embryogenesis of the fruit fly *Drosophila Melanogaster.* We found that the hypothesis he puts forward concerning the preference of the model for forming striped patterns is not necessary. We showed that there is a condition (3.85) upon the form of the reaction kinetics, which is satisfied by the class of kinetics which are asymmetric - the hypothesis of Nagorcka, which is the true reason a striped pattern is likely to form. We also showed that the initial and boundary conditions are crucial in determining the pattern.

In the next chapter we briefly examined gradients in the model parameters for reaction diffusion systems and showed that one dimensional gradients, of a size to be analytically manageable, do not effect the pattern forming potential of the model on a two dimensional domain. Only when large gradients, relative to the size of the parameters, are use is there any noticable effect when one dimensional stripe patterns form perpendicular to the gradients.

We then examined a model of a different form based upon known cellular processes suggested by Goldwasser *et al.* (1989) to model the growth and splitting of branches in arborescent bryozoans. We showed that this model, while difficult to analyse in full, can, under certain restrictions, give analytical solutions in the form of both stationary one humped patterns and standing waves in one dimension. A combination of the two types of solution was shown, in theory, to give rise to both the branching and oscillating behaviour known to occur.

Finally we considered briefly a genetic switch mechanism suggested to model the development of certain pattern elements on a butterfly wing. We considered one such element, an eyespot, in detail and examined how, by reducing the values of certain model parameters, we could could compare the behaviour of the solution with the experimental effect of a coldshock to the wing.

Bibliography

[1] Almirantis, Y. and Nicholis, G (1987). Morphogenesis in an Asymmetric Medium. *Bull. Math. Biol.* **49** p519-530.

[2] Arcuri, P. and Murray, J.D. (1986). Pattern Sensitivity to Boundary and Initial Conditions in Reaction Diffusion Models. *J. Math. Biol.* **24** p141-165.

[3] Baldwin, D.I. (1984). Pattern Formation in Reacting and Diffusing Systems. *D. Phil. Thesis. Oxford.*

[4] Bard, J.B.L. and Lauder, I. (1974). How well does Turing's Theory of Morphogenesis work? *J. Theor. Biol.* **45** p501-531.

[5] Bell, A. (1976). Computerized Vegetative Mobility in Rhizomatous Plants. In: *Automata, Languages, Development.* (ed. A. Lindemayer and G. Rosenberg) North-Holland p3-14.

[6] Bell, A. (1986). The Simulation of Branching Patterns in Modular Organisms. *Phil. Trans. R. Soc. Lond.* **B313** p143-159.

[7] Berding, C. (1987). On the Heterogeneity of Reaction Diffusion Generated Pattern. *Bull. Math Biol.* **49** p233-252.

[8] Britton, N.F. (1986). Reaction Diffusion Equations and their Applications to Biology. New York: Academic Press.

[9] Bunow, B., Kernevez, J.-P., Joly, G. and Thomas, D. (1980). Pattern Formation by Reaction Diffusion Instabilities: Application to Morphogenesis in *Drosophila*. *J.Theor. Biol.* **81** p389-400.

[10] Carroll, S.B. and Scott, M.P. (1986). Zygotically Active Genes that Affect the Spatial Expression of *fushi tarazu* Gene during Early *Drosophila* Embryogenesis. *Cell* **45** p113-126.

[11] Cohen, D.S. and Murray, J.D. (1981). A Generalised Diffusion Model for Growth and Dispersal in a Population. *J. Math. Biol.* **12** p237-249.

[12] Conway, E.D., Hoff, D. and Smoller, J. (1978). Large Time Behaviour of Solutions of Systems of Nonlinear Reaction Diffusion Equations. *SIAM J. Appl. Math.* **35** p1-16.

[13] Crick, F. (1970). Diffusion in Embryogenesis. *Nature* **225** p420-422.

[14] Edelstein-Keshet, L. and Ermentrout, B. (1989). Models for Branching Networks in Two Dimensions. Preprint.

[15] Ermentrout, B., Campbell,B. and Oster, G.F. (1986). A Model for Shell Patterns Based on Neural Activity. *The Veliger* **28** p369-388.

[16] Fife, P.C. (1979). Mathematical Aspects of Reacting and Diffusing Systems. *Lect. Notes in Biomath.* **28**. Springer, Berlin-Heidelberg-New York.

[17] Foe, V.E. and Alberts, B.M. (1983). Studies of Nuclear and Cytoplasmic Behaviour during the Five Mitotic Cycles that Precede Gastrulation in *Drosophila* Embryogenesis. *J. Cell Sci* **61** p31-70.

[18] Gierer, A. and Meinhardt, H. (1972). A Theory of Biological Pattern Formation. *Kybernetic* **12** p30-39.

[19] Goldwasser, L. (1988). Branching Patterns, Generating Rules and Astogenetic Trajectories in Arborescent Bryozoans. *J. Theor. Biol* **132** p179-201.

[20] Goldwasser, L., Maini, P.K. and Murray, J.D. (1989). Splitting of Cell Clusters and Bifurcation of Bryozoan Branches. *J. Theor. Biol* **137** p271-286.

[21] Goodwin, B.C. (1984). Calcium is a Candidate for the Morphogen in *Acetabularia.* European Developmental Biology Congress, Southampton. *J. Embryol. exp. Morph.* **82** (Supplement) p171.

[22] Harris, A.K. (1983). Cell Migration and its Directional Guidance. In: *Cell Interactions and Development: Molecular Mechanisms.* (ed. K. Yamada) Wiley: New York p123-151.

[23] Harrison, L.G. and Kolař, R.M. (1988). Coupling between Reaction Diffusion Prepattern and Expressed Morphogenesis, applied to Desmids and Dasyclads. *J. Theor. Biol.* **130** p493-515.

[24] Kath, W.L. and Murray, J.D. (1985). Analysis of a Model Biological Switch. *SIAM J. Appl. Math.* **45:6** p943-955.

[25] Kauffman, S.A., Shymko, R. and Trabert, K. (1978). Control of Sequential Compartment Development in *Drosophila. Science* **199** p259-270.

[26] Kühn, A. and Von Engelhardt, M. (1933). Über die Determination des Symmetriesystems auf dem Voderflügel von *Ephestia kühniella. Wil. Roux Archiv. EntwMech. Org.* **130** p660-703.

[27] Kurata, K., Kishimoto, K. and Yanagida, E. (1989). The Asymptotic Transectional/Circumferential Homogeneity of the Solutions of Reaction Diffusion Systems in/on Cylinder like Domains. Preprint.

[28] Lacalli, T.C. and Harrison, L.G. (1979). Turing's Conditions on the Analysis of Morphogenetic Models. *J. Theor. Biol.* **76** p419-436.

[29] Lacalli, T.C. and Harrison, L.G. (1987). Turing's Model and Branching Tip Growth: Relation of Spatial Scales in Morphogenesis with Applications to *Micrasterias. Can. J. Bot.* **65** p1308-1319.

[30] Lacalli, T.C., Wilkinson, D. and Harrison, L.G. (1988). Theoretical Studies of Stripe Formation and their Relevance to the Pattern of *ftz* Expression in *Drosophila. Development* **104** p105-114.

[31] Lara-Ochoa, F. and Murray, J.D. (1983). A Nonlinear Analysis for Spatial Structure in a Reaction Diffusion Model. *Bull. Math. Biol.* **45** p917-930.

[32] Lewis, J., Slack, J.M.W. and Wolpert, L. (1977). Thresholds in Development. *J. Theor. Biol.* **65** p579-590.

[33] Macdonald, P.M. and Struhl, G. (1986). A Molecular Gradient in Early *Drosophila* Embryos and its Role in Specifying Body Pattern. *Nature* **324** p537-545.

[34] Matkowsky, B.J. (1970a). A Simple Nonlinear Dynamic Stability Problem. *Bull. Amer. Math. Soc.* **76** p620-625.

[35] Matkowsky, B.J. (1970b). Nonlinear Dynamic Stability: a Formal Theory. *SIAM J. Appl. Math.* **18** p872-883.

[36] Mehrtens, J.M. (1987). Living Snakes of the World. Sterling Publishing Co..

[37] Meinhardt, H. (1986). Hierarchial Inductions of Cell States: a Model for Segmentation of *Drosophila*. *J. Cell Sci. Suppl.* **4** p357-381.

[38] Meinhardt, H. and Klinger, M. (1987). A Model for Pattern Generation on the Shells of Molluscs. *J. Theor. Biol.* **126** p63-89.

[39] Mimura, M. and Murray, J.D. (1978). On a Diffusive Prey-Predator Model which Exhibits Patchiness. *J. Theor. Biol.* **75** p249-262.

[40] Murray, J.D. (1977). Nonlinear Differential Equation Models in Biology. Oxford: Clarendon Press.

[41] Murray, J.D. (1979). A Pattern Formation Mechanism and its Application to Mammalian Coat Markings. In: *Vito Volterra Symposium. Lect. Notes. in Biomath.* **39** Springer-Verlag, Berlin p360-399.

[42] Murray, J.D. (1981a). A Pre-pattern Formation Mechanism for Animal Coat Markings. *J. Theor. Biol.* **88** p161-199.

[43] Murray, J.D. (1981b). On Pattern Formation Mechanisms for Lepidopteran Wing Patterns and Mammalian Coat Markings. *Phil. Trans. R. Soc. Lond.* **B295** p473-496.

[44] Murray, J.D. (1982). Parameter Space for Turing Instability in Reaction Diffusion Mechanisms: A Comparison of Models. *J. Theor. Biol.* **98** p143-163.

[45] Murray, J.D. (1989). Mathematical Biology. Springer-Verlag. Heidelberg.

[46] Murray, J.D. and Oster, G.F. (1984a). Generation of Biological Pattern and Form. *I.M.A. J. Math. Appl. in Medic. and Biol.* **1** p51-75.

[47] Murray, J.D. and Oster, G.F. (1984b). Cell Traction Models for Generating Pattern and Form in Morphogenesis. *J. Math. Biol.* **19** p265-279.

[48] Nagorcka, B.N. (1988). A Pattern Formation Mechanism to Control Spatial Organisation in the Embryo of *Drosophila Melanogaster. J. Theor. Biol.* **132** p277-306.

[49] Nijhout, H.F. (1978). Wing Pattern Formation in Lepidoptera: A Model. *J. exp. Zool.* **206** p119-136.

[50] Nijhout, H.F. (1980). Pattern Formation in Lepidopteran Wings: Determination of an Eyespot. *Devl. Biol.* **80** p267-274.

[51] Nijhout, H.F. (1984). Colour Pattern Modification by Coldshock in Lepidoptera. *J. Embryol. exp. Morph.* **81** p287-305.

[52] Oster, G.F., Murray, J.D. and Harris, A.K. (1983). Mechanical Aspects of Mesenchymal Morphogenesis. *J. Embryol. exp. Morphol.* **78** p83-125.

[53] Russell, M.A. (1985). Positional Information in Insect Segments. *Dev. Biol.* **108** p269-283.

[54] Schnackenberg, J. (1979). Simple Chemical Reaction Systems with Limit Cycle Behaviour. *J. Theor. Biol.* **81** p389-400.

[55] Schneider, D. (1963). Normal and Phototropic Growth Reactions in the Marine Bryozoan *Bugula avicularia.* In: *The Lower Metazoa.* (ed. E.C. Dougherty). Univ. Cal. Press. Berkeley p357-371.

[56] Schwanwitsch, B.N. (1924). On the Groundplan of Wing Patterns in Nymphalids and Certain Other Families of Rhopalocerous Lepidoptera. *Proc. zool. Soc. Lond.* **34** p509-528.

[57] Shapiro, A.M. (1980). Testing Visual Species Recognition in *Precis* using Coldshock Phenocopy. *Psyche* **90** p59-65.

[58] Sibatani, A. (1980). Wing Homeosis in Lepidoptera: A Survey. *Devl. Biol.* **79** p1-18.

[59] Smoller, J. (1983). Shock-Waves and Reaction Diffusion Equations. Springer, Berlin-Heidelberg-New York.

[60] Sondhi, K.C. (1963). The Biological Foundations of Animal Patterns. *Q. Rev. Biol.* **38** p289-327.

[61] Tautz, D., Lehman, R., Schnürch, H., Schuh, R., Seifert, E., Kienlin, A., Jones, K. and Jäckle, H. (1987). Finger Protein of Novel Structyre Encoded by *hunchback*, a Second Member of the Gap Class of *Drosophila* Segmentation Genes. *Nature* **327** p383-389.

[62] Taverner-Smith, R. and Williams, A. (1972). The Secretion and Structure of the Skeleton of Living and Fossil Bryozoa. *Phil. Trans. R. Soc. Lond.* **B264** p97-159.

[63] Thomas, D. (1976). Artificial Enzyme Membranes, Transport Memory and Artificial Phenomena. In: *Analysis and Control of Immobilized Enzyme Systems.* (ed. D. Thomas and J.-P. Kernevez) Springer-Verlag, New York p115-150.

[64] Tickle, C. (1983). Positional Signalling by Retenoic Acid in the Developing Chick Wing. *Prog. Clin. Biol. Res.* **110** p89-98.

[65] Toussaint, N. and French, V. (1988). The Formation of Pattern on the Wing of the Moth *Ephestia kühniella. Dev.* **103** p707-718.

[66] Turing, A.M. (1952). The Chemical Basis of Morphopgenesis. *Phil. Trans. R. Soc. Lond.* **B237** p37-72.

[67] Tyson, J.J. (1976). The Belousov-Zhabotinski Reaction. *Lect. Notes in Biomath.* **10** Springer, Berline-Heidelberg-New York.

[68] Tyson, J.J., Alexander, K.A., Manoranjan, V.S. and Murray, J.D. (1989). Spiral Waves of Cyclic-AMP in a Model of Slime Mold Aggregation. *Physica D* **34** p193-207.

[69] Vogel, O. (1977). Regionalisation of Segment Forming Capacities during Early Embyogenesis in *Drosophila Melanogaster. Roux's Arch. Dev. Biol.* **182** p9-32.

[70] Wolpert, L. (1969). Positional Information and the Spatial Pattern of Cellular Differentiation. *J. Theor. Biol.* **25** p1-47.

[71] Wolpert, L. (1981). Positional Information and Pattern Formation. *Phil. Trans. R. Soc. Lond.* **B295** p441-450.